PERFORMANCE

OF

A MULTISTAGE FLUIDIZED-BED ION-EXCHANGE CONTACTOR

WITH

FLUID-DIODE DOWNCOMERS

By

CONRAD YIU-FOOK LAW

A Research Report

Submitted to the School of Graduate Studies

in Partial Fulfilment of the Requirements

for the Degree

Master of Engineering

McMaster University

February, 1974

MASTER OF ENGINEERING (1974)
(Chemical Engineering)

McMASTER UNIVERSITY
Hamilton, Ontario

TITLE: Performance of a Multistage Fluidized-Bed Ion-Exchange Contactor with Fluid-Diode Downcomers

AUTHOR: Conrad Yiu-Fook Law, B.Eng. (McMaster University)

SUPERVISOR: Dr. L. W. Shemilt

NUMBER OF PAGES: xiv, 203

ABSTRACT

A study was carried out on the operational and mass-transfer performance of a multistage fluidized-bed continuous countercurrent ion-exchange contactor with fluid-diode downcomers. For the mass-transfer study, the ion-exchange system Na^+/H^+ with Dowex-50W-x8 resin was used. The total solution concentration used was 0.06 meq/ml.

The fluid-diode downcomer design significantly reduces the bypassing of liquid up the downcomer. Easy start-up and shut-down were observed and the resin was evenly distributed on each mass-transfer stage. The effects of fluid-diode lateral displacement, weir height, weir shape and resin particle size on the operational performance (in terms of liquid-bypassing and resin fluidization) of the solid-liquid contactor were investigated.

A one-quarter replicate of a factorial experimental design to 7 factors at 2 levels successfully and efficiently revealed the main factors and interactions which significantly affect the overall stage efficiency of the ion-exchange column operation. The significant main factors are resin feed-rate, process solution flow-rate, weir length and weir height. The significant interactions are between resin feed-rate and weir length, process solution flow-rate and weir length, and weir height and weir length.

The mass-transfer study has shown that the solid-liquid contact time in the contactor determines the overall stage efficiency. The composition dependence of

the mass-transfer coefficients in both the solid and liquid sides also plays a role in affecting the overall mass-transfer.

The relative specific volumes calculated from the experimental results justify further development of the present contactor in the consideration for industrial scale applications. The present type of contactor is simple in design and requires simple control strategy, providing operational stability, and large solid and liquid handling capacity.

ACKNOWLEDGEMENTS

The author wishes to express his sincere appreciation to his research supervisor, Dr. L. W. Shemilt, Dean of Engineering, for his assistance and co-operation during the course of the completion of this study.

Thanks are extended to Dr. A. V. Bapat for contributing some of his ideas to the present study.

Thanks are also extended to Mr. G. De Bore of the Faculty Machine Shop and Messrs. J. Newton and B. Dunn of the Chemical Engineering Machine Shop for their workshop assistance. Special thanks are extended to Mrs. I. Underell for her secretarial help.

Finally, the author wishes to thank his wife, Stella, for her help in preparing the draft for this thesis and her patience and encouragement throughout the course of the research program.

TABLE OF CONTENTS

LIST OF FIGURES

LIST OF TABLES

I. INTRODUCTION

The study of ion-exchange is over a century old and the technology has been applied to industry for more than sixty years. For many years, ion-exchange was commonly used for water softening. The introduction of synthetic resins of reliable physical and chemical properties has greatly broadened the application of ion-exchange. Various successful applications of the ion-exchange process are well known in demineralisation of boiler feed-water, in effluent treatment, in demineralisation of sugar solution and in hydrometallurgy and in the purification of pharmaceuticals.

The fixed-bed ion-exchange technique has been used for more than fifty years and is essentially unchanged except for automation. The fixed-bed process operates on a semi-batch basis and is easy to achieve on a large scale. The advance in this technology has been confined almost entirely to the chemistry of the process, such as through the development of new and better ion-exchange resins. Some of these resins approach theoretical limits with respect to their chemical capacity, efficiency and stability (1). Further improvement on the performance of ion-exchange technology will be in the development of more efficient solid-liquid contactors. In addition, there is still need to solve the problem of a fixed-bed ion-exchange process economically for treatment of a continuous liquid-feed of high concentration where a short cycle-time is required. The development of continuous countercurrent contactors for ion-exchange processes

has been emphasized in recent years. Various contactor designs employ solid resin flow countercurrent to process solution flow in the form of a moving packed-bed, a fluidized bed or a pulsed bed (3, 4, 5). Progress here has also been encouraged by the development of synthetic ion-exchange resins. Continuous countercurrent ion-exchange processes have advantages, including maximum utilization of the ion-exchange resin inventory during the exhaustion and the regeneration cycles. Further, the resin inventory is low, and equipment size and floor space requirements are reduced. The regenerant and wash water requirements are also lowered, indicating a reduction in waste disposal expenditure. The continuous mode of operation requires no shutdown for regeneration, and automatic control can be implemented to adjust the resin and liquid flows in obtaining effluents of desired compositions. Hence overall labour requirement may be reduced. In general, the continuous countercurrent ion-exchange processes can offer savings in capital and operating costs per unit output, above some threshold capacity, when compared to the conventional fixed-bed operation. For the treatment of dilute solutions (0.0005 gm/cc), this threshold has been put between 6000 and 30,000 gal/hr (15) which varied for different operable contactor designs. A large number of contactors have been developed but very few have become commercially successful (2).

The present research is on the development of a truly continuous countercurrent ion-exchange contactor. This is a multistage fluidized-bed contactor. The resin flows under gravity from one stage to the next through a fluid-diode downcomer. Unlike other countercurrent ion-exchange contactors, this one handles truly continuous solid and liquid flows within the optimal range of operation

conditions. The development of the present contactor originates from the research of Souhrada (6) who has applied the controlled cycling technique in the design of a multistage fluidized-bed ion-exchange column with downcomers similar to those in a gas-liquid contactor. Egan (7) reported on the application of the fluid diode in designing a downcomer to eliminate the problem of liquid bypassing. Cha's (8) investigation has extended to demonstrating the ability of the contactor to perform under a continuous liquid-flow. Although these intermittent and continuous liquid-flow operations showed approximately the same mass-transfer performance, the simplicity of the continuous liquid-flow operation appears economically more advantageous.

The purpose of the present study is to extend the investigation on the operational and mass-transfer performance of the multistage fluidized-bed contactor with fluid-diode downcomers when operated under continuous liquid-flow. A further aim is to compare the performance (in terms of the chemical efficiency and the volumetric throughput) of this ion-exchange contactor with others, including some which have been used industrially.

2. LITERATURE REVIEW

2.1 Fluid Diode

Considerable interest in fluidic (fluid logic) systems and devices has arisen, largely from the work done at the Harry Diamond Laboratories (14). These devices are generally characterized by having no mechanical moving parts and rely on the interaction of entering fluid streams with each other and with shaped walls to produce the desired response in the output fluid stream (9, 10, 11).

The fluid diode was invented by Telsa (12) in 1920. The device consisted of a channel with many branching and returning loops which behaved like an electrical diode in offering far more resistance to flow in one direction than to flow in the reverse direction.

Ringleb (13) investigated the flow patterns of an incompressible inviscid fluid in various single cusp-cavity shapes. The general theory of standing vortices based on potential-flow consideration was applied to the computation of velocity distributions along the walls of various cusp-cavities. Ringleb also suggested the general form of a mapping function to generate these cusp-cavity shapes.

Thompson (14) has utilized the principle of the fluid diode to develop an intermittent-flow countercurrent liquid-liquid contactor. The contactor makes use of the flow-interference effects of the designed fluid-diode structure to convert an alternating applied pressure into a net countercurrent motion of the two liquid phases.

Egan (7) implemented the idea of the fluid diode in his design and construction of a new downcomer structure to overcome the undesirable downcomer liquid-bypassing in the intermittent-flow multistage fluidized-bed ion-exchange column developed by Souhrada (6). Egan tested three cusp shapes for the fluid-diode downcomer design. The design is essentially similar to that used in Thompson's fluid-diode contactor but each fluid-diode downcomer consisted only of two or three pairs of cusp-cavities.

2.2 Continuous Countercurrent Ion Exchange

A large number of continuous countercurrent ion-exchange (CCIX) contactors have been proposed and tried in pilot-plant scale. However few of the designs have met with any degree of commercial success (2). The main problem to overcome in the designs is to achieve smooth, even and continuous counterflows of solid resin and process solution where there is a small density difference between the two phases. Various ingenious methods employed to overcome this problem include solution downflow, resin agitation and various other mechanical and hydraulic techniques.

Various mixer-settlers have been patented for CCIX processes. The horizontal mixer-settler system patented by Morris (16) was tested as a continuous countercurrent ion-exchange contactor. Hiester (17) has developed a mixer-settler device using air agitation in the mixer cells. Other mixer-settler systems have been examined by Iwasyk and Thodos (18) who claimed favourable results for these contactor systems in the extraction of phenol by ion-exchange.

There are some unusual designs in the mechanical transport of the ion-exchange material continuously and countercurrently through the liquid phase. These are McCormack and Howard's (19) endless tube of cloth filled with resin, Muendel and Selke's endless belt of phosphorylated ion-exchange cotton and the rotating helical tubes of Miles (21) and Schulman (22). These designs were only for laboratory operations.

Weiss, McNeill and Swinton (23) have adapted the ore dressing operation of jigging and developed multideck jigs for CCIX. The authors felt that the large capacity, ruggedness, flexibility and ease of maintenance of the contactor more than balanced the lower efficiency.

Various contactor designs have employed the moving fixed-bed technique in the transfer of resin through the exhaustion, regeneration and washing stages. Some of these designs have become very successful in industrial applications. These systems use the principle of periodically removing a portion or slug of exhausted resin from one end of a fixed bed, and replacing it with an equal volume of regenerated resin at the other end. Such systems are usually not truly continuous since the flow of process solution is momentarily stopped during the transfer of resin in and out of the column. Peebles and co-workers (24) have developed one such system where a single column of resin is divided into zones for treatment, rinsing and regeneration, and resin is pumped from the bottom to the top of the column forming a complete loop. A serious difficulty with this design is the balancing of differential pressures within the unit.

One of the most successful moving fixed-bed designs is the Higgins contactor

(25) which is also a single-loop system. The resin is transferred around the loop by regular hydraulic pulses. Further development of the process by Higgins and Chopra (26) at the Chemical Separations Corporation results in the addition of the "down flow" design to the single-loop system and has enhanced its versatility as a process in both water and chemical process demineralisation applications. The process is now marketed as the Chem-Seps CCIX contactor. The Chem-Seps process is claimed to require a resin inventory as low as 15% and rarely over 30% of that required for conventional fixed-bed systems. The countercurrent flow efficiency of this continuous process has also given a reduction of regenerant consumption by one half and the rinse-water requirement by one-tenth. The Chem-Seps process also has a lower equipment cost than the conventional fixed bed process. The comparison is based on the treatment of a feed flow of 380,000 U.S. gals/day and a removal of TDS from 1800 ppm to 5 ppm.

The Asahi process and the Permutit CCIX systems employing the moving fixed-bed technique have also been successful in large scale industrial operations throughout the world (27). Levendusky (3) recently described the Graver C.I. process which also employed the moving-bed and intermittent-flow techniques. The process has been successful in pilot-plant scale after eight years of research. The design has the versatility in controlling the adsorption and desorption and washing operations separately. Another version of the same design can handle a mixed-resin bed. The new process is expected to challenge conventional fixed-bed and existing CCIX processes.

Recent research has been in the development of multistage fluidized-bed

contactors for CCIX. The fluidized-bed ion-exchange contactors may have a lower chemical efficiency than that of fixed-bed and moving-bed contactors. However, the reduction in capital and operational costs due to simpler design requirements in fluidized-bed contactors may compensate for the slight loss in efficiency. The movement of resin from one stage to another countercurrent to the solution flow has been achieved in a variety of ways. The horizontal contactor design of Cloete and Streat (4) uses a momentary reversal of liquid-flow. Grimmett and Brown (5) used the pulsing technique to assist the downward movement of resin through the tubular downcomers in their vertical multistage fluidized-bed column. Slater (28) has studied a similar pulse column. Church and Turner (29) developed and studied a 16 plate fluidized-bed column with stage and downcomer structures similar to those of a sieve-plate distillation column. Results indicated that the column was relatively easy to operate at steady state but there were difficulties in starting up and allocating equal amounts of resin in each stage.

The principal difficulty in stagewise contactor columns with downcomers has been the prevention of liquid bypassing up the downcomers. Externally controlled fluidized seal pots under the downcomers (30) or rubber flaps or valves in the downcomers (31) to reduce liquid bypassing have been suggested. However, individual seals of this nature cannot be regulated to give equal solid flow from each stage without a complex control system.

Souhrada (6) has applied the principle of controlled cycling to achieve a stable operation in a CCIX column similar to that of Turner (29). The intermittent flow of liquid through the multistage column did provide easy start-up and shut-

down, and increased the stability of the steady state operation. However problems were still encountered in liquid bypassing up the downcomers resulting in a lower contacting efficiency.

Egan (7) applied the fluid dynamic properties of a fluid diode in designing a new type of downcomer for the intermittent-flow multistage fluidized-bed column of Souhrada. The fluid-diode downcomer succeeded in reducing the undesirable liquid bypassing. Cha (8) has showed that the multistage fluid-bed column can be operated satisfactorily not only by an intermittent but also by a continuous liquid-flow. The mass-transfer performance of the two modes of operation was shown to be approximately the same. However, the truly continuous operation should be able to process resin and liquid feed streams of larger volumetric throughput. The elimination of the intermittent-flow control is a further economic advantage, especially when the contactor is applied to large scale industrial operations.

3. THEORY

3.1 Fluid Diode

Ringleb (13) investigated the formation of standing vortices by a two-dimensional incompressible inviscid fluid in single cusp-cavities. He suggested a general form of mapping function to generate the cusp-cavity shape in which a single standing vortex is automatically created when a parallel flow passes over it. Wall profiles and flow streamlines for families of cusp-cavity shapes were obtained by integrating equations of the form

$$\frac{dF(a)}{da} = \frac{a(a-a_2)\cdots}{(a-a_1)(a-a_3)\cdots} \qquad (3.1.1)$$

where F(a) is the mapping function and a the complex mapping variable; along each streamline its imaginary part is constant. The complex parameters a_1, a_2, a_3, etc. determine the nature of the flow field.

Cusp-cavity of the simplest form requires only one complex parameter in the mapping function (3.1.1). Ringleb (13) and Thompson (14) have suggested expressions of such mapping functions:

$$F(a) = a + a_1^2/(a-a_1) \qquad (3.1.2)$$

$$F(a) = a + a_1 \log (a-a_1) \qquad (3.1.3)$$

where $a_l = m_l + in_l$. The two adjustable parameters are m_l and n_l which determine the shape of the cusp-cavity. When m_l is held constant to fix the scale, a family of cusp shapes can be generated for different non-positive values of n_l by plotting y versus x in the following expression for the shape of a streamline,

$$z = x + iy = F(a) \tag{3.1.4}$$

as a is moved along the real axis. The cusp point corresponds to $a = 0$.

Ringleb's analysis is only helpful in designing the channel of Thompson's contactor (14) for flow in the low pressure-drop direction and serves mainly to establish the kind of cusp-cavity shape that will permit a stable vortex to be established. When fluid flow is reversed, the inviscid model would predict unchanged streamlines.

The mathematical shape generated from the mapping function was modified by Thompson in order to obtain turbulence during reverse flow. The original and adapted shapes are shown in Figures A.1 and A.2 in Appendix A. Thompson has found that if the radius of curvature of the wall C is less than 4 inches, the flow may separate and short-circuit to the cusp endpoint, causing less turbulence in the flow pattern.

The fluid flow patterns in Thompson's fluid-diode contactor are shown in Figures A.3 and A.4. The contactor is constructed of two identical horizontal fluid-diode sections but oppositely oriented. In the low pressure-drop direction (A to B), the main stream follows a direct path through the channel, and it separates from the wall at each cusp point D and a standing vortex is formed in each cavity.

While some turbulence may be generated between these two flows, the general appearance to the flow pattern is very smooth. When the direction is reversed and the stream flows in the high pressure-drop direction (B to A), the stream follows a highly tortuous path. The high velocity portion of the stream becomes attached to wall C and is diverted into the cavity, where it is forced to partially reverse in direction and deflected to the opposite side of the channel.

Egan (7) tested fluid diodes of three different cusp-cavity shapes which are shown in Figure A.5. Results for water flow showed that the friction factor of the fluid diode in the high pressure-drop direction can be 20 times more than that in the low pressure-drop direction as the Reynolds number of the water flow in the channel is increased. The pressure drop for water flow in either direction of the diode is higher than that for pipe flow but the characteristics of flow in the high pressure-drop direction is entirely different from that of pipe flow. Figure D.1 shows that the pressure-drop ratio, $\Delta P_{high}/\Delta P_{low}$, increases with the Reynolds number. The ratio is independent of the fluid-diode lateral displacement in the flow region investigated by Egan. Note that only the ratio is constant but the pressure drop in both directions decreases in the same proportion as the diode lateral displacement is increased.

The fluid diodes with cusp-cavity shapes A and B of Figure A.5 behave almost identically. However, fluidic element C also has a pressure-drop characteristic comparable to shapes 1 and 2. This observation of Egan indicates that the increased number of cusp-cavities per unit length has counteracted the short-circuiting expected since the radius of curvature at point C of shape C is less than

four inches.

When the fluid diode is adapted as a downcomer structure in the multistage fluidized-bed continuous countercurrent ion-exchange contactor developed by Souhrada, the characteristics of fluid flow through the fluid-diode downcomer in the high pressure-drop direction created by the bypassing process solution during startup still hold, and serve the purpose of discouraging liquid bypassing up the downcomers. At steady state a continuous stream of solid resin particles flows down the downcomer in the low pressure-drop direction. The flow pattern of the solid particles with a density slightly higher than that of water is expected to be different from that of an incompressible inviscid fluid. The characteristic of the resin flow through the downcomer will be discussed in Section 8.1.1.

3.2 Ion-Exchange Resin

Ion-exchange resins are insoluble spherical solid particles, whose framework is an elastic matrix consisting of an irregular macromolecular, three-dimensional network of hydrocarbon chains, carrying fixed ionic groups associated with exchangeable cations or anions. These exchangeable ions can be exchanged for a stoichiometrically equivalent amount of other ions of the same charge when the resin is in contact with an electrolytic solution. Carriers of exchangeable cations are called cation exchangers and carriers of exchangeable anions, anion exchangers. There are four main types of ion-exchange resins in commercial use, namely strongly and weakly acidic (cation) resins and strongly and weakly basic (anion) resins.

The Dowex-50Wx8 resin used in the present study is a strongly acidic cation exchanger. It is prepared by the nuclear sulphonation of styrene-divinyl benzene beads and the fixed ionic group is $-SO_3^-$. The resin is stable chemically and physically. The divinyl benzene is a cross-linking reagent, the percentage of which determines the degree of crosslinkage in the resin matrix. The degree of crosslinkage determines the physical and chemical properties of the resin. A decrease in crosslinkage increases the matrix porosity and hence its ability to swell and takes up more water. The increase in porosity also increases the mobility of the counter-ions in the resin and hence the rate of exchange.

A detailed discussion on ion-exchange resins can be found in Helfferich (32).

3.3 Ion Exchange

Ion-exchange is a mass-transfer process between two phases. Ions are transferred from a solution (usually an aqueous phase) to an ion-exchange material (usually a solid and commonly a polymerized resin), while an equivalent number of ions of the same charge, but of different species, are displaced and transferred in the opposite direction. An example of ion-exchange is the Na^+/H^+ exchange on Dowex-50Wx8 resin. The equation of exchange is given by

$$(H^+)\,\text{resin} + (Na^+)\,aq + (Cl^-)\,aq \rightleftharpoons (Na^+)\,\text{resin} + (H^+)\,aq + (Cl^-)\,aq \qquad (3.3.1)$$

This is an interdiffusion between counter-ions, H^+ and Na^+. The co-ion, Cl^-, does not participate in the ion-exchange process; however, there is still some sort of distribution of the chloride ion between the resin and aqueous phases as can be

found in the work by Whitcombe et al (33).

For an ordinary ion-exchange system, the ion-exchange rate controlled by chemical reaction has been ruled out (32). Ion exchange, as a rule, is purely a diffusional phenomenon. Hence the rate of exchange is governed by the same general consideration as for any mass-transfer process. There are mass-trqnsfer resistances in both phases, and the overall rate may be controlled by either (or by both) of these resistances. For either phase, the mass transfer may be described by a rate equation of the form

$$\frac{dq}{dt} = k'A(c-c_i) \qquad (3.3.2)$$

If the two exchanging ions have markedly different diffusion coefficients, then an electric field will be set up in each phase and these fields will affect the diffusion process. One of the consequences is that the rate of exchange can be markedly composition dependent. This phenomenon in the resin phase can be illustrated by the present ion-exchange system, Equation 3.3.1. At the start of an exchange, the hydrogen ions, which have a higher mobility, tend to move off more rapidly than the sodium diffusing in the opposite direction. This leads to a charge separation which proceeds only to a minute extent before an electric field is set up in such direction and of such strength that the hydrogen ions are slowed down, and the sodium ions are speeded up until their opposing fluxes are equal. The effects of these electric fields are allowed for in the Nernst Planck model for diffusion in a resin particle and the interdiffusion coefficient of two monovalent ions, as a function

of resin composition is given by the following expression

$$D = \frac{D_A}{1 + \left(\frac{D_A}{D_B} - 1\right) x_A} \qquad (3.3.3)$$

Note that the model assumes the mobility of an ion to be independent of its surroundings, which is a reasonable assumption for the exchange of ions of equal charges (32).

Turner et al (34) has verified the Nernst Planck model for diffusion in Zeo Karb-225 resin for the exchange of H^+ and Na^+ ions. The self-diffusion coefficient of the hydrogen ions can be more than four times that of the sodium ions depending on their concentrations.

Turner and Snowdon (35) have also applied the Nernst-Planck behaviour in the study of the liquid-film mass-transfer coefficient in the exchange of H^+ and Na^+ ions between aqueous chloride solutions and Zeo Karb-225 ion-exchange resin. It has been shown that where the liquid film plays a significant role in ion-exchange kinetics, the variation of exchange rate with liquid composition should not be ignored. The liquid side mass-transfer coefficient can vary by a factor of more than three as the liquid composition changes.

For the present ion-exchange system, H^+-Dowex-50W-x8-Na^+, Duncan and Lister (36) have shown that the equilibrium constant, K, remains practically constant for a given total solution normality, Co, and is given by

$$K = \frac{y(1-x)}{x(1-y)} \qquad (3.3.4)$$

where x and y are equilibrium mole-fraction compositions on sodium bases in the aqueous and resin phases respectively. The temperature dependence of the equilibrium constant is usually negligible.

Gilliland and Baddour (37) have determined the equilibrium constant for sodium chloride solutions of various normality equilibrated with Dowex-50-x8 ion-exchange resin. The plot of log (Co) vs. K in Figure D.2 gives the following analytical expression

$$K = \frac{-\log (Co) + 17.75}{12.5} \qquad (3.3.5)$$

Note that the present experimental study uses the Dowex-50W-x8 resin which is claimed (38) to have stronger physical properties than the Dowex-50-x8 resin. However, the correlation (3.3.5) is assumed to be the same for Dowex-50W-x8 resin since the chemical properties of the two resins are identical (38).

3.4 Fluidized-Bed Ion Exchange

Mass transfer in fluidized-bed ion-exchange is a volume process*. With the

---

* Beek (42) has made a distinction between surface and volume processes in fluidized-bed operations. Coating, wetting and agglomeration are surface processes, and drying, cooling and freezing are volume processes.

small dependence on temperature, the physical factors which determine the rate of the process include inside and outside particle mass-transfer, the fluid and solids mixing, and the probability of particles encounter.

The mass-transfer rate in a shallow fluidized-bed of ion-exchange resin is commonly controlled by both the solid- and liquid-sides mass-transfer resistances. Turner (39) has shown that the solid-side resistance can account for 20% or more of the total resistance depending on the compositions. When the liquid flow was increased, the liquid boundary layer around the resin particle decreased, the liquid-side mass-transfer resistance was reduced and consequently the overall mass-transfer coefficient was increased. The ion-exchange resin is at a state of particulate fluidization when the incipient fluidization velocity is exceeded by the solution flow. For a shallow fluidized-bed, the resins are perfectly mixed and the liquid passes through the bed in plug flow. However, longitudinal dispersion of liquid cannot be neglected in deep fluidized beds.

The mass transfer study of Petrovic and Thodos (40) on a gas-solid fluidized-bed system contributed to understanding the mass-transfer process in a liquid fluidized-bed system since they worked with an almost homogeneous bed with the fluidized-bed voidage given by

$$\frac{V_o}{V_{ob}} = \left(\frac{\epsilon}{\epsilon_b}\right)^{2.5} \qquad (3.4.1)$$

which is similar to that by Richardson and Zaki (41) for liquid fluidized-beds. The following mass-transfer relations were reported for the fluidized-bed system,

$$\phi = \frac{k_L}{k_{Lb}} = \frac{\epsilon_b}{\epsilon} \left(\frac{V_o}{V_{ob}} \right)^{0.57} \qquad (3.4.2)$$

and

$$\phi \simeq \left(\frac{\epsilon}{\epsilon_b} \right)^{0.44} \qquad (3.4.3)$$

Equation 3.4.2 shows that k_L is proportional to ϵ^{-1} and $V_o^{0.57}$. In Equation 3.4.1 V_o is proportional to $\epsilon^{2.5}$. Hence k_L is proportional to $\epsilon^{0.43}$. Within the range of voidage (0.5 to 0.8) commonly used, the values of $\epsilon^{0.43}$ varied by a maximum of 18%. A consequence of this result is that the k_L value is almost independent of the superficial fluid velocity.

The above conclusion coincides with the findings of Rowe and Claxton (46) that the tendency of increasing Re to increase Sh with fluidized beds is largely nullified by the resulting increase in voidages. For fluidized-bed ion-exchange, the mass transfer between resin particles and the aqueous solution flow is complicated by the composition dependence of both the solid- and liquid-sides mass-transfer coefficients. However, the experimental results of Turner and Snowdon (35) for liquid fluidized-bed ion-exchange shows that the change in liquid-film mass-transfer coefficient, k_L, with bulk solution composition is identical at Reynolds number 7.2 and 8.8 for a total solution normality of 0.01 N.

Snowdon and Turner (39) claimed that less mass-transfer occurred in fluidized beds than in fixed beds when compared at the same Reynolds number, $U_o \rho d/\mu$ (based on liquid superficial velocity). They correlated the mass-transfer results of

both fluidized and fixed beds by

$$Sh = \frac{0.81}{\epsilon} ReSc^{1/3} \qquad (3.4.4)$$

where $Sh = k_L d/D$, $Re = U_o \rho d/\mu$, $Sc = \mu/\rho D$.

However, comparisons of the mass-transfer rate in fixed and fluidized beds on different bases can give different conclusions in the relative effectiveness of the two processes. Beek (42) shows that a correlation between $St.Sc^{2/3}$ and $U_o d/\nu$ can bring the mass-transfer results for packed and fluidized beds close together,

$$St.Sc^{2/3} = (0.81 \pm 0.05)(U_o d/\nu)^{-0.5} \quad \text{for } 5 < U_o d/\nu < 50 \qquad (3.4.5)$$

where $Re = U_o d/(1-\epsilon)$, $Sc = \nu/D$, $Sh = \epsilon k_L d/(1-\epsilon) D$ and $St = \epsilon k_L/U_o$.

The correlation is obtained from the experimental data of Snowdon and Turner (39) for liquid-fluidized ion-exchange beds ($100 < Sc < 1000$, $0.43 < \epsilon < 0.63$). A comparison between both beds gives for equal value of $U_o d/\nu$ equal values of $(k_L/U_o)\epsilon$ and consequently lower k_L values in the fluidized bed. Beek believes that this expression is the most accurate and reliable presentation of today's knowledge for the most important range of Reynolds number, for all Sc values met in practice and for porosities up to 0.75.

The study by Hanna (51) on the residence time distribution of solid particles in a countercurrent fluidized-bed system shows that the mixing of solid particles can be increased by increasing the liquid flow-rate (superficial liquid velocity), by decreasing solid particle throughput and by decreasing the bed height.

3.5 Continuous Countercurrent Multistage Ion Exchange

The continuous countercurrent multistage fluidized-bed ion-exchange contactor under present study operates on continuous solid resin and liquid flows with equal distribution of resin in each stage when steady state is reached. The theory of continuous countercurrent ion-exchange is analogous to that of solvent extraction and the diffusional mass-transfer column operations. The performance is governed by the equilibrium relationship, the mass balance, the rates of mass transfer, and the contacting efficiency of the contactor.

The performance of the ion-exchange column can be analysed by the McCabe-Thiele diagram. This method has been suggested by Moyle (43) and used by Turner and Church (44). A material balance across a section of the column and the bottom of the column (Figure D.3) gives the following component balance

$$L_o c_o x_o + R_{n+1}\ q_{n+1}\ y_{n+1} = L_n c_n x_n + R_1 q_1 y_1 \qquad (3.5.1)$$

The ion-exchange operation is a truly equi-molar counter-diffusion process. The volume flow-rates of the solid and liquid flows in the present system are constant. Hence, we have

$$L_o = L_1 = L_2 = \cdots = L_N = L$$

$$R_1 = R_2 = R_3 = \cdots = R_{N+1} = R \qquad (3.5.2)$$

and $$c_o = c_1 = c_2 = \cdots = c_N = c$$

$$q_1 = q_2 = q_3 = \cdots = q_{N+1} = q$$

Equation 3.5.1 can be reduced to

$$Lc\,x_o + Rq\,y_{n+1} = Lc\,x_n + Rq\,y_1 \qquad (3.5.3)$$

or $$y_{n+1} = \frac{Lc}{Rq}\,x_n + \frac{Rq\,y_1 - Lc\,x_o}{Rq} \qquad (3.5.4)$$

Equation 3.5.4 relates the compositions of the resin phase, y_{n+1}, and the liquid phase, x_n, flowing past each other between stages. The locus of (x_n, y_{n+1}) on the equilibrium diagram plot is a straight operating line as shown in Figure D.4. The linearity of equation 3.5.4 is displayed much more vigorously for ion exchange than the corresponding distillation or absorption, in which the usual simplifying assumptions (45) are usually not strictly true.

The number of theoretical stages (NTS) can be determined from this diagram by a stepping off procedure involving alternate use of the operating line and the equilibrium curve as shown in Figure D.4. The height equivalent to a theoretical stage (HETS) is then obtained by dividing the actual contactor height by the number of theoretical stages.

However, the actual height of the present ion-exchange column useful for mass transfer is that of the weir height in each stage. The calming zones between stages and the stage separation necessary for the installation of the fluid-diode downcomer is determined by the physical operational requirement and should not be considered in the mass-transfer performance study. Hence, it is only proper to calculate the HETS using the total active height of the ion-exchange column; and HETS is thus given by

$$HETS = Z/NTS = WH.\ N/NTS \qquad (3.5.6)$$

In the actual countercurrent multistage contact, the solid and liquid phases leaving a stage are not in thermodynamic equilibrium. An overall stage efficiency may be defined to describe the degree of approach to equilibrium in the contacting operation. The overall stage efficiency is defined as the ratio of the number of equilibrium stages required for a given separation to the number of actual stages required and can be expressed in percentage as

$$E_{os} = (NTS/N) \cdot 100\% \qquad (3.5.7)$$

This stage efficiency is simple to use in calculations, although it does not allow for the variations in efficiency which may occur from stage to stage. The overall stage efficiency depends on many factors such as the time of contact and degree of dispersion of the phases, the geometry of the stages, the rate of mass transfer, and the physical properties and flow rates of the solid and liquid phases.

3.6 Factorial Experimental Design

Experimental design is the planning of data collection from an experiment or a series of experiments so that the desired information can be obtained with sufficient precision. The response of the dependent variable to the independent variables (factors) and to the levels of the factors are of interest to the experimenter. For a given number of factors and levels of the factors, a complete factorial design can evaluate jointly and efficiently the effects of all the possible combinations of factors and levels on the response. Standard works (47, 48) deal extensively with

the theory of experimental design. The following is adapted from Peng (47).

For a design of three factors (A, B, C) at two levels, the eight (2^3) possible combinations (treatments) are

1, a, b, ab, c, ac, bc, abc.

The "1" represents the treatment with all the factors at their low levels. In each of the remaining treatment combinations, the high level of any factor is denoted by the corresponding letter and the low level by the absence of the corresponding letter.

The effect of changing A when the other two factors are at their low levels is

$$a - 1 \tag{3.6.1}$$

Similarly, the effect of changing A when B is at the high level and C at the low level is

$$ab - b \tag{3.6.2}$$

The effect of changing A when B is low and C is high is

$$ac - c \tag{3.6.3}$$

Finally, the effect of changing A when B and C are both at the high level is

$$abc - bc \tag{3.6.4}$$

The main effect of A for the whole experiment is defined to be the mean of these four effects, namely

$$\frac{1}{4}(a + ab + ac + abc - 1 - b - c - bc) \tag{3.6.5}$$

When C is at the low level, the interaction AB is defined to be one-half the difference between the effects of A at the two levels of B, (3.6.1) and (3.6.2), i.e.

$$\tfrac{1}{2}\,((ab - b) - (a - 1)) \qquad (3.6.6)$$

Similarly for C at the high level, the interaction of AB is

$$\tfrac{1}{2}\,((abc - bc) - (ac - c)) \qquad (3.6.7)$$

Hence the AB interaction for the whole experiment (over both levels of C) is the average of (3.6.6) and (3.6.7)

$$AB = \tfrac{1}{4}\,(ab + 1 + abc + c - b - a - bc - ac) \qquad (3.6.8)$$

The ABC interaction is defined to be one-half the difference between the AB interactions for the two different levels of C,

$$ABC = \tfrac{1}{4}\,(abc - bc - ac + c - ab + b + a - 1) \qquad (3.6.9)$$

Thus if AB is the same for both levels of C, ABC is zero.

For a two-level factorial design at higher levels, the equations for forming the main effects and interactions can be generated systematically by one of two methods: effect matrix (47) and Yates' method (48). The methods for generating the equations are illustrated in Tables E.1 and E.2 in Appendix E.

In a complete factorial experimental design the required number of measurements is often beyond the resources of the investigator, or it gives more precision in the estimates of the effects than necessary, or estimates of high-order interaction effects are of less interest. For example, in a 2^8 complete factorial design, 256 treatment combinations are required and each main factor is an average over 128 combinations of the other factors. In many practical situations, a certain degree of continuity and regularity can be expected with regard to the manner in which the response varies and the higher-order interaction effects involving three or more factors are often negligible. Then design requiring only a definite fraction of a

complete factorial may be used to estimate the main effects and two-factor interaction effects in such a way that only the information on the higher-order interactions is lost.

A fractional factorial experimental design can reduce the required treatments of a 2^k complete factorial design by a factor of 2^{-r}, where r = 1, 2, 3 $\cdots$ and r is less than k. The information on one or more interaction effects is sacrificed in order to split up the whole experimental design to 2^r blocks of treatment combinations. These interaction effects are called the defining contrasts. The block which contains the treatment combination "1" is called the principal block and is normally used for experimental purpose. The other blocks can be obtained from the principal block by multiplying (modulo 2) each of its effects with the defining contrasts selected. Examination of the effect matrix generated for all the treatment combinations (2^k) shows that the estimate of a factor or factor-interaction in a block is identical to that of another factor or factor-interaction from each of the other blocks. These factors or factor-interactions which have identical estimates are called aliases. The effect matrix will also show that the defining contrasts have estimates identical to the general mean, and hence their information is lost. The idea of confounding (confusing) in the fractional factorial experimental design is illustrated by the effect matrix generated for a 1/2-replicate of a 2^3 factorial design in Table E.3 of Appendix E.

The determination of the total effects from the experimental results for the fractional experimental design can be achieved by the effect matrix above or by a modified Yates' technique as demonstrated in the present $1/4 \times 2^7$ fractional

factorial design.

The analysis of variance (ANOVA) is a systemmatic method for making a useful investigation even when there are residual variations. An analysis of variance can be performed on the calculated total effects obtained by the Yates' analysis. The high-order interactions which are assumed to be zero are pooled together to form the residual variation (random error). The statistical F-ratios can then be used to distinguish the significance of the effects at various confidence levels. The detailed procedure of the analysis of variance can be found in Table E.8 for the present study of a 1/4-replicate of a 2^7 factorial experimental design.

The magnitude of the effects in an experimental design can be examined by another statistical method. Daniel (49) proposes the use of the half-normal plot and standardized half-normal plot. This approach removes the question as to which effects can reasonably be assumed to be zero and pooled together into the residual, as required in the ANOVA. The method is discussed in Appendix F.

4. EQUIPMENT DESIGN AND APPARATUS

4.1 Ion-Exchange Column System

4.1.1 General

The detail flow sheet of the ion-exchange column and ancillary equipment is shown in Figure A.6. Every part of the system in contact with the sodium chloride process solution, distilled water or ion-exchange resin is made of stainless steel, PVC or Plexiglas materials. Process solution from the storage tanks (T_1, T_2) is pumped into the bottom stage of the multistage ion-exchange column (C_1). The liquid coming out from the top of the column flows through a cyclone for resin removal before going to the drain. Fresh resin is fed to the top stage of the column and the resin flows through the stages down the column by gravity. Before entering into the exhausted-resin collector (B_1) resin from the last stage of the column can be sampled by the sampler (S).

4.1.2 Ion-exchange column

The 4 inches (10.2 cm) I.D. ion-exchange column is 3 feet and 8.5 inches (1.13 m) high. The material of construction is almost entirely Plexiglas. The column consists of 9 sections as shown in Figure A.7 and are joined together at the flanges by 1/4-inch (6.4 mm) nuts and bolts. Sections 1 to 6 are the stages for fluidized-bed ion-exchange. Section 7 is a calming zone for the liquid feed. Section 8 is the liquid feed stage which has three perforated Plexiglas plates to

improve liquid distribution. The detailed structure of sections 7 and 8, and of the liquid distribution plates, are shown in Figures A.8 and A.9. Section 9 is the last section which connects the exit resin-stream to the exhausted-resin collector (B_1). The resin sampler is built into this section and the detailed design is shown in Figures A.10 and A.11.

The stages (sections 1 to 6) of the column for mass transfer are identical in structure except for section 1 which has a cylindrical trough to direct the liquid effluent into the exit hose as shown in Figure A.6. The detailed structure of section 1 is shown in Figure A.12. Each of these stages has identical tray structures: fluidized-bed support, weir shape and fluid-diode downcomer. In the present study, the performance of three different weir shapes is studied, namely straight, conical and cylindrical shape weirs. The performance of the straight weir is also studied at three different weir lengths. The straight weir type also has four different heights. The designs of these weirs and their corresponding tray-support structures are shown in Figures A.13, A.14, A.15, A.16 and A.17.

The three fluid-diode designs used for the downcomers in the preliminary study are shown in Figure A.5. These fluid-diodes were prepared by Egan (1971). The detailed design of the fluid-diode downcomers used in the present mass-transfer study is shown in Figure A.18 and these downcomers are identical in each section for mass transfer except that of section 6, which is shown in Figure A.19. The last fluid-diode downcomer directs the resin flow into a 3/8-inch (9.5 mm) tygon tubing which leads into the sampling section of the column.

Drain holes and vent holes, each 1/4-inch (6.4 mm) diameter, are present at various points in the column for the removal of resin and of trapped air bubbles respectively. Sampling ports for liquid and solid are also made on the walls of the mass-transfer sections as shown in Figure A.7.

The ion-exchange column set up is slightly modified for the column operability studies under various geometrical combinations on the stage structures. The column is made up of sections 1, 2, 6, 7, 8 and 9 only. The qualitative interactions observed in sections 1, 2 and 6 are representative of the entire column operation. The water effluent from the top of the column is recycled to the feed tanks (T_1, T_2) in the experimental runs.

4.1.3 Liquid feed system

The liquid feed system is included in Figure A.6. The two 45-gallon (170 litre) polyethylene tanks (T_1, T_2), connected in series by a 1 1/2-inch (3.8 cm) hose, are sodium chloride feed-solution storage tanks. The solution is pumped through a rotameter (R_1) and into the ion-exchange column at section 8. The liquid feed-rate can be controlled by the stainless steel needle valves on the recycle and feed lines (V_3, V_4). The mixing line is used for preparing a homogeneous solution before an experimental mass-transfer run is started. The temperature of the feed solution can be maintained above room temperature by passing hot water through the stainless steel coil in the storage tank. The temperature is monitored by the thermostat in the tank and the water flow by the on-off solenoid valve (V_5) on the hot water line. The purpose of heating is to displace dissolved air from the solution so as to prevent

the formation of air bubbles in the ion-exchange column.

Contamination of the feed solution is avoided by the use of a PVC pump head, tygon piping, stainless steel and PVC valves, stainless steel and glass rotameters, and polyethylene storage tanks.

4.1.4 Resin feed system

The system is included in Figure A.6. The resin is fed by volumetric displacement as suggested by Slater (28). Distilled water from the 45-gallon (170 litre) polyethylene storage tank (T_3) is pumped into the 3-gallon (11.4 litre) Pyrex glass resin-feed bottle (B_2) and an equal volume of resin and water is displaced out of the bottle through the resin feed line and into the first section of the ion-exchange column. During start-up, air bubbles trapped in the bottle can be released through the toggle valve (V_8). The distilled water flow entering the bottle can be controlled by the two stainless steel needle valves (V_6 and V_7) and monitored by the low-flow rotameter (R_2). Pump (P_2) is a Masterflex tubing pump. The piping consists of 1/4-inch (6.4 mm) tygon and stainless steel tubings to avoid ionic contamination of the distilled water and hydrogen-form resin. All other materials of construction in contact with the resin or distilled water are inert to our chemical system.

The resin feed system produces negligible resin attrition because no mechanical parts are involved in the physical transport of the resin. A solid screw feeder was originally designed as the solid feed system. However, grinding of the resin between the screw threads and the screw housing was considerable. Increasing the clearance between the screw and its housing reduced the grinding but the sensitivity

of the resin flow-rate to the screw rotation was greatly reduced.

4.1.5 Resin sampling system

The detailed design of the sampler is shown in Figure A.10 and A.11. The sampler's teflon plunger has a cavity for the collection of resin coming down into section 9 of the ion-exchange column. The sample cup is screwed onto the sample collector and can be removed. The oscillatory pump (P_3) pumps distilled water into the sample collector and displaces the air from the sample collector and sample cup through the outlet line. A bypass line is provided to adjust the water flow into the sample collector. The piping is made up of 1/4-inch (6.4 mm) tygon tubing.

4.1.6 Exhausted resin collecting system

The bottom end of the ion-exchange column is connected to a 3-gallon (11.4 litres) Pyrex glass bottle (B_1) by a 1-inch (2.54 cm) tygon tube. The downflow of resin and solution can be cut off by closing the PVC globe valve (V_9). From the neck of the bottom through the rubber stopper is a 1/4-inch (6.4 mm) bleeding line. The water flow-rate through the bleeding line is adjusted by a stainless steel needle valve (V_{10}). The purpose of the bleeding is to maintain a smooth flow of resin down the 3/8-inch (9.5 mm) tygon tube in section 8 and also out of section 9 of the ion-exchange column. When the bleeding of water is at the same volumetric flow-rate as the resin feed-rate, resin will not back up or block the resin exit at the bottom of the column.

4.2 Resin Drying System

The resin drying system is shown in Figure A.20. The Plexiglas column (C_2), 39 inches (99.1 cm) high, has an inner diameter of 2 7/16 inches (6.2 cm). Laboratory air supply is used for drying the resin before size screening. The air passes through a filter before entering the column at the bottom. A 3/8-inch (9.5 mm) tygon tubing connects the filter and the air inlet of the column. The top opening of the column is covered by a 60-mesh screen to prevent the carry-over of resin during the drying process.

4.3 Resin Regenerating and Washing System

The system is shown in Figure A.21. The column (C_3) is 4 feet and 2 inches (1.27 m) high with a 4-inch (10.2 cm) I.D. and the material of construction is Plexiglas. The bottom of the column is connected to a Masterflex tubing pump (P_4) which pumps either acid or distilled water into the column for regeneration or washing of the resin. Near the lower end of the column is an outlet valve (V_{20}) (a stop-cock with a 5-mm bore teflon-plug) for resin removal. Bottle (B_4) is the storage for resin to be transferred into the column. Transfer of resin is by volumetric displacement as for the resin feed system. Distilled water is pumped into the bottle and an equal volume of resin and water is forced out of the bottle and into the column at the top. Air trapped in the bottle during start-up can be released through the vent by opening valve V_{26}.

B_5 and B_6 are 5-gallon (18.9 litre) Pyrex glass bottles. Bottle B_5 is for the storage of recycled hydrochloric acid during the last quarter of the regeneration

cycle. Bottle B_6 is the storage for fresh 10% hydrochloric acid. Outlets of the two bottles can be closed by the 5-mm bore teflon-plug stop-cocks (V_{23}, V_{22}). The two outlets are joined together before going through the Masterflex tubing pump (P_4) and finally into the column at the bottom inlet. The suction of the pump is also connected to the 45-gallon (170 litre) distilled water storage-tank (T_3). During resin regeneration or washing, liquid effluent overflows into the trough around the top end of the column and flows either to drain or into recycle acid bottle (B_5).

5. FRACTIONAL FACTORIAL EXPERIMENTAL DESIGN

Seven operational and geometrical parameters for the continuous countercurrent ion-exchange column were chosen as the factors for the factorial experimental design. The response is the overall stage efficiency. The factors chosen are

(i) resin flow-rate,

(ii) solution flow-rate,

(iii) resin particle size,

(iv) weir length,

(v) weir height,

(vi) fluid-diode lateral displacement, and

(vii) downcomer clearance.

These factors showed significant effects (at least visually) on the operational behaviour of the column, including the efficiency of solid-liquid contact. Although the solid and liquid flow-rates were shown to be significant by Egan (7) and Cha (8), these two factors were included in the experimental design to reveal any possible interactions among themselves and the other five main factors. The initial sodium chloride concentration was not included, since the emphasis desired was on geometrical and physical factors.

A level of two for the experimental design was chosen. Hence a complete factorial design of seven factors at two levels required a total of 128 experiments. Experience showed that only two experimental runs at most could be performed in

one day. Thus a complete factorial design was considered not practical for this investigation and a quarter-replicate selected. This required only 32 experimental runs.

A quarter-replicate of a complete factorial design causes every effect to be confounded with three other effects. The three defining contrasts which divide the complete design into four blocks were carefully chosen such that the main effects and 2-factor interactions were not confounded with each other. All possible combinations of defining contrasts were tried and those which produced the least undesirable confounding were selected. Table E.4 is a list of all the possible defining contrasts. The system of defining contrasts that seemed to suit best for the present study was ABCDE, ABCFG and DEFG. The effects of the complete factorial design are split up into four blocks by these three defining contrasts. The principal block is generated by the modulo equations

$$x_1 + x_2 + x_3 + x_4 + x_5 = 0 \pmod 2 \qquad (5.0.1)$$

$$x_1 + x_2 + x_3 + x_6 + x_7 = 0 \pmod 2 \qquad (5.0.2)$$

The principal block generated is shown in Table E.5a. The other three blocks and their corresponding pair of modulo equations are shown in Table E.5b. The four alias groups are shown in Table E.6. The four effects in each row are confounded with each other due to the blocking. The three defining contrasts (ABCDE, ABCFG and DEFG) are confounded with the general mean, I, hence their information is lost. The loss of information about interactions with more than two factors is of no concern

because interactions involving more than two factors are often negligible, and hence can be assumed to be zero. All main factors, and fifteen of the twenty-one 2-factor interactions, are confounded with interactions of second order or higher. Three pairs of 2-factor interactions are confounded with each other as indicated in Table E.6. The pattern of confounding for the 2-factor interactions is shown in Figure E.1. In order to overcome undesirable confounding of the 2-factor interactions, the factors (solid flow, liquid flow, etc.) were assigned to the letter (A, B, C, etc.) in such a way that one of the 2-factor interactions in each of these three pairs was very likely to be zero. Thus, the assignment of factors to the letters are as follows

A = resin flow-rate

B = solution flow-rate

C = resin particle size

D = weir height

E = fluid-diode lateral displacement

F = downcomer clearance

G = weir length

Referring to the 2-factor confounding pattern, it can be seen that DG (interaction between weir height and weir length) which might be significant is confounded with EF (interaction between fluid-diode lateral displacement and downcomer clearance) which is very likely to be negligible in terms of its effect on the overall stage efficiency of the ion-exchange column.

In normal practice, treatment combinations in the principal block are chosen for experimental work. Experiments of different treatment combinations of an experimental design should be carried out randomly. However, in order to save time and labour, treatment combinations of the principal block were performed in the order shown in Table E.7. Each day two experimental runs were performed. These two runs involved the same internal stage structures in the multistage column, hence the column was dismantled after every two runs rather than after every run. The two experimental runs in each day used a resin particle size different from the day before because the exhausted resin required one day's time for regeneration and washing before it could be used again. It is claimed that such practical planning is not against the principle of randomization in statistical experimental designs.

6. EXPERIMENTAL PROCEDURE

6.1 Analytical Techniques

6.1.1 Displacement of hydrogen ions from resin by sodium chloride solution

3 ml (bulk volume) samples of hydrogen-form resin (-30 +35 mesh) were equilibrated with 100 ml of sodium chloride solution of concentrations = 0.25, 0.5, 1.0, 2.0 and 4.0 N. Interparticle water content in the bulk volume of measured resin was removed by suction in a Büchner funnel before the resin was added to the sodium chloride solution. The calomel and glass electrodes connected to the Orion digital meter were used to follow the change in pH value of the resin and sodium chloride solution mixture which was agitated by a magnetic stirrer. The change of pH value, i.e. hydrogen ion liberated, as a function of time is shown in Figure B.1.

It can be seen that equilibrium was obtained in 2.5 to 4.0 minutes. The more concentrated sodium chloride solution required less time for equilibrium to be reached. Hence five minutes of mixing were enough before the mixture could be titrated for the determination of resin capacity.

Figure B.2 shows that the hydrogen ion liberated increases with the initial sodium ion concentration.

6.1.2 Concentration of sodium chloride solution for resin sample titration

A measured bulk sample volume of -30 +35 mesh hydrogen-form resin was mixed with a given volume of sodium chloride solution of various concentrations,

and the change in pH value of the solution mixture during the titration with 0.1 N sodium hydroxide solution was followed using the calomel and glass electrodes connected to the Orion digital pH/mV meter. The plotting of the pH value as a function of the volume of titrant added yields the titration curve. The end point of titration is at the point of inflexion. Figure B.3 shows the titration curves for 5 ml (bulk volume) of resin mixed with 100 ml of sodium chloride solutions of concentrations 0.25, 0.10 and 3.0 N. Figure B.4 shows the titration curves for 3 ml of resin in 100 ml of 4.0 and 5.0 N sodium chloride solution. These experimental results indicate that the titration end point is independent of the concentration of sodium chloride solution used. 4.0 N sodium chloride solution was chosen to treat resin samples in the analysis of resin capacities.

6.1.3 Determination of resin capacity

The capacity of resin can be obtained from the end-point of a titration curve as shown in Section 6.1.2. A faster way to obtain the resin capacity is by the Fisher Automatic Titrimeter. About 3.0 ml of resin was transformed with a 10 ml pipet into a 10 ml measuring cylinder. The packed bed volume was recorded. The resin was then rinsed with distilled water in a Büchner funnel, and interparticle moisture content removed by suction. After the addition of the resin to 100 ml of 4.0 N sodium chloride solution in a 250 ml beaker, the beaker was placed on a Flexa-Mix and the mixture agitated by a magnetic stirrer for about five minutes. The mixture was then titrated with 0.1 N sodium hydroxide solution prepared from concentrated volumetric solution. The change in pH value was followed by the

calomel/glass electrodes connected to the calibrated automatic titrimeter. The titrimeter automatically stopped the titrant flow when the end point was reached. The resin capacity in meq/ml wet volume was then calculated as

$$\text{resin capacity} = \frac{V_{NaOH}\, N_{NaOH}}{V_{Resin}\,(1-\epsilon)} \qquad (5.1.3.1)$$

The accuracy of the analytical results using the Fisher Automatic Titrimeter and the Orion pH/mV digital meter were compatible as had been confirmed experimentally. In fact, the main source of error in the resin capacity analysis is in the measurement of resin sample volume and in reading the titrant volume. The accuracy can be improved by measuring the resin sample on a weight basis. However, the drying of resin sample in an oven is time consuming and this slight gain in accuracy is likely to be masked by the random errors in other parts of the mass-transfer experiment.

6.1.4 Determination of chloride concentration in solution

Chloride concentration in a sample solution was measured directly by the Orion digital pH/mV meter with chloride specific ion and double junction reference electrodes. A relative mV reading was obtained from the digital meter, and the chloride concentration read from the calibration curve prepared with standard sodium chloride solutions. Before a series of measurements, the Orion meter was re-calibrated against the existing calibration curve with a standard solution.

It was later discovered that the mV measurement by the electrodes was a function of the acidity of the soluion. Figures B.5 and B.6 show the change in

mV reading with changing hydrogen-ion concentration and pH values respectively. Each data point was obtained by pipetting 100 ml of acid solution of the desired hydrogen-ion concentration into a weighed sample of sodium chloride (10.35 gm for a 0.06 N solution) and the relative mV reading was taken after thorough mixing. Sulphuric acid and nitric acid solutions were used to prepare the solutions. Results showed that the relative mV measurements were independent of the sulphate and nitrate anions. Figure B.6 shows that the relative mV reading is constant from a pH value of 3.5 to at least 7.0. Hence the chloride concentrations in solutions with pH values between 3.5 and 7.0 can still be correctly estimated by direct measurement using the Orion digital pH/mV meter calibrated against a standard sodium chloride solution having a pH value in the same range.

6.1.5 Determination of hydrogen-ion concentration in solution

The pH value of an aqueous solution was determined by direct measurement with the Orion digital pH/mV meter using calomel and glass electrodes. The meter was calibrated against buffer solutions of pH values 7.0 and 4.0 with adjustment for solution temperature different from 25°C.

It was experimentally confirmed that the pH value measurement by the calomel and glass electrodes was independent of the sodium and chloride ion concentrations in the solution.

6.1.6 Determination of packed resin bed voidage

The voidages of packed resin beds were found experimentally. The result for all particle-size distributions (-20+30, -30+35 and -35+50 mesh) is 0.33. About

10 ml of resin with interparticle moisture removed by suction were added to about 15 ml of distilled water in a measuring cylinder. The measuring cylinder was vibrated until the volume of the packed resin bed became constant and the volume was recorded. The actual volume of resin added was obtained by the difference between the volumes indicated by the first and second water levels in the measuring cylinder. With the resin bulk volume and actual volume, the resin voidage can be calculated.

6.2 Calibrations

The necessary calibration curves were obtained as discussed below.

6.2.1 Process solution feed rotameter

The calibration curve of the volumetric flow of liquid against the rotameter reading is shown in Figure B.7. The calibration was performed with tap water at room temperature.

6.2.2 Resin feed rotameter

The volumetric calibration curve of the resin feed rotameter is shown in Figure B.8. Water was used for the calibration.

6.2.3 Variable speed Masterflex tubing pump

The calibration of water volume-flow against the pump-controller's speed setting is shown in Figure B.9. The calibration was only a guide to the approximate pumping rate. The liquid flow-rate changed with the aging of the 1/4-inch (6.4 mm) tygon tubing in the pump head, and it also depended on the liquid-head

pressure.

6.2.4 Resin feed

The calibration curves of the resin volume flow-rate versus the resin-feed rotameter reading for the three different resin particle-size distributions (-20+30, -30+35 and -35+50 mesh) are shown in Figure B.10. The actual resin volume-flow was considered in the calibration curves. The volume flow of resin at each rotameter reading is higher for smaller particles, i.e. fraction of water in the resin feed is less. Figure B.11 shows the change in the volume fraction of the resin in the total flow as a function of the rotameter reading. The curves indicate that at high total flow-rates the volume fraction of resin in the feed becomes constant.

6.2.5 Water in resin feed

The calibration curves of water flow in the resin feed for the three different resin particle-size distributions are shown in Figure B.12. For the same total volume-flow (water and resin) the volume fraction of water is higher in the resin feed of larger particle-size distribution.

6.2.6 Chloride-ion concentration

The calibration of chloride-ion concentration versus the electrode potential reading (mV) of the Orion digital pH/mV meter with chloride specific ion and double junction reference electrodes is shown in Figure B.13. Sodium chloride solutions of concentrations 0.1, 0.08, 0.06, 0.04 and 0.02 N were prepared with distilled water. The electrode potentials were then measured with the digital meter.

The logarithmic value of the chloride-ion concentration was plotted against the corresponding mV reading as shown. Subsequent measurement of chloride-ion concentration was obtained by reference to the calibration curve, justified only for solutions having a pH value between 3.5 and 7.0.

6.3 Resin Drying

The resin drying column is shown in Figure A.20. About I litre of resin was poured into the column at the top and then air was turned on at a moderate flow-rate to dry the resin. Each batch of resin required about twenty hours to become free flowing. The free flowing resin was removed at the bottom outlet after disconnecting the air hose.

6.4 Resin Size Screening

The Dowex-50W-x8 hydrogen-form resin had a wet size-distribution of -20+50 mesh. Batches of 500 ml air-dried resin was placed on a column of sieves with 20, 30, 35 and 50 mesh screens and was vibrated by an electric sieve-shaker. Each batch of resin required about three hours for a reasonable separation into size-distributions: -20+30, -30+35 and -35+50 mesh.

After screening the resin was re-hydrated with concentrated hydrochloric acid as a precaution against resin-cracking during hydration. The resin and acid mixture was then diluted gradually with distilled water so that the resin could swell slowly without cracking up.

6.5 Resin Regeneration

Figure B.14 shows the change in resin capacity during regeneration by 10% (by weight) hydrochloric acid. The resin bed was about 40 inches (1.0 m) deep. This regeneration represented the elution by three bottles of 6 lb. hydrochloric acid (37%) diluted to 10%. The acid flow-rate was 10.0 ml/sec. The elution curve indicates that 12 lb. of concentrated acid can adequately regenerate the column of resin completely when a lower elution flow-rate is used. As a precaution, 2.5 gallons (9.5 litre) of spent acid at the end of one regeneration run were used before the 5 gallons (18.9 litre) of fresh 10% acid.

The resin-regeneration system is shown in Figure A.21. Distilled water was pumped into the exhausted-resin bottle (B_4), at an initial rate of about 4.0 ml/sec and gradually increased to 10.0 ml/sec when a smooth resin flow was obtained from the bottle, through the 1/4-inch (6.4 mm) tubing and into the regeneration column. While the column was being filled, a slow flow of distilled water was pumped through the column to keep the resin bed loose for the regeneration acid flow later. When all the resin was transferred to the column, the pump (P_2) was turned off and the pressure in the bottle released. Recycled acid in bottle B_5 was pumped through the column of resin at about 4.0 ml/sec. Then the 5 gallons (18.9 litre) of fresh 10% hydrochloric acid was pumped through the resin at the same flow rate. When approximately 2.5 gallons (9.5 litre) of fresh acid was left in bottle B_6, the liquid effluent from the regeneration column was switched over from the drain to the recycle-acid bottle. The 2.5 gallons (9.5 litre) of acid collected was used for the next regeneration run.

During the regeneration cycle, the acid feed was occasionally increased to about 11.0 ml/sec to mix the resin bed in order to obtain a homogeneous regeneration.

6.6 Resin Washing

Resin washing was performed in the regeneration column as shown in Figure A.21.

A resin bed, 40 inches (1.0 m) deep, required a wash time in the order of 12 hours at a distilled water flow-rate of 10 ml/sec as shown in Figure B.15. About two hours were required to wash out the acid in the bed void and then ten hours to remove the acid inside the resin particles. An increase in water flow satisfactorily reduced the time of displacing the acid from the bed void but did not help much in reducing the washing time in the diffusion stage.

During the washing cycle, the acid bottles were isolated by closing valves V_{22} and V_{23}. Then valve V_{21} was opened and distilled water in the storage tank (T_3) was pumped through the bed of resin. Washing was stopped when the liquid effluent had a pH value of about 5.2

To obtain an effluent pH value of 7.0 was not found possible. This may be due to the fact that Dowex-50W-x8 ion-exchange resin is strongly acidic and whose dissociation thus causes the wash effluent to remain slightly acidic.

6.7 Factors' Levels for the Fractional Factorial Experimental Design

The two levels for each factor (dimensions of geometrical structures on each tray and the resin particle-size distribution) for the fractional factorial experimental

design are listed below

resin particle size: -20+30, and -35+50 mesh

weir length: 3.380 and 3.970 inches (8.59 and 10.08 cm)

weir height: 1.0 and 2.0 inches (2.54 and 5.08 cm)

fluid-diode lateral displacement: 1/20 and 3/20 inche (1.27 and 3.81 mm)

downcomer clearance: 1.0 and 1.50 inches (2.54 and 3.81 cm).

The two levels for the solid and liquid flows had to be chosen such that the continuous countercurrent ion-exchange column was operable under the various treatment combinations.

To observe the operability of the column under various treatment combinations, the modified ion-exchange column system, discussed in Section 4.1.2, was used. Observations of the solid and liquid interaction in Sections 1, 2 and 6 were enough for the present study.

It was believed that the downcomer clearance would not affect the solid-liquid interaction extensively. Hence, the present study used only one level of downcomer clearance, 1.0 inch (2.54 cm), so as to reduce the number of experimental runs by one-half.

Various combinations of the two levels of the factors (weir height, weir length and fluid-diode lateral displacement) were installed on the trays of the column. For each structural combination, the ion-exchange column operation was started as discussed in Section 6.9, with distilled water as the feed liquid. The "perfectly" operable ranges of liquid flow-rate were observed at resin flow-rates of 0.6 and

2.25 ml/sec. The column is considered "perfectly" operable when the resin bed is evenly fluidized and the resin flow through the downcomer is not cyclic. These observations were made for both resin particle-size distributions (-20+30 and -35+50 mesh), and the results are tabulated in Tables B.1 and B.2. The operable ranges of the liquid flow-rates for the two tabulations are clearly displayed in Figure B.17. An extremely narrow range of liquid flow-rate around 53.0 ml/sec is operable for all the treatment combinations with the resin flow-rates at either 0.6 or 2.25 ml/sec.

A study of Figure B.17 shows that the operable range of liquid flow can be increased by trying to reduce the lower limit of operability of the runs with large resin size-distribution (-20+30 mesh) and to raise the upper limit of operability of the runs with small resin size-distribution (-35+50 mesh).

The upper limit of operable liquid flow-rate for the runs with the small size resin can be raised by using resin of -30+50 mesh size-distribution instead. A decrease in solid feed-rate also helps. Hence overfluidization for operations with the low size-level of resin will occur only at a higher liquid flow-rate. The decrease in resin flow-rate also reduces the lower limit of the liquid flow-rate below which flooding of downcomer will occur. Hence for the two level experimental design the levels of particles size were chosen at -20+30 and -30+35 mesh and solid flow-rates at 0.84 and 1.6 ml/sec. The operable range of liquid flow-rate was broadened and its levels for the experimental design were chosen to be 40.0 and 79.2 ml/sec. The difference between these two levels of liquid flow-rate was sufficient for the factorial experimental design.

6.8 Operational Performance of the Ion-Exchange Column

The equipment set up for the operational performance study was similar to that for Section 6.7. Various weir shapes (straight, cylindrical and conical), weir heights and fluid-diode lateral displacements were installed in the three sections (1, 2 and 6) of the ion-exchange column. The column was started as discussed in Section 6.9, but distilled water was used as the feed liquid. At a given resin flow-rate, the operational behaviour in terms of fluidization, flooding and the continuity of resin downflow in each stage was noted as the liquid flow-rate was gradually decreased such that the resin bed changed from the state of over-fluidization to the state of flooding of the feed stage through sluggish resin movement. Near incipient fluidization, the column operation became unstable and a quick decrease in liquid flow would cause premature flooding of the feed stage.

6.9 Mass-Transfer Experiment

The mass-transfer experiment to determine the overall stage efficiency of a particular column operation was performed by the equipment as shown in Figure A.6.

A weighed quantity of sodium chloride was added to the two storage tanks (T_1, T_2) of distilled water. Valves V_1 and V_2 were opened while V_3 and V_4 were closed. The solution was then mixed by pumping in a closed loop. After two hours of mixing, the chloride concentration in the two tanks was measured with the Orion digital pH/mV meter using the chloride specific ion and double junction reference electrodes. Extra sodium chloride was added when required. Four or five hours of mixing were normally required before the 90 gallons (340 litre) of sodium chloride

solution became homogeneous.

The temperature of the feed solution was raised above room temperature by the heating coil so as to liberate some of the dissolved air. The thermostat was set at the desired temperature, and the on-off control was turned on. The hot water coil raised the solution in the tanks to the desired temperature, and maintained it at the set temperature. The heating ensured the avoidance of air bubbles being liberated when the solution was rising through the column. Bubbles trapped under the screen of each stage would have affected the liquid distribution.

During start-up all the 1/4-inch (6.4 mm) drain holes and vent holes except V_{16} were closed by spring clamps on the connecting 1/4-inch (6.4 mm) tygon tubing. Valve V_2 was closed and valves V_3 and V_4 opened, and feed solution was pumped into the column at about 3.0 ml/sec. A slow liquid flow was needed to avoid trapping air bubbles under the liquid distributors and screens. When the column was filled to section 6, the solution overflowed into the downcomer area and into section 9. Valves V_9 and V_{10} were opened so that the resin bottle (B_1) was also filled. When the bottle was filled, valve V_{10} was closed. When section 9 was filled, valve V_{16} was closed. While section 9 was being filled, the cavity at the end of the sampler's plunger was turned upward so that air bubbles would not be trapped in the cavity. Gradually the entire column was filled and the solution overflowed into the trough and to the cyclone. Since there was no air vent in the resin collector, B_3, the cyclone and the bottle were disconnected to release the air while the bottle was being filled. Then solution feed to the column was shut off until the resin-feed system was ready. Valve V_4 was closed and valve V_3 opened

to recycle the feed solution.

The resin-feed system was started up by opening valves V_6, V_7, V_8 and V_{12} while closing valves V_{11}, V_{13} and V_{14}. The Masterflex tubing pump, P_2, was activated and distilled water was pumped from storage tank, T_3, to the resin-feed bottle (B_2). When all the air was displaced through the air vent, valve V_8 was closed and valve V_{11} was opened. The resin feed-rate to the column was then adjusted by the needle valves V_6 and V_7.

Before the sampler could be used, the sample collector was filled with distilled water by activating pump P_3. When all the air was displaced and the pump was turned off, valves V_{17}, V_{18} and V_{19} were closed. This procedure prevented the introduction of air into section 9 of the column during sampling.

The mass-transfer experiment was then ready to be started. The desired resin and process solution feed-rates were set and the continuous countercurrent operation usually would start automatically. When a run involved a low liquid-flow (e.g. 40 ml/sec) and a high solid-feed (e.g. 1.6 ml/sec) flooding of the feed stage would occur during start-up. Hence a higher liquid flow-rate had to be used and gradually reduced to the desired flow after a continuous and smooth resin flow was obtained down the whole column.

When steady state was reached, four 100 ml samples of process feed solution were taken at the recycle outlet. Four samples of liquid effluent were collected at the outlet of the cyclone. The assurance of steady state could be obtained by checking the pH value of the liquid effluent from the column. Figure B.16 shows the change in pH value of the liquid effluent for a typical run. Steady state was

obtained in about 10 minutes from start-up. Resin effluent was sampled at section 9. Resin was drawn into the sample collector for two or three times. The plunger was moved slowly to avoid disturbances to the resin downflow. The sampler cup was unscrewed and resin transferred to 1000 ml of distilled water. The resin sample was washed, by two litres of distilled water in a Büchner funnel. The sample was then stored in 200 ml of distilled water. About 20 ml of resin from the feed bottle was also collected at the feed line for the analysis of initial resin capacity. Each fresh and exhausted resin sample was enough for four chemical analyses.

7. DATA REDUCTION

7.1 Mass-Transfer Experiment

For each mass-transfer experimental run, the results from the chemical analyses were used to evaluate the mass-transfer performance of the ion-exchange operation. A computer program was written in Fortran IV to perform the computation. The program was processed by the CDC 6400 Computer at McMaster University.

The overall stage efficiency, the volumetric efficiency as well as other experimental conditions and results were calculated. Mass balances on hydrogen ion and chloride bases were checked. The second half of the computer program programmed the Benson-Lehner plotter to plot the equilibrium diagram for each experimental run. The equilibrium diagram showed the analysis operating line and also the flow operating line if the difference between the slopes of the two operating lines was greater than the tolerance set in the computer program. The stepping off of the theoretical stages was included.

The general flow chart of the computer program is shown in Figure G.1. A sample computer output and the program listing are shown in Appendix G.

7.2 Fractional Factorial Experimental Design

A general computer program was written in Fortran IV to perform the analysis

of variance for fractional factorial experimental designs. The program was divided into three functional parts. The pass number in the data deck controlled the section of the program to be used. The following results were obtained in the computer output when appropriate pass number and data were supplied in the data deck

Pass 1: Yates' Analysis, and absolute average effects listed in ascending order

Pass 2: Those of Pass 1 and standardized absolute average effects listed in ascending order

Pass 3: Those of Pass 2 and analysis of variance table.

The general flow chart of the computer program is shown in Figure H.1. A sample computer output and the computer program listing are shown in Appendix H.

8. RESULTS AND DISCUSSION

8.1 Fluid Diodes as Downcomers

8.1.1 Effects of the fluid-diode designs on resin flow

The three fluid-diode shapes shown in Figure A.5 were installed as separate downcomers in the multistage ion-exchange column. The qualitative operational effects of the three different fluid-diode shapes (A, B and C) on the resin flow were observed. The comparisons were performed at zero fluid-diode lateral displacement for the downcomer in each stage and with the 3.78-inch (9.6 cm) straight weirs. In the present study the fluid-diode lateral displacement was defined as the distance between the cusp end points of the two opposing fluidic elements when observed lengthwise.

A qualitative comparison shows that fluid-diode types A and B give less resistance to resin flow than type C and hence resin flows faster through these downcomers. The smaller resistance to resin flow enables a column to handle a higher resin feed-rate before the flooding of the feed stage occurs.

However, at a low resin flow-rate, operations with these fluid-diode shapes (A and B) are more susceptible to cyclic flow of resin, i.e. alternating solid-flow down and liquid-bypass up the downcomers. This is because the resin goes down the downcomer so fast that there is not enough resin to maintain an equilibrium resin-head in the downcomer area against the upward flow of liquid. Hence liquid bypasses up the downcomer. The resin then accumulates in the downcomer area to

such a height that the resin downflow can be initiated again.

The downcomers with fluid-diode shape C offer higher resistance to the liquid flow and hence require a lower solid-head to initiate resin flow and also a lower equilibrium resin-head to maintain a continuous downflow of resin. A higher resistance to resin flow in the downcomer also means a slower response of the column to any change in resin or liquid flows in re-establishing steady state operation.

A comparison between types A and B also indicates that the extended cusp ends of the former offer higher resistance to liquid flow and hence require a lower resin-head to initiate resin flow and to maintain a continuous downflow of resin.

Downcomers of different fluid-diode shapes have different ranges of operability in terms of the resin and liquid flow-rates. A change in liquid flow-rate changes the voidage of the fluidized bed, the pressure-drop across the fluidized bed and hence the pressure drop across the fluid-diode downcomer. The operable range of the column would be smaller if the fluid-diode downcomers installed in the column are more pressure sensitive.

8.1.2 Effects of fluid-diode lateral displacement on resin flow

Experimental runs were performed with the 3.78-inch (9.6 cm) straight weirs and using type B fluid-diode downcomer. The fluid-diode lateral displacement was varied between $^{1}/_{32}$ and $^{3}/_{32}$ inch (0.79 and 2.38 mm).

For a given liquid flow-rate, a decrease in fluid-diode lateral displacement reduces the resin-head required to initiate the downflow of resin in the downcomer, and also the equilibrium resin-head required to maintain a continuous flow of resin.

A larger fluid-diode lateral displacement such as $^3/_{32}$ inch (2.38 mm) not only increases the resin-head requirement but also causes cyclic flow of resin from stage to stage. Increasing the resin feed-rate will reduce the frequency of intermittent resin flow until the maximum solid handling capacity is reached.

The effect of fluid-diode lateral displacement on the resin flow can be qualitatively explained by considering the balance of forces acting on the bulk of resin in and immediately above the downcomer. When the resin flow in the fluid-diode is fully developed, the forces acting on the resin are the weight of the solid resin (mg), the buoyancy force (f_b), pressure force across the fluid-diode downcomer ($(p_2-p_1)A$), and the fluid-diode's force of resistance to the downward flow of resin (R_1). Hence,

$$F = mg - f_b - ((p_2-p_1)A) - R_1 \qquad (8.1.2.1)$$

where p_1 and p_2 are the hydraulic pressures at the entrance and exit of the fluid-diode downcomer respectively, and A is the area of the openings at the ends of the downcomer. An increase in fluid-diode lateral displacement increases the hydraulic pressure force ($(p_2-p_1)A$) across the fluid-diode downcomer but decreases the fluid-diode's resistance (R_1) to resin flow. Apparently, the increase in pressure force is higher than the reduction in fluid-diode resistance and hence, as observed, a higher resin-head (mg) is required to maintain a continuous resin flow.

Similarly, a force balance can be written at the moment of impending resin downflow

$$(mg - f_b) = (p_2-p_1)A - R_2 \qquad (8.1.2.2)$$

where R_2 is the fluid-diode's force of resistance to the bypassing flow of liquid and mg the resin-head required to initiate resin flow. An increase in fluid-diode lateral displace-

ment increases the pressure force but reduces R_2, resulting in a higher resin-head for the initiation of resin flow.

8.2 Operational Performance of the Ion-Exchange Column

8.2.1 Effects of resin and liquid flow-rates

Figure C.1 shows the performance of the column under various combinations of resin and liquid flow-rates. Each stage has a straight weir and the dimensions of the stage structures are included in the diagram.

The performance diagram can be divided into six regions. In all the regions, except the one to the left of the dotted line and labelled "liquid bypassing", resin flows through the downcomers are continuous and the rates are constant, at least visually. At the centre is the region of "perfect" operation. In this region the resin bed in each stage is fluidized completely and smoothly (i.e. homogeneous). In the fluidization area the height of the fluidized resin-bed is slightly higher than the weir height and the resin in the fluidization area overflows smoothly into the downcomer area. In this region above (labelled "over-fluidization of fines"), the resin particles experience a high superficial liquid velocity. The terminal velocity is reached for the smaller resin particles at one end of the size distribution and also for the cracked resin pieces. The fine particles float above the fluidized bed and even stay on the lower surface of the screen above. In this region, the column is perfectly operable. A further increase in liquid superficial velocity over-fluidizes the majority of the resin particles. The fluidized-bed height becomes equal to the stage spacing and flooding occurs. The boundaries, AB and CD, curve down as the resin flow-rate is increased since, at the high resin flow-rates, the fluidized

bed is churned up by the strong transverse flow of resin. The momentum transfer causes the resin bed to become over-fluidized at a lower superficial liquid velocity.

When the superficial liquid velocity is lowered below the region of "perfect" operation, the resin bed in each stage becomes partly fluidized due to channeling. Further reduction in liquid flow-rate causes sluggish resin movement across the fluidization area and also down the fluid-diode downcomer which has become filled with resin by then. Finally the feed stage is flooded because the resin feed-rate is higher than the flow-rate of resin down the column. The boundary for flooding (EF) goes up as the resin feed-rate is increased, because the higher the resin feed-rate the sooner the resin downflow fails to cope with the input feed.

Cyclic flow of resin in the fluid-diode downcomers occurs left of the dotted line. The resin flow is still continuous and some liquid-bypassing is obvious. For a given resin feed-rate (e.g. 0.4 ml/sec), liquid-bypassing occurs at some intermediate range of superficial liquid velocity (0.7 to 1.6 cm/sec). This must be the region that the fluid-diode downcomer experiences the highest pressure drop, as the superficial velocity is increased the fluidized-bed's voidage increases and hence the resin hold-up decreases, resulting in a decrease in the pressure drop across the fluidized bed. Near the incipient fluidization velocity channeling occurs in the resin bed, causing a decrease in the pressure drop across the bed. Channeling frequently occurs at incipient fluidization when screens are used as liquid distributors (50). Liquid-bypassing does not occur at higher resin flow-rates because the plentiful supply of resin is sufficient to maintain an equilibrium resin-head in the downcomer area to counteract the unfavourably high pressure drop.

8.2.2 Effects of resin particle-size distribution

The performance of the ion-exchange column with the same stage set-up as discussed in Section 8.2.1, but operated with -20+30 mesh resin, is shown in Figure C.2. The basic performance pattern is the same as in Figure C.1.

The region for over-fluidization is missing because the terminal velocity of these larger resin particles is higher. The large particle-size and hence the reluctance to mobilize increases the areas of the partial mobilization and flooding regions. The larger particle-size distribution also gives a smaller fluidized-bed voidage and a larger resin holdup resulting in a higher pressure drop across the resin bed. The increase in pressure drop is the reason for the larger region of liquid-bypassing in the performance diagram.

8.2.3 Effects of fluid-diode lateral displacement

The performance diagram for the column operation in Section 8.2.1 with the fluid-diode lateral displacement increased to 3/20 inch (3.81 mm) is shown in Figure C.3. The result is an increase in the regime of liquid-bypassing up the downcomers and can be explained by the same principles discussed in Section 8.1.2. The region of partial mobilization is extended to the right and its boundary meets the flooding line at a higher resin feed-rate. The increase in fluid-diode lateral displacement lowers the fluid-diode resistance to resin flow. Hence the resin flow in the downcomer is less sluggish even at a low superficial liquid velocity and the column can cope with a higher resin flow-rate before the flooding of feed stage takes place.

8.2.4 Effects of weir height

The performance diagram of the column operation of Section 8.2.1 but with 1-inch (2.54 cm) height for the weirs is shown in Figure C.4. The basic pattern is the same as in Figure C.1. This shallower fluidized-bed means a lower pressure-drop across the tray and hence no apparent liquid-bypassing in the downcomer. The region of partial mobilization is more dominant due to the poor liquid distribution in a shallow bed and hence serious channeling. A lower weir height also means a shorter downcomer seal. Hence the resin flow out of the downcomer is less restricted and flooding becomes independent of the resin feed-rate. Flooding of the feed stage occurs at a very low superficial velocity which is close to the minimum fluidization velocity.

Figure C.5 shows the performance diagram of the column when the fluid-diode lateral displacement is also changed. The fluid-diode lateral displacement is increased to 3/20 inch (3.81 mm). The performance diagram is the same as that in Figure C.4 except for the extra region of intermittent resin flow (in the downcomers). The intermittent resin flow is partly due to liquid-bypassing, and partly due to some stagnant resin particles, blocking the downcomer's exit.

8.2.5 Effects of conical weir

The performance of the column with conical weirs of diameters 1.28 inches (3.25 cm) and heights 2 inches (5.08 cm) is shown in Figure C.6. The other structural parameters of the tray are as shown in the diagram.

The performance diagram can be divided into six regions similar to those for

straight weir operations. However, the area of the region for "perfect" column operation is reduced due to excessive fluidization at a lower, and partial mobilization at a higher, superficial liquid velocity. The lowering of the upper boundary may be caused by the interaction between the diverging shape of the conical weir and the upward liquid flow. The liquid going up the side of the conical weir deflects resin particles away from the downcomer area. Hence flooding (i.e. fluidized-bed height equals stage spacing) occurs at a slightly lower superficial liquid velocity when compared to the operation with straight weirs. The interaction between the conical weir and the inside column wall may also have caused the occurrence of partial mobilization of the resin bed at a higher superficial liquid velocity. The conical weir is situated near the column wall as shown in Figure A.16. The transverse flow of resin from the downcomer side to the weir side of the tray results in some stagnant resin areas on the sides of the weir away from the downcomer (areas labelled "A" in Figure A.16). These stagnant resin areas become dominant as the superficial liquid velocity is lowered.

The patterns of liquid-bypassing and the flooding of the feed stage are similar to column operations with straight weirs.

Figure C.7 is the performance diagram of the column with a conical weir of smaller diameter, 1.03 inches (2.62 cm), but of the same weir height. Figures C.6 and C.7 are similar. The upper limit of superficial liquid velocity for "perfect" operation is about the same for both sizes of conical weirs. The larger area of partial mobilization for the operation with smaller conical weir may be due to larger stagnant areas at the weir and due to the lower effective fluidization super-

ficial velocity experienced by the resin as can be understood from the difference in steepness of the side walls of the two sizes of conical weirs.

The effects of resin particle size, fluid-diode lateral displacement and weir height on the performance of the column operating with conical weirs are shown in Figures C.8, C.9, C.10 and C.11 in Appendix C. The performance patterns of these operations can be explained as in the corresponding straight weir operations. The regions of liquid-bypassing for the conical weir operations occur at a lower resin feed-rate than those for the straight weir operations. This is certainly due to the elimination of dead downcomer areas inside the conical weirs. Hence the solid head of resin can be more efficiently maintained by the fluidized resin particles overflowing over the weir and into the downcomers.

8.2.6 Effects of cylindrical weir

The performance diagram of the column operation with cylindrical weirs is shown in Figure C.12. The basic pattern of the performance is similar to that for straight and conical weir operations. The upper boundary of "perfect" operation is slightly higher than that for the corresponding conical weir operation. This is due to the smoother pattern of liquid-flow around the vertical outside wall of the cylindrical weir. The existence of large dead resin area between the cylindrical weir and the inside column wall (areas labelled "A" in Figure A.17) is the reason for the large region of partial mobilization at lower superficial liquid velocity.

The inner sloping wall of the cylindrical weir eliminates dead downcomer areas and hence liquid-bypassing occurs only at a very low resin flow-rate.

Figure C.13 is the performance diagram for the column operation with the cylindrical weirs using -20+30 mesh resin.

8.3 Fractional Factorial Experimental Design

The 32 treatment combinations were performed for the 1/4-replicate factorial experimental design for 7 factors at 2 levels. The experimental runs which had mass-balance discrepancies in hydrogen ion greater than 6.5% or an initial sodium ion concentration deviation greater than 0.0035 N were repeated. A positive mass-balance discrepancy was likely due to errors in the sampling of resin and liquid effluents before the steady state was reached. The level of the initial sodium ion concentration in all treatment combinations was chosen to be 0.06 N.

The results of the mass-transfer experiments were processed by the computer program discussed in Section 7.2. The yield of the experimental design is the overall stage efficiency of the countercurrent ion-exchange operation. The analysis of variance on the average effects shows that out of the seven main factors and twenty-one 2-factor interactions the following are significant:

Main effects:	resin flow-rate
	liquid flow-rate
	weir length
	weir height
interactions:	liquid flow-rate and weir length
	solid flow-rate and weir length
	weir height and weir length.

The analysis of variance table in Table E.8 of Appendix E shows that these main effects and interactions are significant at the 95.0% and 99.0% levels of confidence. The other main factors (resin particle size, fluid-diode lateral displacement and downcomer clearance) and other interactions are not considered to be significant in affecting the overall stage efficiency of the ion-exchange column because their effects are not as large as those due to random experimental errors.

The use of half-normal and standardized half-normal plots confirmed the above results as shown in Figures E.2 and E.3.

8.4 Effects of the Main Factors and the Significant Interactions on the Mass-Transfer Performance

8.4.1 Resin feed-rate

The resin flow-rate is significant in determining the overall stage efficiency of the ion-exchange operation. As shown in Figure B.18a, the increase in resin flow-rate normally reduces the overall stage efficiency. Figure B.19 shows the equilibrium diagram (with operating lines) of the experimental runs.

The faster the resin travels through a stage of the column, the shorter is its contact time with the flow of process solution. Hence the degree of approach towards thermodynamic equilibrium is less. The decrease in solid mixing in each stage as the solid feed-rate is increased also accounts for some decrease in the overall stage efficiency. The decrease in contact time decreases the transfer of sodium ion to each resin particle. The mole fraction of sodium in the exit resin is

thus reduced as shown in Figure B.18b. However, the increase in resin feed-rate increases the overall rate of counter-ions (Na^+ and H^+) exchanged in the contactor between the solution and resin phases as shown in Figure B.18d. Hence the mole fraction of sodium ion in the liquid phase decreases as shown in Figure B.18c.

Under the present experimental conditions ($Re_p = 10.0$), both the solid and liquid sides play a significant role in the ion-exchange kinetics. In the multistage ion-exchange column, the steady state compositions of the resin and solution phases in each stage vary as the resin feed-rate is increased. Examination of Figures B.18b and B.18c shows that the hydrogen-ion content both in the resin and the liquid phases increases with the increase in resin feed-rate. Hence mass-transfer coefficients in both the solid and liquid sides decrease as the resin feed-rate increases. This increase in overall mass-transfer resistance also causes the decrease in overall stage efficiency as the resin feed-rate is increased.

When the ion-exchange operation is concerned with the extraction of ions (Na^+) from a solution (NaCl), Figure B.18e shows that it is not economical to increase the extraction yield beyond 65% by increasing the resin feed-rate. When the operation is concerned with the extraction of material (H^+) from the resin particles, Figure B.18f shows that the fraction of ions extracted from the resin decreases as the resin feed-rate is increased. Figure B.18e is equivalent to Figure B.18d and Figure B.18f to Figure B.18b.

8.4.2 Process solution flow-rate

The process solution flow-rate is significant in determining the overall stage efficiency. Figure B.20a shows that the overall stage efficiency decreases as the process solution feed-rate increases. Figure B.21 shows the equilibrium diagram (with operating lines) of these experimental runs.

It has been shown that the increase in mass-transfer rate by increasing the liquid flow in fluidized-bed mass-transfer is nullified by the increase in bed voidage (46). However, in the present operation of a multistage fluidized-bed column the increase in voidage also results in a decrease in resin holdup in each stage and hence a decrease in resin residence time in the column. For a given resin feed-rate, the increase in liquid flow-rate also decreases the contact time of a given volume of process solution with the resin. On the other hand, the increase in liquid flow improves the resin mixing in each stage. Apparently the degree of approach to chemical equilibrium is reduced due to the more significant effect of decreasing the resin and liquid contact time.

The increase in solution flow-rate results in an increase in the mole fraction of sodium in the resin phase, as shown in Figure B.20b, because each volume of resin is exposed to more sodium-ion contact. Hence the higher flow-rate of sodium ion compensates for more than the decrease in the residence time of the resin.

For the solution phase, the decrease in residence time of the solution reduces the transfer of sodium ion from the solution per unit volume as shown in Figure B.20c. However, the overall rate of ion-exchange is increased as the solution flow is increased as shown in Figure B.20d. The mass-transfer coefficients in the solid

and liquid sides increase when the liquid flow-rate increases because of the corresponding decrease in hydrogen-ion mole fractions in both phases.

When the ion-exchange process is designed for the extraction of ion (Na^+) from solution, Figure B.20e shows that the increase in solution flow only reduces the fraction of ions removed. However, when the extraction of ion (H^+) from the resin is of concern, the increase in solution flow does increase the fraction of ions removed from the resin as shown in Figure B.20f.

8.4.3 Weir height

The weir height is a significant factor in affecting the overall stage efficiency. Figure B.22a shows that the overall stage efficiency increases as the weir height is increased from 0.5 to 2.0 inches (1.27 to 5.08 cm). The equilibrium diagram showing the changes in the operating line with the changes in weir height is shown in Figure B.23.

For given resin and process solution flow-rates, the increase in weir height increases the resin holdup in each stage. Thus the resin residence time in the column is increased. The mole fraction of sodium ion in the resin effluent is increased and consequently the mole fraction of sodium ion in the liquid effluent is decreased as shown in Figures B.22b and B.22c, respectively. With the increase in weir height, the compositions in the resin and liquid phases change in the direction of increasing the solid-side mass-transfer coefficient and decreasing the liquid-film mass-transfer coefficient, respectively.

The increasing lack of ideal solid mixing with the increase in weir height

apparently does not seem to override the other factors in reducing the overall stage efficiency.

Figure B.22 d shows that as the weir height is increased the overall rate of ion-exchange increases and again can be explained by the longer residence time of the resin in the contactor. Figure B.22 d also indicates that the increase in the overall rate of ion-exchange approaches a constant value as the weir height is increased. Hence there is a maximum weir height beyond which the overall rate of ion-exchange does not increase significantly.

The fraction of sodium ion adsorbed from the solution by the resin flow and the fraction of hydrogen ion extracted from the resin by the liquid flow follow the same trend as the overall rate of ion-exchange when the weir height is increased. These are shown in Figures B.22 e and B.22 f.

8.4.4 Weir length

The straight weir length is a significant factor in affecting the overall stage efficiency. Figures B.24a, B.25a, and B.26a show that for a given resin feed-rate, liquid flow-rate and weir height, respectively, the overall stage efficiency of the ion-exchange column increases with a decrease in the length of the straight weir. In the present tray design, the decrease in the length of the straight weir corresponds to an increase in fluidization area. The increase in fluidization area corresponds to an increase in resin holdup and hence an increase in resin residence time. For a given liquid flow-rate, the increase in fluidization area also decreases the fluidization superficial velocity and hence a further increase in resin holdup due

to a decrease in fluidized-bed voidage. On the other hand, the decrease in superficial liquid velocity causes an increase in the liquid-film mass-transfer resistance. Apparently, the experimental results of the present study indicate that the effect on the overall stage efficiency due to resin holdup is dominant over that due to increasing liquid-film mass-transfer resistance.

Since the change in weir length affects the process efficiency mainly through the resin holdup, the change in compositions of the resin and solution effluents and the overall rate of ion-exchange will follow the same trends as those discussed for weir height changes in Section 8.4.3.

8.4.5 Fluid-diode lateral displacement

The change of fluid-diode lateral displacement between 1/20 and 3/20 inch (1.27 and 3.81 mm) (a 3-fold change) does not show a significant effect on the mass-transfer performance of the ion-exchange column. The absence of significant interactions between the fluid-diode lateral displacement and the other six main factors also indicates its negligible effect under any operating conditions.

Hence the increase in liquid-bypassing up the downcomers when the fluid-diode lateral displacement is increased from 1/20 to 3/20 inch (1.27 and 3.81 mm) does not affect the mass transfer to a significant extent. The bypassing represents only a very small fraction of the total solution flow, and the bulk of mass transfer still takes place in the fluidization area on each stage.

8.4.6 Downcomer clearance

The downcomer clearance as well as its interactions with the other six factors are not significant in determining the overall mass-transfer stage efficiency. The levels of the downcomer clearance were 1.0 and 1.5 inches (2.54 and 3.81 cm) and so the downcomer seal varies from -0.5 to 1.0 inch (-1.27 to 2.54 cm) (a three fold change). Hence, the effect of the downcomer seal on the resin's residence time in each stage is not large enough to cause any significant difference in mass-transfer performance.

8.4.7 Resin particle size

The change in resin particle-size distribution from -30+35 mesh to -20+30 mesh is not significant in affecting the mass-transfer efficiency.

The mean particle diameter is varied from 0.507 to 0.718 mm and is a 40% increase in diameter. However, the result of the experimental design shows that this change in resin particle-size is not significant in affecting the overall stage efficiency. A smaller resin particle has a larger surface area to volume ratio and also a lower mass-transfer effect due to solid-side resistance (when compared to that of the liquid-side). However, for a given weir height and a given superficial liquid velocity the resin holdup in the fluidization area is lower for the smaller particle-size distribution. The decrease in mass transfer due to a lower resin holdup may possibly just cancel out the net increase in mass transfer due to a larger surface area to volume ratio and a lower mass-transfer effect due to solid-side resistance. Hence the overall stage efficiency is indifferent to the change in

particle size.

8.4.8 Resin feed rate - weir length interaction

The interaction between the resin feed-rate and the length of the straight weir (i.e. fluidization area) on the overall stage efficiency is shown in Figure B.24a. The term "interaction" means that the effect of the resin feed-rate on the overall stage efficiency is different for different weir lengths. The effects on the overall stage efficiency due to the change in resin feed-rate and weir length were discussed in Sections 8.4.1 and 8.4.4 respectively. Figure B.24a shows that the response of the overall stage efficiency to the resin feed-rate is very significant at the shortest weir length especially in the region of low resin feed-rates.

At a weir length of 3.38 inches (8.59 cm), the decrease in resin residence time and overall mass-transfer coefficient due to increasing resin feed-rate can account for the corresponding decrease in overall stage efficiency. However, at a weir length of 3.97 inches (10.08 cm) (smaller fluidization area) the overall stage efficiency is indifferent to the change in resin residence time and overall mass-transfer coefficient. One possible explanation for this behaviour at the weir length of 3.97 inches (10.08 cm) is that the initial part of the ion-exchange takes place in a very short time as can be understood by the graphs in Figure B.1. The resin residence time provided by the holdup in each stage is more than enough for the completion of this part of the reaction. The decrease in resin residence time by increasing the resin feed is not significant enough to affect the completion of this reaction. As can be seen from Figure B.24b and B.24 c, the change in resin and

solution compositions is relatively small as the resin feed-rate is increased. Hence the overall stage efficiency remains practically unchanged.

The same concept may be used to explain the approach toward a constant value of overall stage efficiency with increasing resin feed-rate for the operations with straight weirs of lengths 3.38 and 3.78 inches (8.59 and 9.60 cm).

8.4.9 Process solution flow rate - weir length interaction

Figure B.25a shows the decrease in the overall stage efficiency as the process solution flow is increased for the three weir lengths. The effects of the change in solution flow-rate and weir length on the overall stage efficiency were discussed in Sections 8.4.2 and 8.4.4 respectively.

Figure B.25a shows that the effect of the change in process solution flow-rate on the overall stage efficiency is slightly more significant for greater weir lengths (i.e. for smaller fluidization areas). The decrease in resin holdup is the main cause for the lowering of the overall stage efficiency when the weir length is increased.

At a weir length of 3.38 inches (8.59 cm), the change in solution flow from 40.0 to 94.2 ml/sec corresponds to a change in particle Reynolds number from 7.2 to 16.8. Both the solid and liquid sides are significant in determining the overall mass-transfer coefficient which is increasing with the increase in solution flow-rate due to the favourable composition changes as shown in Figures B.25b and B.25c. The liquid-film resistance also is decreasing with the increase in superficial liquid velocity. The change in liquid flow-rate corresponds to a change in the super-

ficial liquid velocity from 0.61 to 1.44 cm/sec which would significantly increase the mixing of the resin particles in each stage. These increases in overall mass-transfer coefficient and in resin mixing counteract part of the effect of the decrease in solid-liquid contact as the solution flow-rate is increased.

However, at a greater weir length, e.g. 3.97 inches (10.08 cm), the same change in solution flow-rate corresponds to a change of particle Reynolds number from 11.7 to 26.4 and the superficial velocity from 1.0 to 2.3 cm/sec. The solid-side mass transfer becomes the controlling step, especially at the high range of liquid flow-rates. The increase in superficial liquid velocity no longer has a significant effect in increasing the overall mass-transfer rate by reducing the liquid-film mass-transfer resistance. The effect of increasing the solid mixing by increasing the solution flow-rate is less significant because of the high superficial liquid velocity already experienced by the resin bed at the low range of liquid flow-rate. Hence, the increase in the overall mass-transfer coefficient and the resin mixing with increasing solution flow-rate is less significant at greater weir lengths (smaller fluidization areas). The decrease in solid-liquid contact due to increasing solution flow-rate becomes more dominant for operations with smaller fluidization area. Hence the solution flow-rate has a more significant effect on the overall stage efficiency as the weir length is increased.

8.4.10 Weir height - weir length interaction

Figure B.26a shows the response of the overall stage efficiency at three different weir lengths as the weir height is increased. The increase in the overall

stage efficiency as the weir height and fluidization area are increased was discussed in Sections 8.4.3 and 8.4.4 respectively.

Figure B.26a shows that the response of the overall stage efficiency to the weir height is more significant at a smaller weir length, i.e. larger fluidization area. For the operations with different weir lengths, Figures B.26b and B.26c show the same pattern of composition change (in the solid and liquid phases) with different weir lengths. Hence the composition dependence of the overall mass-transfer coefficient is not the reason for the interaction between the weir height and the weir length. Besides, the solid-side mass transfer may be controlling at the weir length of 3.97 inches (10.08 cm) ($Re_p = 33.2$), and the change in resin composition due to increasing weir height is increasing the solid-side mass-transfer coefficient.

One reason for the interaction between the weir height and weir length is that the residence time distribution of the resin is more significantly increased by the increase in weir height when the fluidization area is large (short weir length). Hence the more significant increase in resin residence time causes a more significant increase in overall stage efficiency.

8.5 Effects of the Initital Sodium-Ion Concentration in the Process Feed Solution on Mass-Transfer Performance

Figure B.27a shows the increase in overall stage efficiency as the initial sodium-ion concentration is increased. Experiments were performed at two process solution feed-rates: 40.0 and 79.2 ml/sec. The mean resin particle-size is 0.735

mm (-30 + 35 mesh). The equilibrium diagrams showing the operating lines are shown in Figures B.27b and B.27c. The equilibrium constant for the ion-exchange system remains practically constant when the initial concentrations of the sodium ion vary between 0.02 and 0.1 N.

The particle Reynolds numbers for the experimental run range from 5.98 to 11.9, indicating that the mass transfer is controlled by both the solid- and liquid-side resistances. As the initial sodium-ion concentration is increased, the increase in sodium-ion mole fraction in both the resin and liquid phases (as shown in Figures B.27d and B.27e) tends to increase the solid-side and liquid-side mass-transfer coefficients. This is one reason for the increase in the degree of approach towards thermodynamic equilibrium.

Figure B.27f shows that the increase in initial sodium-ion concentration increases the overall rate of ion-exchange but the fraction of sodium ion extracted by the resin from the solution decreases as shown in Figure B.27g. If the objective of the operation is to elute ions from the resin phase, the increase in eluant concentration will significantly increase the fraction of ion extracted from the resin phase as shown in Figure B.27h.

8.6 Effects of Weir Shapes on Mass-Transfer Performance

Experiments on mass-transfer performance were performed on the multistage ion-exchange column with cylindrical weirs installed in each tray. The cylindrical weir has a weir height of 2 inches (5.08 cm) and a diameter of 1.69 inches (4.29 cm) which gives a downcomer catching-area equal to that of the tray design with the

3.38-inch (8.59 cm) straight weir.

The overall stage efficiency of the experimental runs with different resin feed-rates are shown in Figure B.28. The overall stage efficiency decreases with increasing resin feed-rate as expected. Figure B.28 also indicates that the overall stage efficiency for an operation with cylindrical weir is always lower than that for an operation with 3.38-inch (8.59 cm) straight weir. Under the same operating conditions of resin and liquid flows, the resin holdup in both tray-designs are the same because the downcomer areas and weir heights are the same. Difference in resin mixing may not be the main reason for the difference in overall stage efficiency because small resin particle-size (-30 + 35 mesh) and high superficial liquid velocity (1.2 cm/sec) were used. A comparison of the two designs indicates that the distance between the fluid-diode downcomer (from the tray above) and the downcomer area is much shorter for the tray-design with cylindrical weir. Hence the resin residence time is smaller in the tray-design with cylindrical weir, resulting in a lower overall stage efficiency.

Figure B.28 also shows the experimental results for ion-exchange column operations with 2-inch (5.08 cm) high conical weirs. The overall stage efficiency for these runs is higher than that for the runs with straight weirs and cylindrical weirs. This is because the fluidization area and hence the resin holdup are slightly larger for the tray-design with conical weir.

Among the various weir-shape designs, the resin residence time (determined by the resin holdup and the distance between the downcomer of one stage and the weir of the next) in each tray determines the overall stage efficiency of the ion-

exchange column operation. The design of weir shapes mainly affects the operational performance of the column in terms of the flooding and cyclic resin-flow characteristics as discussed in Sections 8.2.5 and 8.2.6.

8.7 Mass-Transfer Performance Factor

The overall stage efficiency has been used in assessing the mass-transfer performance of the ion-exchange column under various operating conditions. This performance factor indicates the lack of thermodynamic equilibrium. However, it does not account for the volumetric throughput rate of the operation. With the resin feed-rate approaching zero, we can have an overall stage efficiency approaching 100% but with little or no output at all. The response of the overall stage efficiency to the resin feed-rate at 3.97-inch (10.08 cm) weir length in Figure B.24a does not indicate that the ion-exchange operation at point A is actually handling nearly three times the resin feed-rate at point B, although the overall stage efficiency is unchanged.

In Egan's optimization study on the operation of the ion-exchange column the volumetric efficiency

$$E_v = \frac{F_S + F_L}{(HETS).(A)} \qquad (8.7.1)$$

was used as the mass-transfer performance factor. The HETS is calculated from the physical height of the contactor and A is the cross-sectional area of the column. In the continuous countercurrent ion-exchange operation using the present contactor and the other contactors, the solid feed-rate is much smaller than the flow of process

solution. The volume flow-rate of the solution can be more than one hundred times that of the resin. Hence the response of the volumetric efficiency to a change in resin throughput is extremely sluggish when compared to that for a change in solution flow. This factor accounts for the total volumetric throughput but neglects the chemical compositions of the solution and resin feed-streams.

Hence a modified volumetric mass-transfer performance factor can be proposed

$$(E_v)_m = \frac{F_s q_o + F_L c_o}{(HETS)_f . (A)_f} \qquad (8.7.2)$$

As discussed in Section 3.5, only the active height of the column should be considered in calculating the HETS. Hence the $(HETS)_f$ in Equation 8.7.2 is calculated from the total of the weir heights or more accurately fluidized-bed heights of the multistage column. By the same argument, the fluidization area $(A)_f$, rather than the cross-sectional area, A, of the column is used in Equation 8.7.2. Similar to the volumetric efficiency, the modified volumetric efficiency may be interpreted as the mass-transfer volume of the ion-exchange column required to handle the ion flows for the necessary separation. For any separation, a large value of the volumetric efficiency is desirable. For a given column (fixed weir lengths and weir heights) and handling feed streams of constant compositions (constant q_o and c_o), the modified volumetric efficiency $(E_v)_m$ is equivalent to the original volumetric efficiency, E_v, with the response to resin flow magnified.

8.8 Comparison of the Performance of Different Ion-Exchange Contactors

Slater (2) has used the specific volume in comparing existing ion-exchange

contactors on the basis of their chemical performance and total volumetric throughput capacity. For stagewise processes, the specific volume is given by

$$V = \frac{HETS}{u + v} \tag{8.8.1}$$

where $u + v$ is given by

$$u + v = \frac{F_S + F_L}{\text{X-sectional area of column}} \tag{8.8.2}$$

The specific volume, for which a small value is desirable, may be interpreted as the volume of a theoretical stage for unit total volumetric throughput. This performance index is actually the reciprocal of the volumetric efficiency in Equation 8.7.1.

The specific volume index also serves to compare the performance between fixed bed and continuous countercurrent contactors without solving for the concentration profile in the fixed bed. For sodium/hydrogen ion exchange, Moison's data (52) for fixed bed and Turner's (29) for fluidized bed are shown in Figure 8.29. Data from the present study are also included. The present CCIX operations appear to be much more efficient than a similar column developed by Turner (29). The reason is that the present contactor design using fluid-diode downcomers makes stable column operation possible at high resin and process solution throughput rates. Our experimental data have much higher $(u + v)$ values. The HETS values calculated from the active height of the column are essentially the same because both are multistage fluidized-bed operations having the same chemical system, solution concentration, and resin particle-size distribution.

If it may be assumed that the comparison of specific volumes of different contactors for a given total flow velocity and chemical system will hold for other chemical systems, then all contactors may be compared with each other and with a fixed bed of specific volume, V_f. This has been done by Slater (2). The standing of the multistage fluidized-bed ion-exchange contactor with fluid-diode downcomers among other existing ion-exchange contactors is shown below:

Contactor	Relative Specific Volume (V_f/V)
Fixed bed	1.0
Fluidized moving bed (Selke)	0.6
Pulsed stages (Grimmett)	0.6 to 0.3
Moving bed (force) (Higgins)	0.5
Moving bed (gravity) (Selke)	0.5
Present study	0.36 to 0.13
Jigged bed (McNeill)	0.25
Fluidized stage (Turner)	0.06
Coil (Schulman)	0.06

The relative specific volume for the present operations ranges from 0.36 to 0.13 with a mean at 0.18. Before the calculation of the relative specific volume, the specific volume data from the present study have been approximately adjusted to account for the difference in solution concentrations between Moison's data and our data. The performance of the present contactor is much better than that of Turner's fluidized-stage contactor. The performance is in the same range as the

other commercially successful moving-bed contactors.

Slater (2) believes that the above comparison is very approximate and relates to capital cost principally. The lower the relative specific volume the lower must be the total contactor cost to be competitive with a fixed bed. The specific volume of a fixed bed concerns only the height of one transfer unit. The actual volume of a fixed-bed contactor is in fact several times greater than that of a continuous countercurrent contactor with the same duty because most of the resin inventory in a fixed bed is not active. However, the relative specific volume would serve well in the comparison among other CCIX processes.

The specific volume of a fluidized-bed contactor would likely be always larger than that for moving fixed-bed contactors due to the larger bed voidage. However, the simplicity in contactor design, the large solid and liquid handling capacity, and the excellent operational stability of the present design may compensate for the slight loss in chemical efficiency. The required control on the resin and process solution flow is much simpler than that for the moving fixed-bed operations. The continuous use of the resin for about two hundred experimental runs has shown that resin attrition in this continuous countercurrent operation is negligible because no mechanical parts are involved in the resin transport and the entire operation involves only moderate pressure changes.

9. CONCLUSION

The multistage fluidized-bed CCIX column with fluid-diode downcomers from the work of Cha was modified and improved. The entire ion-exchange column system and the regeneration and washing systems were redesigned and rebuilt. The system of resin feed by volumetric displacement proved to be controllable and produced no noticeable resin attrition. The modified ion-exchange column had improved liquid distribution. The effluent resin no longer backed up at the exit. The resin sampling system proved to be very efficient.

The study has shown that the implementation of fluid diodes in the design of downcomers is successful in minimizing liquid-bypassing up the downcomers ensuring a smooth and continuous flow of resin from stage to stage down the column. Easy start-up and shut-down were observed and the resin was evenly distributed on each mass-transfer stage. Fluid-diode downcomers are pressure sensitive devices, the performance of which can be predicated by a pressure-drop consideration. The more pressure sensitive is a fluid-diode design, the more unstable will be the column operation towards any sudden change in resin and process solution flows.

The tray structures and resin particle-size distribution can significantly affect the contactor's operational performance in terms of resin fluidization in the fluidization area and liquid-bypassing in the downcomers. The increase in fluid-diode lateral displacement increases the possibility of liquid-bypassing. A large resin particle-size distribution increases the pressure drop across the fluid-diode

downcomers resulting in significant liquid-bypassing. The increase in weir height improves liquid distribution in the fluidized bed and hence reduces channeling. The conical and cylindrical weir design has shown that the elimination of dead area in the downcomer area has the effect of minimizing liquid-bypassing up the downcomer because the equilibrium resin-head is more effectively maintained in the downcomer area. Hence the operation of the column at very low resin but moderately high liquid flow-rates becomes feasible. The interaction of the conical and cylindrical weirs' wall with the inner wall of the column reduces resin mobility in the fluidization area. Hence the straight weir with sloping inside walls would be the best design for the present solid-liquid contactor.

The 1/4-replicate of a factorial experimental design to 7 factors at 2 levels has efficiently and successfully revealed the operational and structural parameters as well as the interactions among these parameters which are significant in determining the overall stage efficiency of the present ion-exchange operation. The experimental design showed that the resin feed-rate, process solution flow-rate, weir length and weir height are significant main factors. The interactions between resin feed-rate and weir length, process solution flow-rate and weir length, and weir height and weir length are significant interactions. The resin particle size, fluid-diode lateral displacement, and downcomer clearance (or seal) are not significant in affecting the overall stage efficiency between the levels investigated.

Further mass-transfer study has shown that resin residence time is the main factor in determining the overall stage efficiency of an operation. The dependency of the solid- and liquid-side mass-transfer coefficients on the chemical compositions

of the solid and liquid phases also plays a role in affecting the overall stage efficiency.

Experimental results from the present study have demonstrated that the multistage fluidized-bed CCIX contactor with fluid-diode downcomers has a favourable chemical efficiency and volumetric capacity when compared to other ion-exchange contactors on the basis of relative specific volume. The fluidized-bed operation has a slightly lower chemical efficiency than the moving fixed-bed operations. However, the simplicity in contactor design and in control requirements together with the operational stability, and large solid and liquid handling capacities, may compenstate for the slightly lower chemical efficiency in large industrial applications.

NOTATIONS

a	complex mapping variable
A	cross-sectional area of ion-exchange column; opening area of fluid-diode downcomer (cm^2)
A_f	fluidization area (cm^2)
c	concentration (meq/ml)
c_i	interfacial concentration (meq/ml)
C_o	initial sodium-ion concentration (meq/ml)
d	particle diameter (cm)
D	interdiffusion coefficient in resin (cm^2/sec)
D_A	self-diffusion coefficient of species A in resin (cm^2/sec)
D_B	self-diffusion coefficient of species B in resin (cm^2/sec)
DC	downcomer clearance (cm)
DLD	fluid-diode lateral displacement (mm)
DP	resin particle size (mm)
E_{os}	overall stage efficiency
E_v	volumetric efficiency (l/hr)
$(E_v)_m$	modified volumetric efficiency (meq/sec-cm^3)
F	force (dyne)
f_b	bouyancy force on resin (dyne)
F_{HE}	fraction of hydrogen ion extracted

F_{SA}	fraction of sodium ion adsorbed
FL	process solution flow-rate (ml/sec)
FS	resin feed-rate (ml/sec)
g	acceleration due to gravity (cm/sec^2)
HETS	height equivalent to a theoretical stage (feet, cm)
$(HETS)_f$	height equivalent to a theoretical stage based on active contactor height (feet, cm)
k_L	liquid-side mass-transfer coefficient (cm/sec)
k_{Lb}	liquid-side mass-transfer coefficient at bubble point (cm/sec)
k'	mass-transfer rate constant ($cm^3/meq\text{-}sec$)
L	process solution flow-rate (ml/sec)
N	number of stages
NTS	number of theoretical stages
P_1, P_2	pressure ($dyne/cm^2$)
q	resin capacity (meq/ml)
R	resin flow-rate (ml/sec)
R_1, R_2	resistances of fluid-diode downcomer to flows (dyne)
R_{IOX}	rate of ion exchanged (meq/sec)
t	time (sec)
u	resin flow velocity in terms of fluidization area (ft/hr)
U_o	superficial velocity (cm/sec)
v	velocity of process solution flow in terms of fluidization area (ft/hr)

V	specific volume (hr)
V_f	specific volume of a fixed bed (hr)
V_o	superficial velocity (cm/sec)
V_{ob}	superficial velocity at bubble point
WH	weir height (cm)
WL	weir length (cm)
x, XB, XT	mole fraction of sodium-ion in liquid phase, B = bottom inlet stream, T = top outlet stream
y, YB, YT	mole fraction of sodium ion in resin phase, B = bottle outlet stream, T = top inlet stream
Z	active height of contactor (cm)

Dimensionless groups

Re	Reynolds number
Sc	Schmidt number
Sh	Sherwood number
St	Stanton number

Greek Letters

ϵ	voidage
ϵ_b	voidage at bubble point
μ	dynamic viscosity (gm/sec)
ν	kinematic viscosity (cm^2/sec)
ρ	density (gm/cm^3)
ϕ	k_L/k_{LB}

REFERENCES

1. Slot, G.S., Soc. Chem. Ind. Conf. on Ion-Exchange, p. 85 (1970).
2. Slater, M.J., Brit. Chem. Eng., 14, 41 (1969).
3. Levendusky, J.A., Chem. Eng. Prog. Symp. Ser., 65, 113 (1969).
4. Cloete, F.L.D., and Streat, M., Nature, 200, 1199 (1963).
5. Grimmett, E.S., and Brown, B.P., Ind. Eng. Chem., 54, 24 (1962).
6. Souhrada, F., unpublished work, Dept. of Chem. Eng., University of New Brunswick, Fredericton (1969).
7. Egan, S.M., M.Eng. Thesis, McMaster University, Hamilton (1971).
8. Cha, C.Y., unpublished work, Dept. of Chem. Eng., McMaster University, Hamilton (1972).
9. Wood, L.O., and Fox, H.L., Intern. Sci. Technology, 23, 44 (1963).
10. Various Authors, Fluid Amplification Symposium, HOL (1964).
11. Various Authors, Fluid Amplifier State of the Art, NASA, CR 102 (1964).
12. Telsa, N., United States Patent 1,399,559 (1920).
13. Ringleb, F.O., Symp. on Fully Separated Flows (ASME Meeting), p. 33 (1964).
14. Thompson, D.W., Can. J. Chem. Eng., 48, 236 (1970).
15. Stevenson, D.G., Soc. Chem. Ind. Conf. on Ion Exchange, p. 114 (1969).
16. Morris, W., Brit. Patent 885,503 (1958).
17. Hiester, N.K., et al., Ind. Eng. Chem., 45, 2402 (1953).
18. Iwasyk, J.M., and Thodos, G., Chem. Eng. Prog., 54, 69 (1958).

19. McCormack, R.H., and Howard, J.F., Chem. Eng. Prog. 49, 404 (1953).

20. Muendel, C.H., and Selke, W.A., Ind. Eng. Chem., 47, 374 (1955).

21. Miles, J.H., Brit. Patent 1,054,578 (1968).

22. Schulman, H.L., et al., Ind. Eng. Chem. Proc. Des. Dev., 5, 257 (1966).

23. Weiss, D.E., McNeill, R., and Swinton, E.A., J. of Metals, 7, 955 (1955).

24. Peebles, F.N., Chem. Eng. News, 34, 5200 (1956).

25. Higgins, I.R., Ind. Eng. Chem., 53, 635 (1961).

26. Higgins, I.R., and Chopra, R.C., Soc. Chem. Ind. Conf. on Ion Exchange, p. 121 (1969).

27. Gilwood, M.E., Chem. Eng., 74, p. 83, Dec. 18 (1967).

28. Slater, M.J., Soc. of Chem. Ind. Conf. on Ion Exchange, p. 127 (1969).

29. Turner, J.C.R., and Church, M.R., Trans. Instn. Chem. Engrs., 41, 283 (1963).

30. Stermerding, S., et al., Soc. Chem. Ind. Symp. on Fluidization (1964).

31. Cox, M., Trans. Instn. Chem. Engrs., 36, 29 (1958).

32. Helferrich, F., Ion Exchange, McGraw-Hill Book Co., Inc. (1962).

33. Whitcombe, J.A., Banchero, J.T., and White, R.R., Chem. Eng. Prog. Symp. Ser., 50, 73 (1954).

34. Turner, J.C.R., Church, M.R., Johnson, A.S.W., and Snowdon, C.B., Chem. Eng. Sci., 21, 317 (1966).

35. Turner, J.C.R., and Snowdon, C.B., Chem. Eng. Sci., 23, 221 (1968).

36. Duncan, J.F., and Lister, B.A.J., J. Chem. Soc., 3285 (1949).

37. Gilliland, E.R., and Baddour, R.F., Ind. Eng. Chem., 45, 330 (1953).

38. Dowex: Ion Exchange, Dow Chemical Co., Midland, Michigan (1958).

39. Snowdon, C.B., and Turner, J.C.R., Proc. Int. Symp. on Fluidization, Eindhoven, p. 599 (1967).

40. Petrovic, J.J., and Thodos, G., Proc. Int. Symp. on Fluidization, Eindhoven, p. 586 (1967).

41. Richardson, J.F., and Zaki, W.N., Trans. Instn. Chem. Engrs., 32, 35 (1954).

42. Beek, W.J., Proc. Int. Symp. on Fluidization, Eindhoven, p. 507 (1967).

43. Moyle, F.J., Australian J. of App. Sci., 10, 433 (1954).

44. Turner, J.C.R., and Church, M.R., Trans. Inst. Chem. Engrs., 41, 283 (1963).

45. Foust, A.S., et al., Principal of Unit Operations, J. Wiley and Sons, New York (1960).

46. Rowe, P.N., and Claxton, K.T., Trans. Inst. Chem. Eng., 43, 321 (1965).

47. Peng, K.C., The Design and Analysis of Scientific Experiments, Addison-Wesley Publishing Co., Massachusetts (1967).

48. Johnson, N.L., and Leone, F.C., Statistics and Experimental Design: In Engineering and the Physical Sciences, Vol. 2, John Wiley and Sons, Inc., New York (1964).

49. Daniel, C., Technometrics, 1, 311 (1959).

50. Leva, M., Fluidization, McGraw-Hill Book Co., Inc., New York, p. 35 (1959).

51. Hanna, M.R., M.Sc. Thesis, University of New Brunswick, Fredericton (1970).

52. Moison, R., and O'Hern, H., Chem. Eng. Prog. Symp. Ser., 55, 71 (1959).

APPENDIX A

Equipment Design and Apparatus

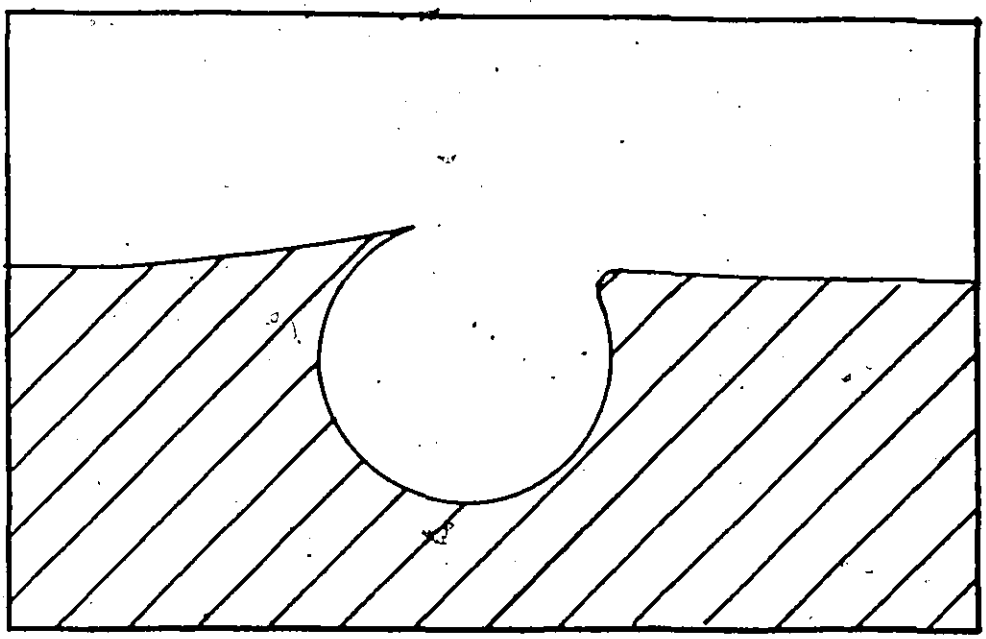

FIGURE A.1 Theoretical contour of cusp-cavity shape

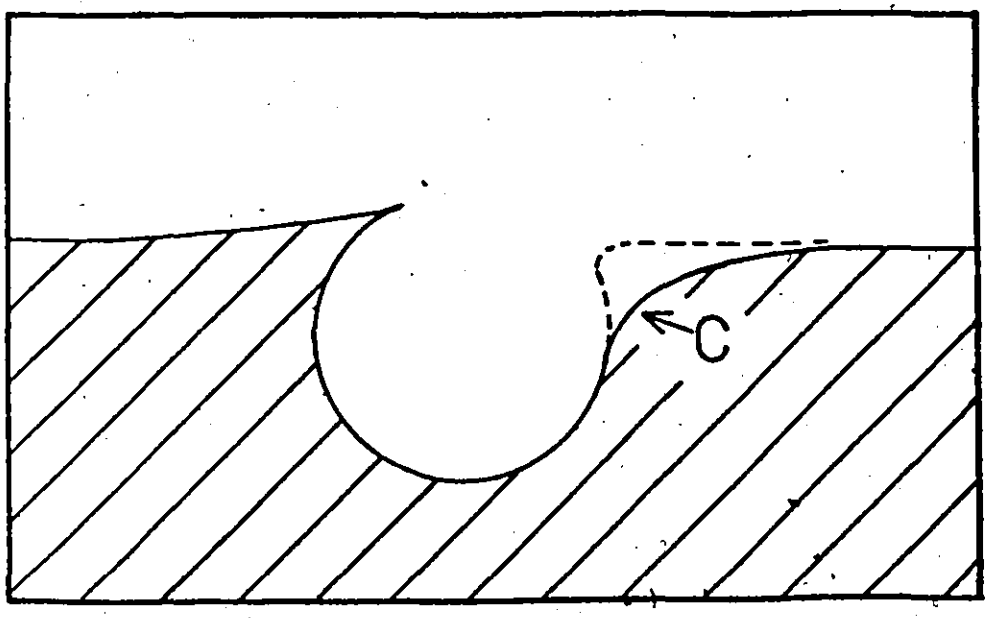

FIGURE A.2 Modified contour of cusp-cavity shape

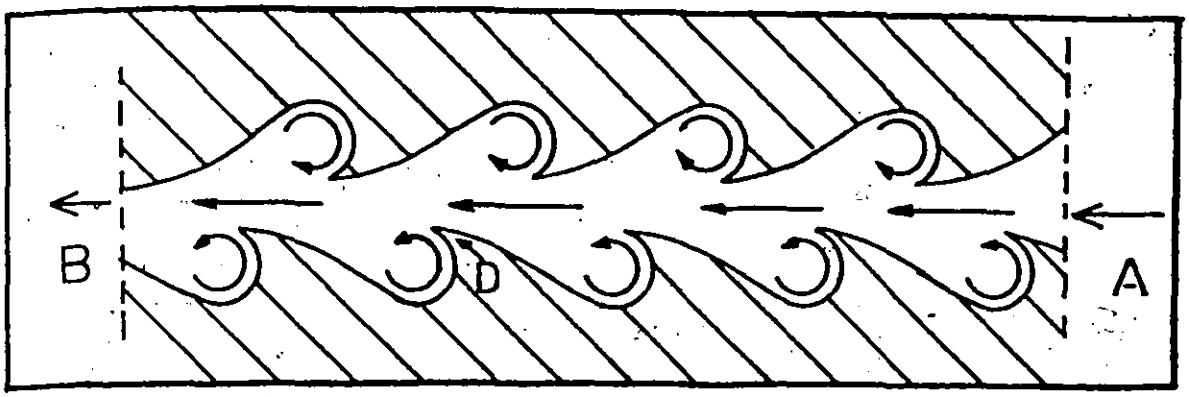

FIGURE A.3 Flow pattern - low pressure-drop direction

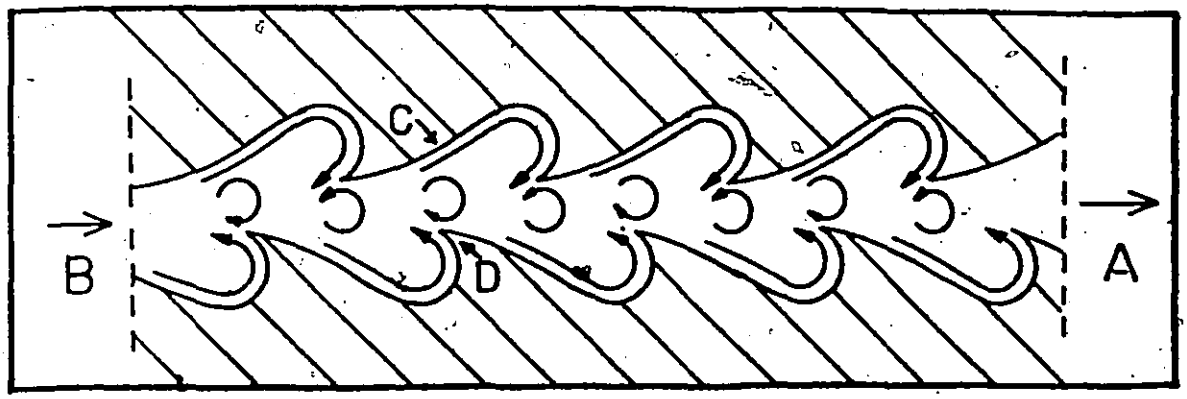

FIGURE A.4 Flow pattern - high pressure-drop direction

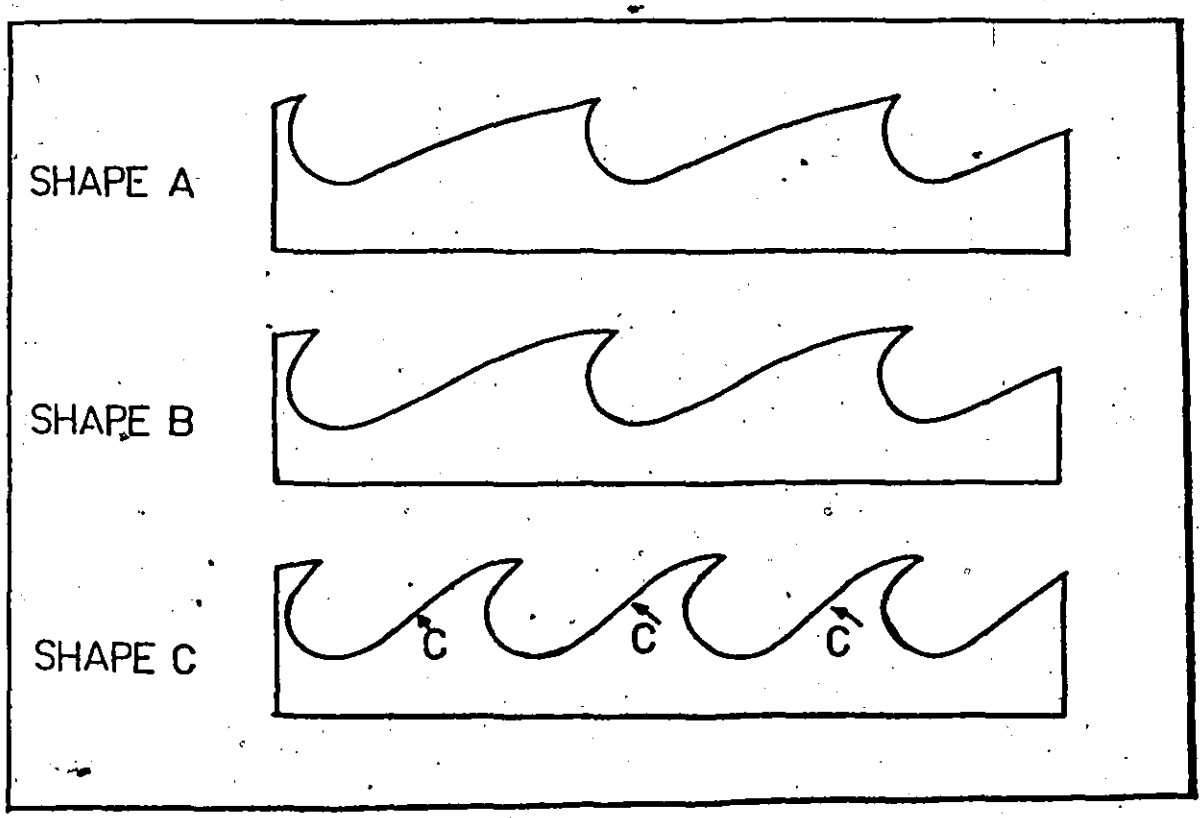

FIGURE A.5 Cusp-cavity designs

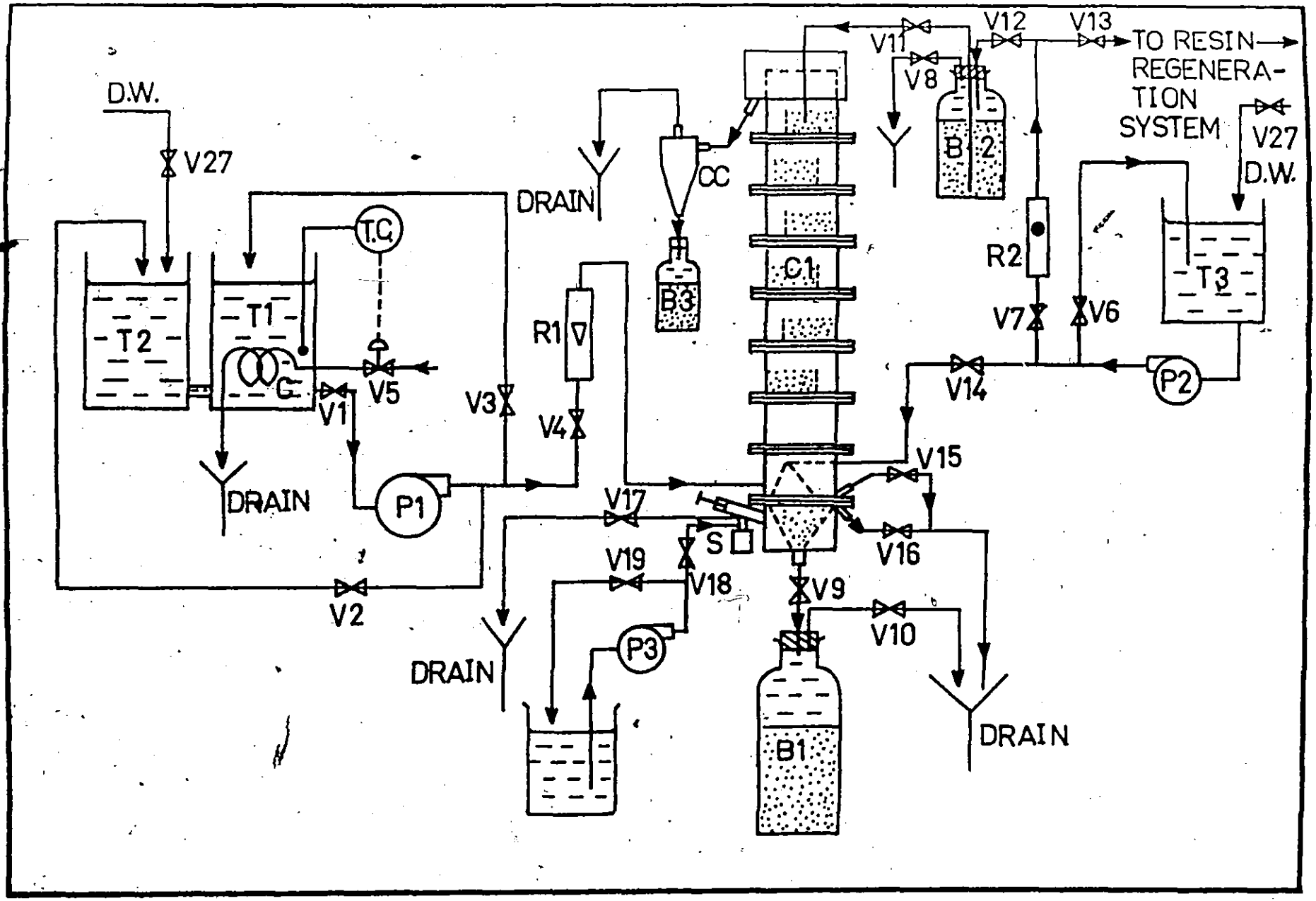

FIGURE A.6 Ion-exchange column system

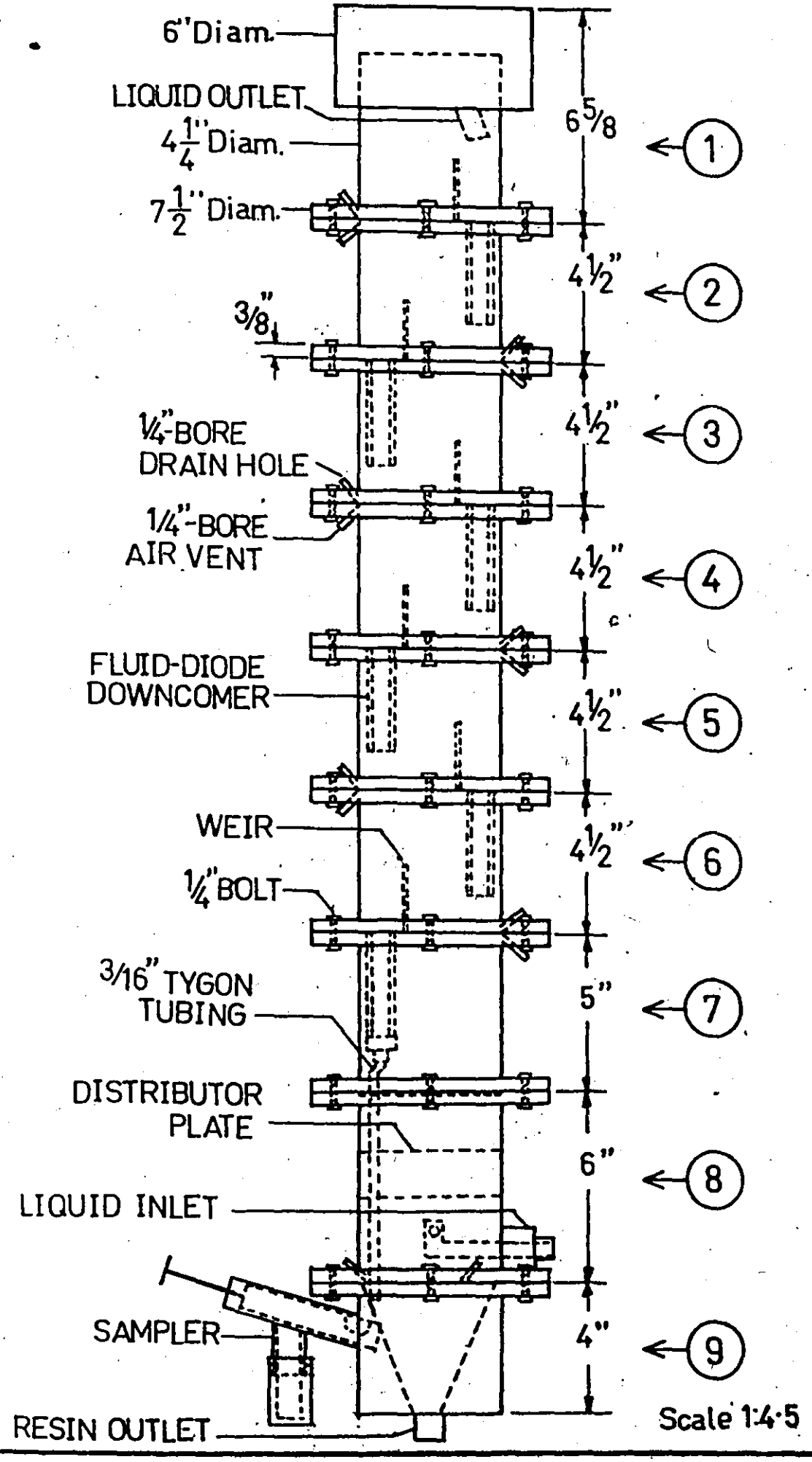

FIGURE A.7 Multistage ion-exchange column

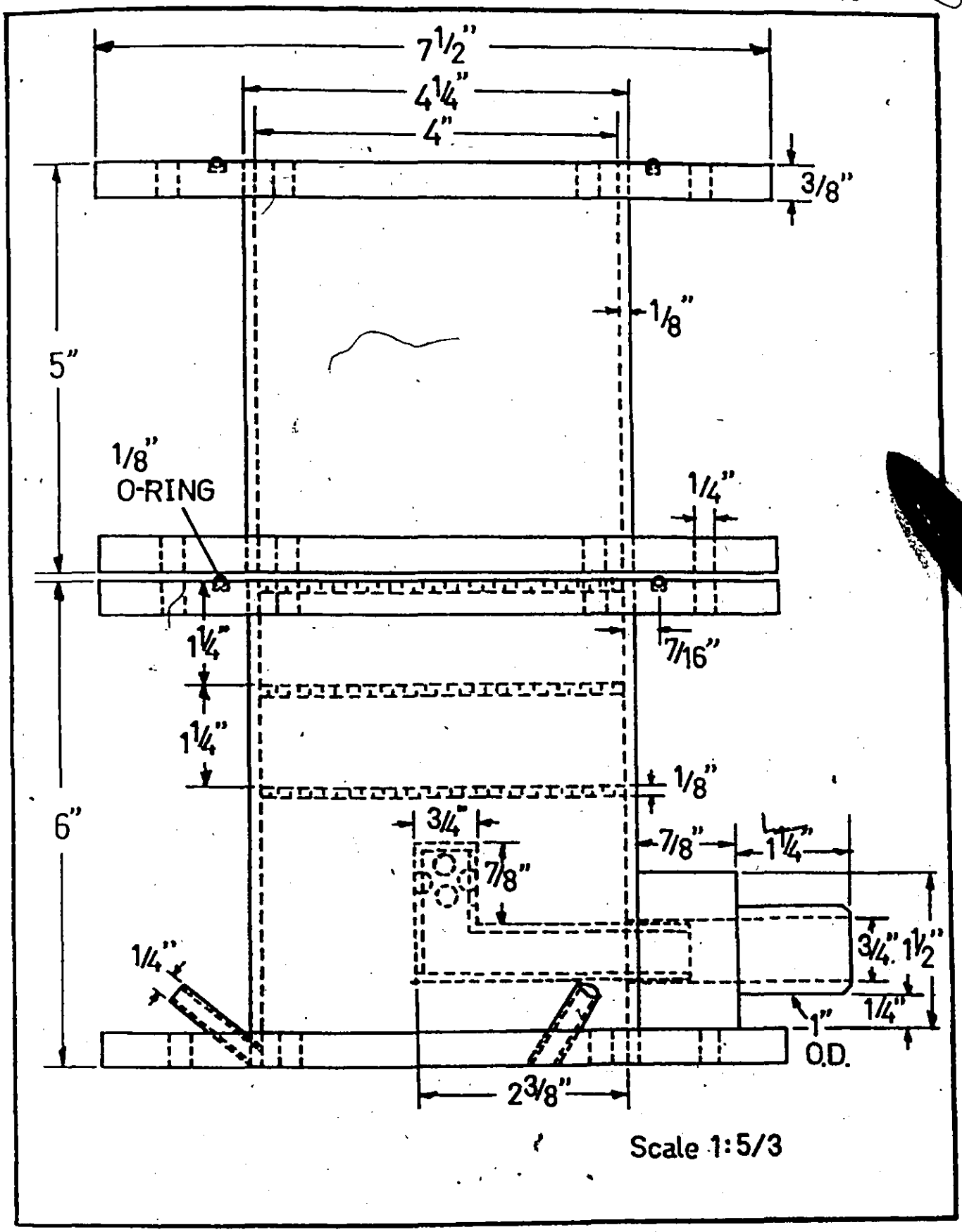

FIGURE A.8. Sections 7 and 8 of ion-exchange column

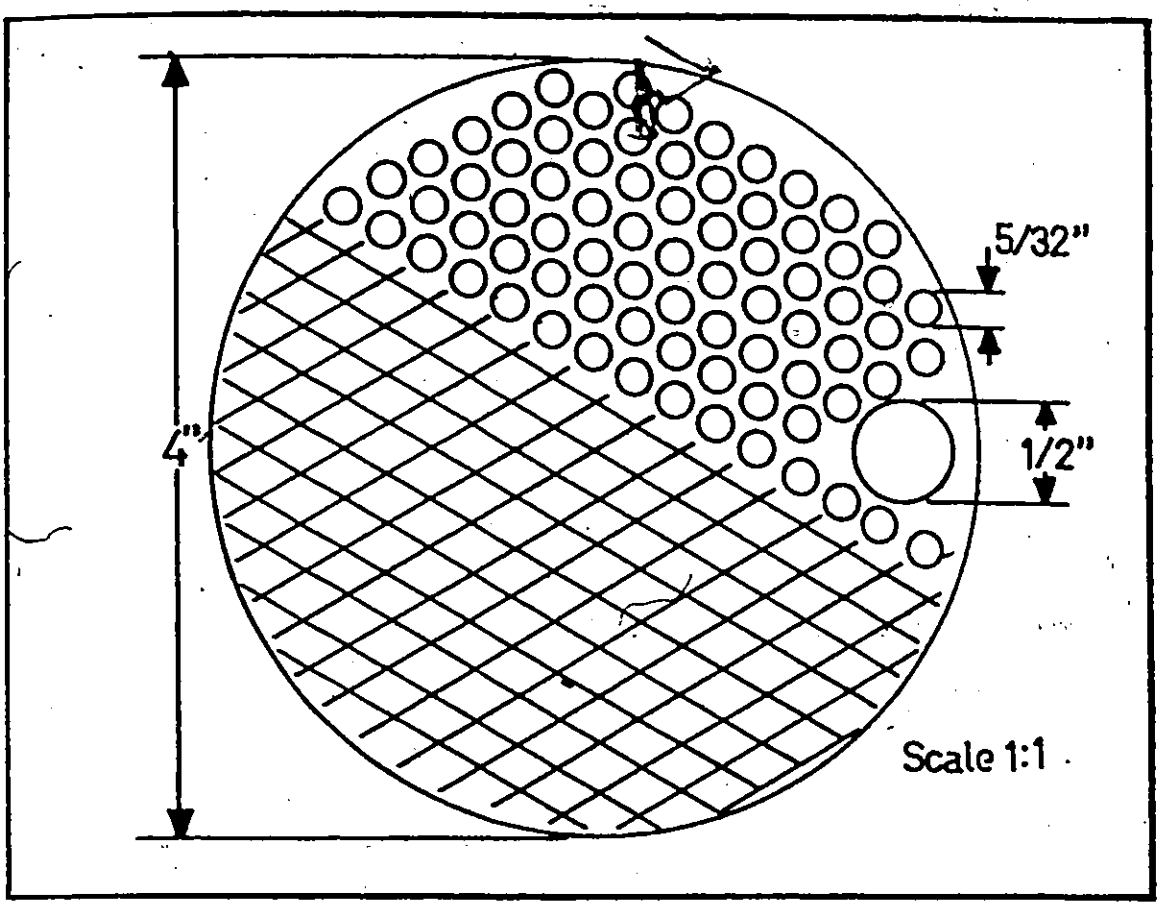

FIGURE A.9 Liquid distributor plate

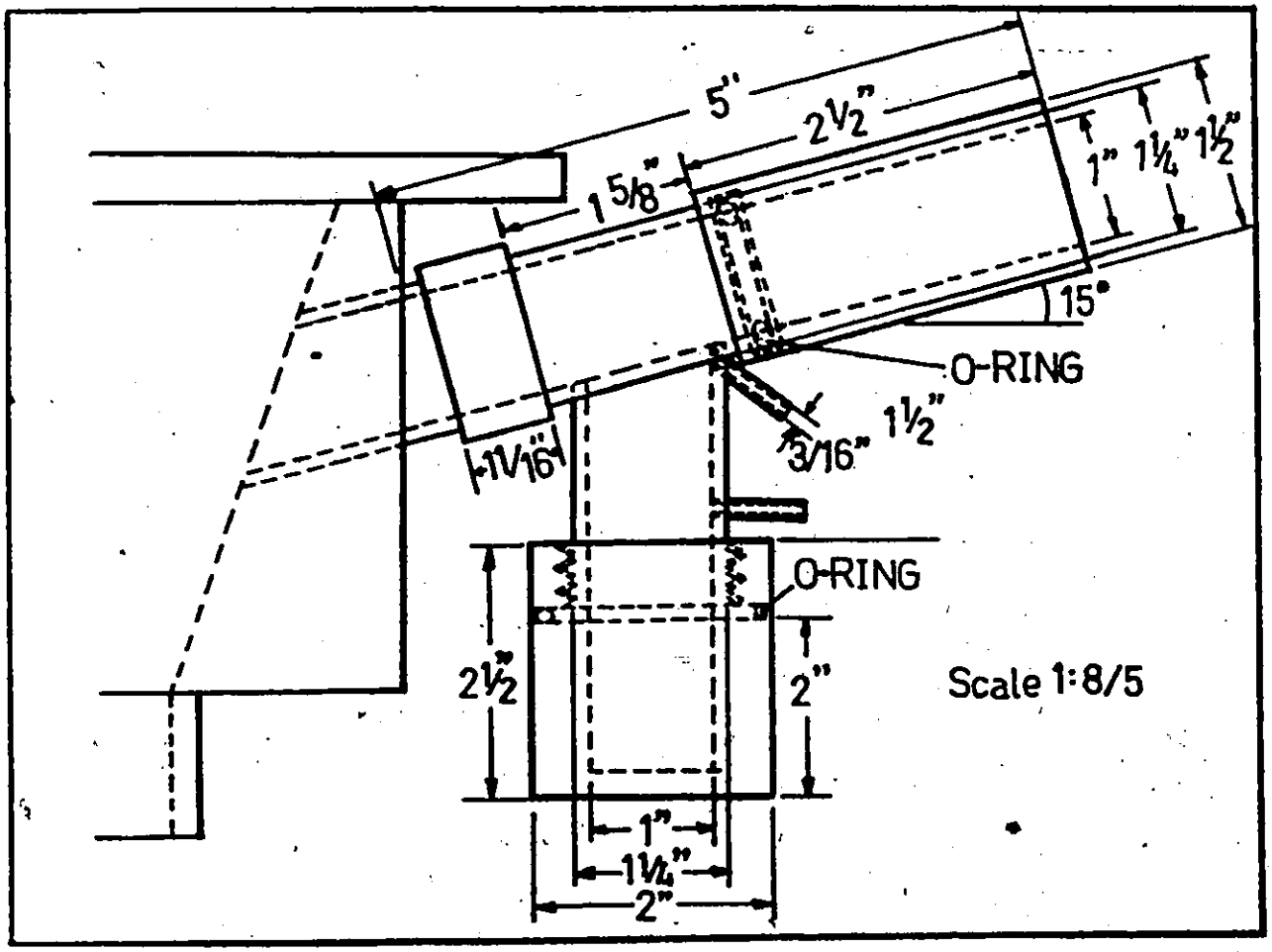

FIGURE A.10 Resin sampler

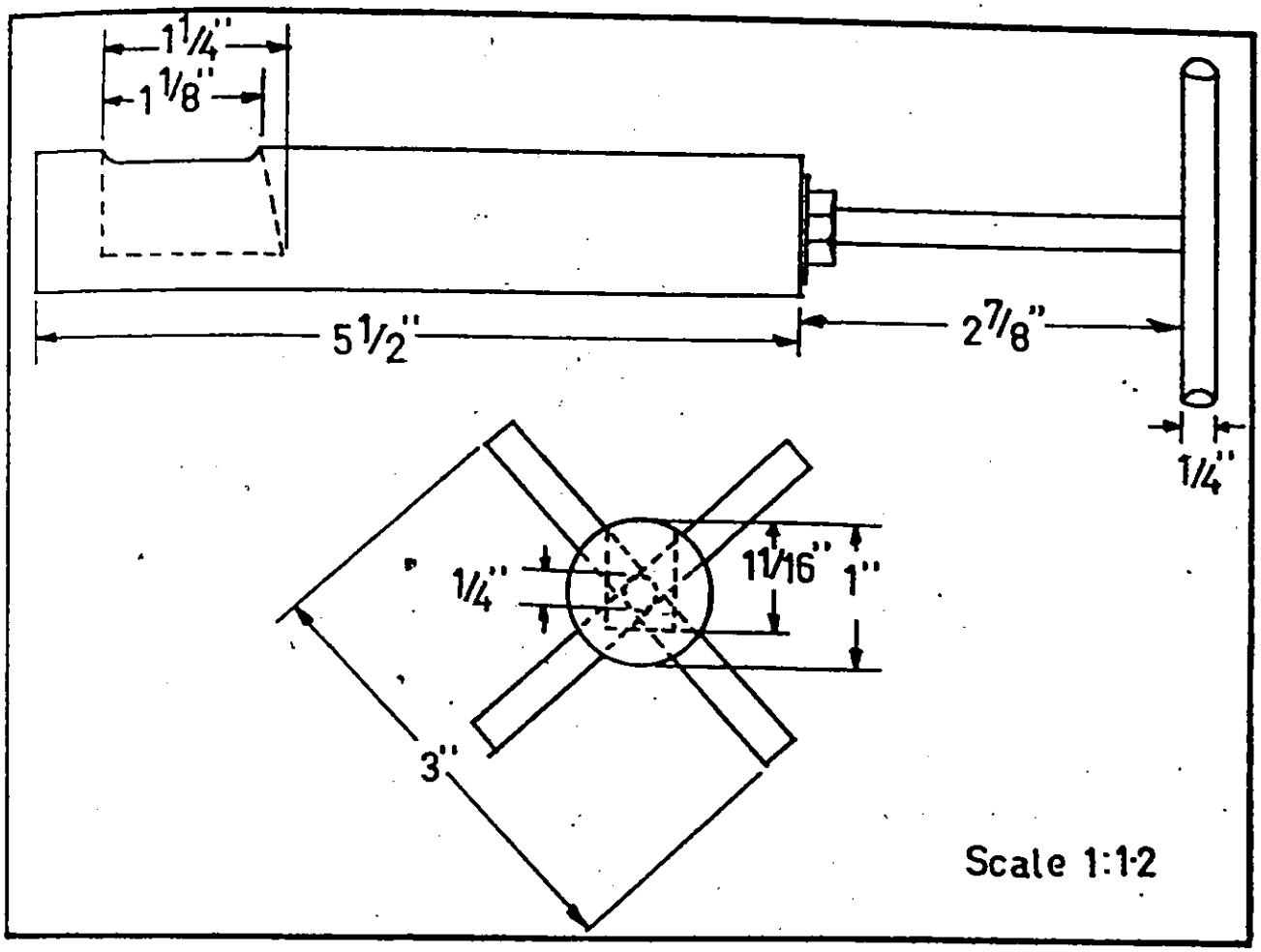

FIGURE A.11 Resin sampler's plunger

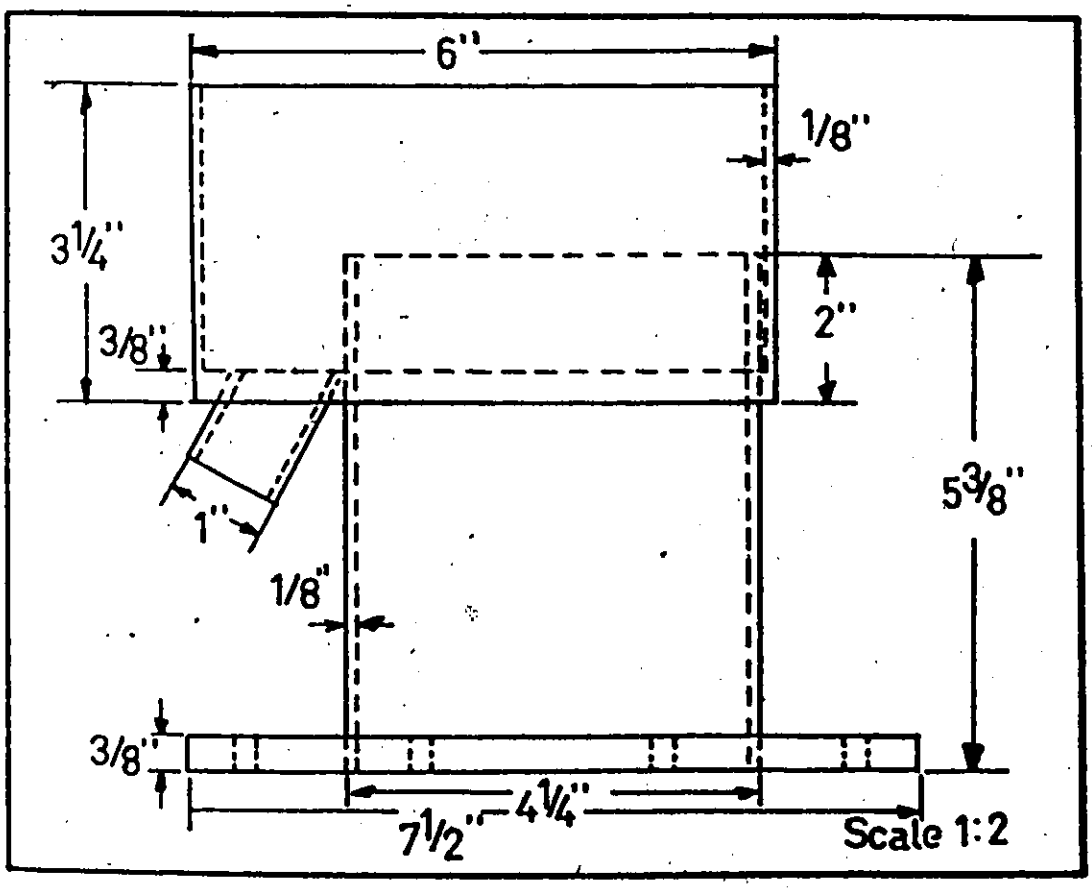

FIGURE A.12 Section I of ion-exchange column

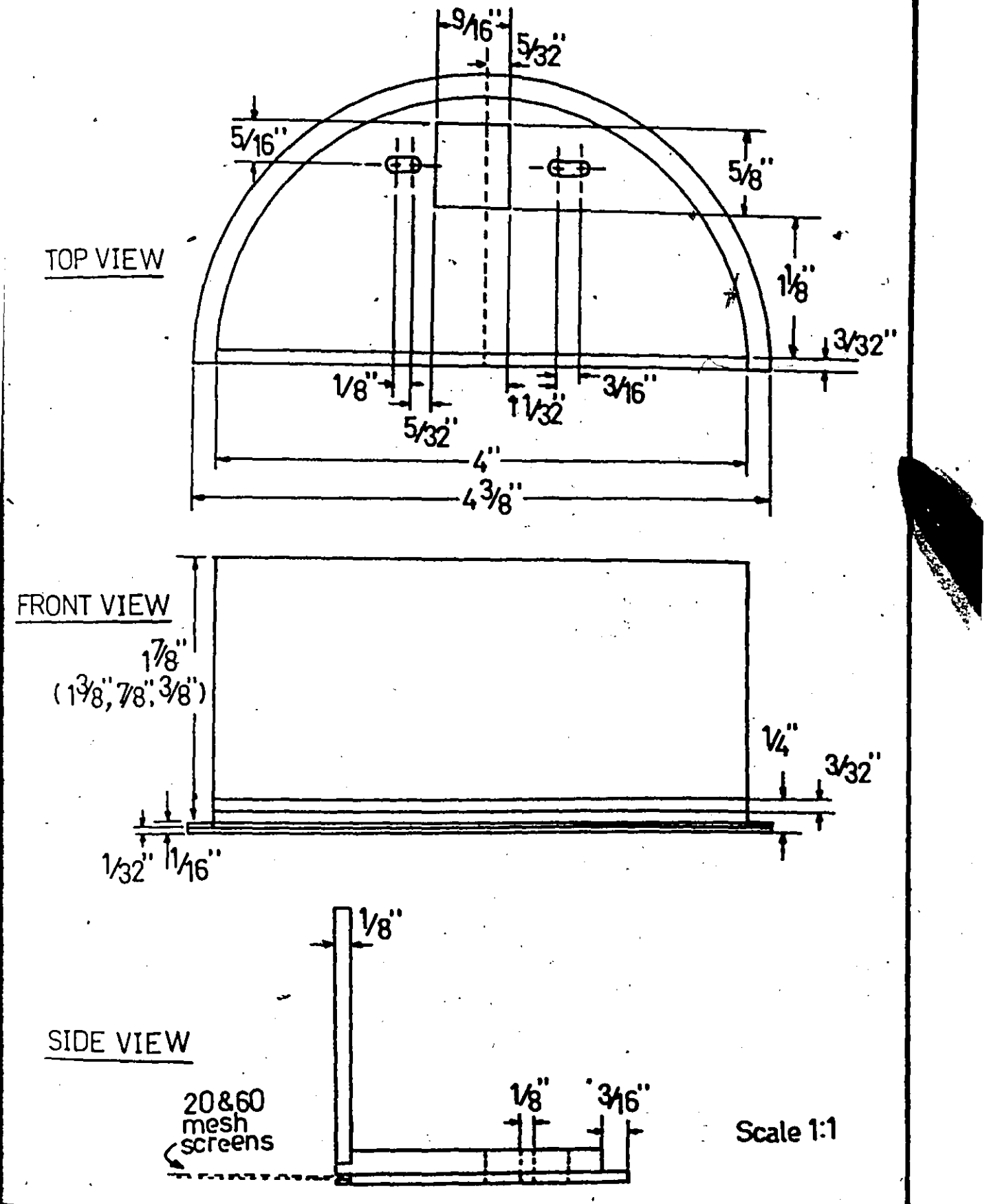

FIGURE A.13 Tray design with 4" straight weir

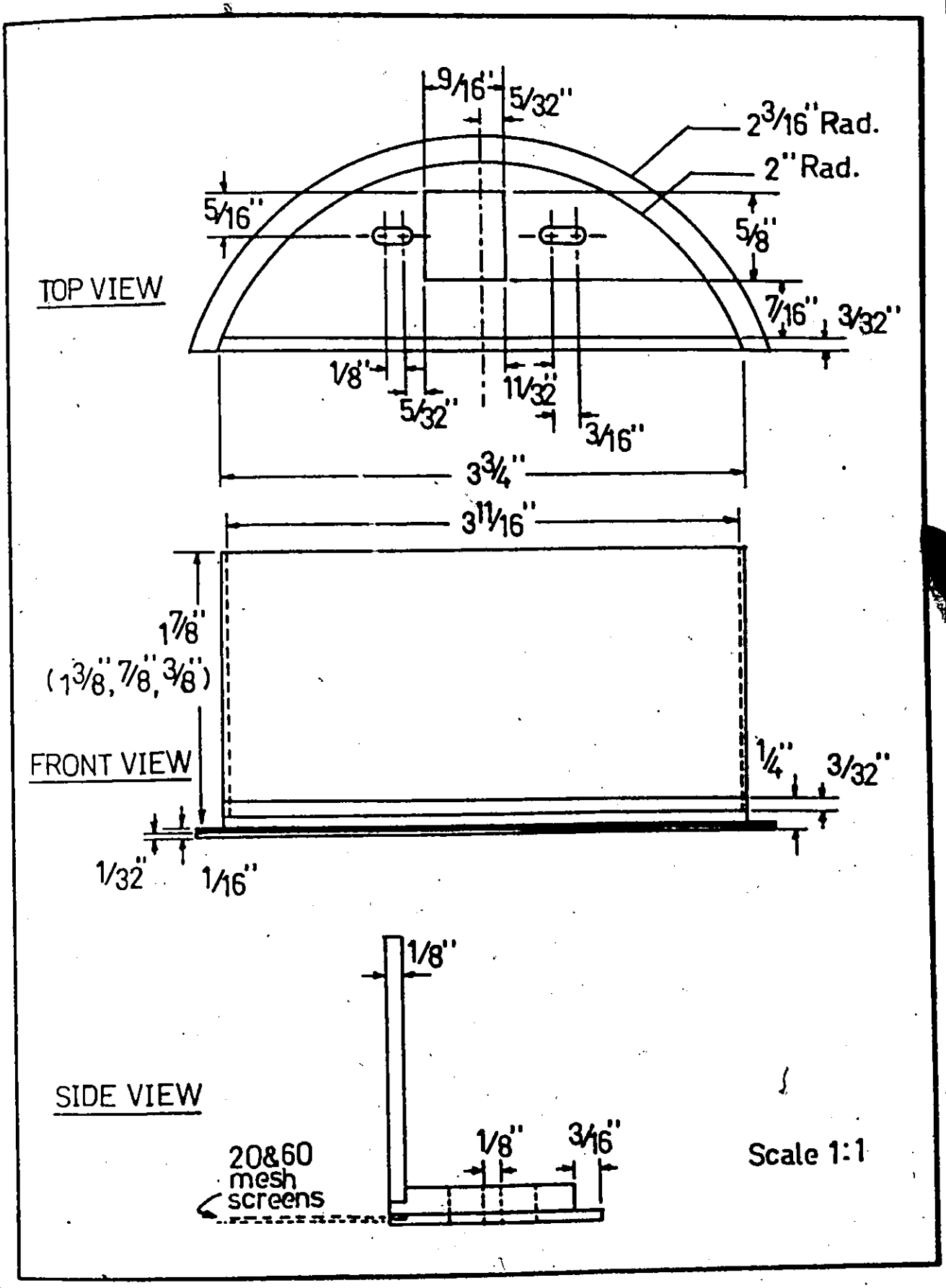

FIGURE A.14 Tray design with 3 3/4" straight weir

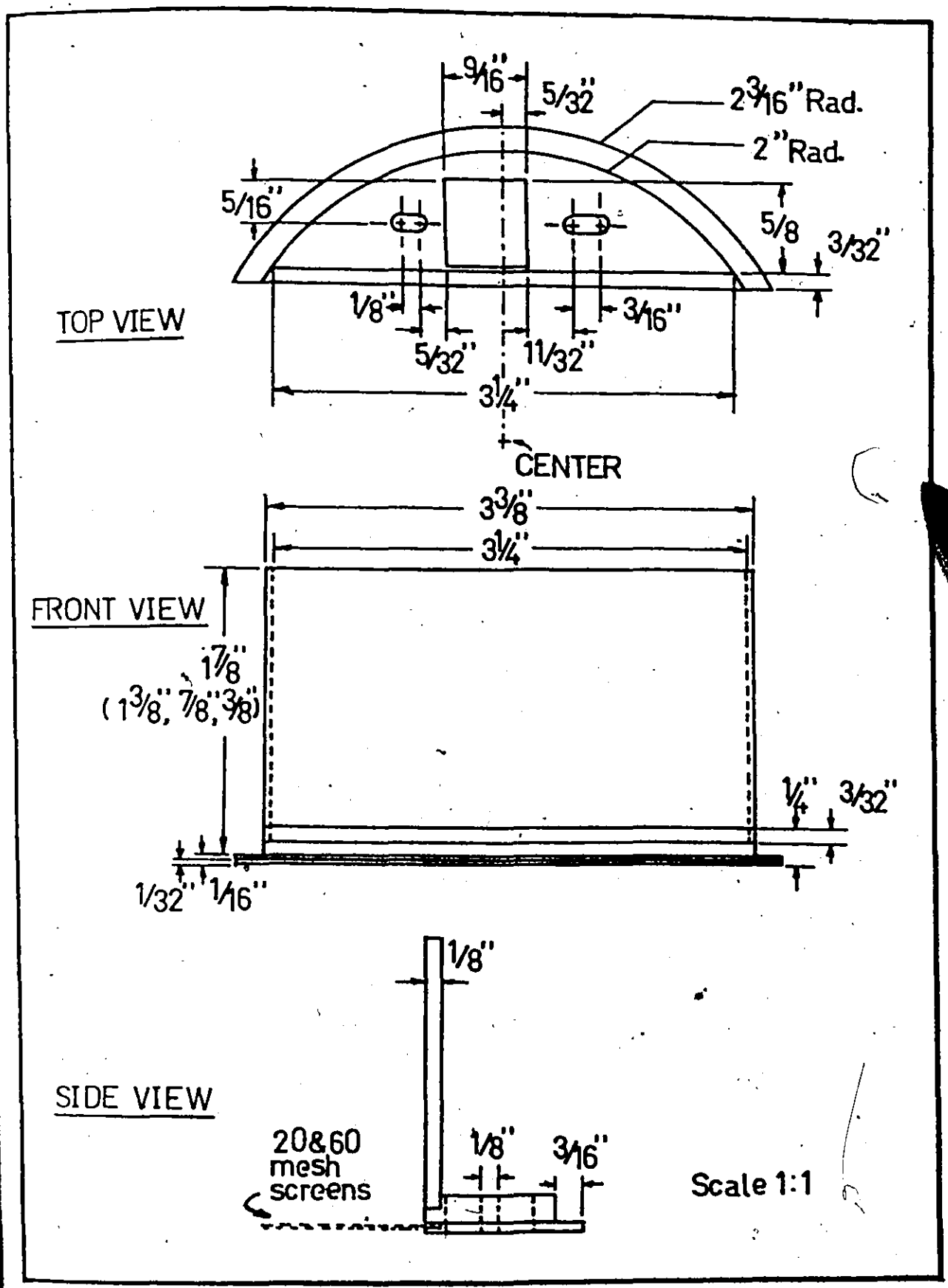

FIGURE A.15 Tray design with 3 1/4" straight weir

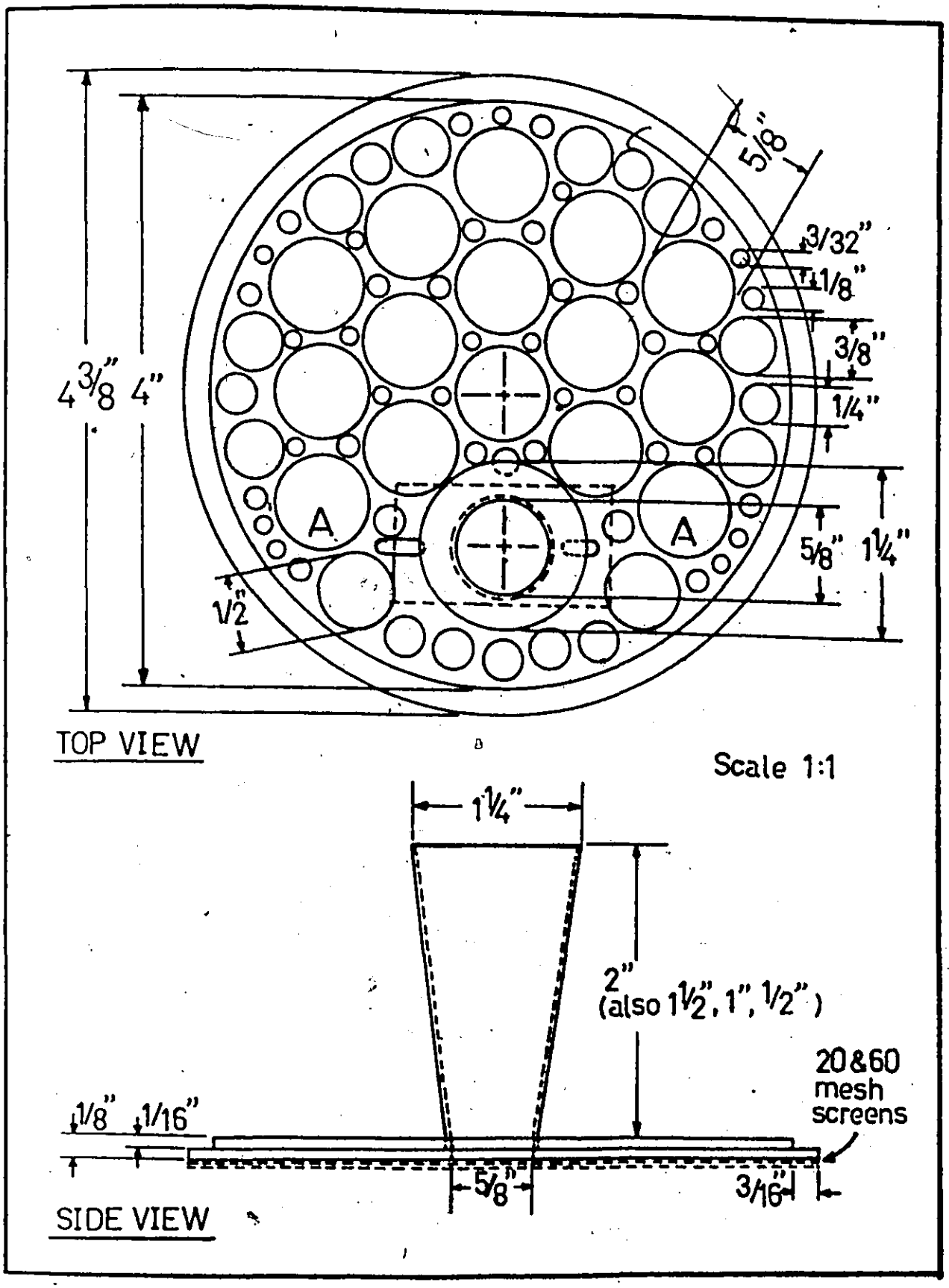

FIGURE A.16 Tray design with conical weir

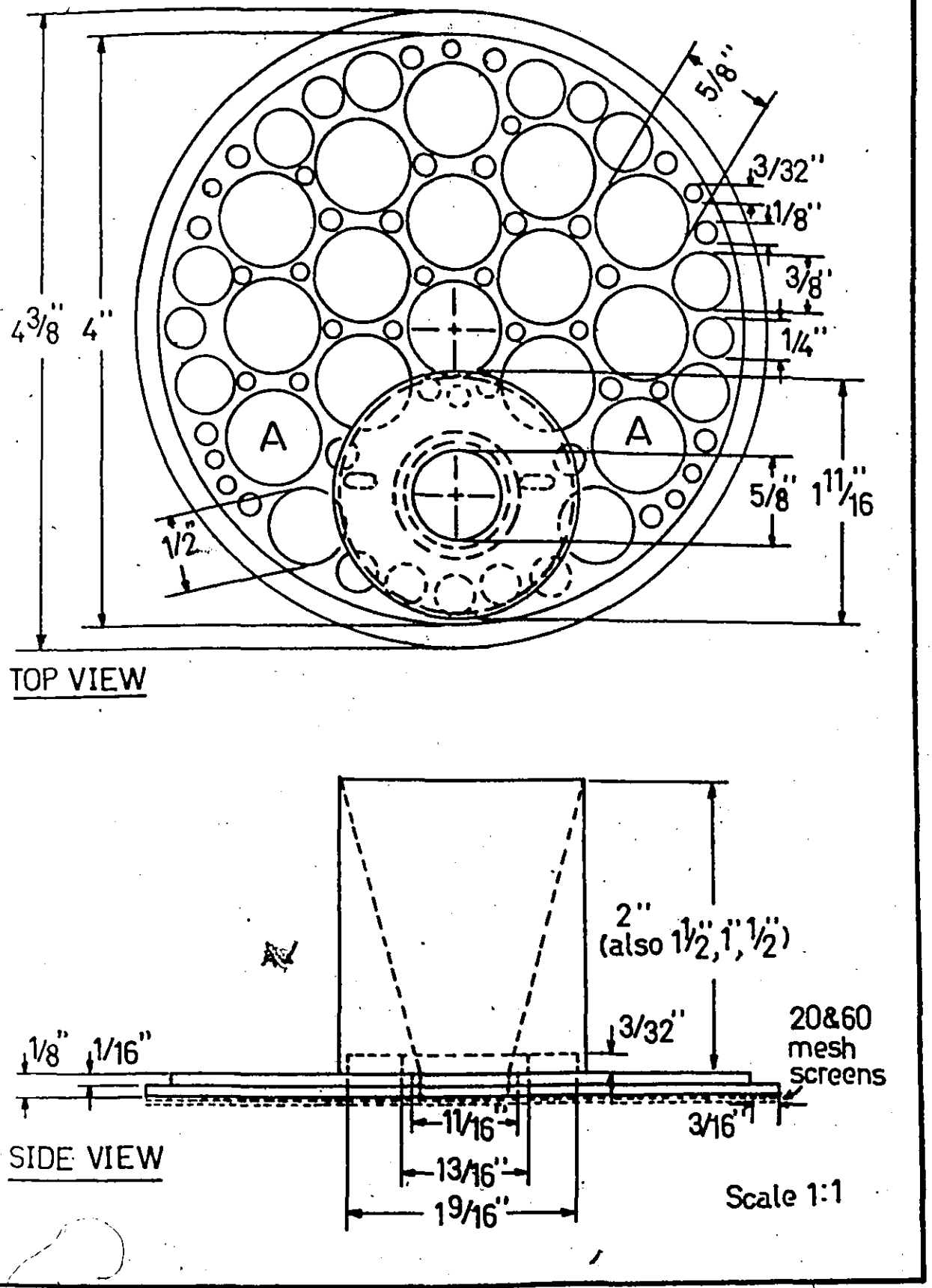

FIGURE A.17 Tray design with cylindrical weir

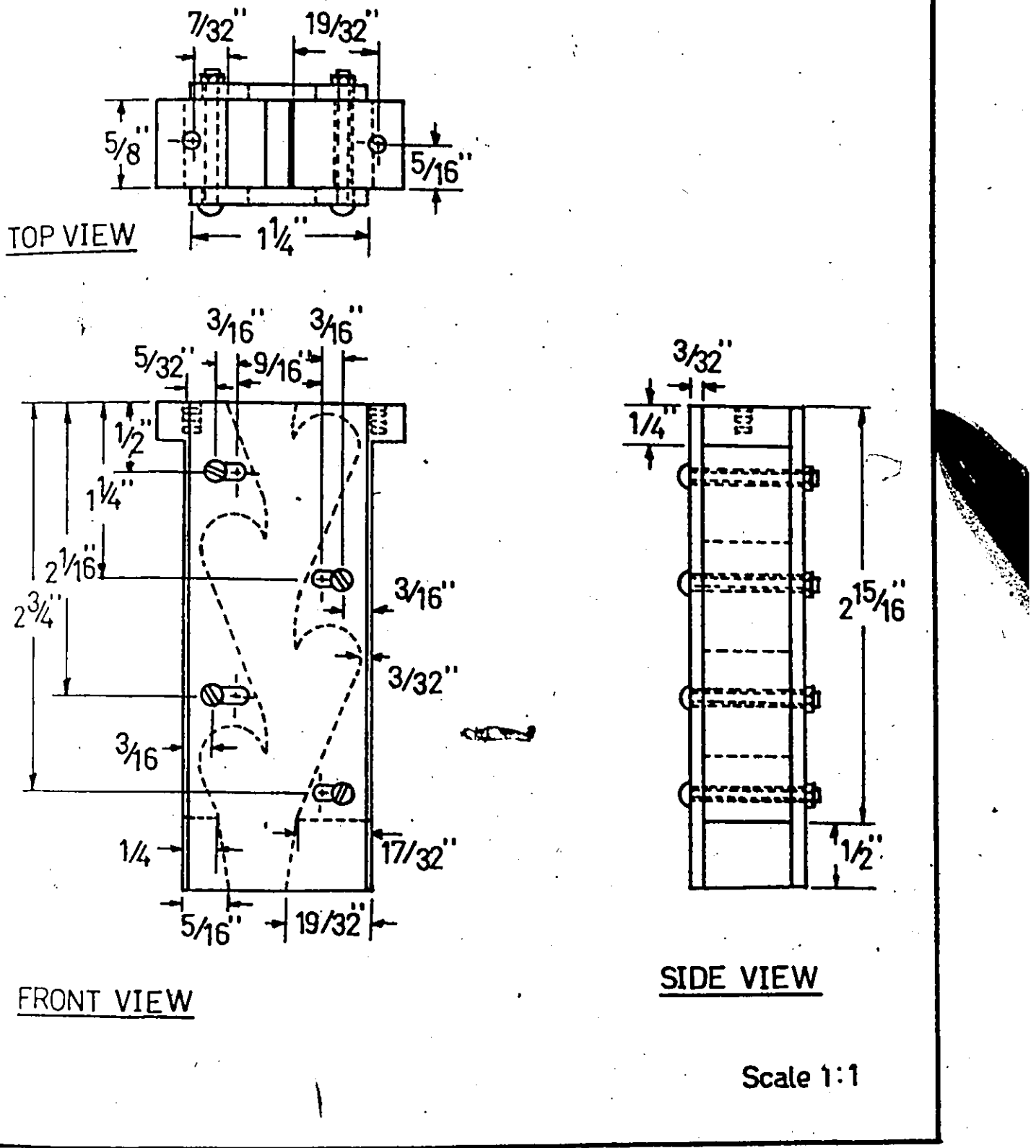

FIGURE A.18 Typical fluid-diode downcomer

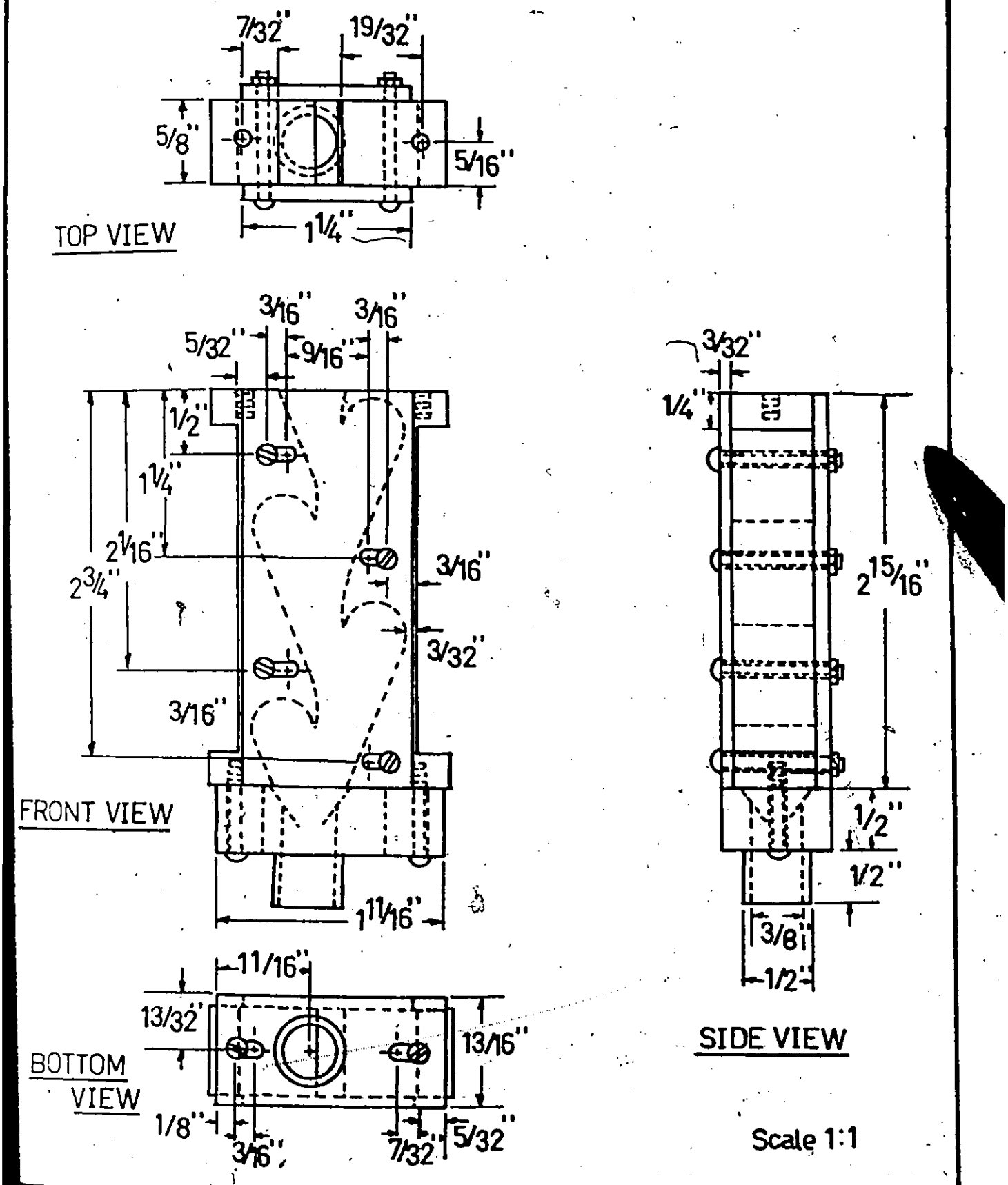

FIGURE A.19 Fluid-diode downcomer in section 6 of ion-exchange column

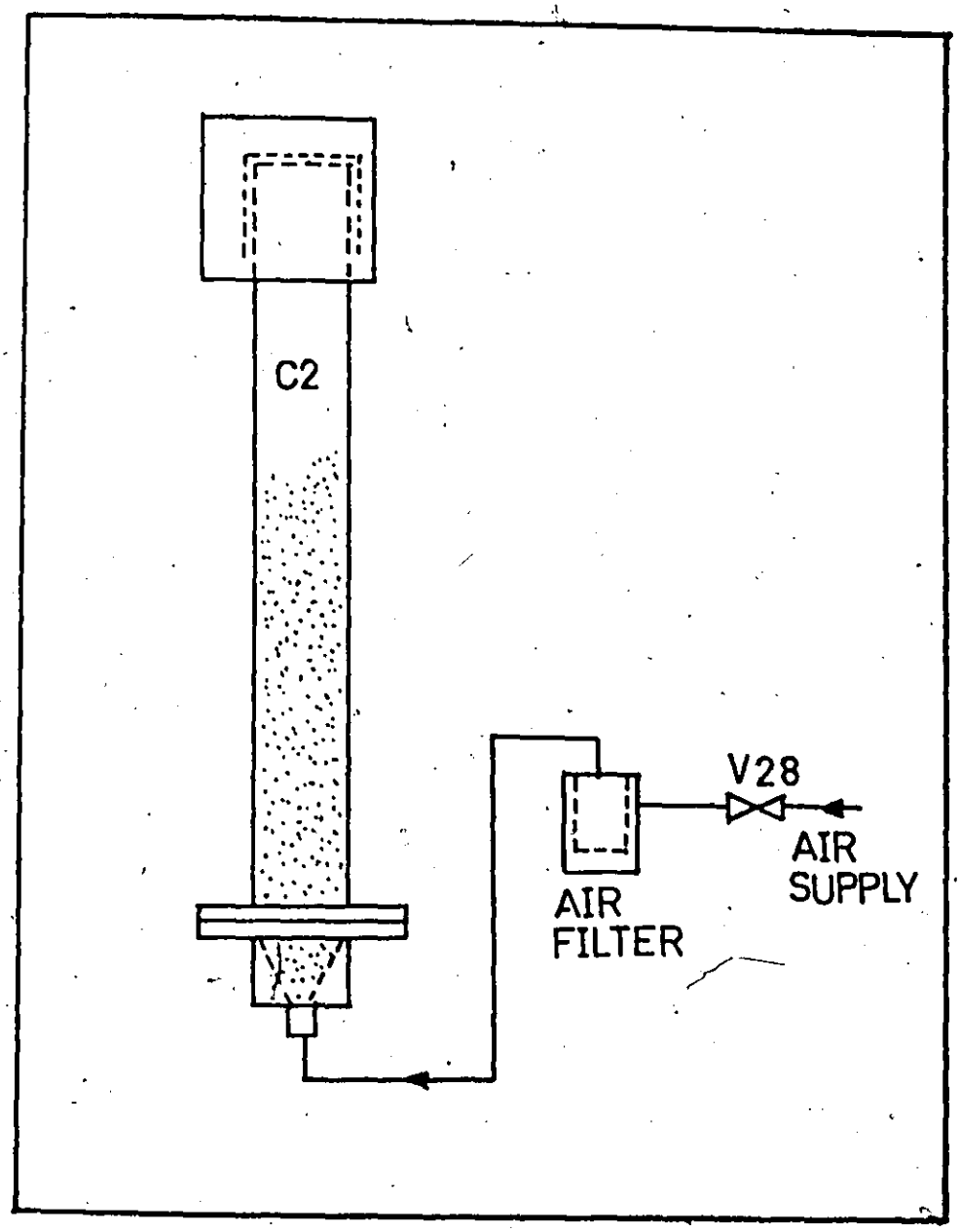

FIGURE A.20 Resin drying system

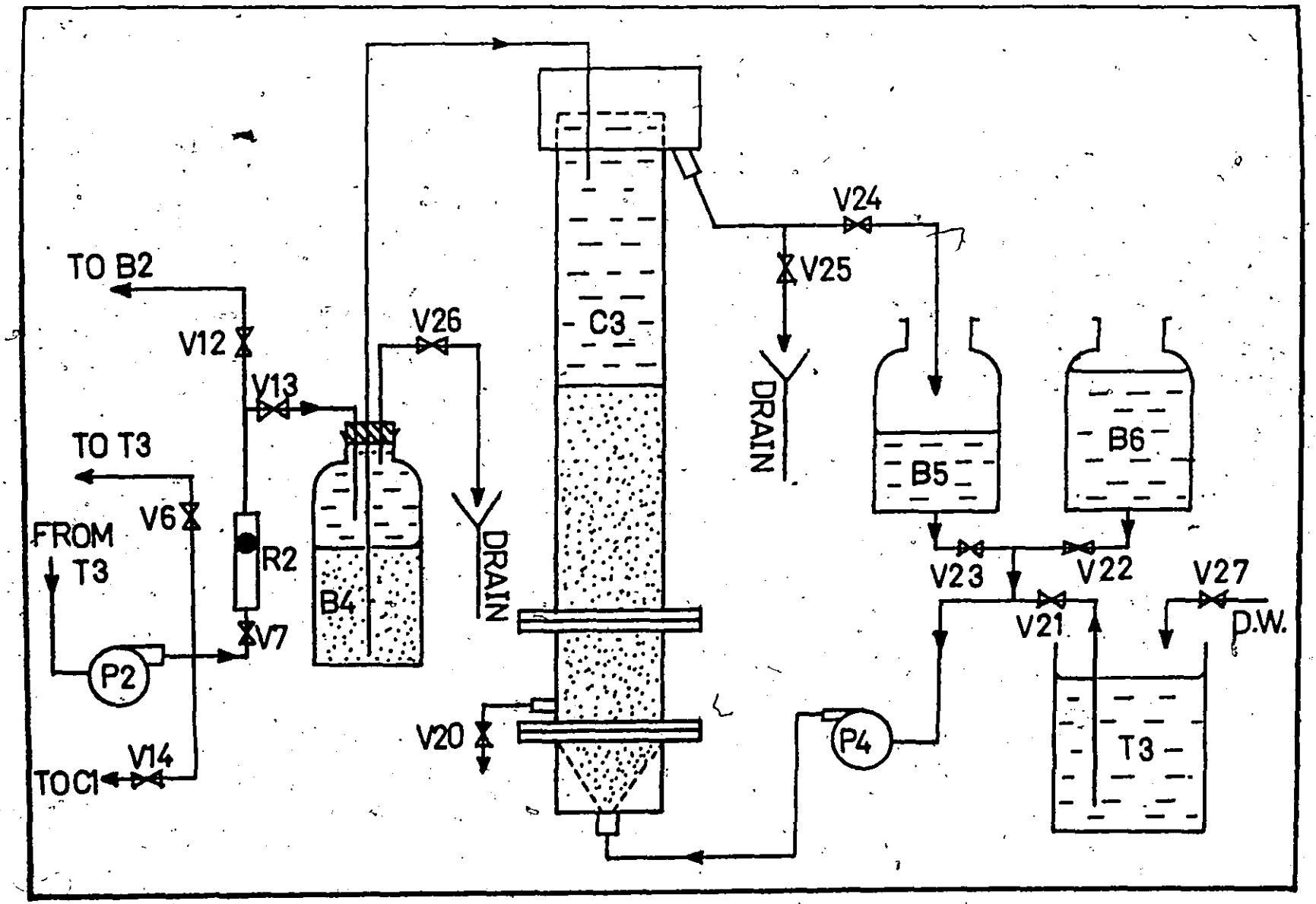

FIGURE A.21 Resin regeneration and washing system

APPENDIX B

Experimental Results

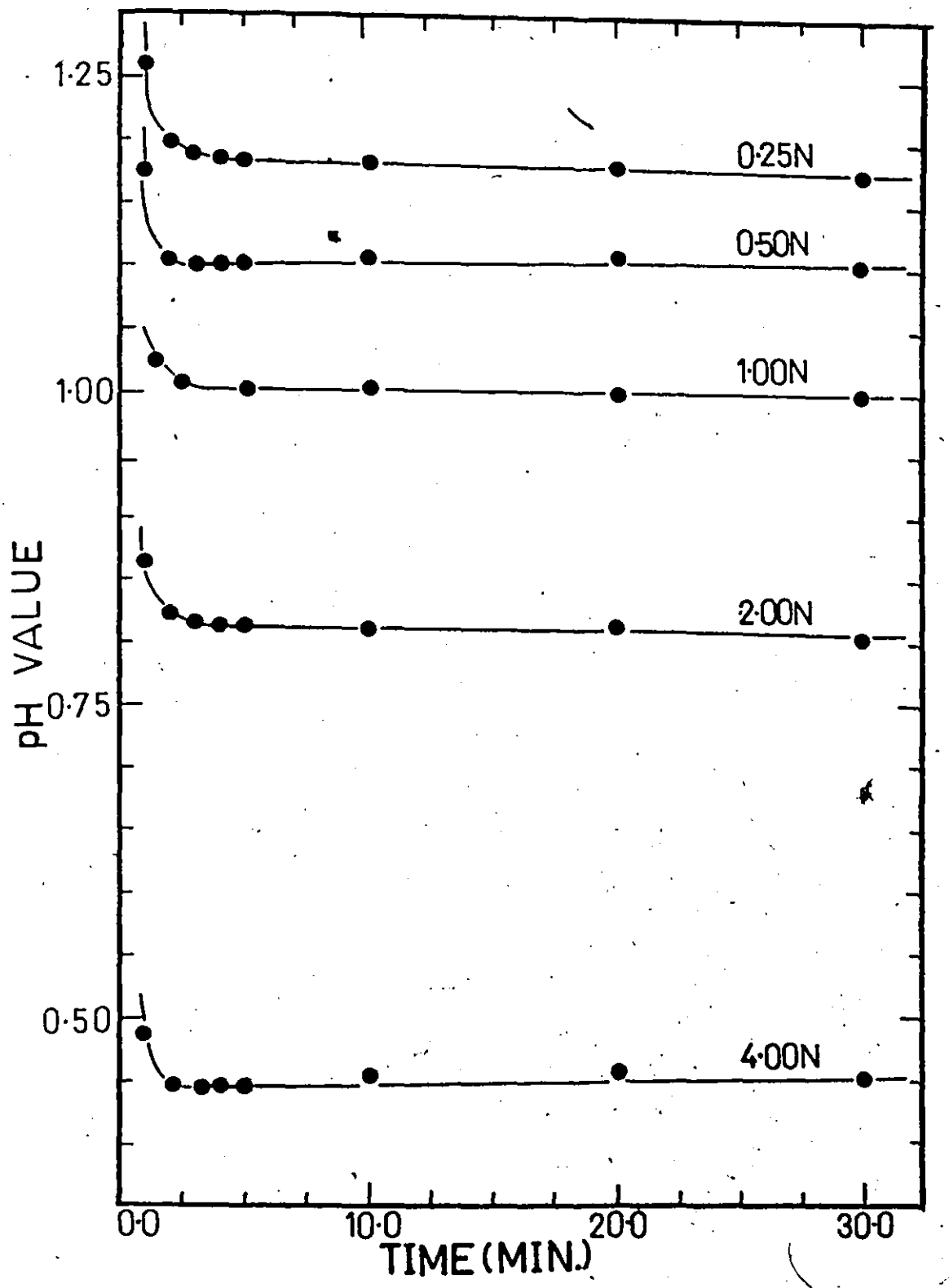

FIGURE 8.1 Change in the pH value of mixtures of resin and sodium chloride solution with time. 3 ml (bulk volume) samples of H^+ form resin was added to 100 ml NaCl solution of various concentrations.

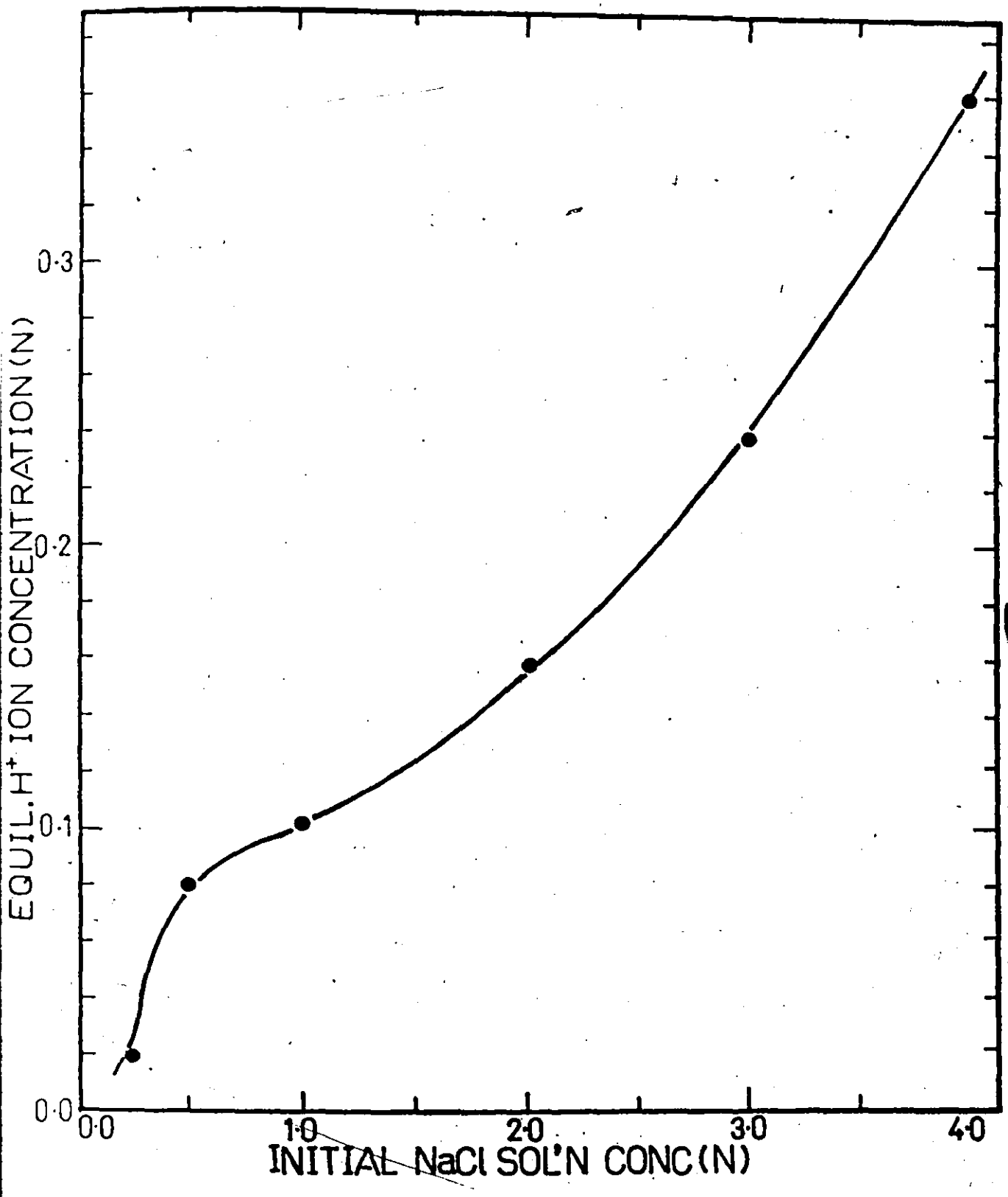

FIGURE B.2 Equilibrium hydrogen-ion concentration versus initial sodium-ion concentration in solution

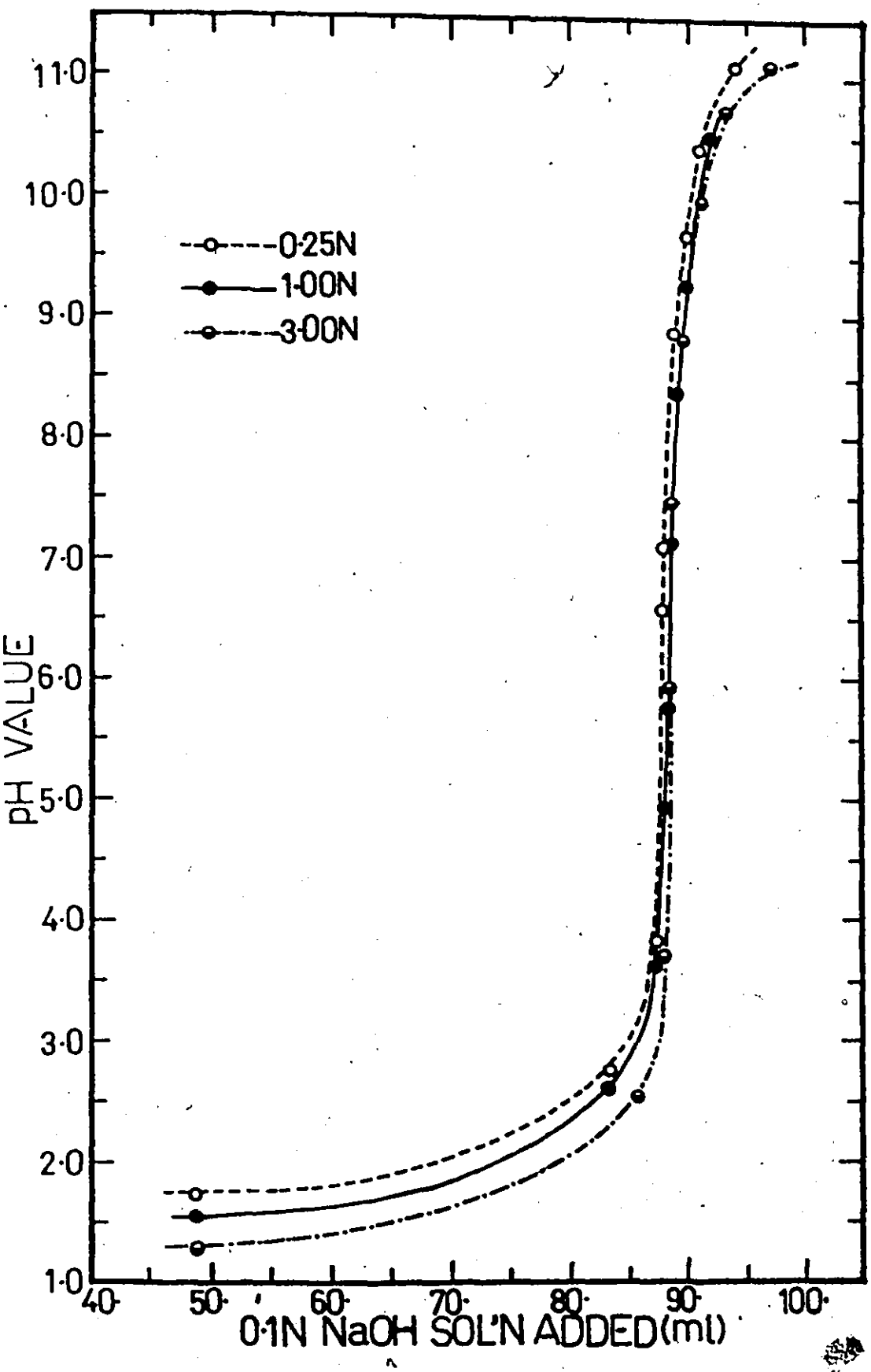

FIGURE B.3 Titration curves. 5 ml samples of H^+-form resin in 100 ml NaCl solutions of various concentrations

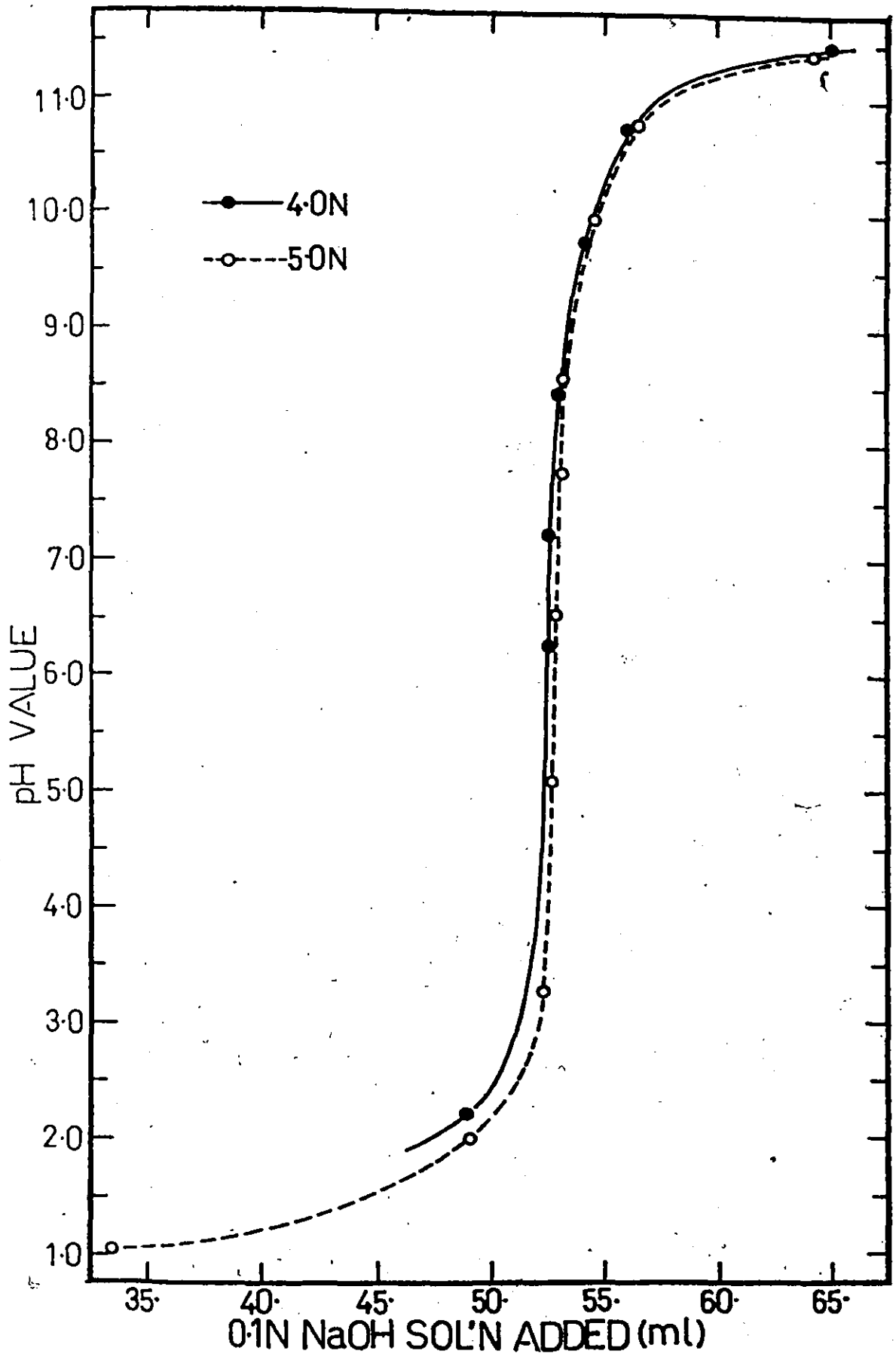

FIGURE B.4 Titration curves. 3 ml samples of H^+-form resin in 100 ml NaCl solutions of various concentrations

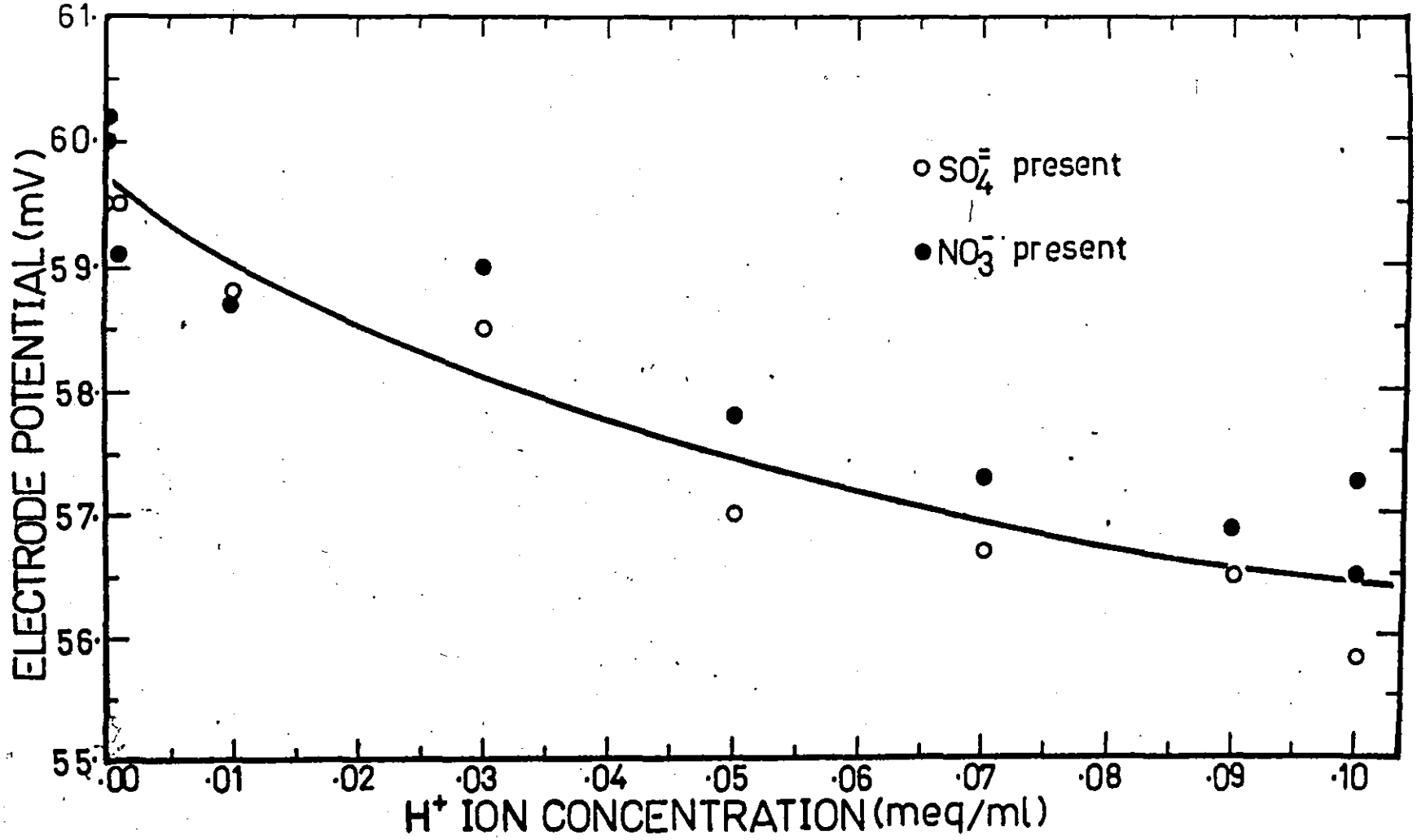

FIGURE B.5 Measured electrode potentials versus hydrogen-ion concentrations in solution

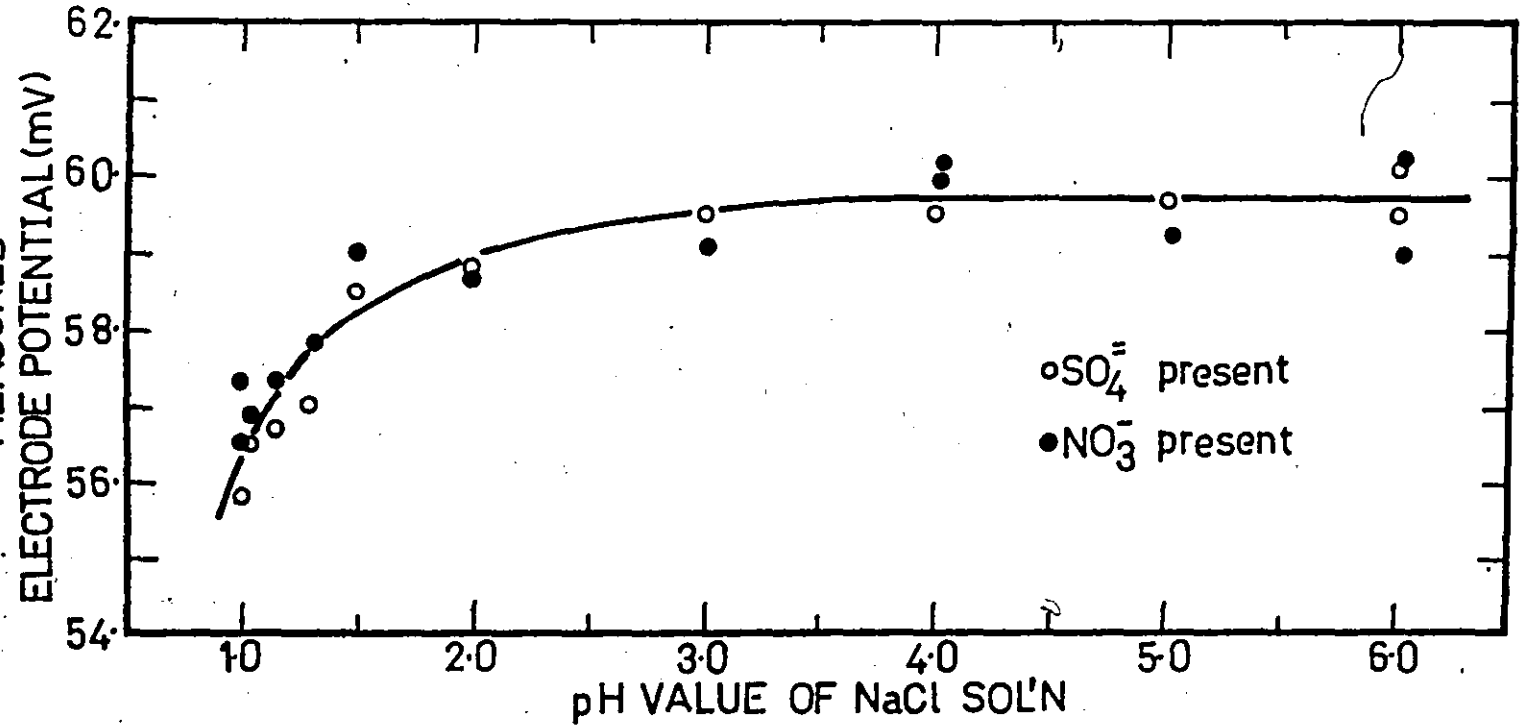

FIGURE B.6 Measured electrode potentials versus pH values of solution

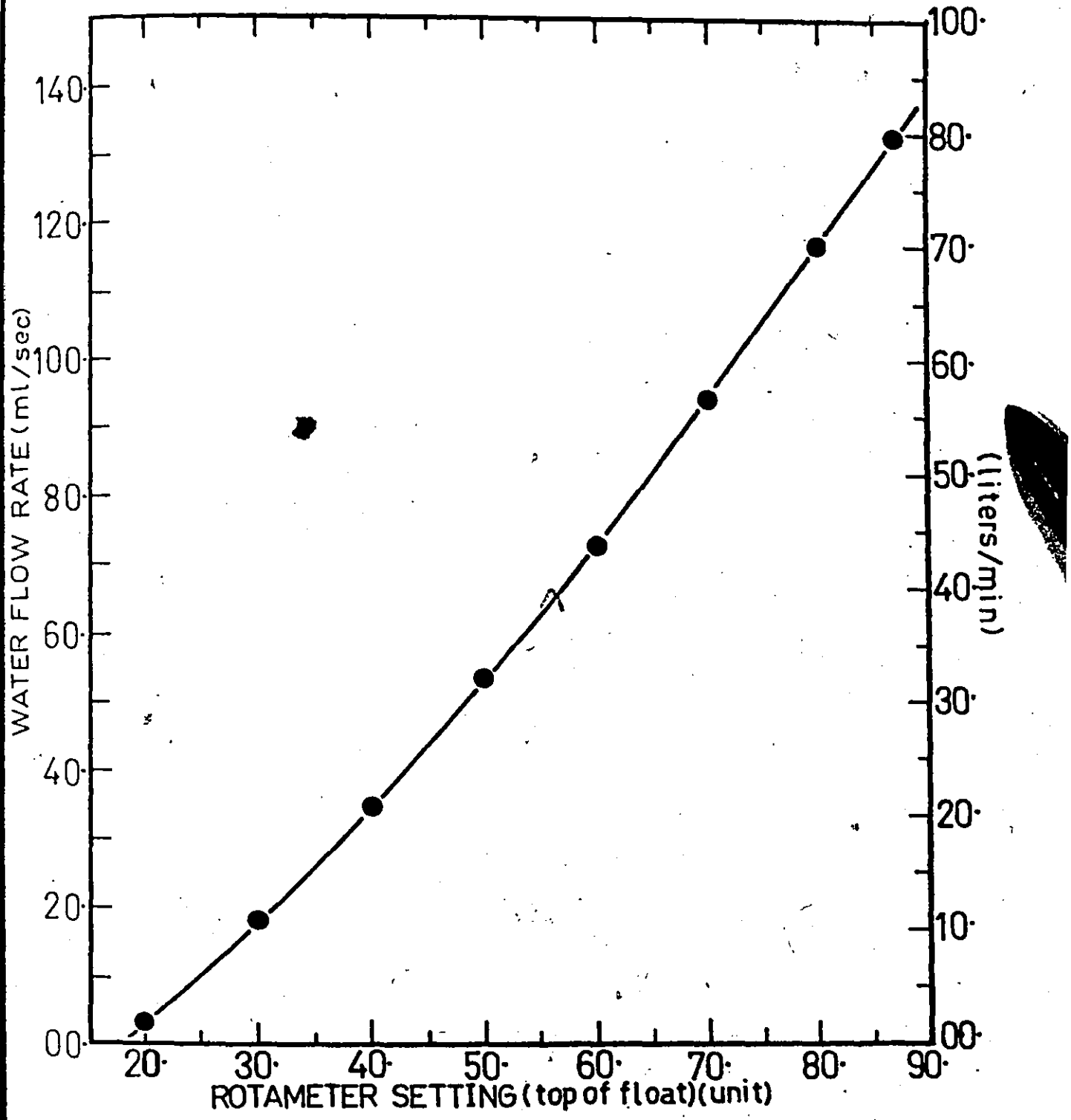

FIGURE B.7 Calibration curve of the rotameter for process solution feed

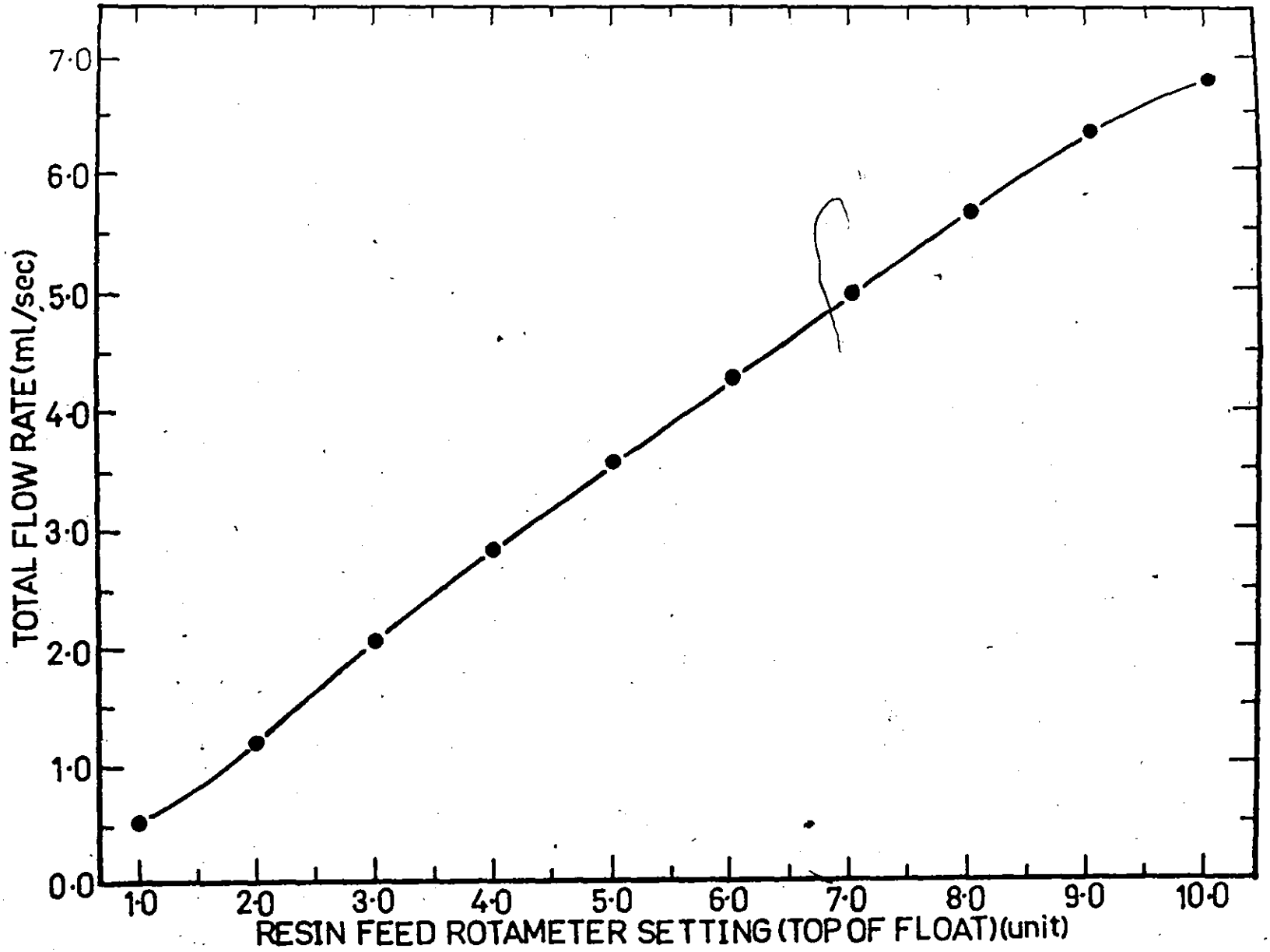

FIGURE B.8 Calibration curve of the rotameter for resin feed

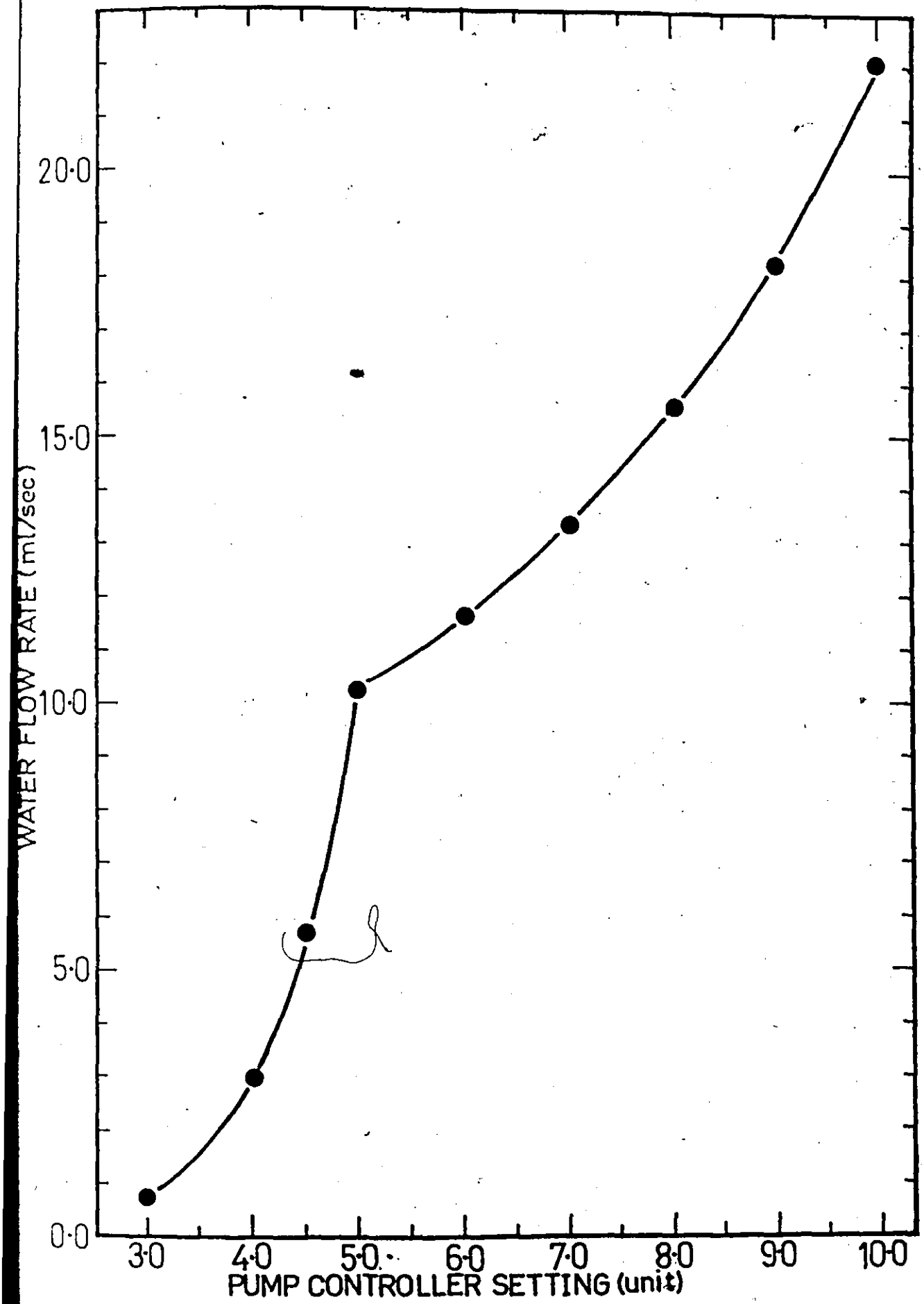

FIGURE 8.9 Calibration curve for Masterflex tubing pump's speed-controller

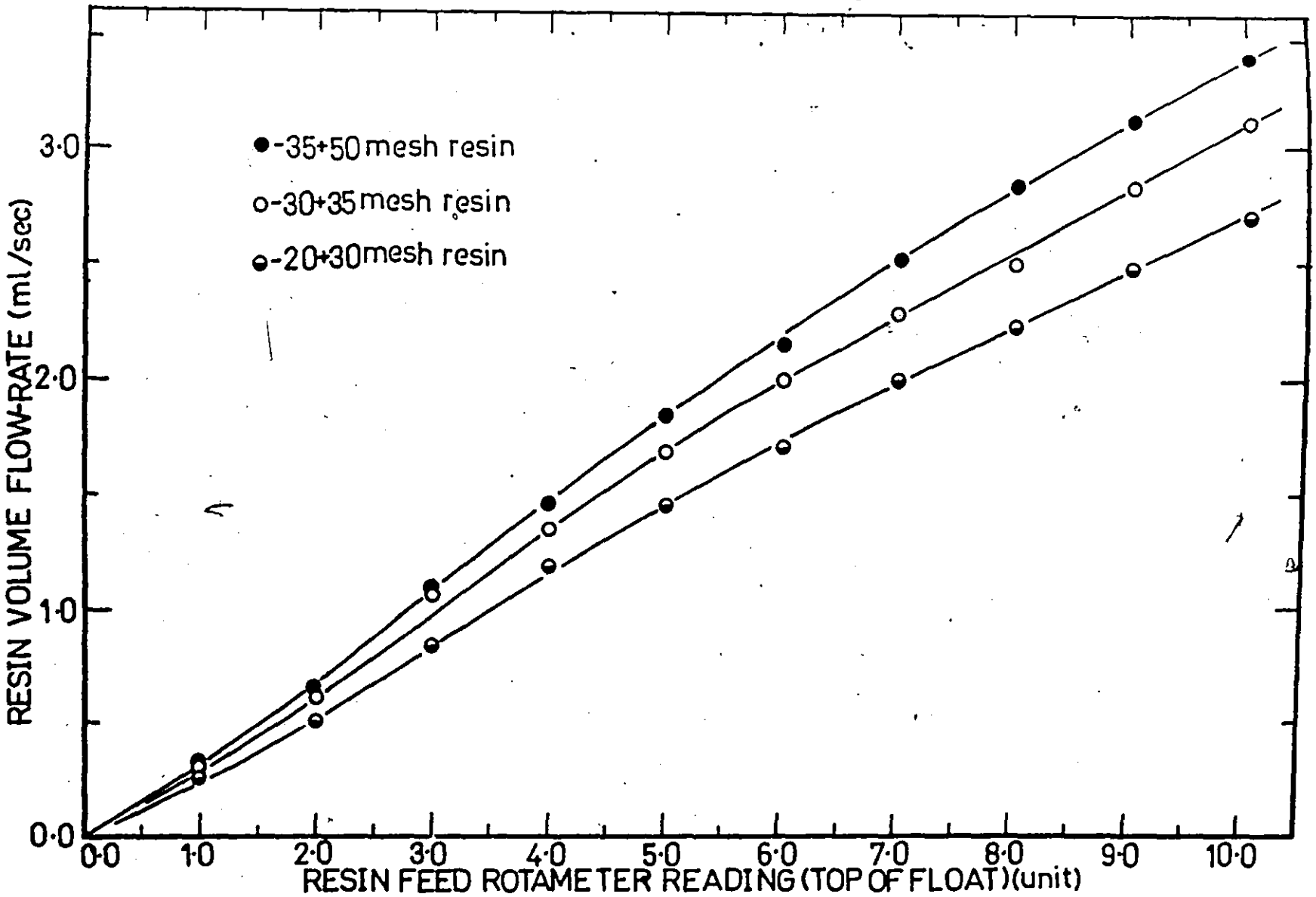

FIGURE B.10 Calibration curves for resin feed

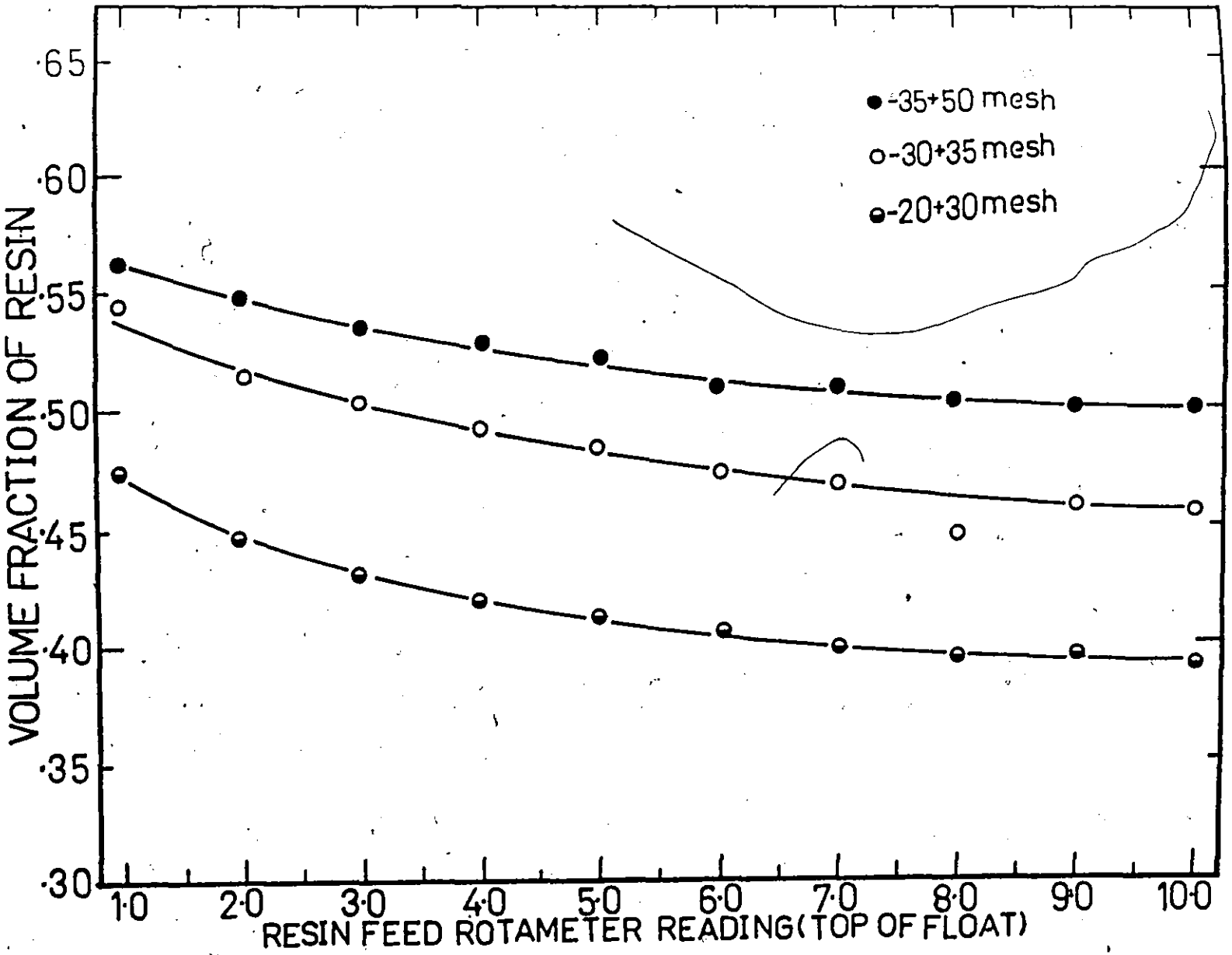

FIGURE B.11 Volume fraction of resin in feed versus resin-feed rotameter's reading

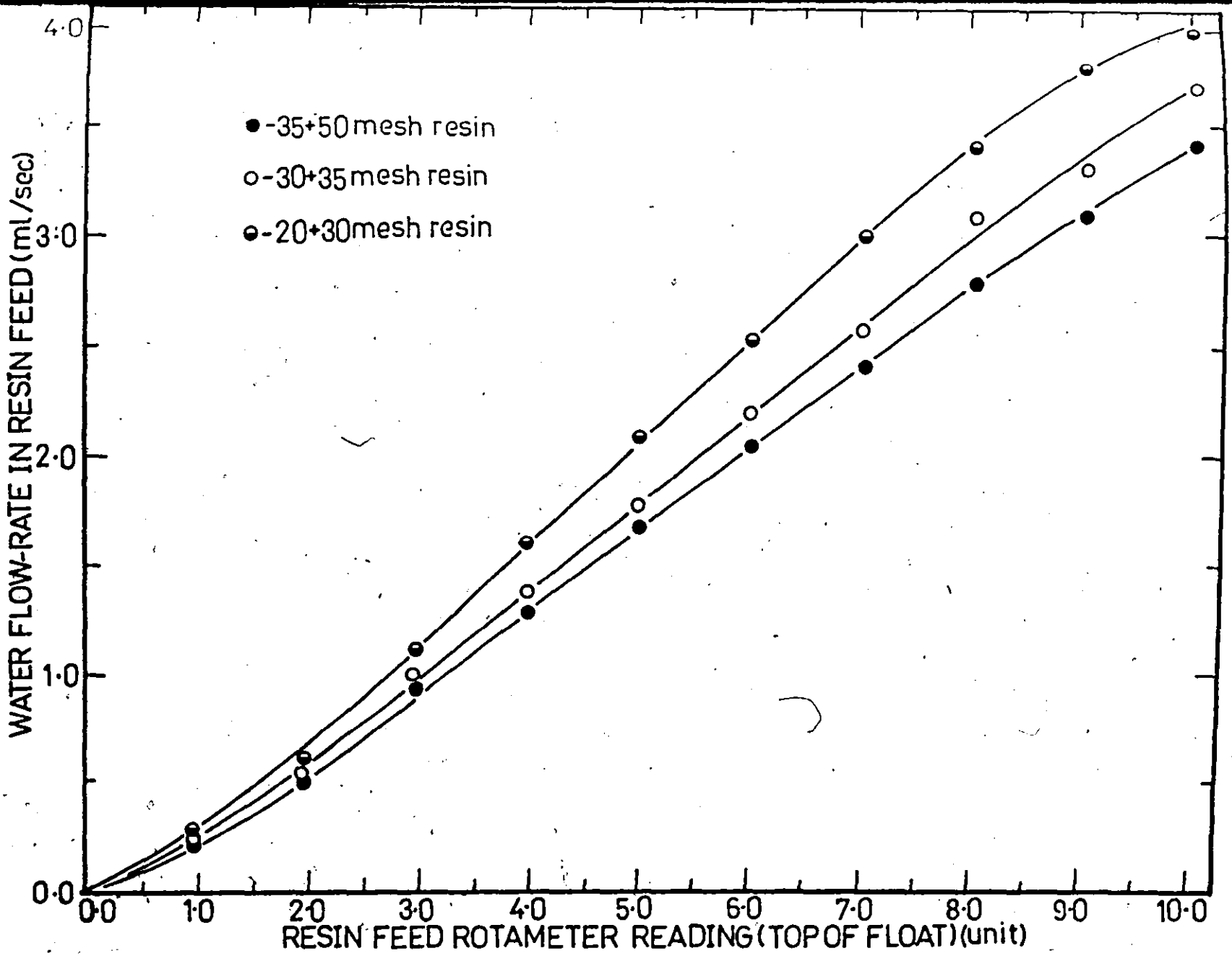

FIGURE B.12 Calibration curves for water flow in resin feed

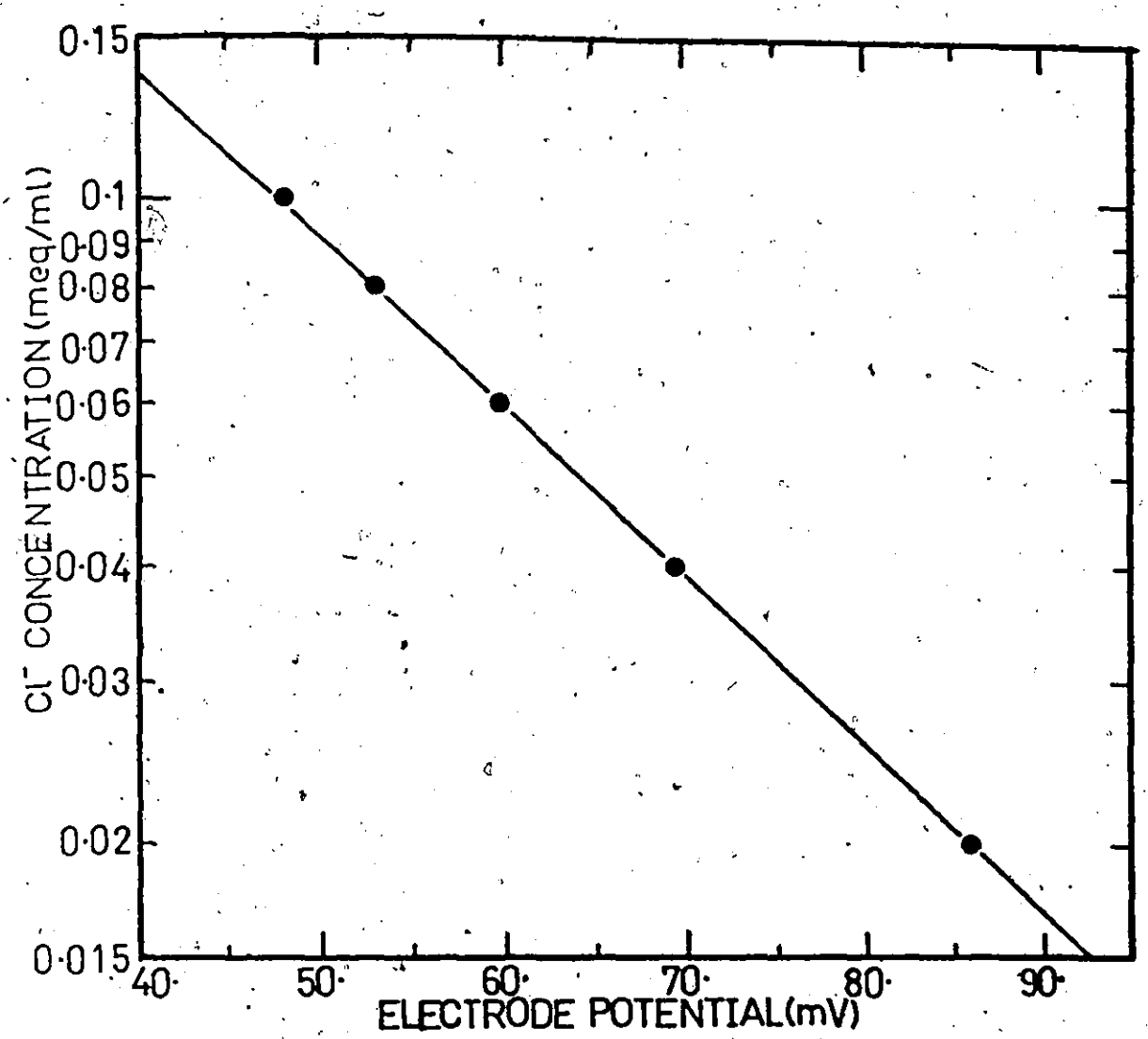

FIGURE B.13 Calibration curve for chloride-ion concentration measurements.

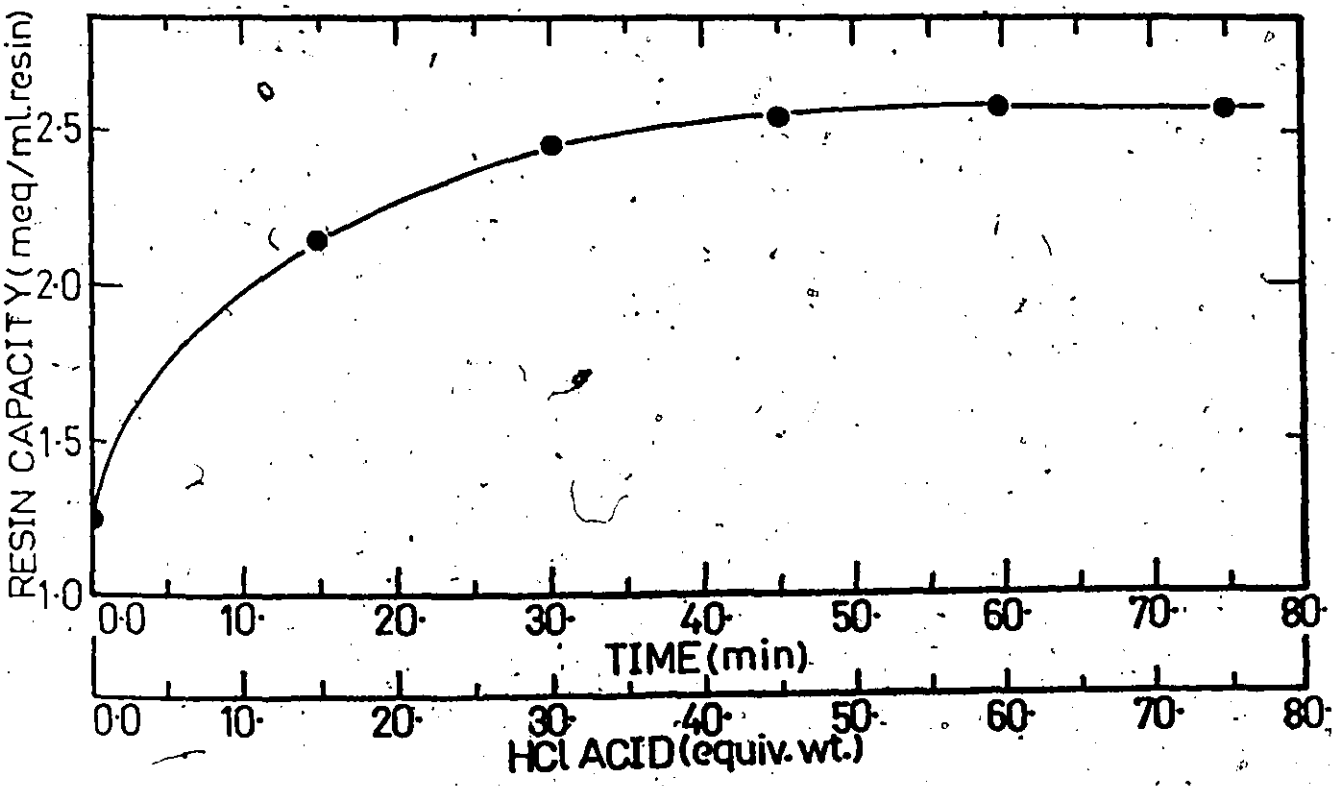

FIGURE B.14 Change in resin capacity during regeneration

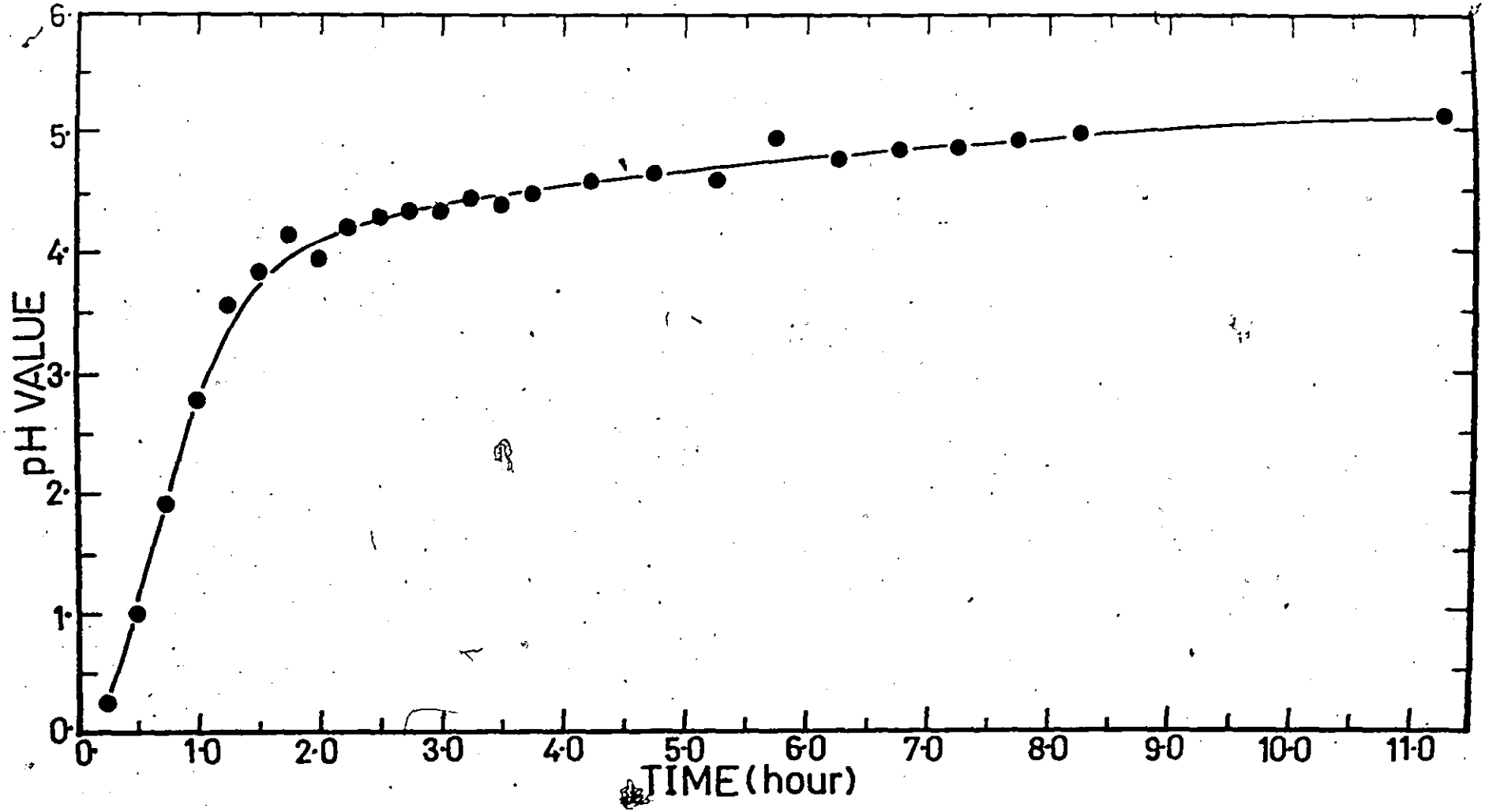

FIGURE B.15 Change in pH value of liquid effluent with time during resin washing

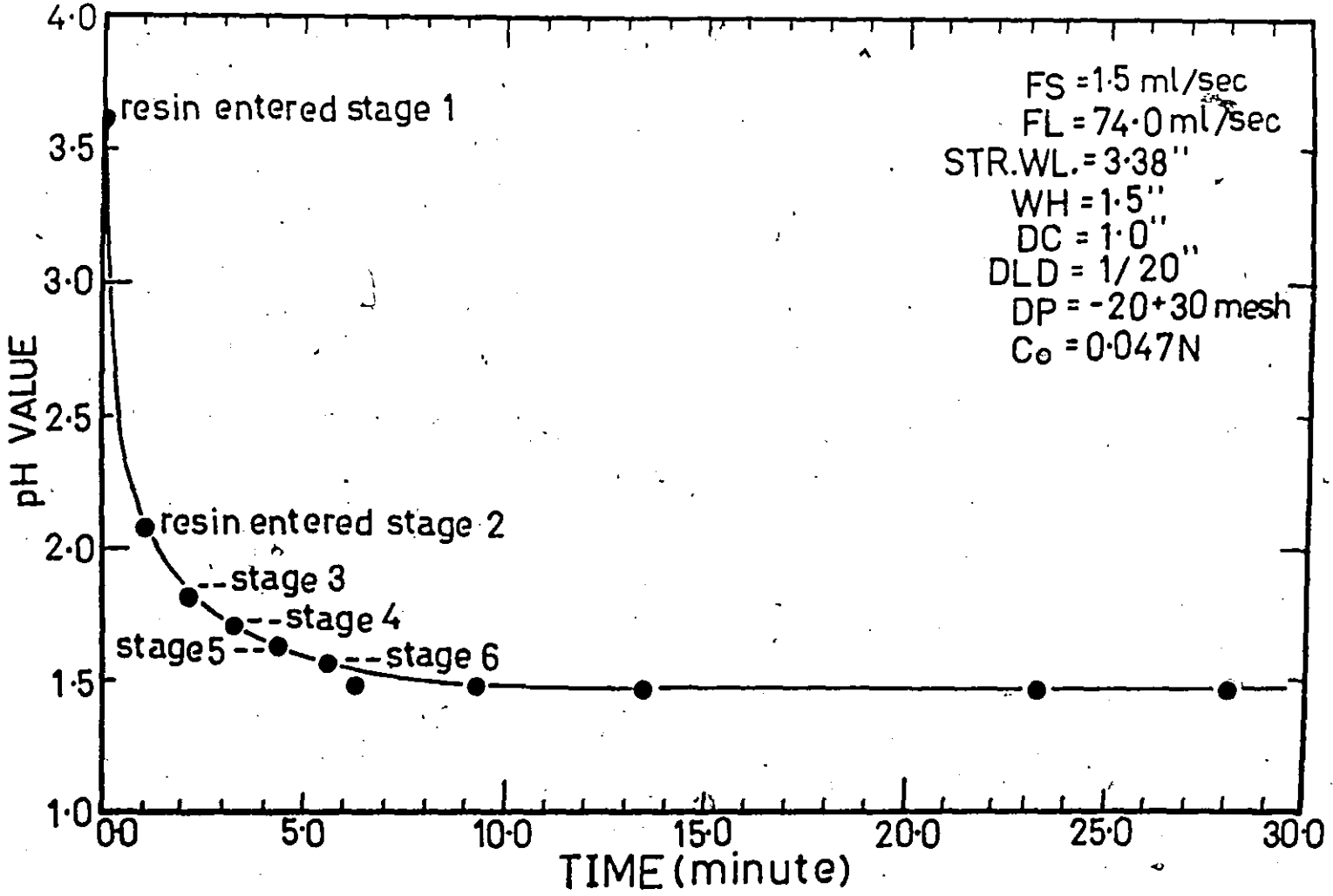

FIGURE-B.16 Change in the pH value of liquid effluent from the ion-exchange column as a function of time

	WEIR LENGTH = 3·38"				
	WH = 1"		WH = 2"		
	DLD = 1/20"	DLD = 3/20"	DLD = 1/20"	DLD = 3/20"	
FS	≤ 34·stagn. < 53·p.mob.	< 24·stagn. ≤ 53·p.mob.	≤ 18·stagn. < 24·p.mob.	≤ 24·stagn. < 34·p.mob.	
0·6 ml/sec	FL = 53·–120·	53·–120·	FL = 24·–120·	34·–120·	'perfect'
2·25 ml/sec	≤ 18·stagn. < 53·p.mob.	< 18·stagn. < 53·p.mob.	≤ 34·d.flood. < 44·p.mob.	≤ 34·d.flood. < 44·p.mob.	
	FL = 53·–106·	53·–106·	FL = 44·–106·	44·–106·	'perfect'
	> 106·o.fluid.	> 106·o.flui.	> 106·o.fluid.	> 106·o.fluid.	

-20+30 mesh resin

	WEIR LENGTH = 3·97"				
	WH = 1·"		WH = 2·"		
	DLD = 1/20"	DLD = 3/20"	DLD = 1/20"	DLD = 3/20"	
FS	≤ 18·stagn. < 26·p.mob.	≤ 18·stagn. < 26·p.mob.	≤ 12·stagn. < 24·p.mob.	≤ 18·stagn. < 24·p.mob.	
0·6 ml/sec	FL = 26·–94·	26·–94·	FL = 24·–63·	24·–73·	'perfect'
	> 94·o.fluid.	> 94·cyc.	> 63·cyc. ≥ 83·d.flood.	> 73·cyc.	
2·25 ml/sec	≤ 10·stagn. < 18·p.mob.	≤ 10·stagn. < 18·p.mob.	≤ 34·d.flood. < 44·p.mob.	≤ 18·stagn. < 44·p.mob.	
	FL = 18·–94·	18·–94·	FL = 44·–83·	44·–83·	'perfect'
	> 94·o.fluid.	> 94·	> 83·o.fluid.	> 83·o.fluid.	

TABLE B.I Operational behaviour of the ion-exchange column at different liquid flow-rates (-20+30 mesh resin used). In each tray setup, the range of liquid flow-rate which gave "perfect" operational behaviour was determined. FL is in ml/sec, stagn. = stagnant resin bed, p.mob. = partial mobilization, d.flood. = downcomer flooding, cyc. = cyclic resin flow, o.fluid. = over-fluidization

	WEIR LENGTH = 3·38"				
	WH = 1·"		WH = 2·"		
	DLD = 1/20"	DLD = 3/20"	DLD = 1/20"	DLD = 3/20"	
FS	≤10· stagn. <34· p.mob.	≤10·stagn. <34· p.mob.	≤10·stagn. <25·cyc.	≤10·stagn. <25· p.mob.	
0·6 ml/sec	FL = 34· – 73·	34· – 73·	FL = 25· – 63·	25· – 63·	'perfect'
	>73· o.fine ≥83· o.fluid.	>73· o.fine ≥88· o.fluid	>63· o.fine ≥73· o.fluid.	>63· o.fine ≥73· o.fluid	
2·25 ml/sec	≤10·stagn. <26 p.mob.	≤10· stagn. <26· p.mob.	<18·cyc.	≤10· stagn. <18· p.mob.	
	FL = 26· – 63·	26· – 63·	FL = 18· – 53·	18· – 53·	'perfect'
	>63· o.fine ≥73· o.fluid.	>63 o.fine ≥73 o.fluid	>53·o·fine ≥73· o.fluid.	>53·o·fine ≥73·o·fluid.	

-35+50 mesh resin

	WEIR LENGTH = 3·97"				
	WH = 1·"		WH = 2·"		
	DLD = 1/20"	DLD = 3/20"	DLD = 1/20"	DLD = 3/20"	
FS	≤10·stagn. <18· p.mob.	≤10·stagn. <18· p.mob.	≤5·stagn. <10· p.mob.	≤5· stagn. <10·p.mob.	
0·6 ml/sec	FL = 18· – 73·	18· – 73·	FL = 10· – 53·	10· – 53·	'perfect'
	>73· o.fine ≥83· o.fluid.	>73· o.fine ≥83·o. fluid	>53· o.fine ≥83· o.fluid.	>53·o·fine ≥83·o.fluid.	
2·25 ml/sec	≤10· stagn. <18· p.mob.	≤10·stagn. <18· p.mob.	≤10· d.flood. <18· p.mob.	≤10·stagn. <18· p.mob.	
	FL = 18· – 53·	18· – 53·	FL = 18· – 53·	18· – 53·	'perfect'
	>53·o.fine ≥73·o·fluid.	>53·o.fine ≥73·o.fluid	>53· o.fluid.	>53· o. fluid.	

TABLE 4.2 Operational behaviour of the ion-exchange column at different liquid flow-rates (-35+50 mesh resin used). In each tray setup, the range of liquid flow-rate which gave "perfect" operational behaviour was determined. FL is in ml/sec, stagn. = stagnant resin bed, p.mob. = partial mobilization, d.flood. = downcomer flooding, cyc. = cyclic resin flow, o.fine = overfluidization of fines, o.fluid. = overfluidization

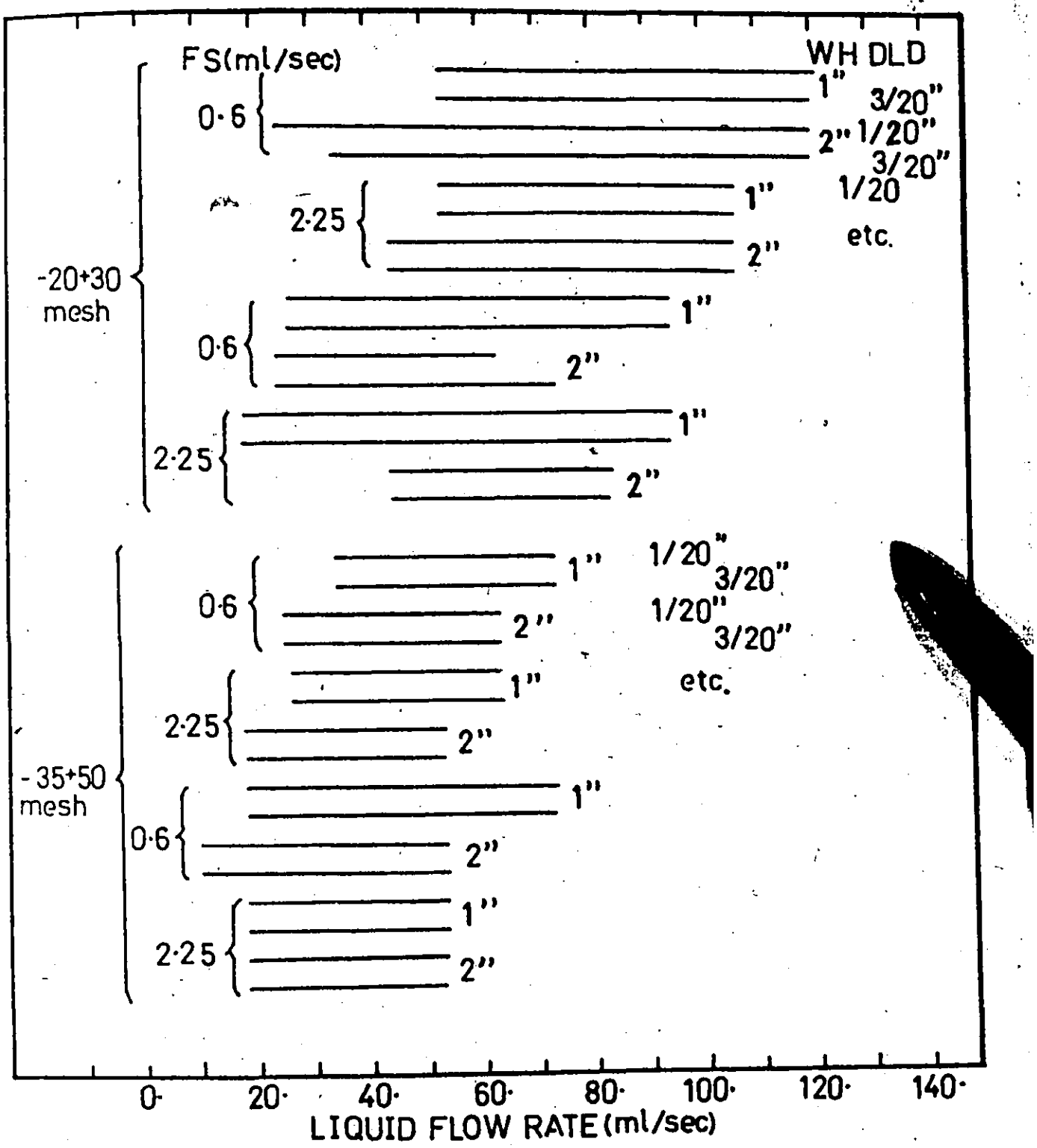

FIGURE B.17 Ranges of liquid flow-rate which gave "perfect" operational behaviour in the ion-exchange column

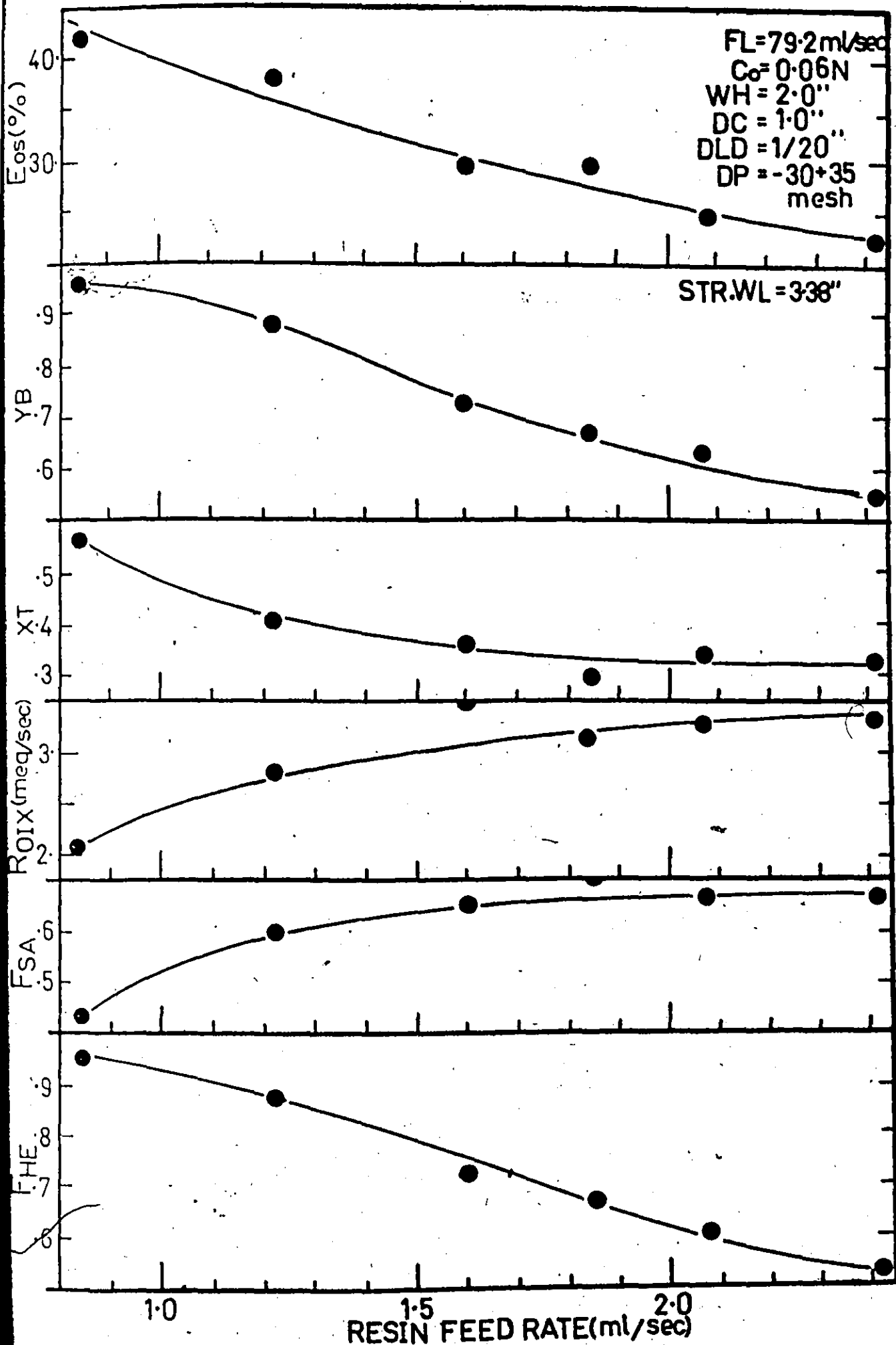
FL=79·2 ml/sec
Co= 0·06N
WH = 2·0"
DC = 1·0"
DLD = 1/20"
DP = -30+35 mesh
STR.WL = 3·38"
Eos(%)
YB
XT
ROIX(meq/sec)
FSA
FHE
a
b
c
d
e
f
1·0
1·5
2·0
RESIN FEED RATE(ml/sec)

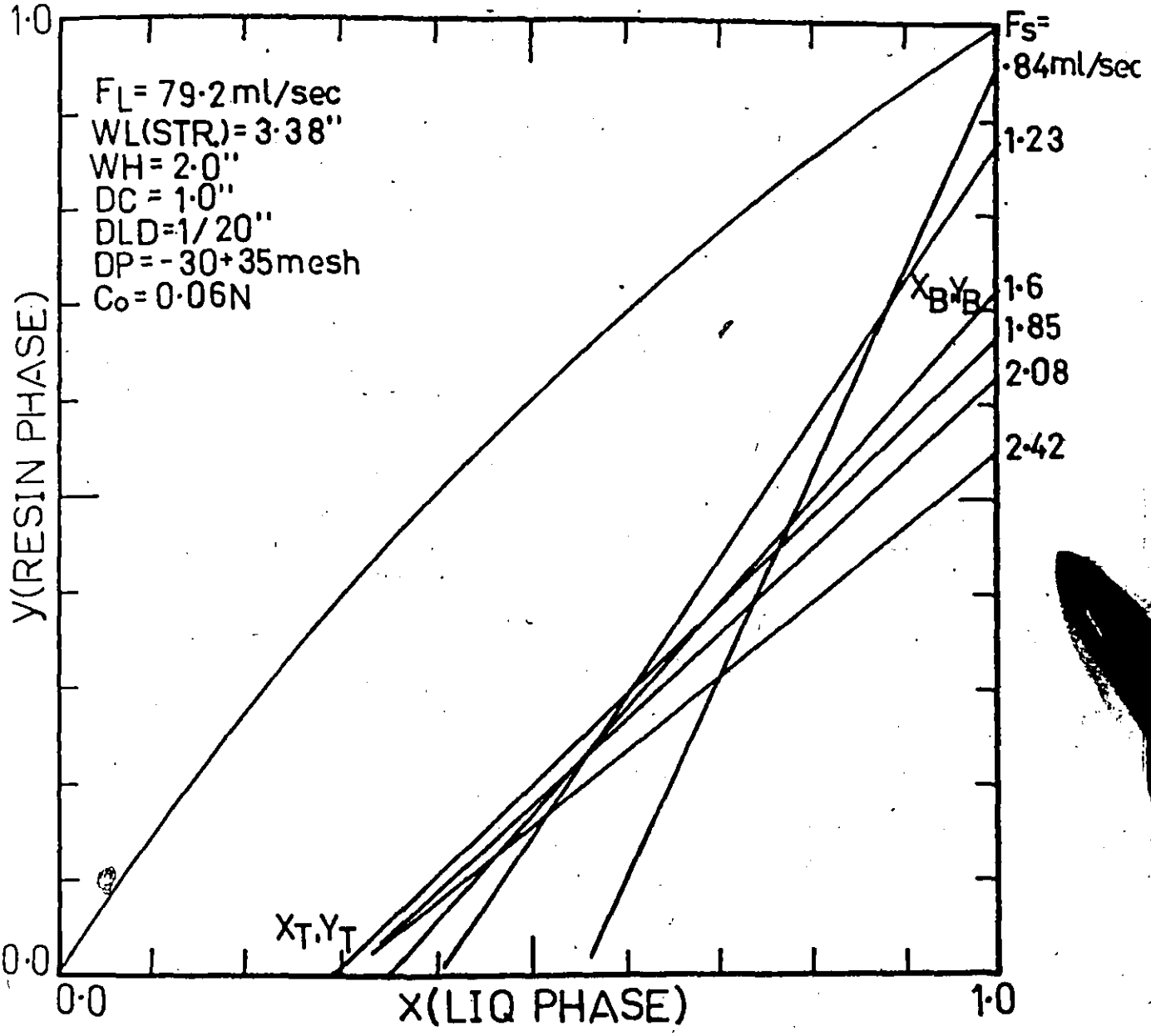

FIGURE 8.19 Effects of resin feed-rate on the operating line

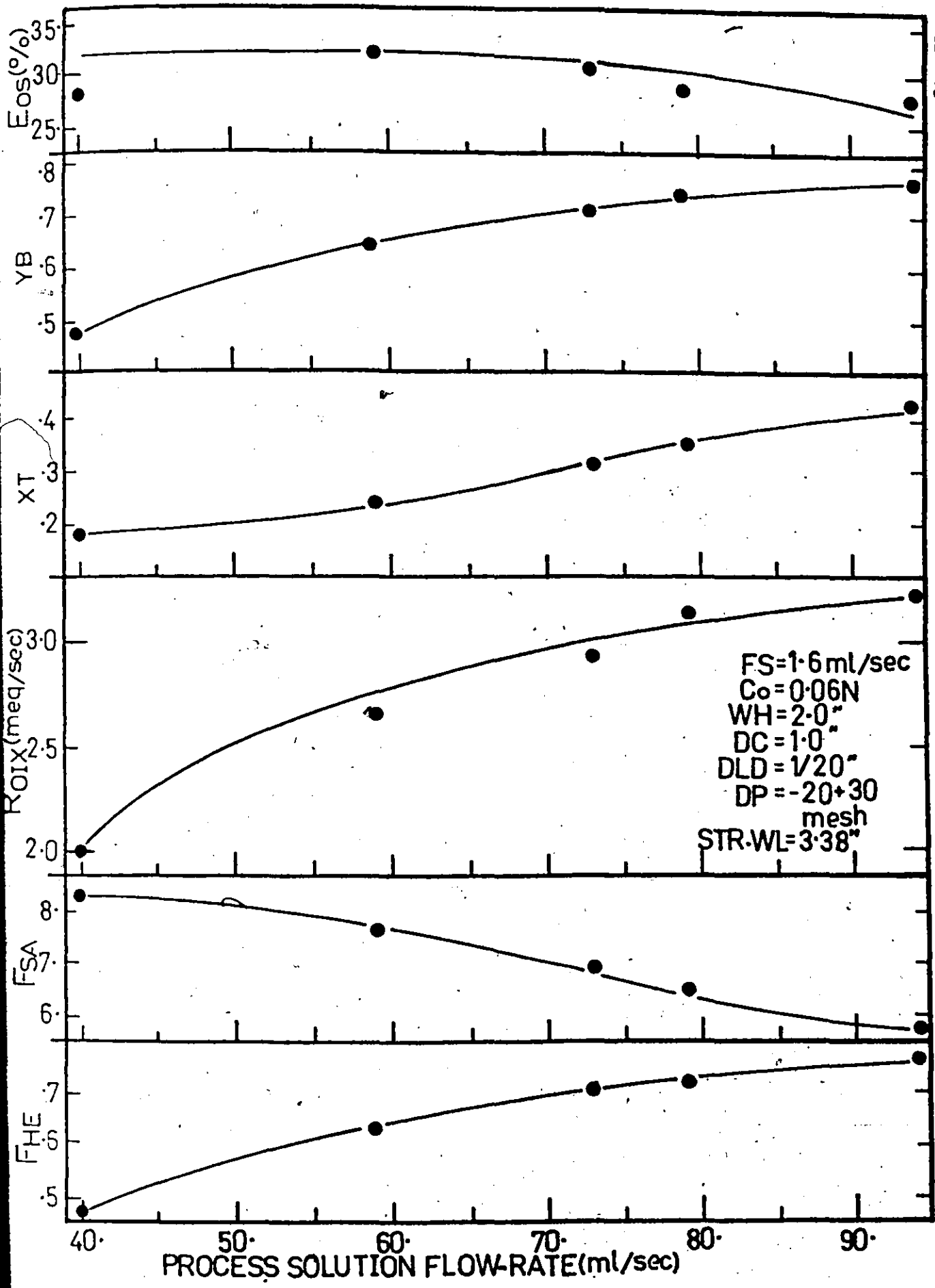

FIGURE B.20 Effects of process solution flow-rate

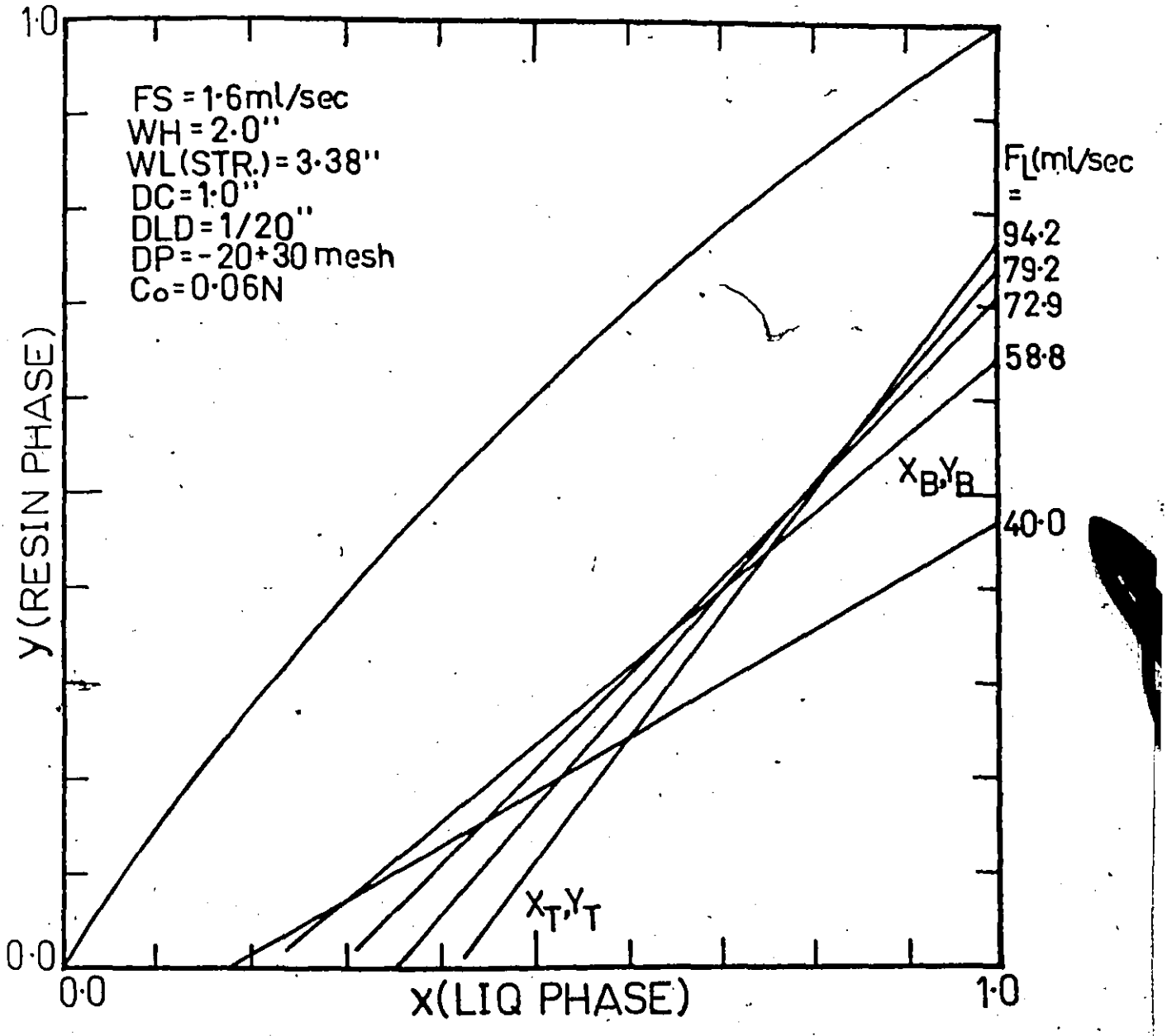

FIGURE B.21 Effects of process solution flow-rate on the operating line

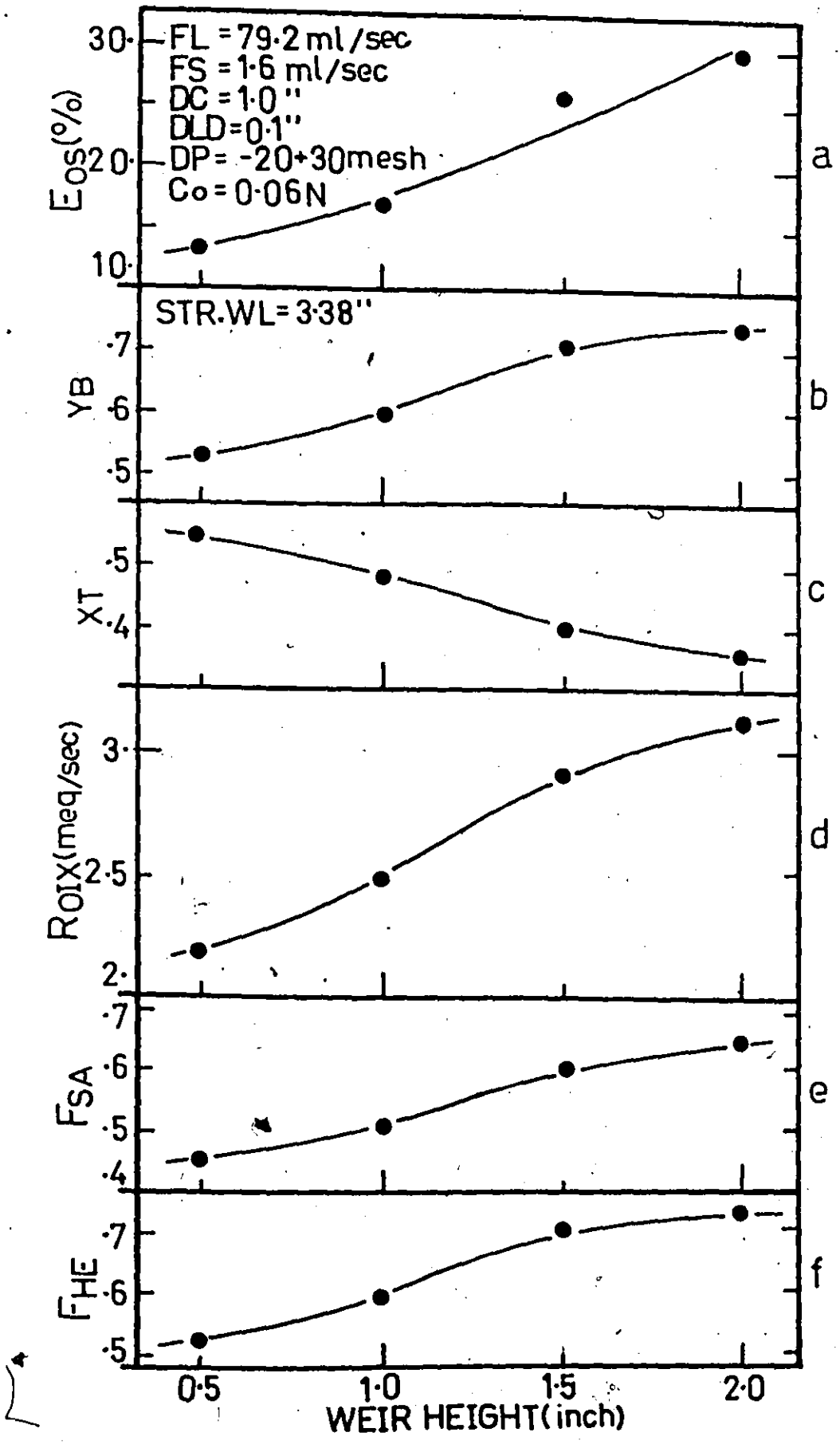

FIGURE B.22 Effects of weir height

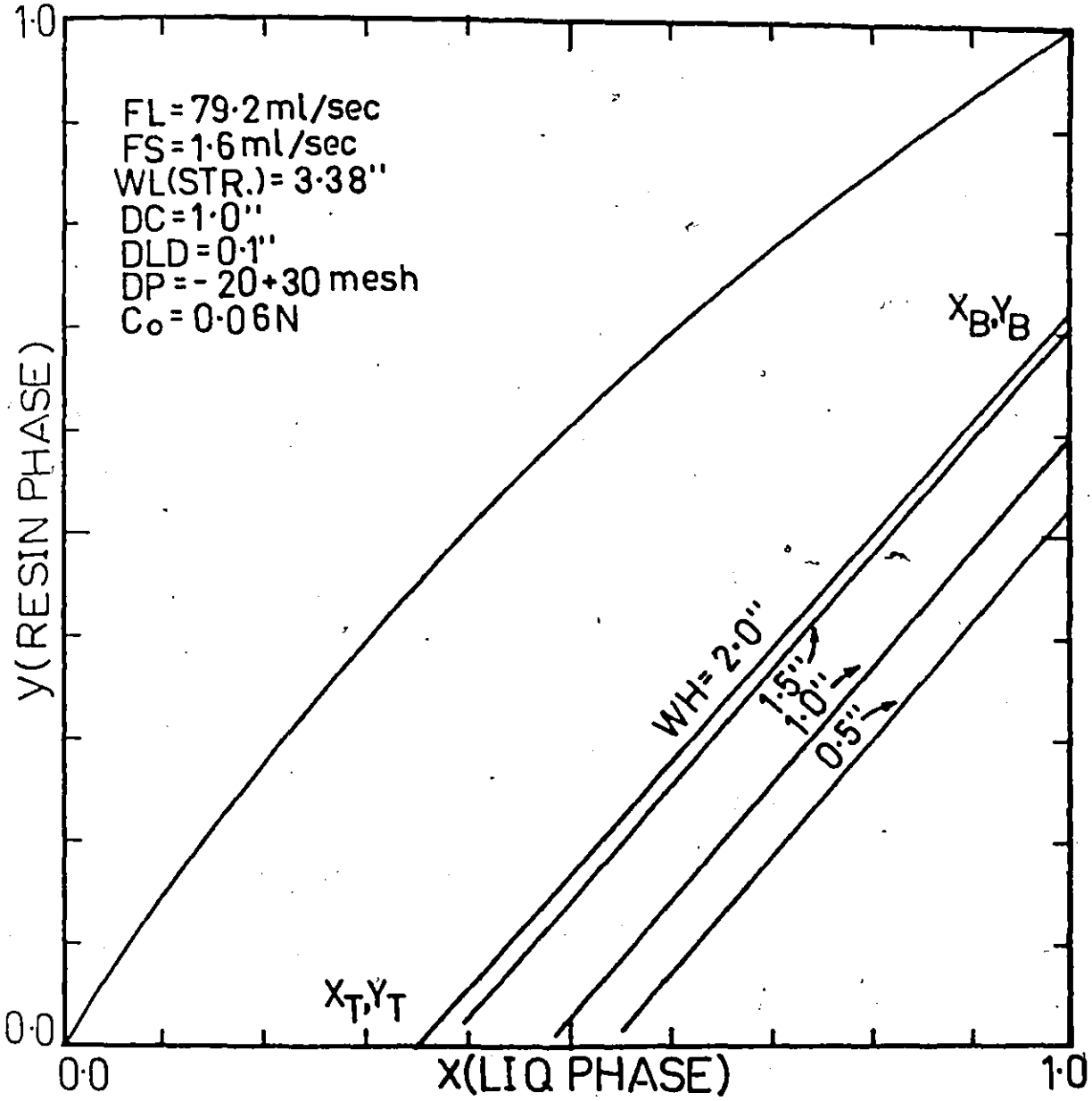

FIGURE B.23 Effects of weir height on the operating line

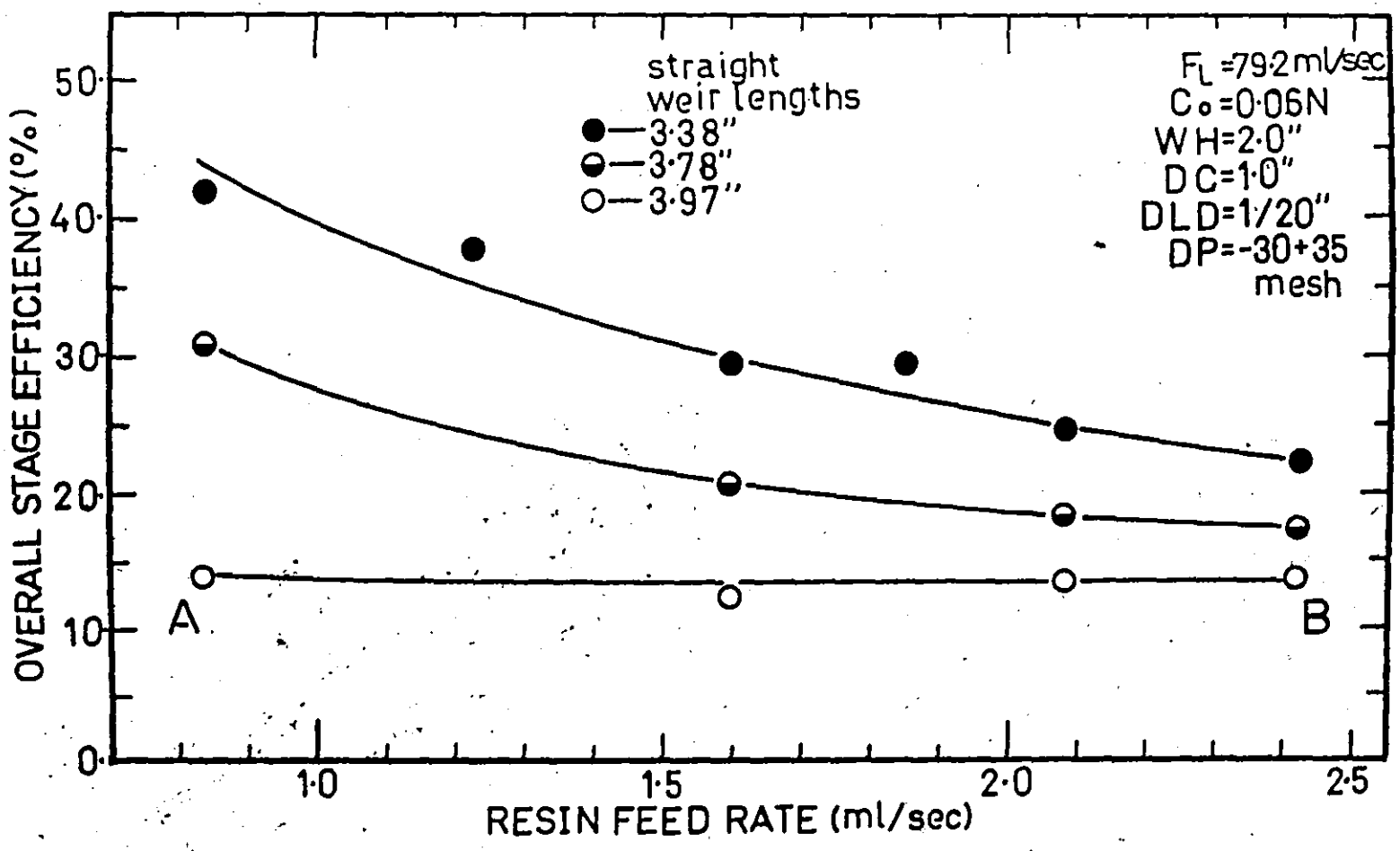

FIGURE B.24a Effects of resin feed-rate on the overall stage efficiency at different weir lengths

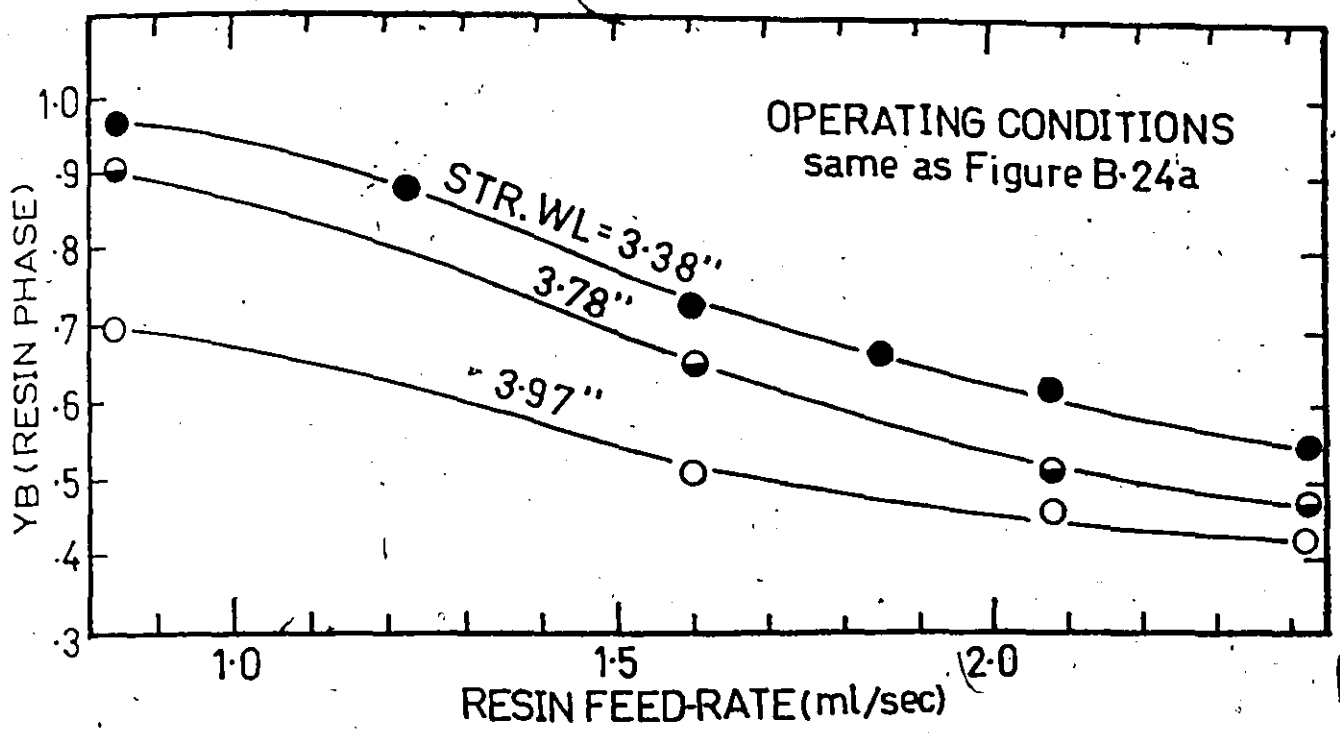

FIGURE B.24b Effects of resin feed-rate on the composition of resin effluent. YB is the mole fraction in sodium-ion basis

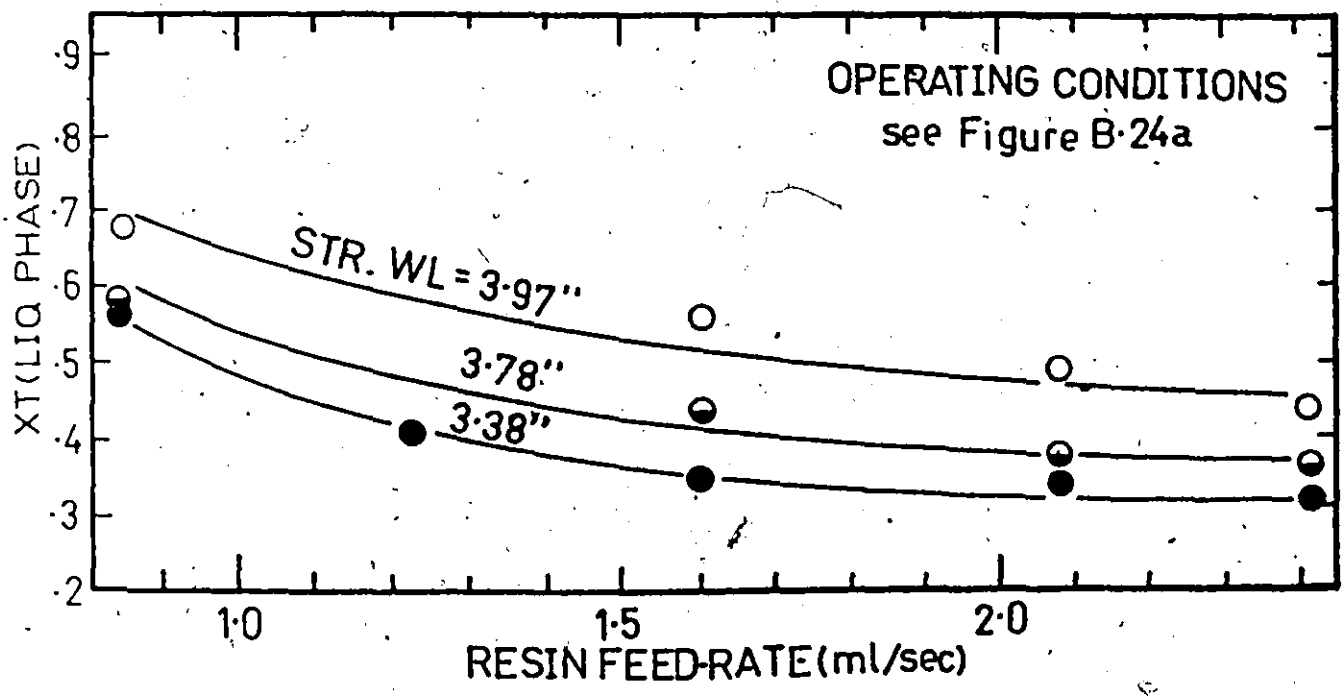

FIGURE B.24c Effects of resin feed-rate on the composition of liquid effluent. XT is the mole fraction in sodium-ion basis

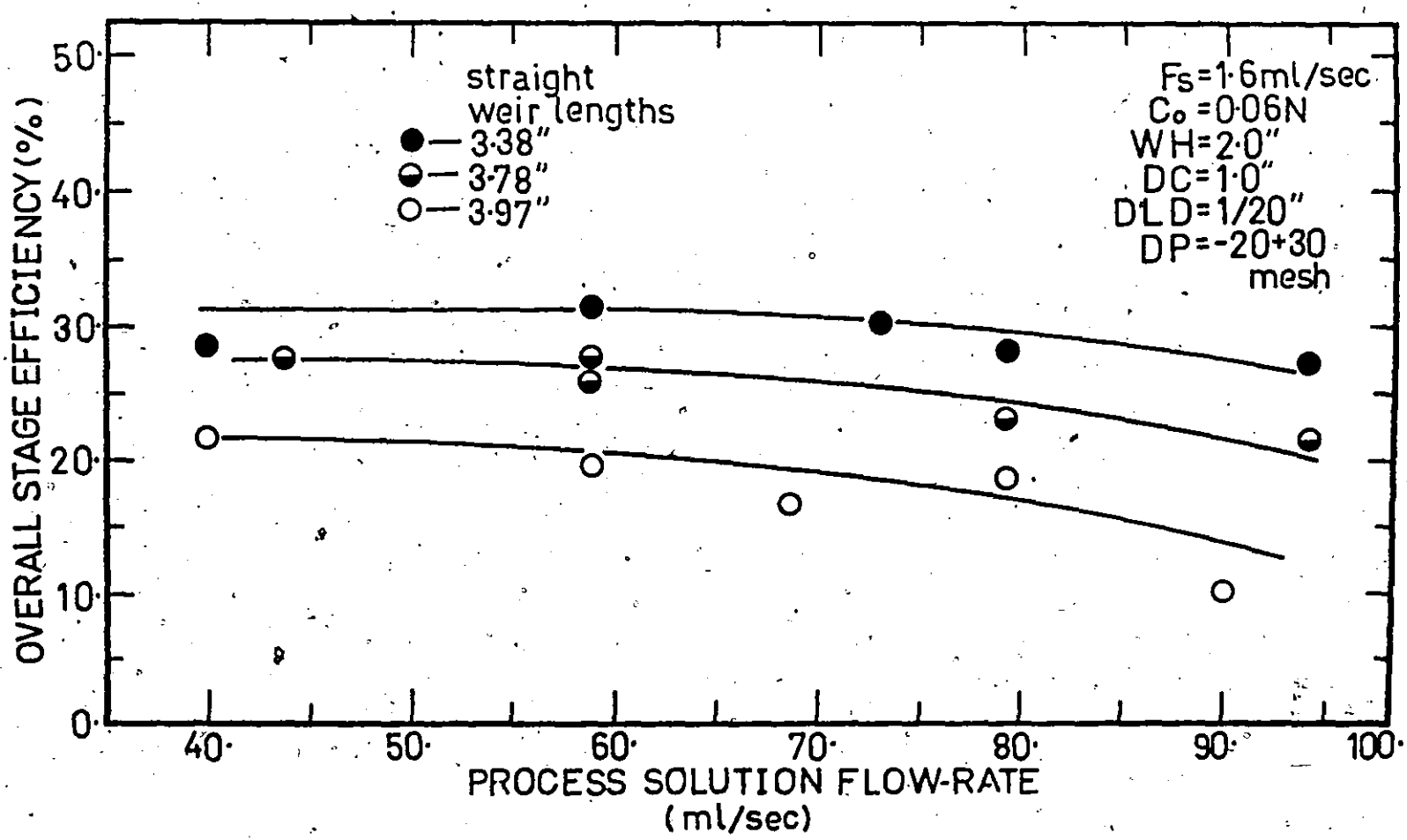

FIGURE B.25a Effects of process solution flow-rate on the overall stage efficiency at different weir lengths

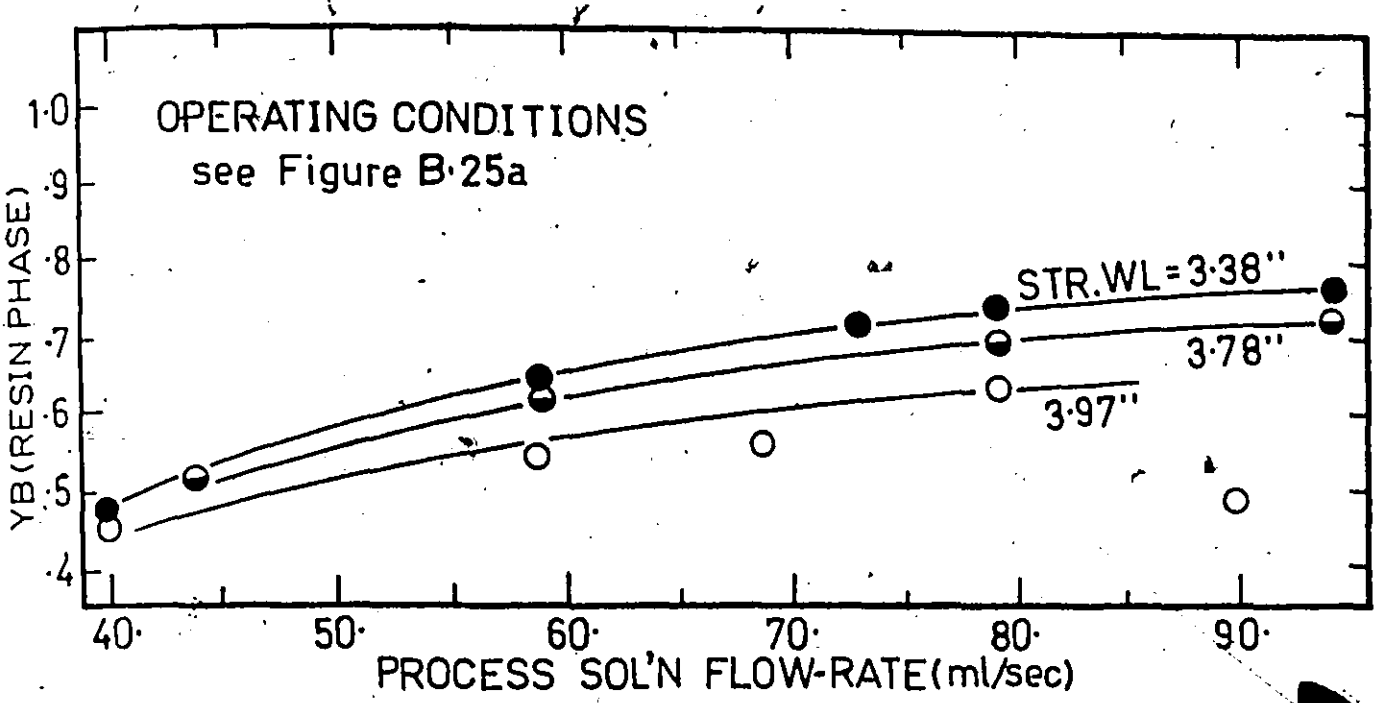

FIGURE B.25b Effects of process solution flow-rate on the composition of resin effluent. YB is the mole fraction in sodium-ion basis

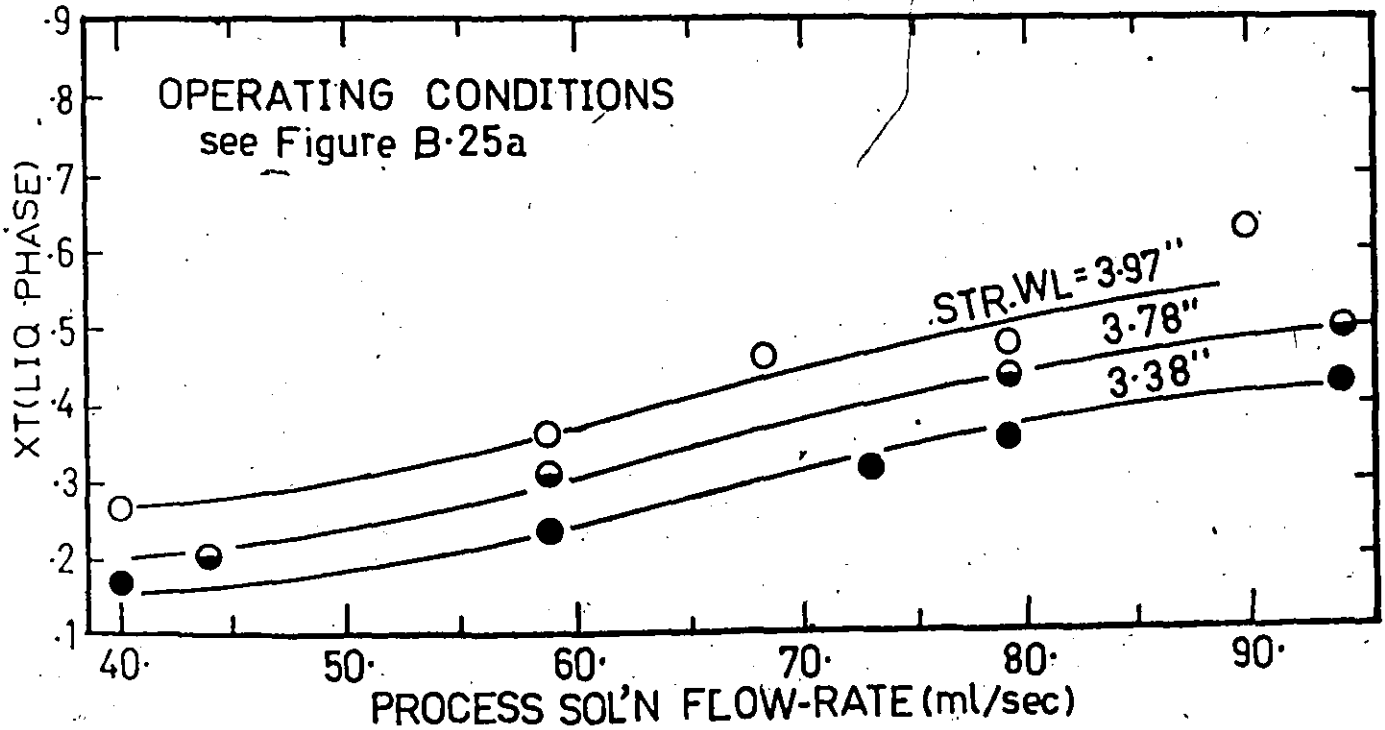

FIGURE B.25c Effects of process solution flow-rate on the composition of liquid effluent. XT is the mole fraction in sodium-ion basis

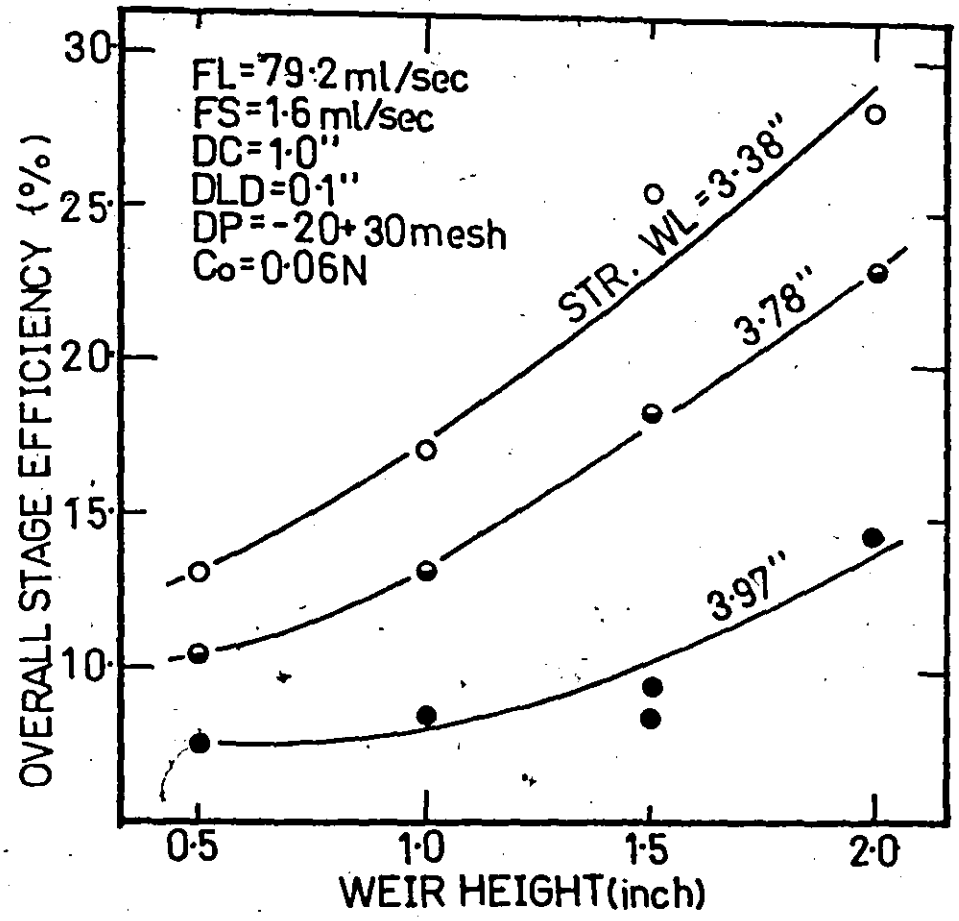

FIGURE B.26a Effects of weir height on the overall stage efficiency at different weir lengths

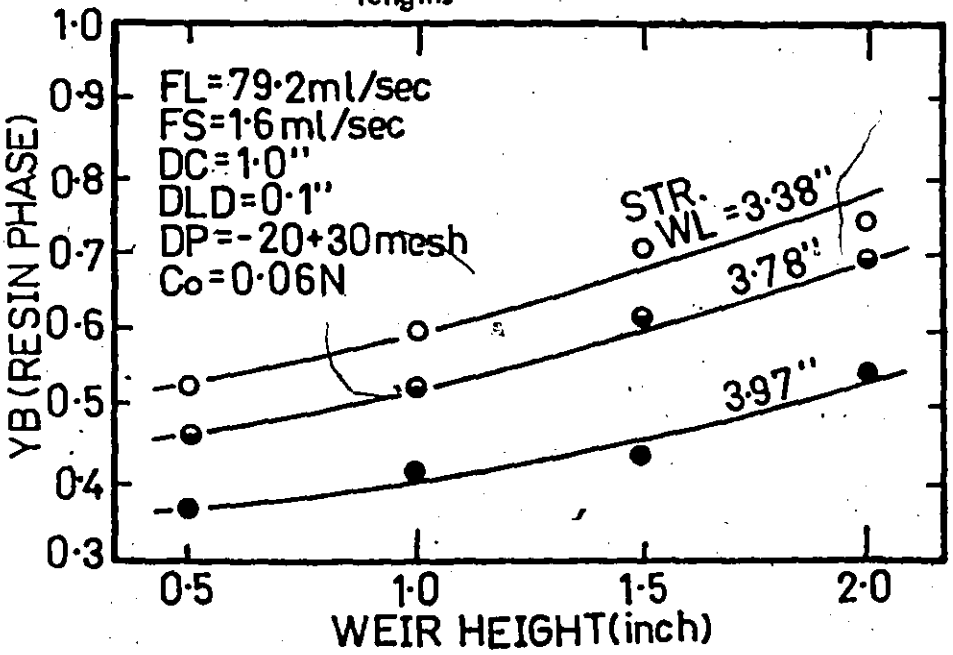

FIGURE B.26b Effects of weir height on the composition of resin effluent. YB is the mole fraction in sodium-ion basis

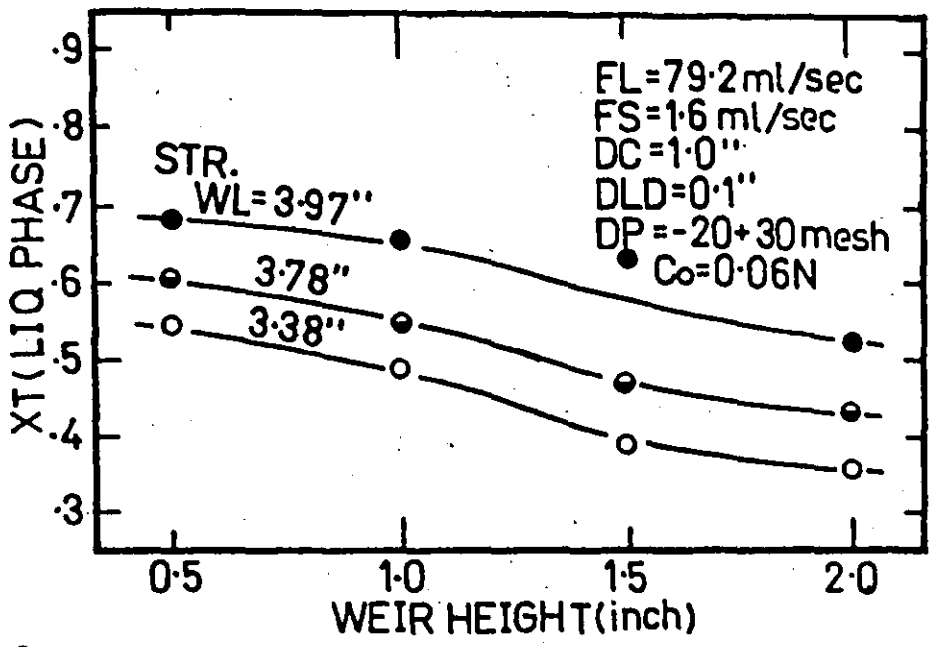

FIGURE B.26c Effects of weir height on the composition of liquid effluent. XT is the mole fraction in sodium-ion basis

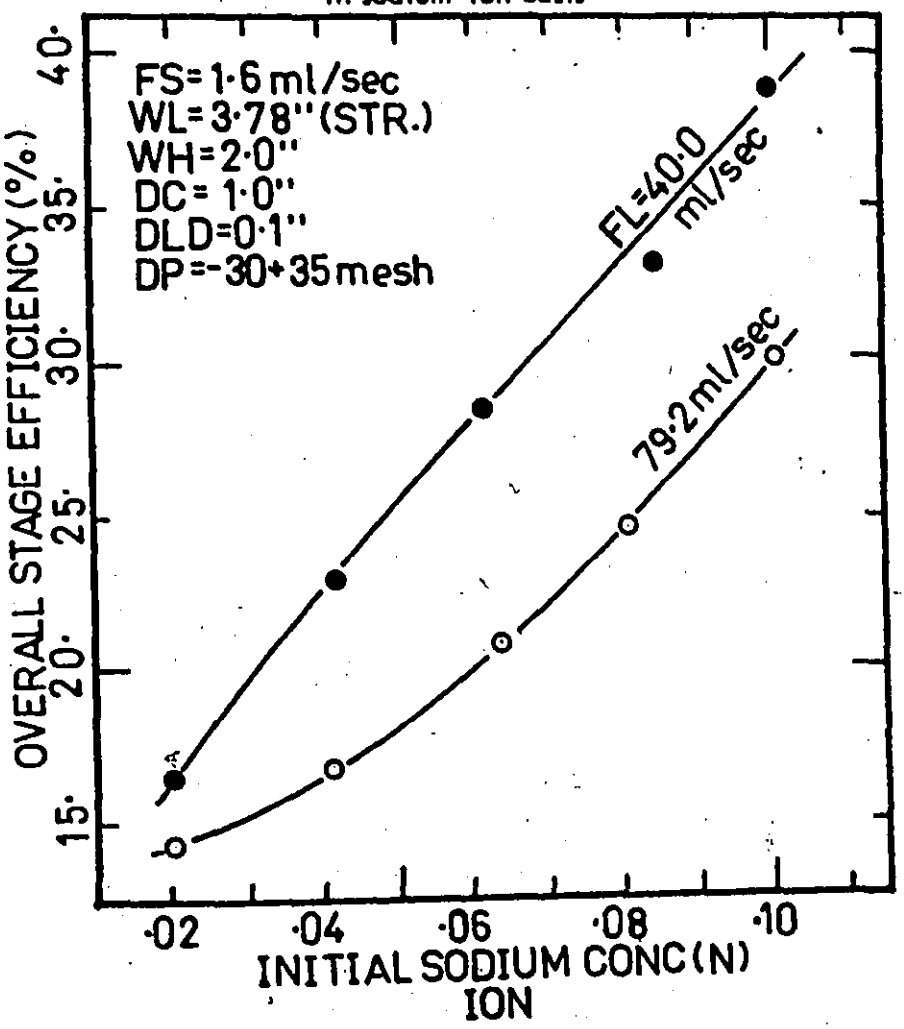

FIGURE B.27a Effects of initial sodium-ion concentration on the overall stage efficiency

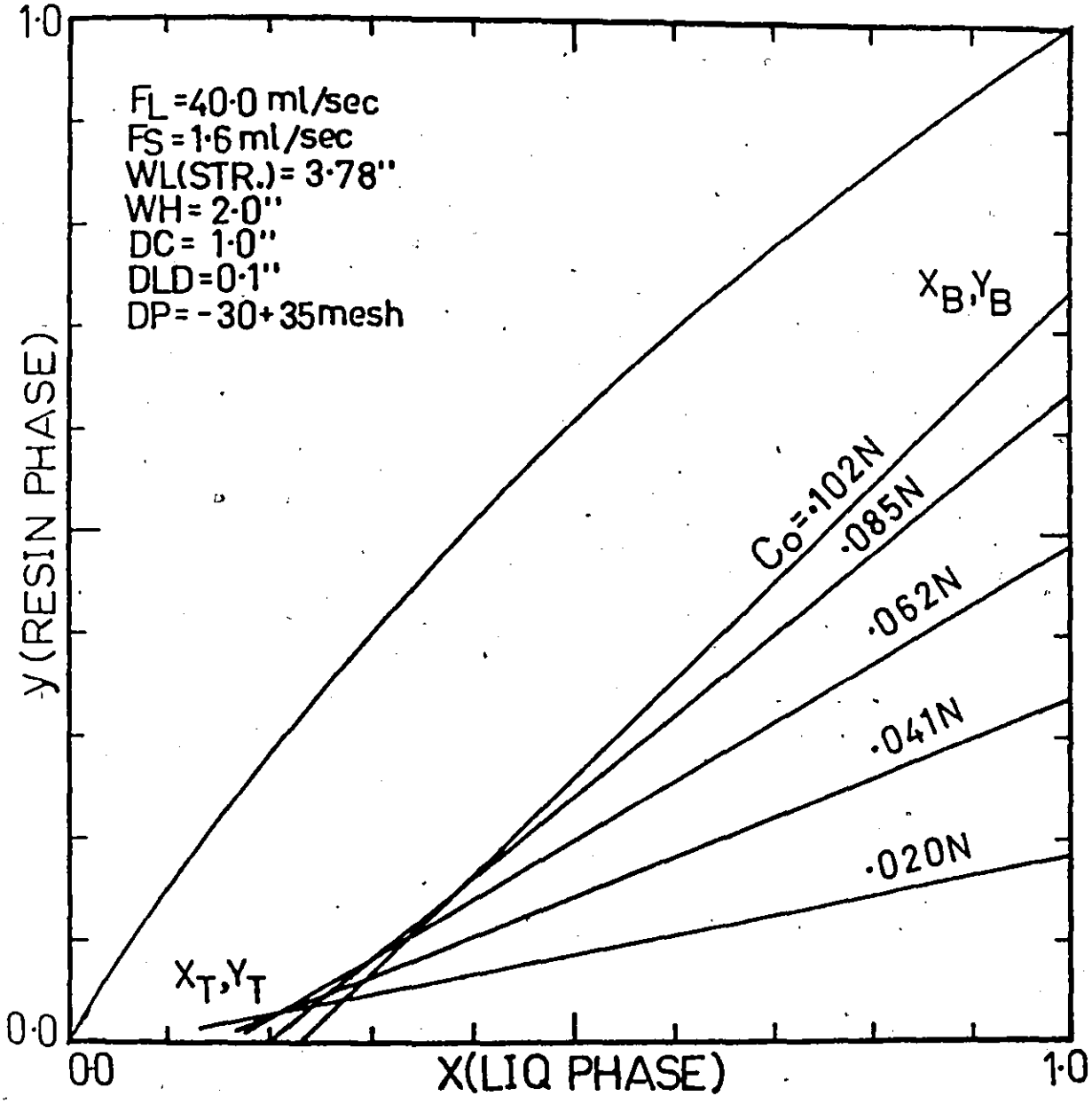

FIGURE 8.27b Effect of initial sodium-ion concentration on the operating line with solution flow-rate at 40.0 ml/sec.

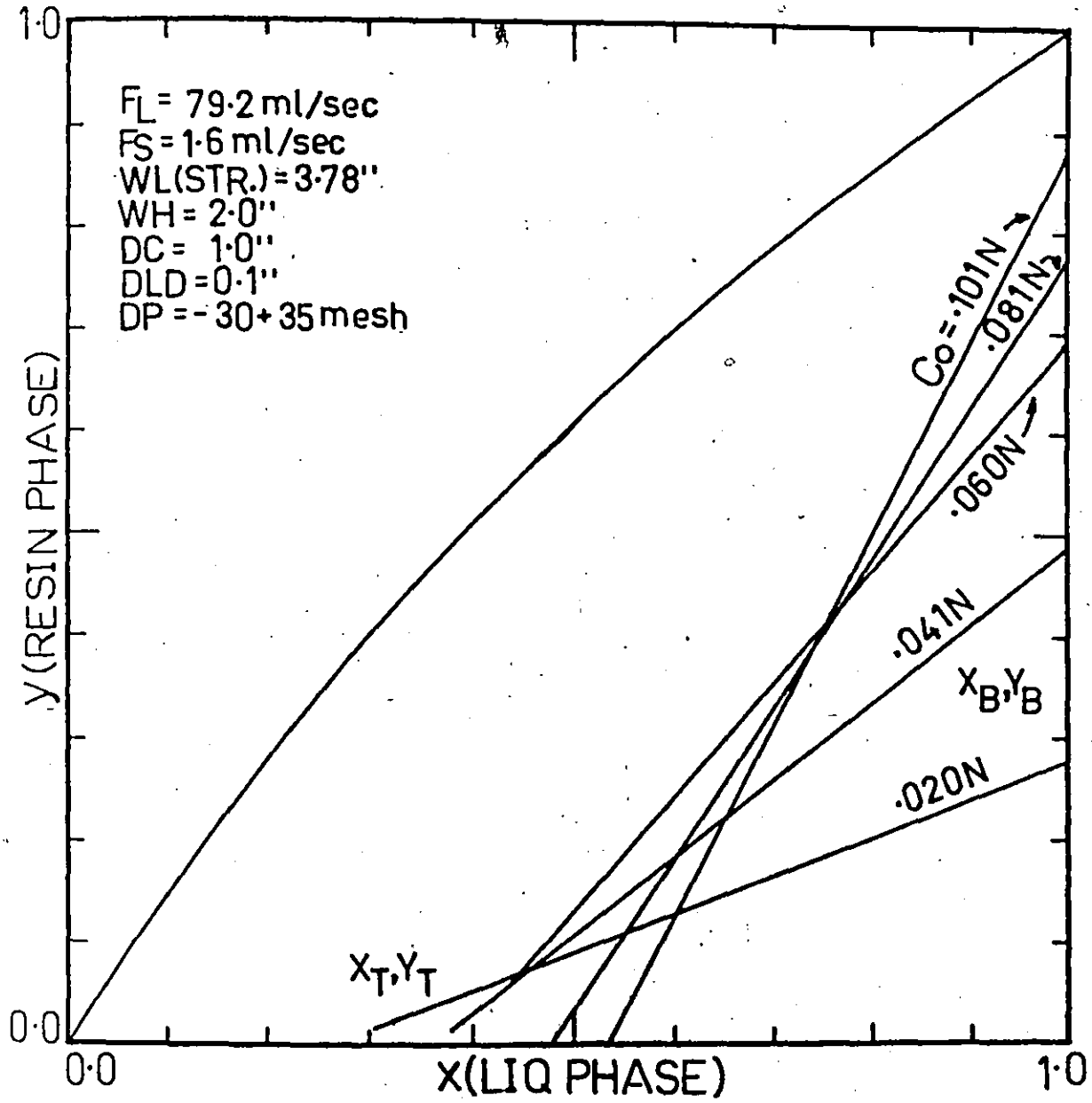

FIGURE B.27c Effects of initial sodium-ion concentration on the operating line with solution flow-rate at 79.2 ml/sec.

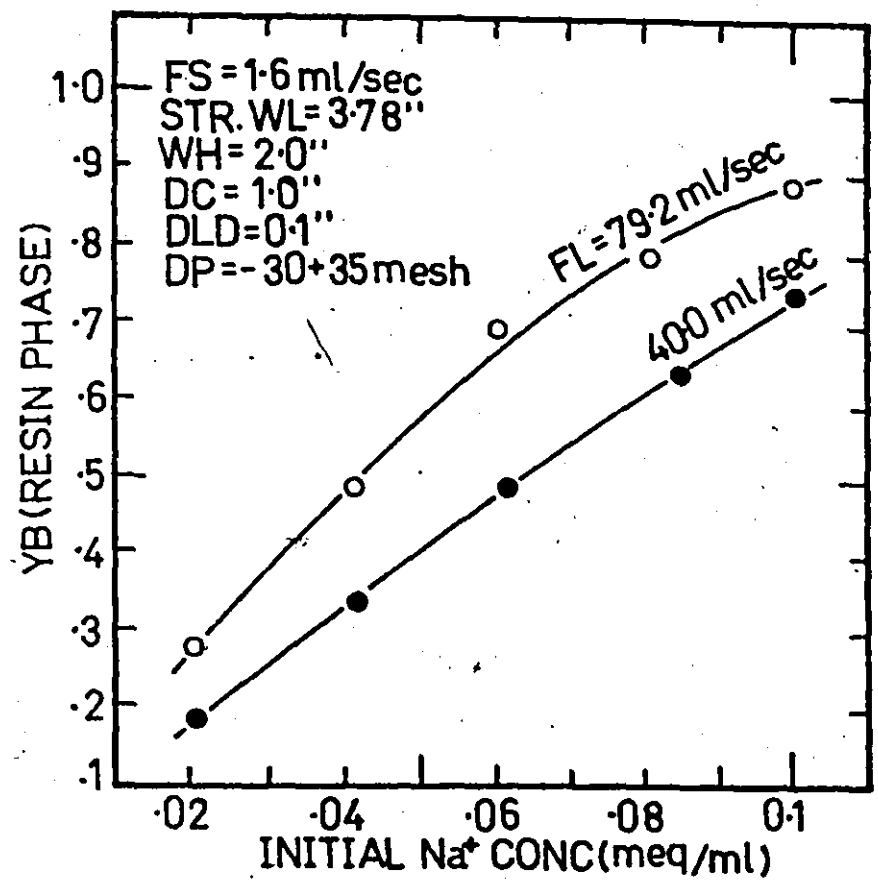

FIGURE B.27d Effects of initial sodium-ion concentration on the composition of resin effluent. YB is the mole fraction in sodium basis

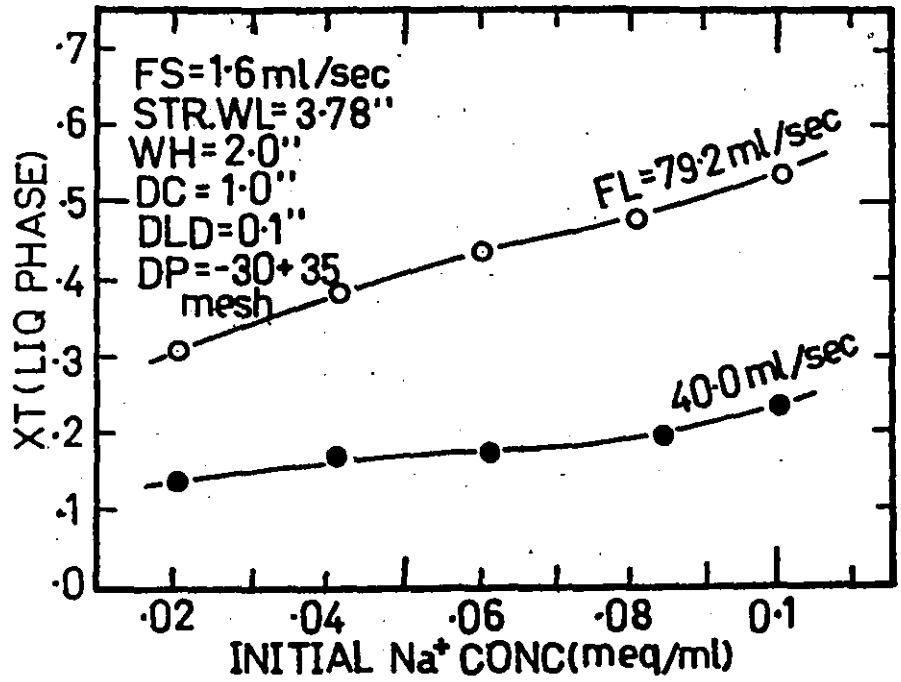

FIGURE B.27e Effects of initial sodium-ion concentration on the composition of liquid effluents. XT is the mole fraction in sodium basis

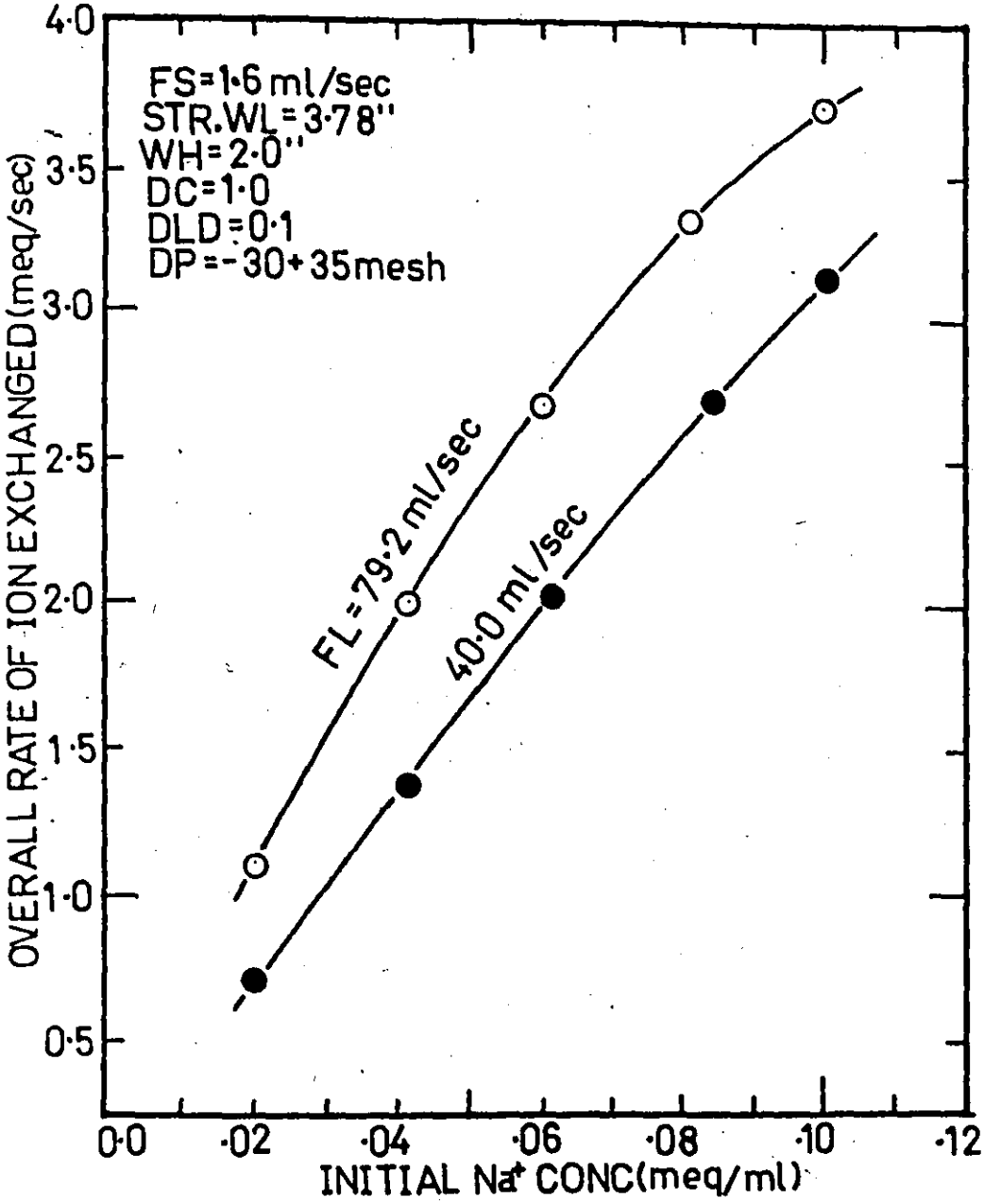

FIGURE B.27f Effects of initial sodium-ion concentration on the overall rate of ion exchanged

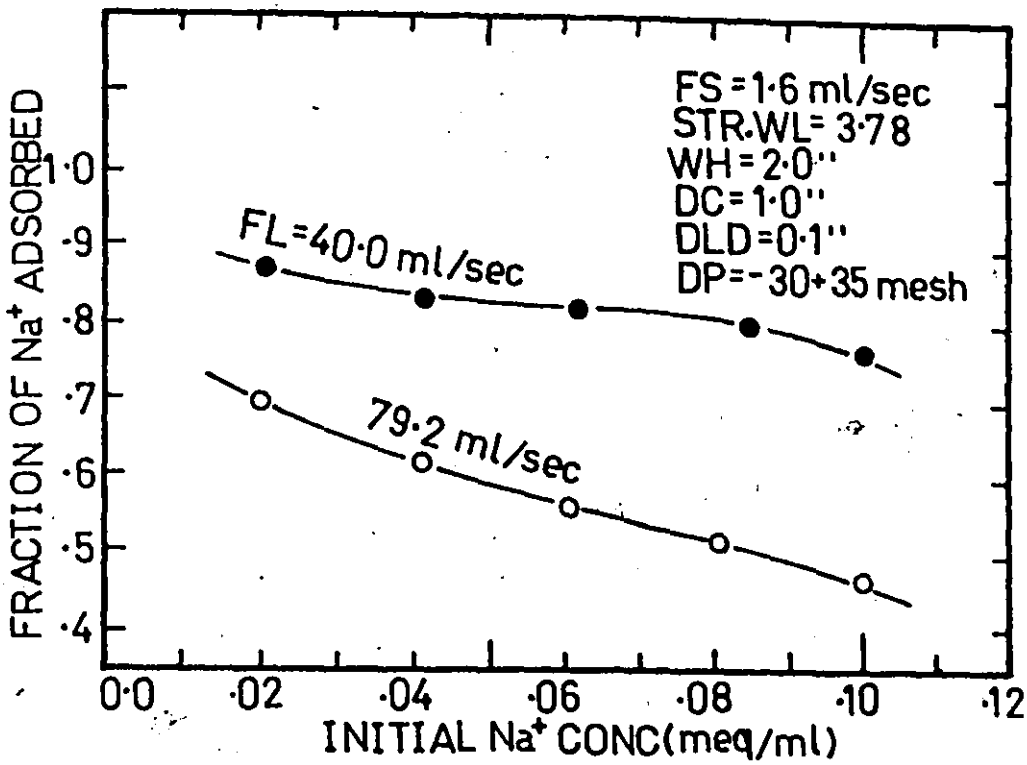

FIGURE B.27g Effects of initial sodium-ion concentration on the fraction of input sodium-ion adsorbed by the resin phase

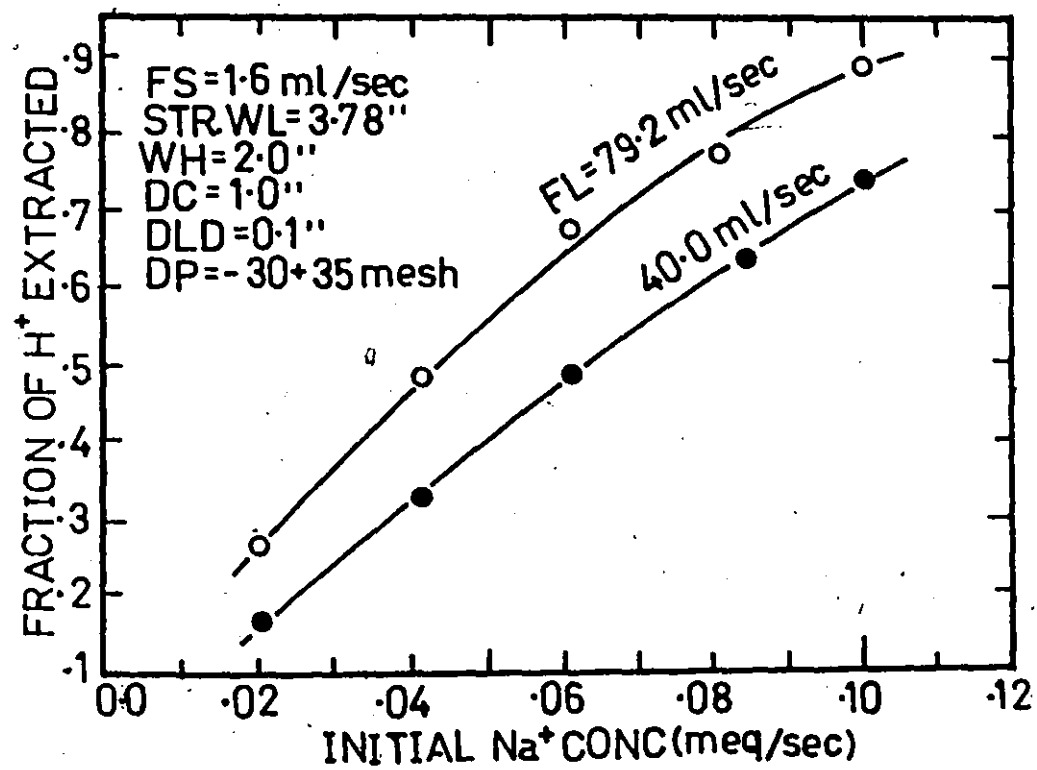

FIGURE B.27h Effects of initial sodium-ion concentration on the fraction of input hydrogen-ion extracted by the liquid phase

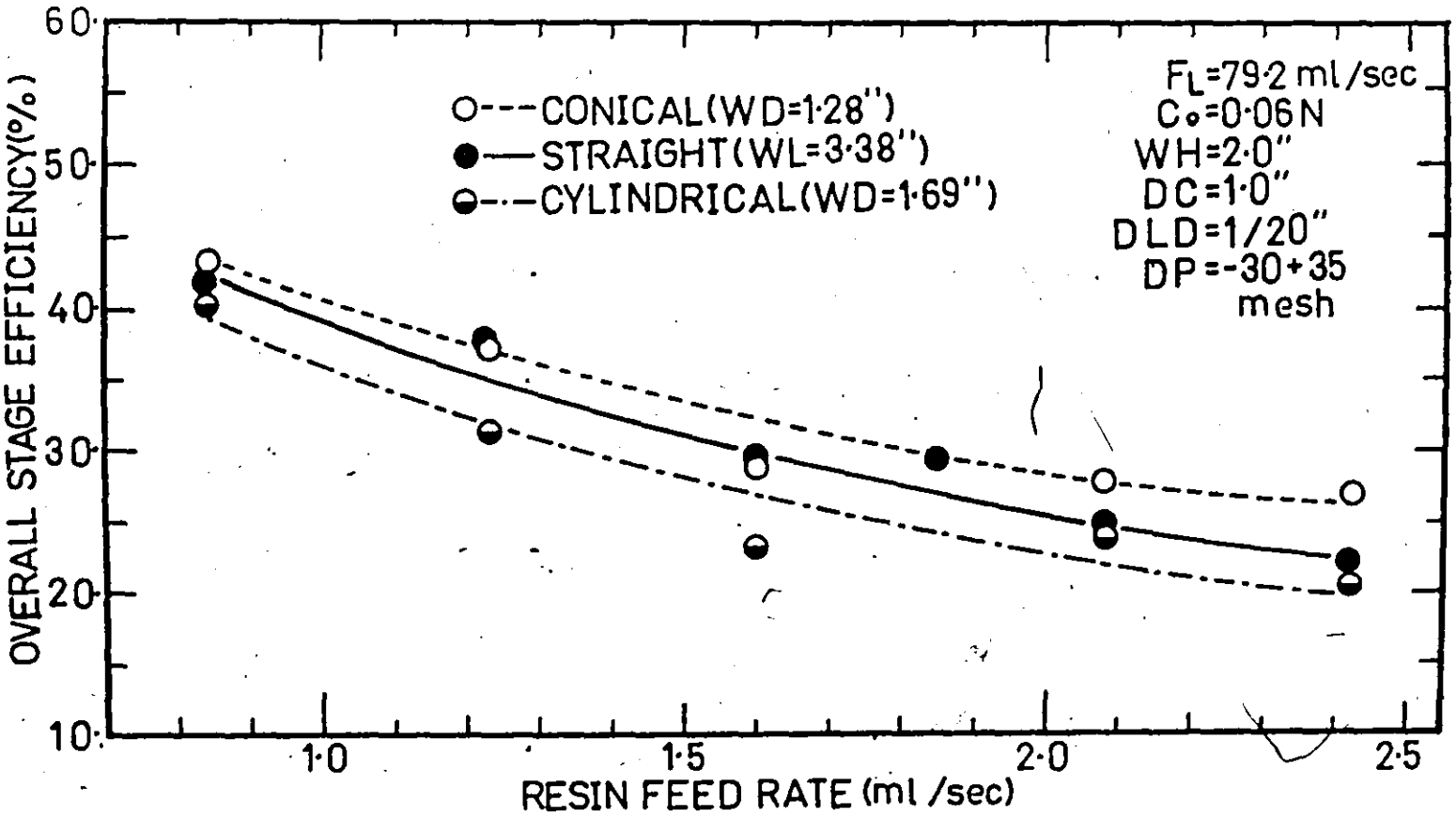

FIGURE B.28 Effects of the resin feed-rate on the overall stage efficiency for different types of weir

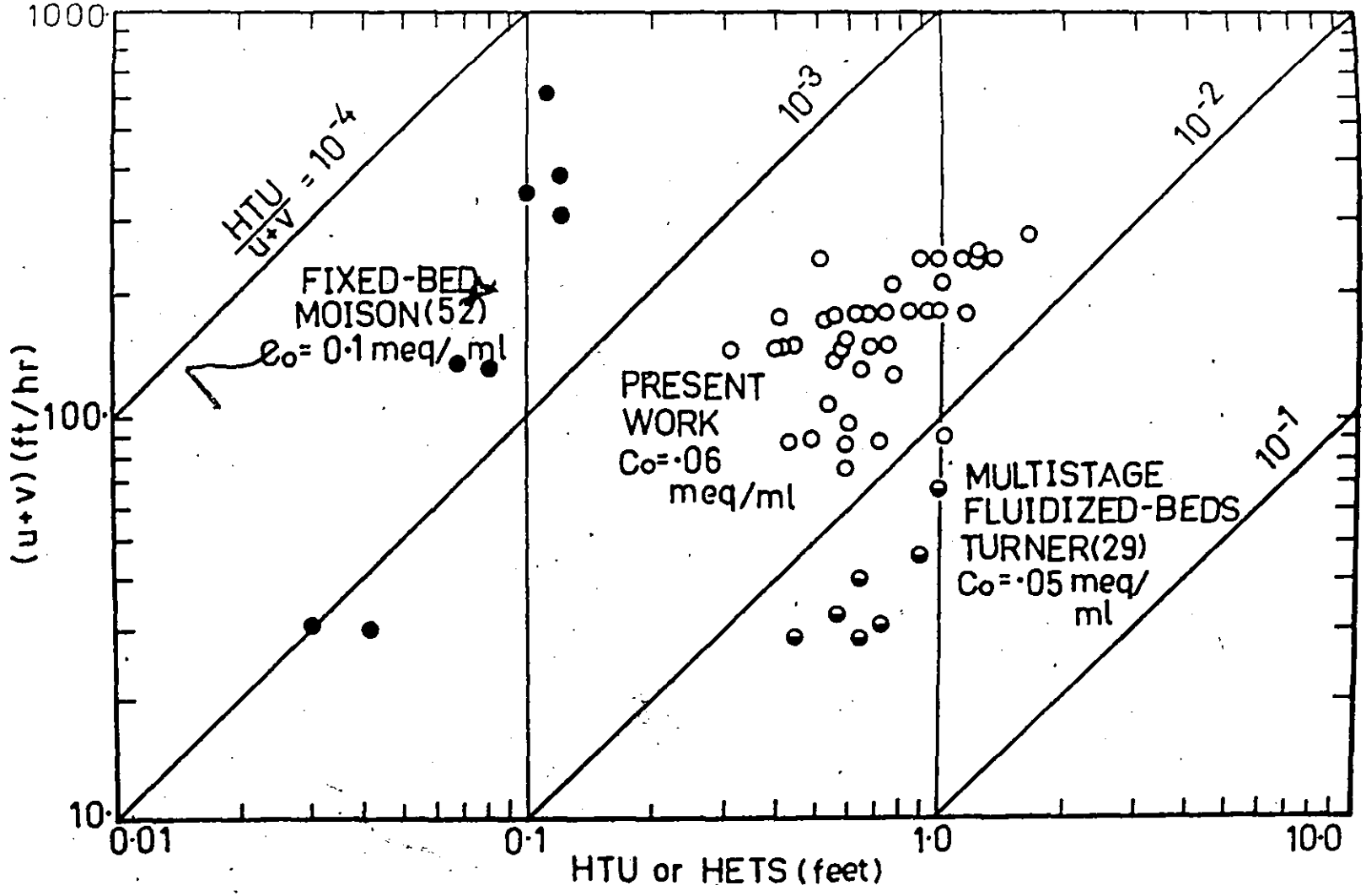

FIGURE 8.29 A log-log plot of total flow velocity (u + v) versus HTU or HETS

APPENDIX C

Operational Performance Diagrams

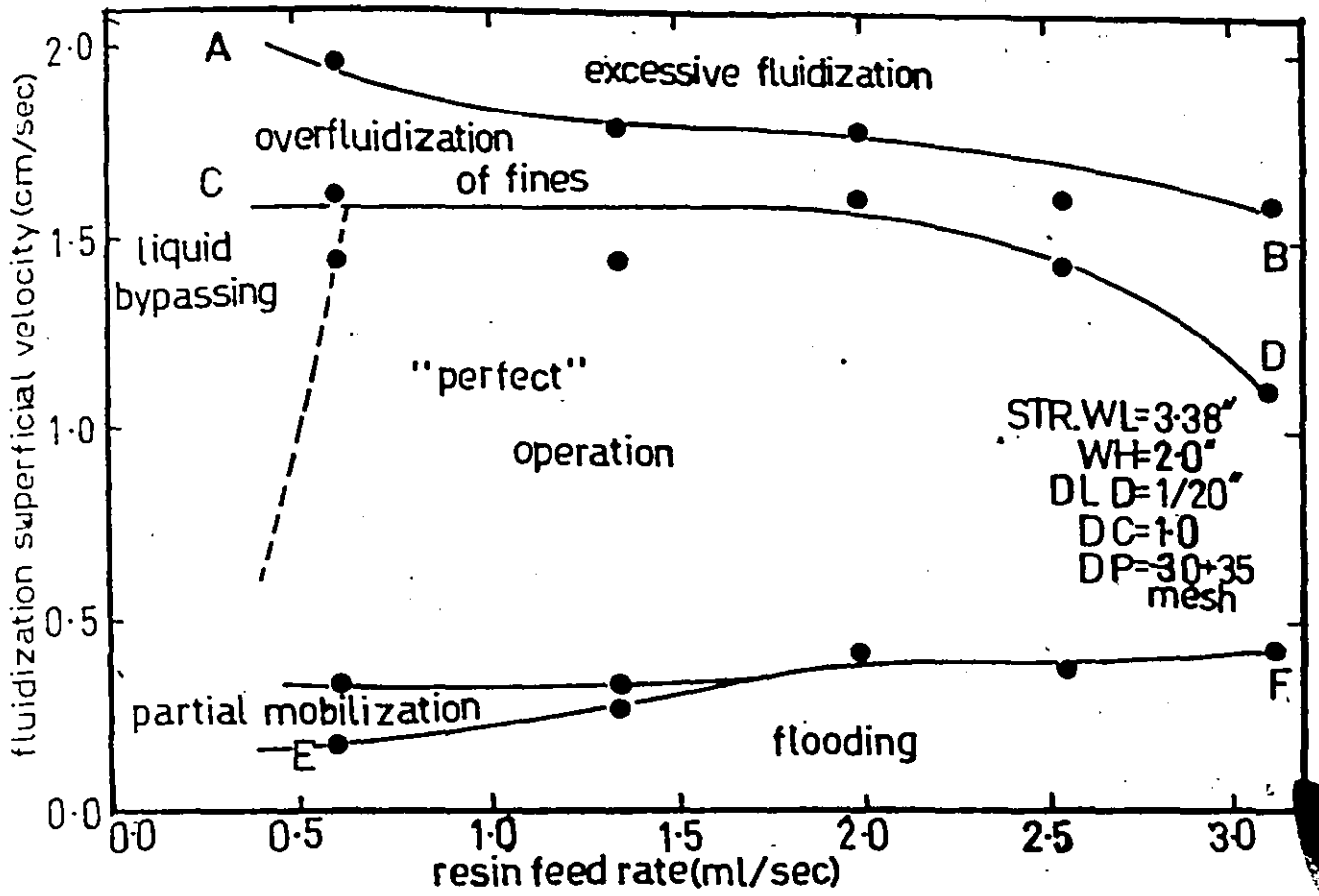

FIGURE C.1. Straight weir–effects of resin and liquid flow-rates

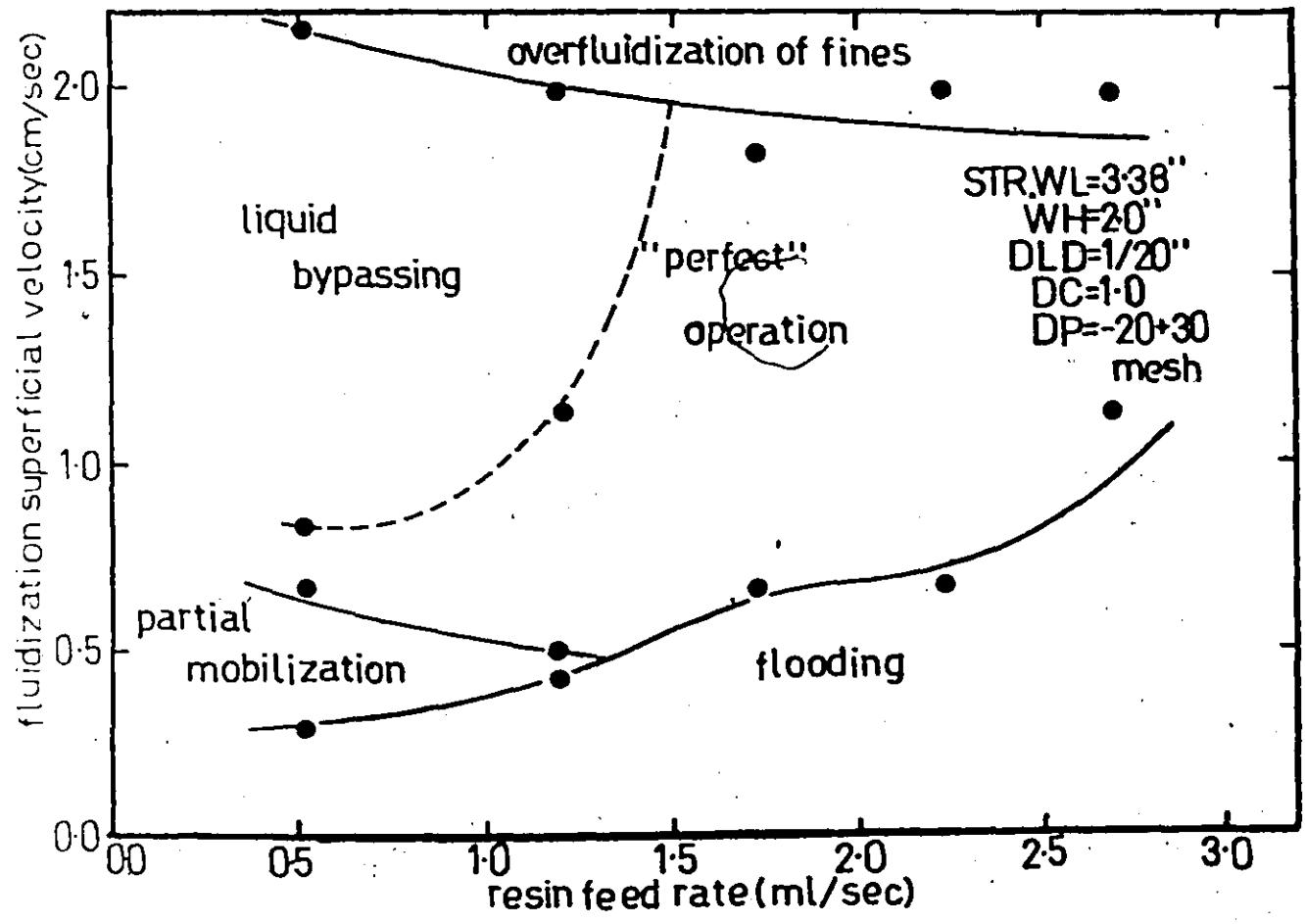

FIGURE C.2 Straight weir–effects of resin particle-size distribution.

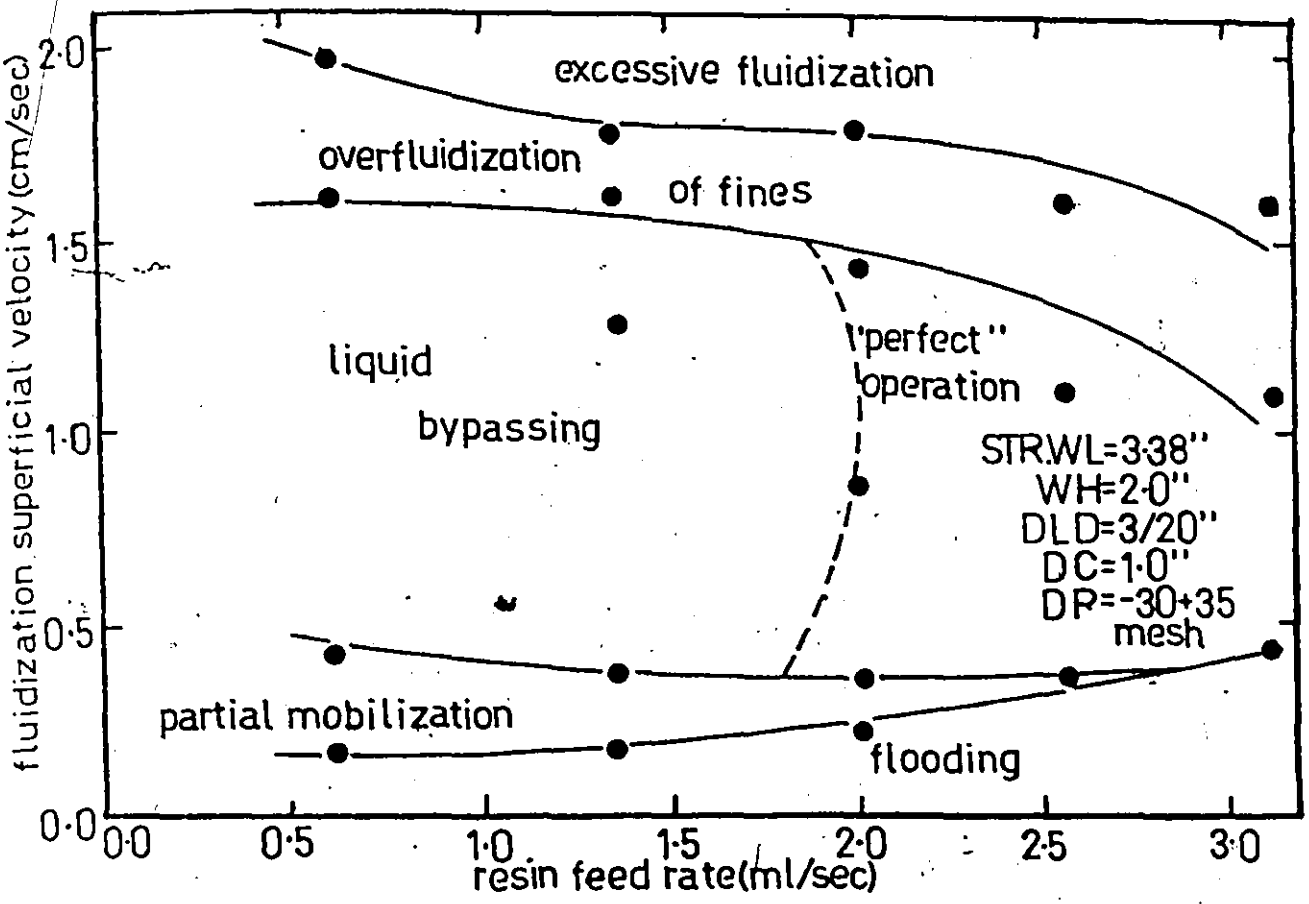

FIGURE C.3. Straight weir – effects of fluid-diode lateral displacement

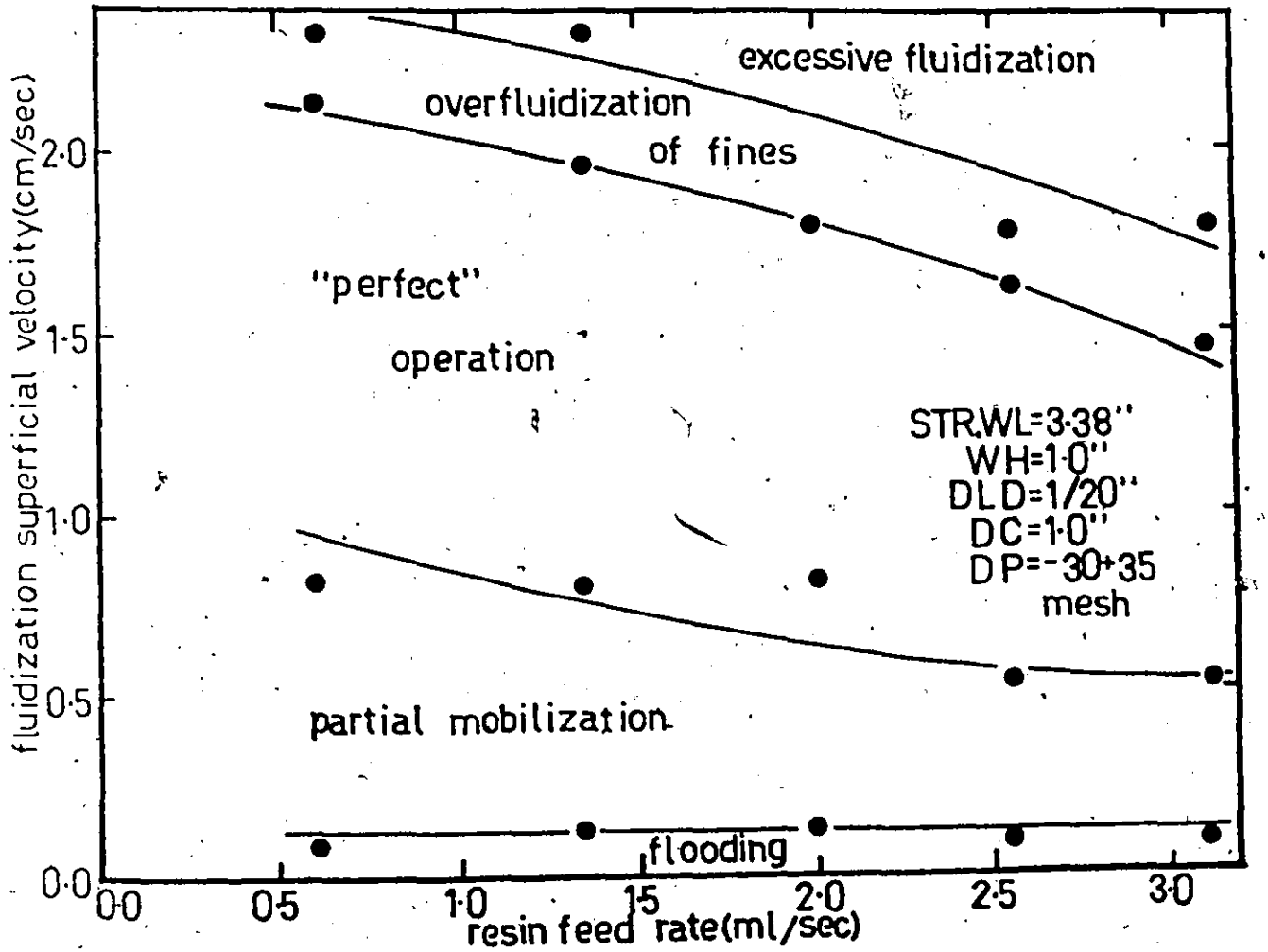

FIGURE C.4 Straight weir – effects of weir height at 1/20 inch fluid-diode

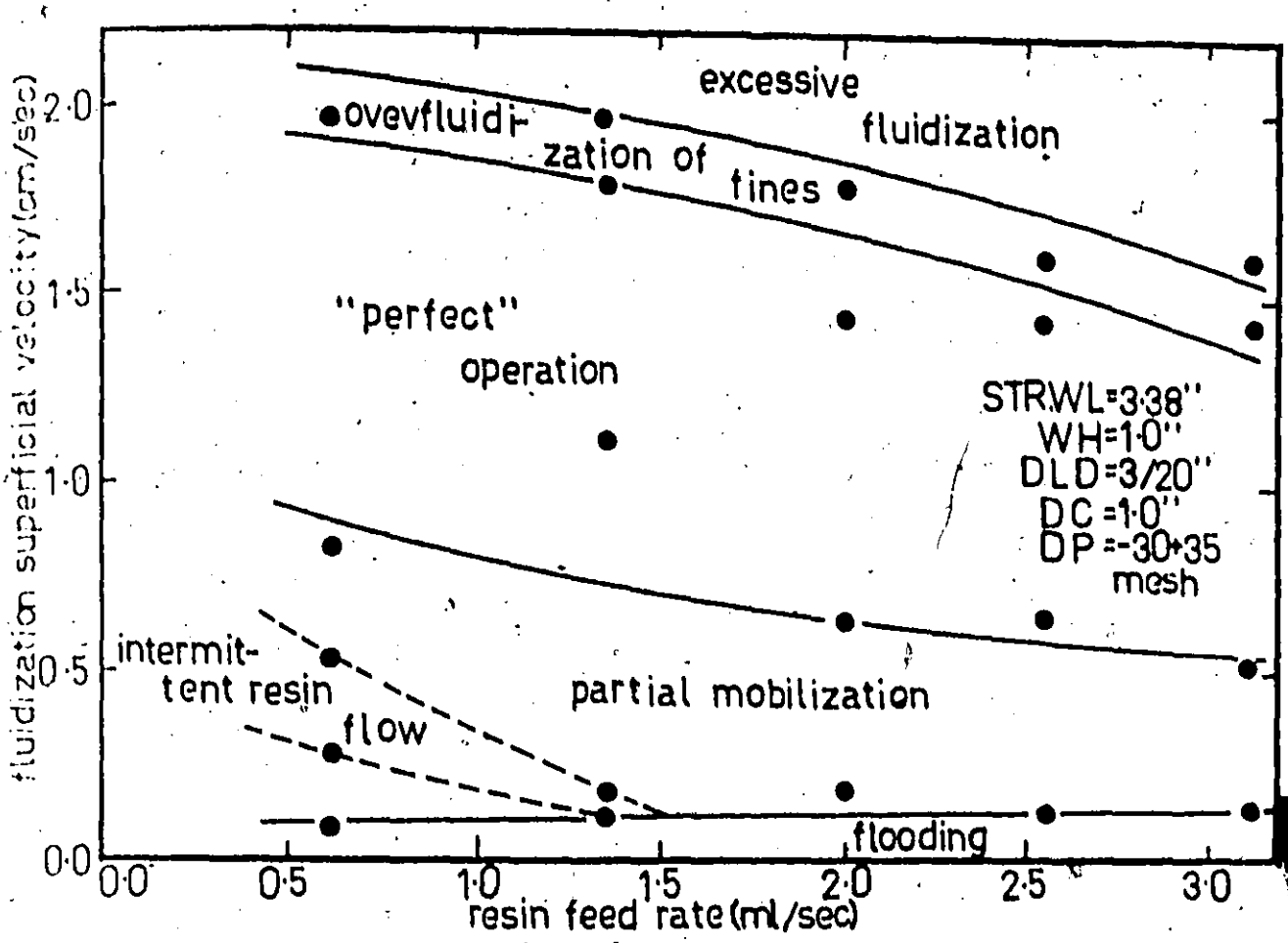

FIGURE C.5. Straight weir - effects of weir height at 3/20 inch fluid-diode lateral displacement

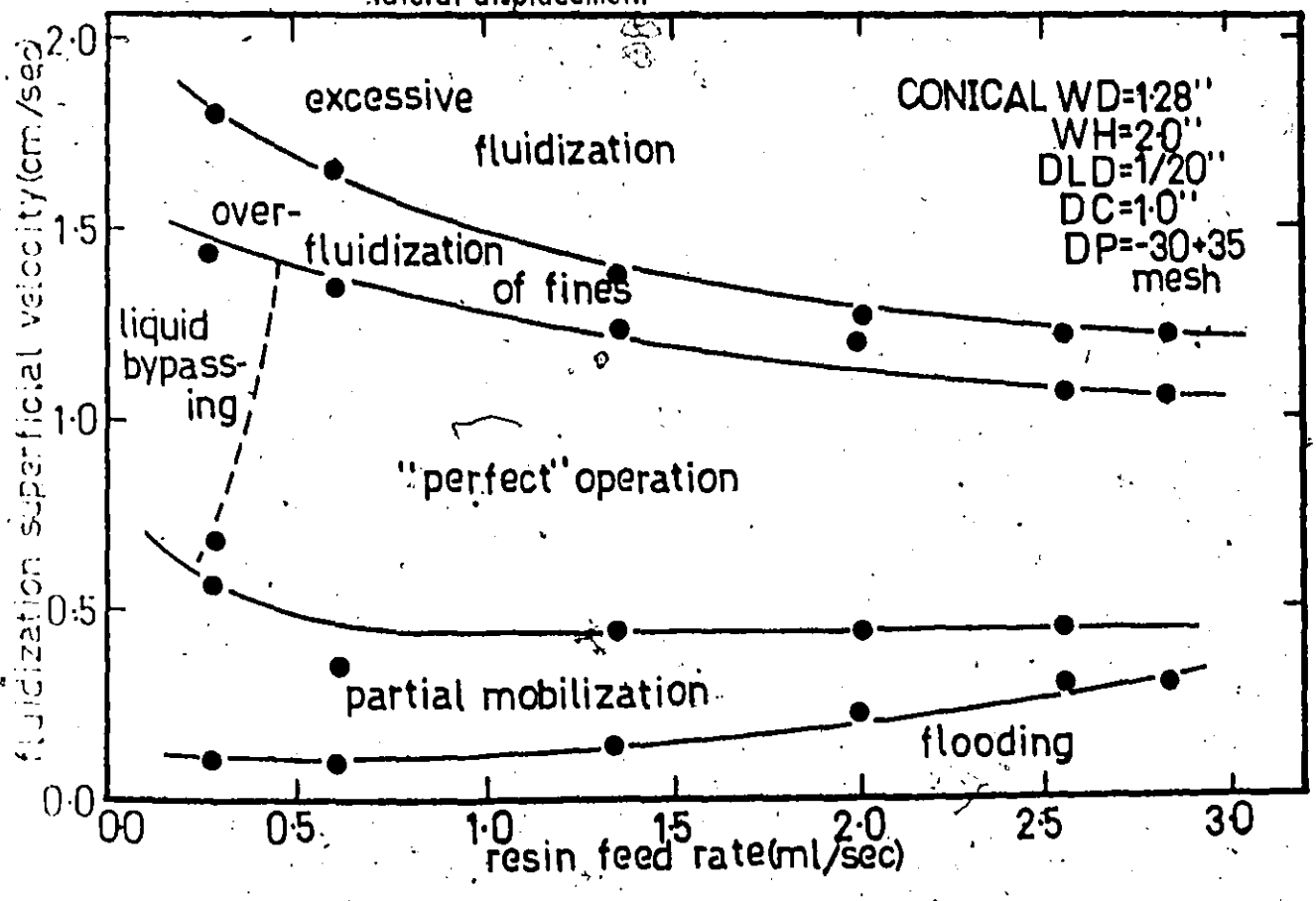

FIGURE C.6 Conical weir - effects of resin and liquid flow-rates

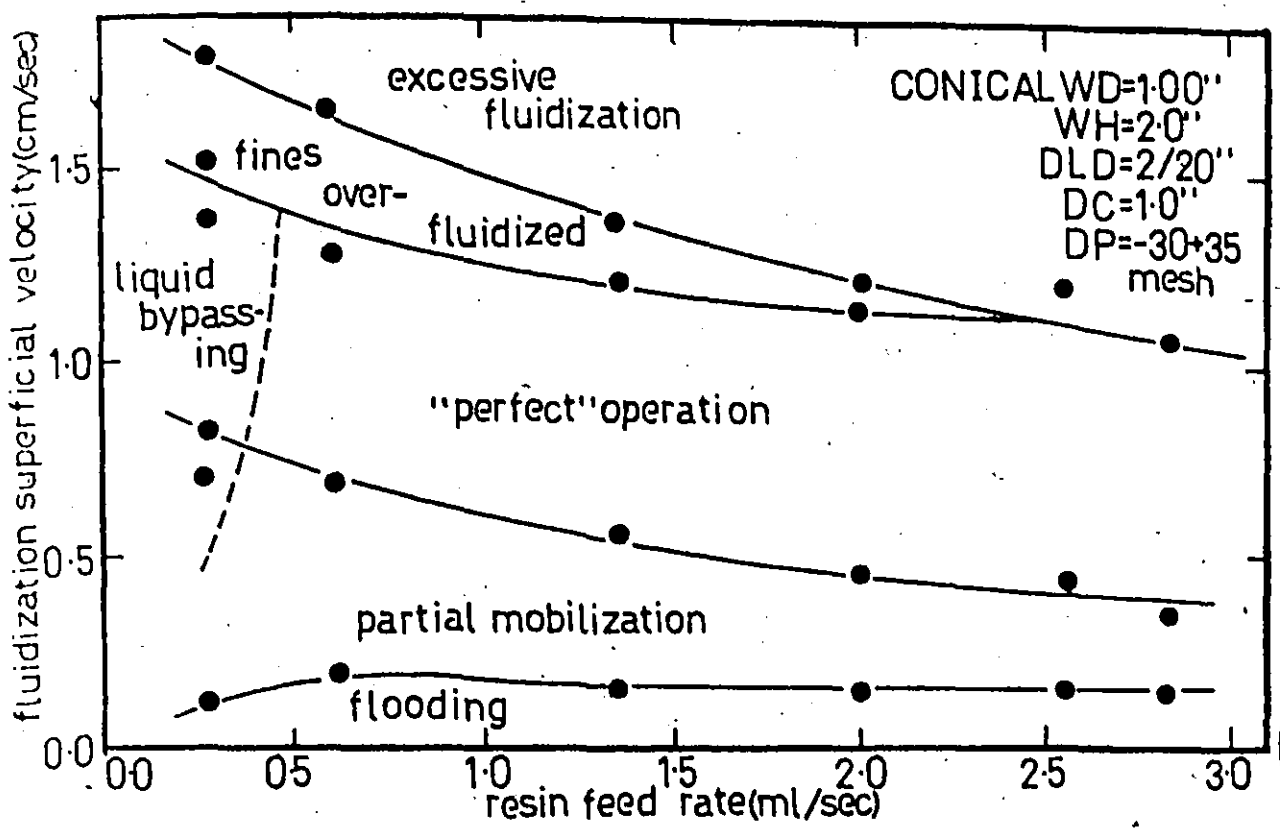

FIGURE C.7. Conical weir - effects of weir diameter

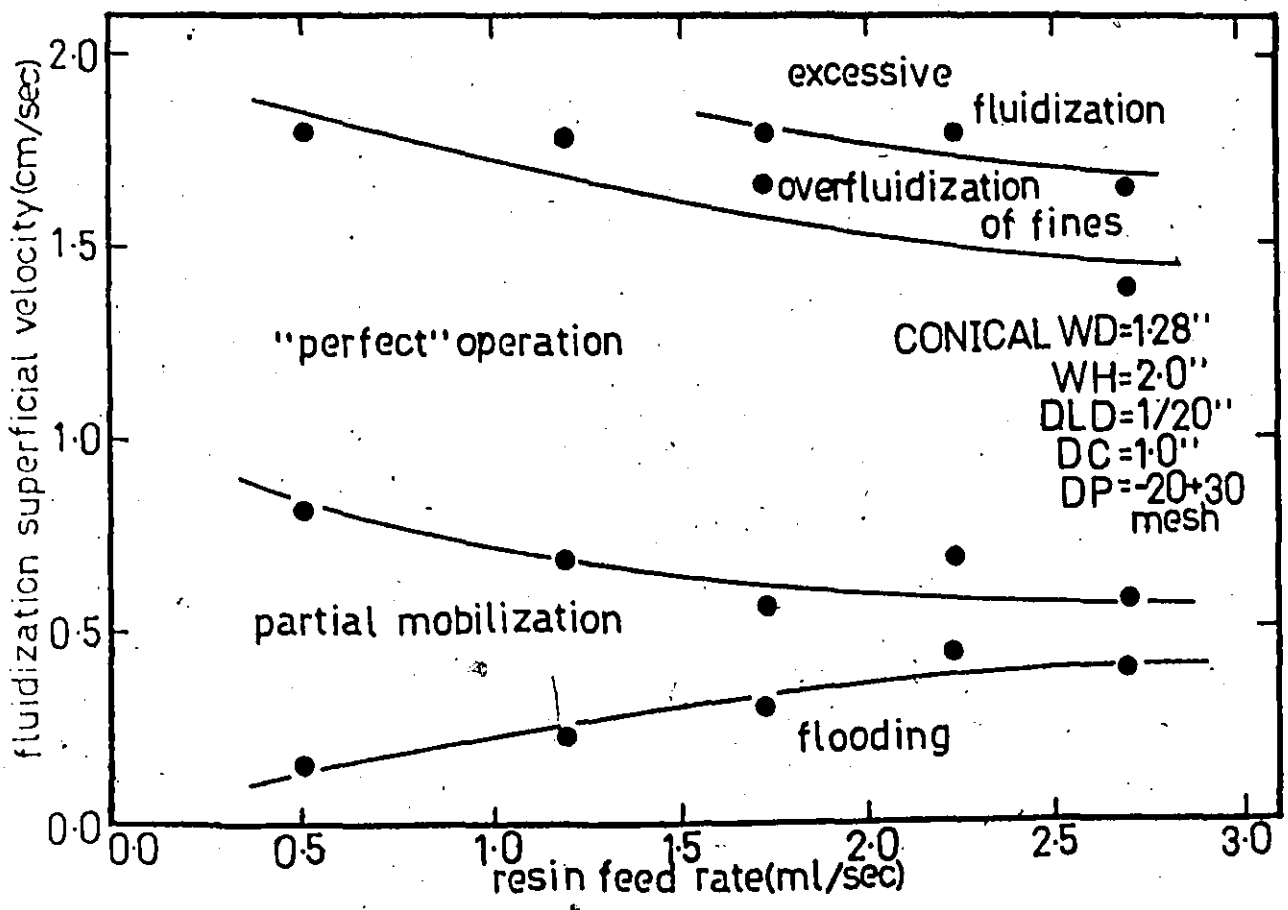

FIGURE C.8 Conical weir - effects of resin particles-size distribution

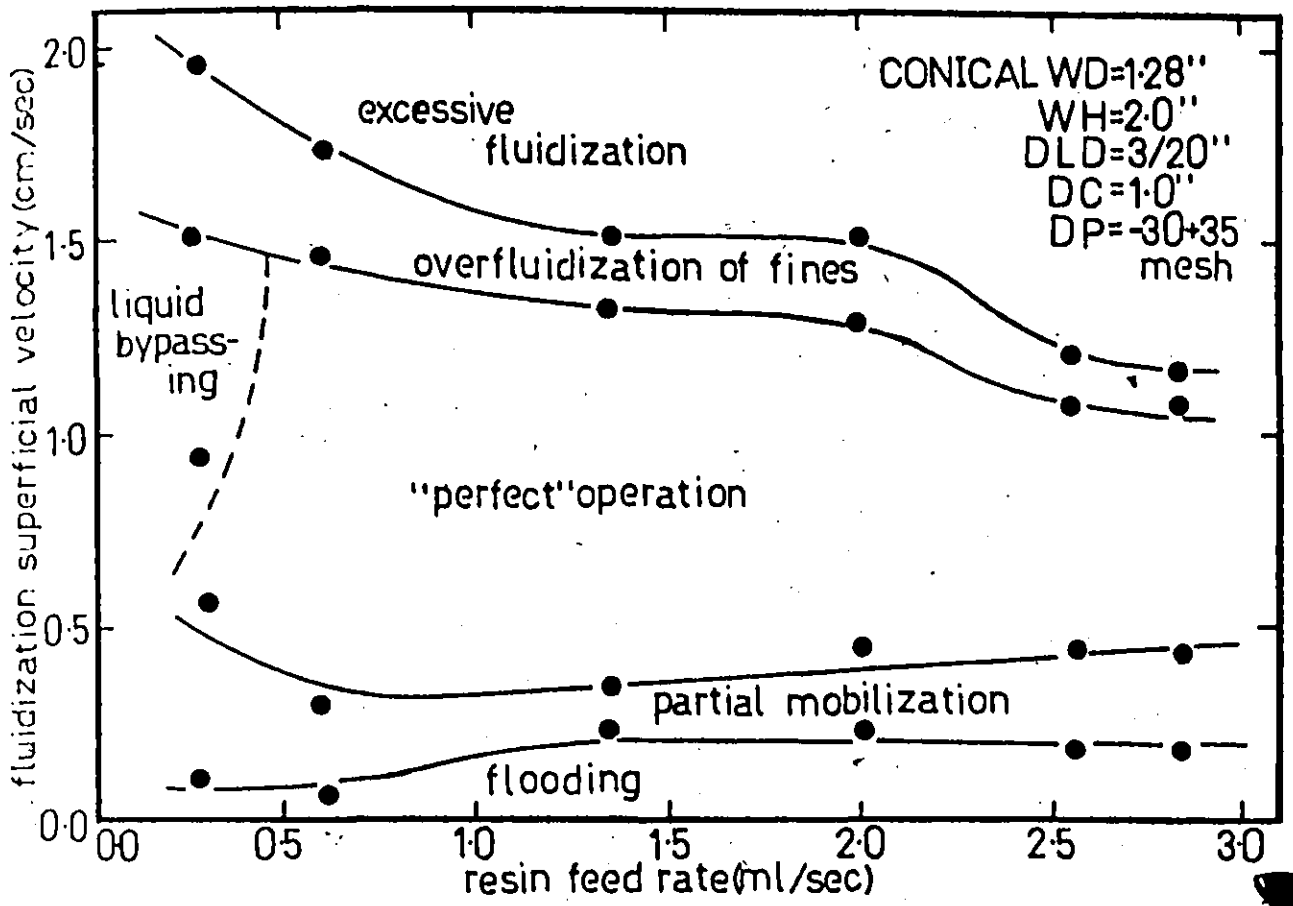

FIGURE C.9. Conical weir - effects of fluid-diode lateral displacement

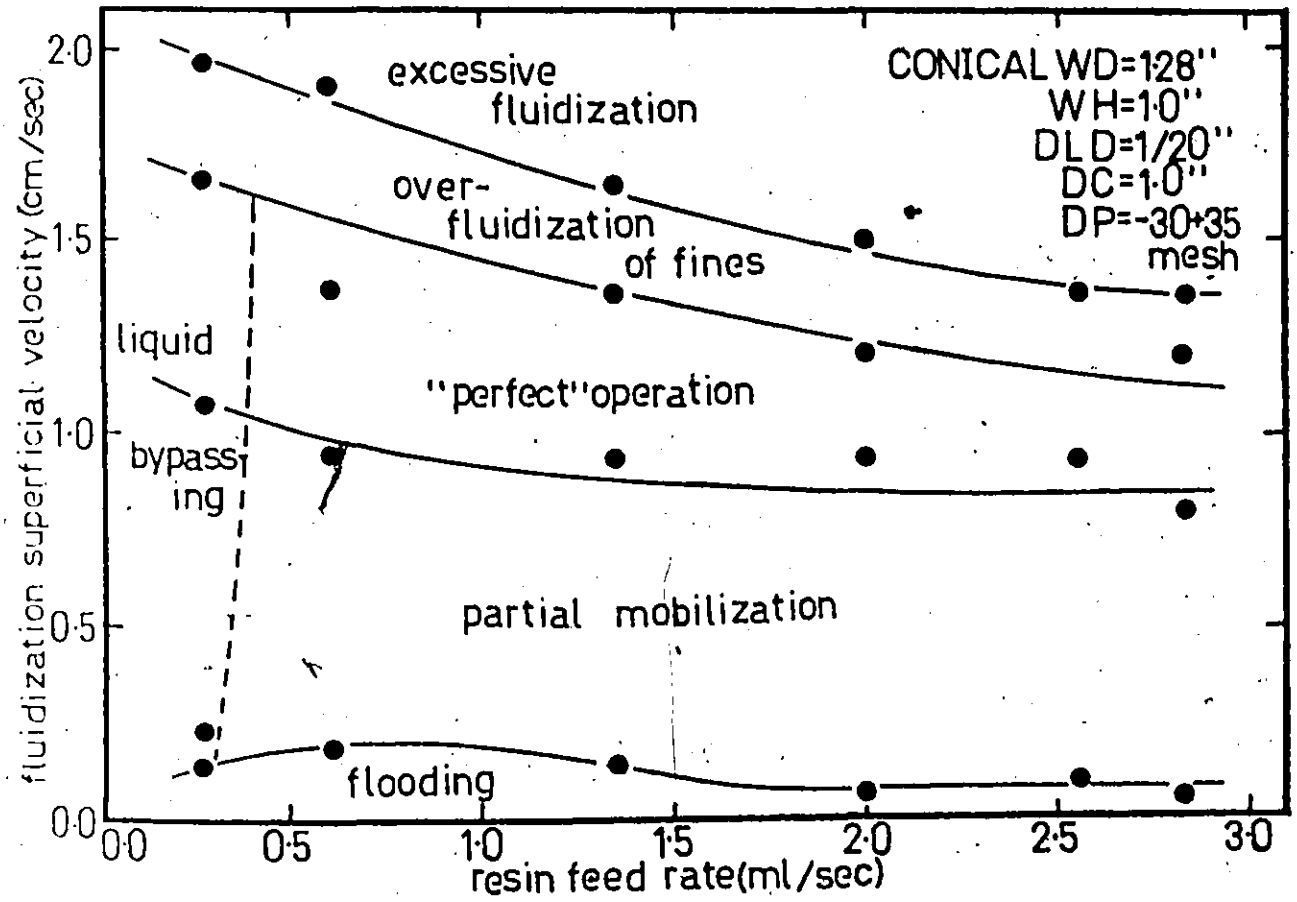

FIGURE C.10 Conical weir - effects of weir height at 1/20 inch fluid-diode lateral displacement

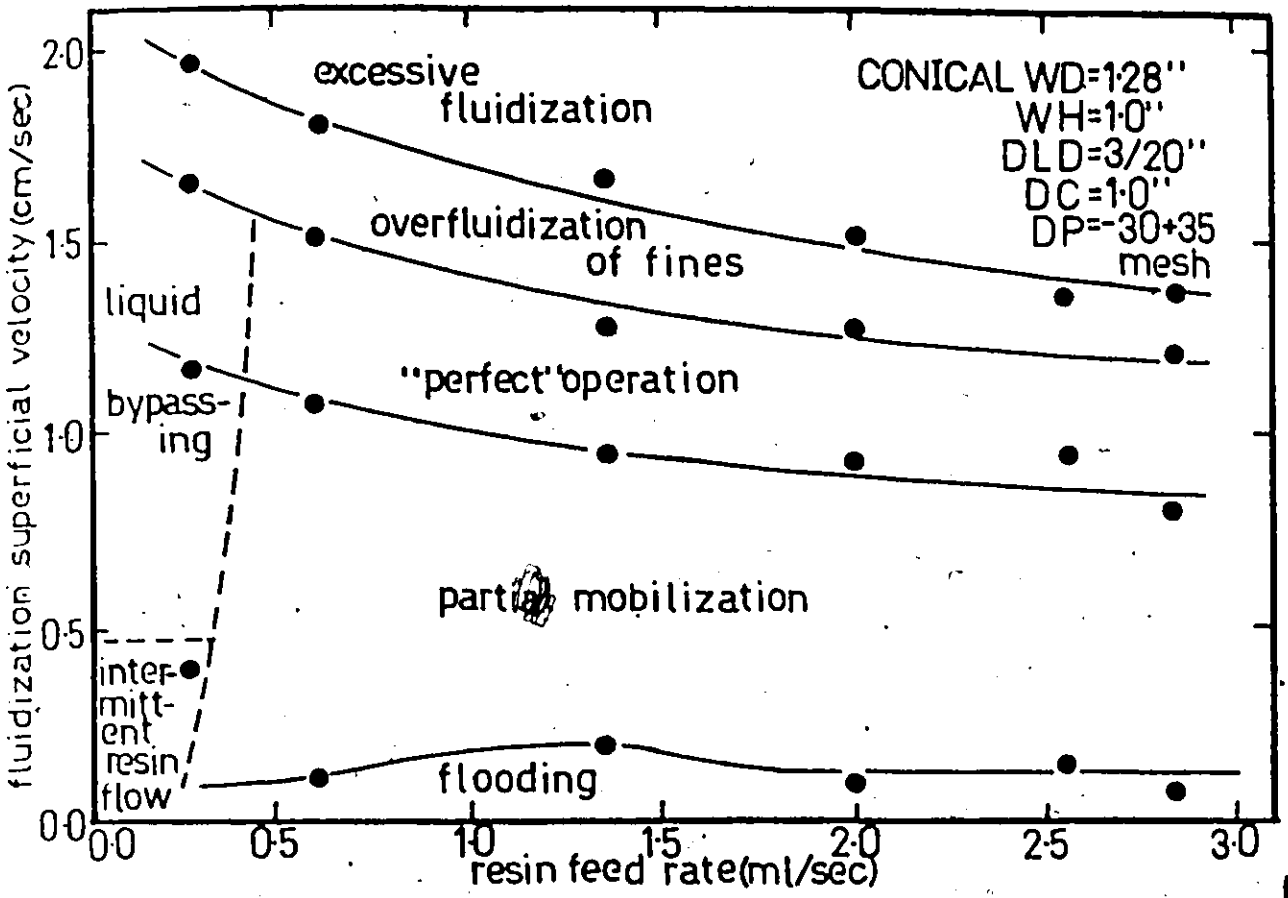

FIGURE C.11. Conical weir – effects of weir height at 3/20 inch fluid-diode lateral displacement

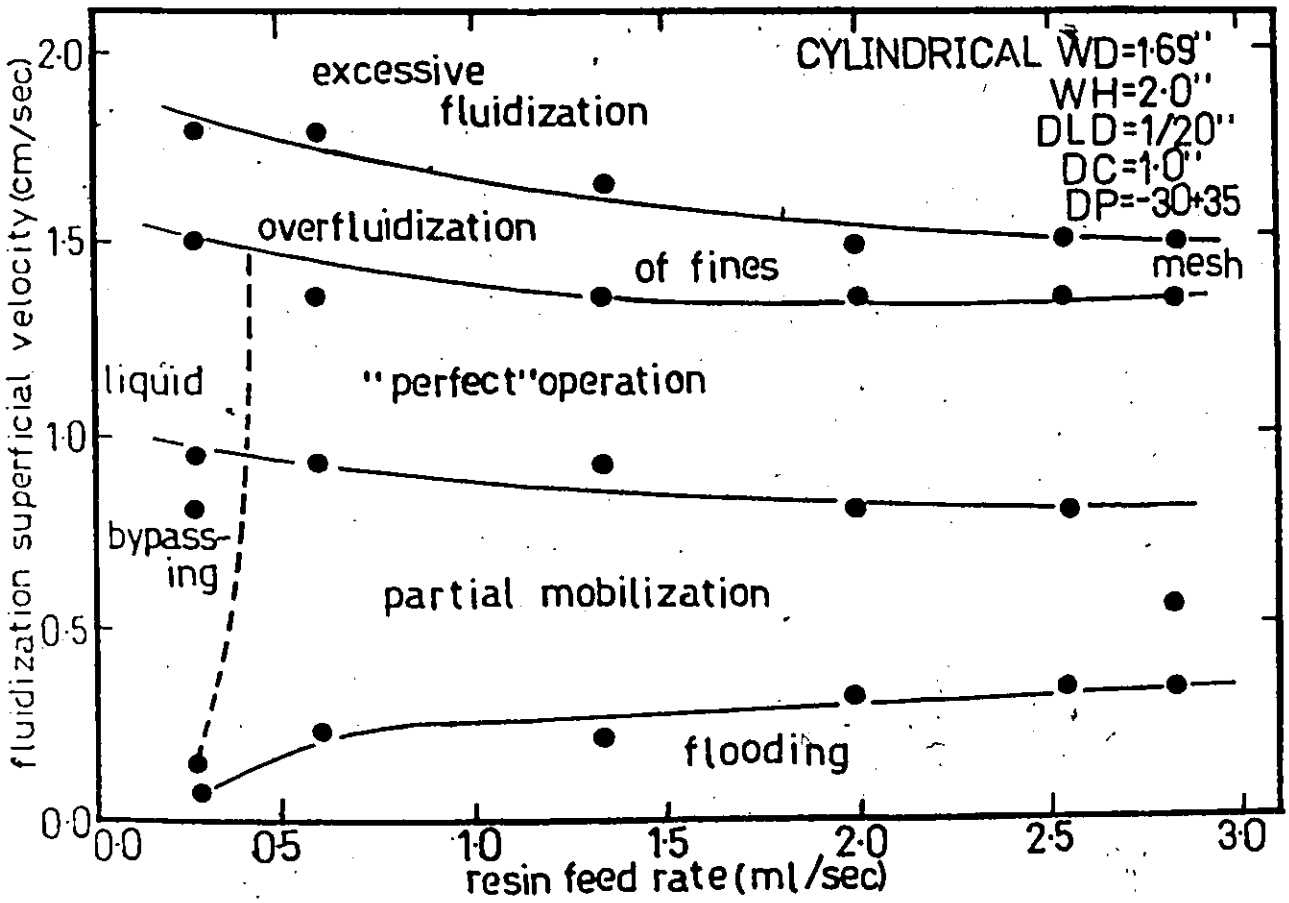

FIGURE C.12 Cylindrical weir – effects of resin and liquid flow-rates

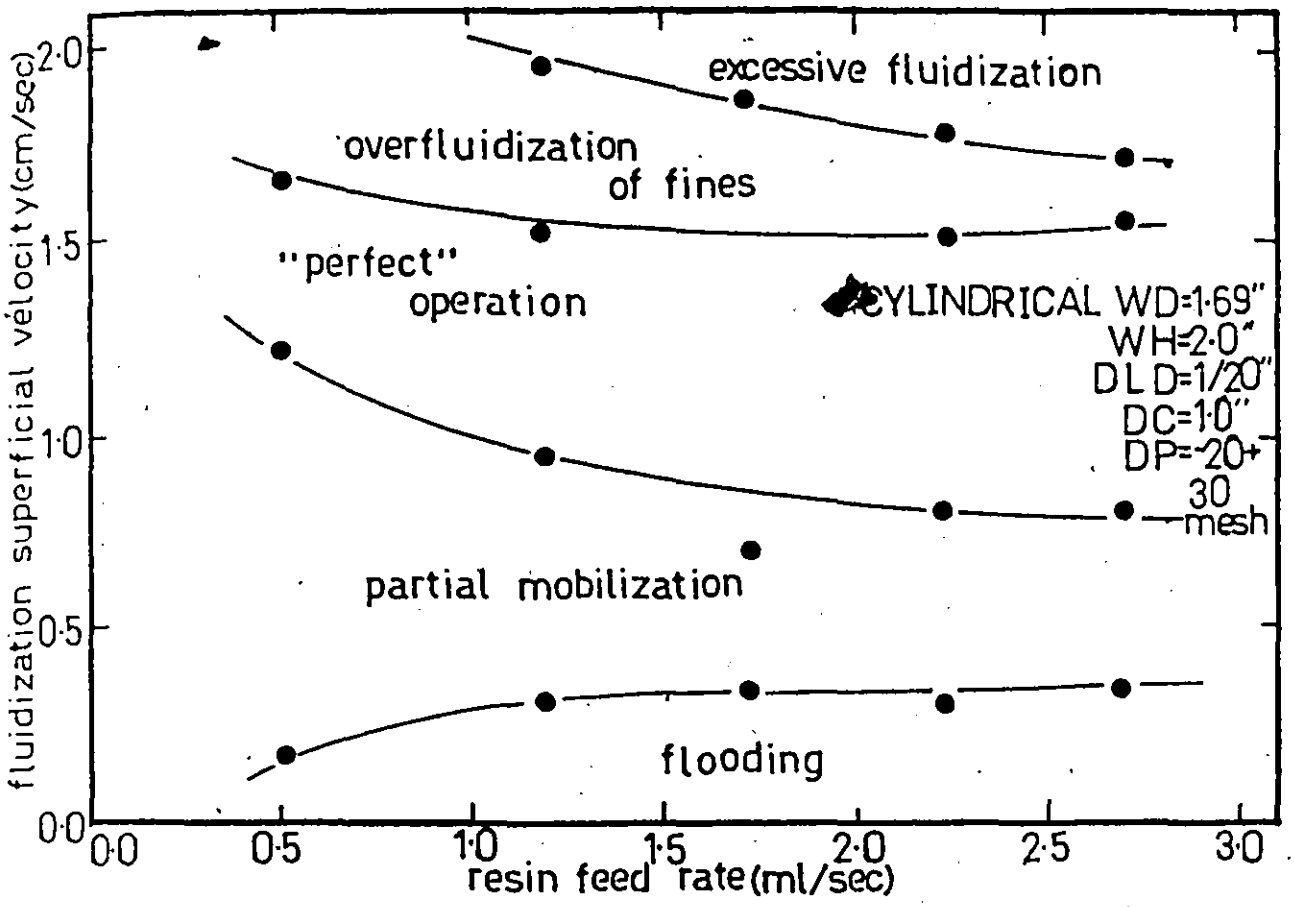

FIGURE C.13 Cylindrical weir - effects of resin particle-size distribution

APPENDIX D

Miscellaneous Figures

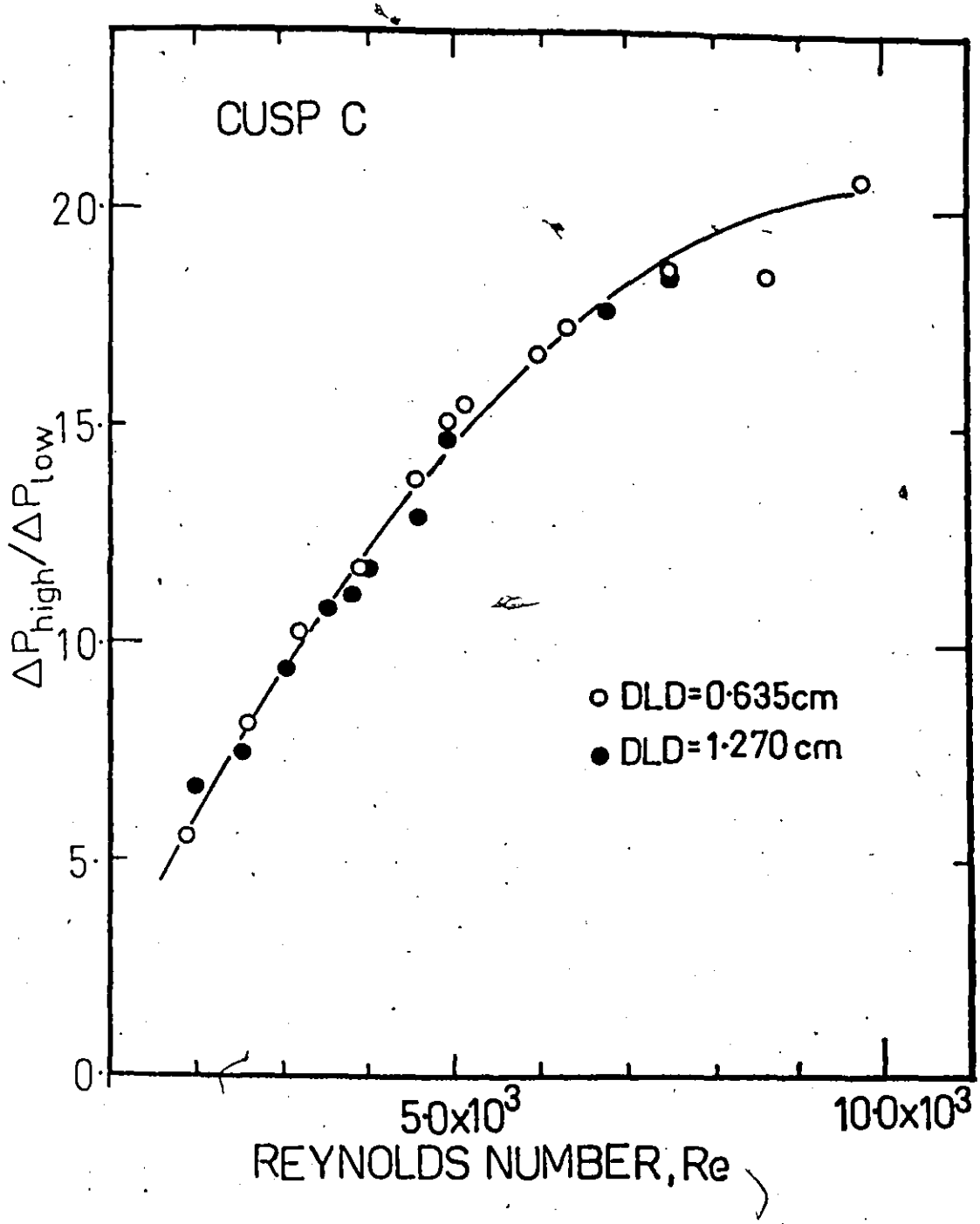

FIGURE D.1 A plot of pressure-drop ratios (high/low) versus Reynold numbers with data from the work of Egan (7)

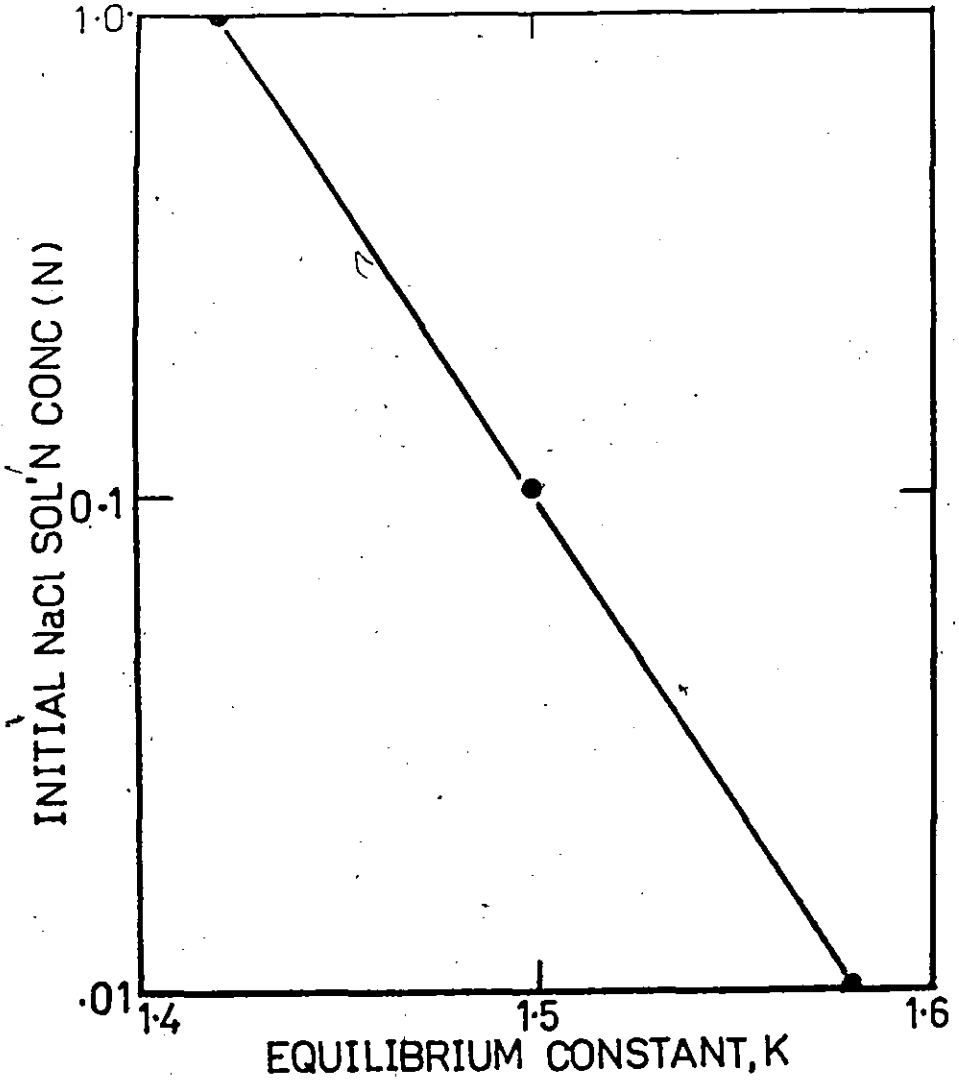

FIGURE D.2 A plot of initial sodium chloride concentration in solution versus the equilibrium constant for hydrogen/sodium exchange on Dowex-50-x8 resin. Data is from the work of Gilliland and Baddour (37)

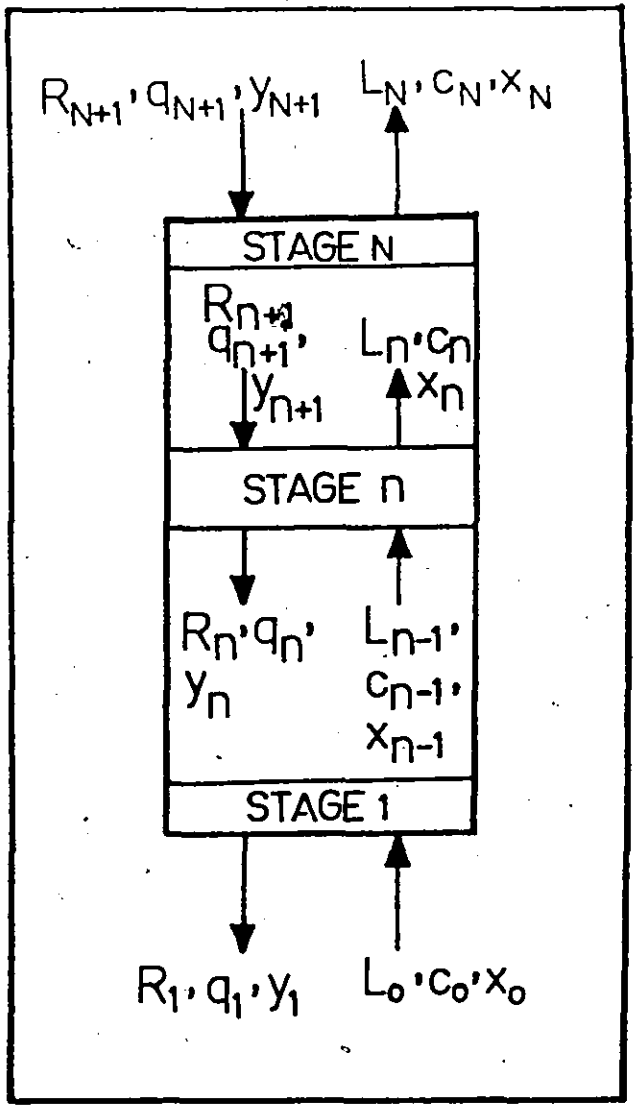

FIGURE D.3. Continuous countercurrent multistage operation

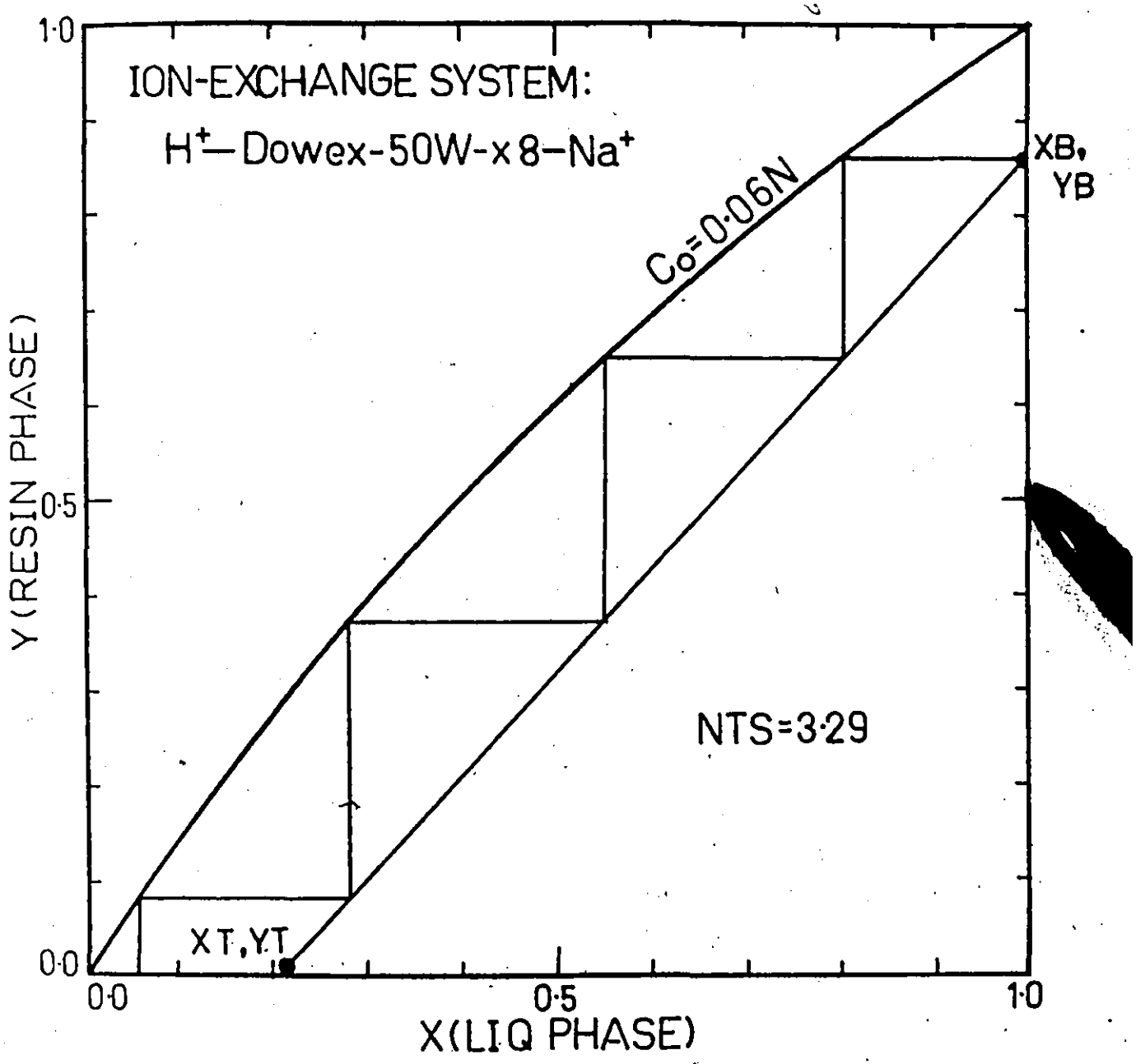

FIGURE D.4 Equilibrium diagram for the ion-exchange system showing the operating line and the number of theoretical stages for a typical continuous countercurrent operation

APPENDIX E

Factorial Experimental Design

Treatment combination	Representation by signs			Effect matrix							
	A	B	C	Mean	A	B	AB	C	AC	BC	ABC
1	-	-	-	+	-	-	+	-	+	+	-
a	+	-	-	+	+	-	-	-	-	+	+
b	-	+	-	+	-	+	-	-	+	-	+
ab	+	+	-	+	+	+	+	-	-	-	-
c	-	-	+	+	-	-	+	+	-	-	+
ac	+	-	+	+	+	-	-	+	+	-	-
bc	-	+	+	+	-	+	-	+	-	+	-
abc	+	+	+	+	+	+	+	+	+	+	+

TABLE E.1 Effect matrix generated for a 2^3 factorial design with factors: A, B and C. In any treatment combination, the low levels are denoted by "-" signs and the high levels by "+" signs. An interaction effect column is obtained by multiplying the columns of those factors appearing in the interaction. To compute any effect, the particular effect column is associated with the treatments and the algebraic sum multiplied by $(1/2)^{3-1}$.

Treatment combination	(1)	(2)	(3)
1	1+a	1+a+b+ab	1+a+b+ab+c+ac+bc+abc = Total
a	b+ab	c+ac+bc+abc	a-1+ab-b+ac-c+abc-bc = 4A
b	c+ac	a-1+ab-b	b+ab-1-a+bc+abc-c-ac = 4B
ab	bc+abc	ac-c+abc-bc	ab-b-a+1+abc-bc-ac+c = 4AB
c	a-1	b+ab-1-a	c+ac+bc+abc-1-a-b-ab = 4C
ac	ab-b	bc+abc-c-ac	ac-c+abc-bc-a+1-ab+b = 4AC
bc	ac-c	ab-b-a+1	bc+abc-c-ac-b-ab+1+a = 4BC
abc	abc-bc	abc-bc-ac+c	abc-bc-ac+c-ab+b+a-1 = 4ABC

TABLE E.2 Yates' technique for generating the total effects for a 2^3 factorial design with factors: A, B and C. The order of treatment combinations in the column must be maintained. The first half of column (1) is obtained by adding the responses of the treatment combinations in adjacent pairs and the second half by subtracting the responses in pairs (first from second of the pair). Column (2) is obtained in the same manner. The process is carried out 3 times for a 2^3 experiment.

Treatment combination	Effect matrix							
	Mean	A	B	AB	C	AC	BC	ABC
a	+	+	−	−	−	−	+	+
b	+	−	+	−	−	+	−	+
c	+	−	−	+	+	−	−	+
abc	+	+	+	+	+	+	+	+

TABLE E.3 Effect matrix generated for a $1/2 \times 2^3$ factorial design with A, B and C as the factors and ABC the defining contrast. The estimate of ABC interaction effect is identical to that of the general mean. The estimates of the pairs A and BC, B and AC, and AB and C are also identical.

	Defining contrasts beginning with main effects					
176	167*	156*	145*	134*	123*	112*
	165	154	143	132	121	
...	beginning with 2-factor interaction effects					
275	266	257*	246*	235*	224*	213*
	264	255	244	233	222	
		253	242	231*		
...	beginning with 3-factor interaction effects					
374	365	356*	347*	336*	325*	314*
	363	354	345*	334*	323*	312*
		352*	343	332*	321*	
			341*			
...	beginning with 4-factor interaction effects					
473	464	455	446*	437*	426*	415*
	462*	453*	444	435*	424*	413*
		451*	442*	433*	422*	
				431*		
...	beginning with 5-factor interaction effects					
572	563*	554*	545*	536*	527*	516*
	561*	552*	543*	534*	525*	514*
			541*	532*	523*	
...	beginning with 6-factor interaction effects					
671	662*	653*	644*	635*	626*	617*
		651*	642*	633*	624*	615*
...	beginning with 7-factor interaction effects					
	761*	752*	743*	734*	725*	716*

TABLE E.4 All the possible sets of defining contrasts for splitting the 2^7 factorial design (with factors A, B, C, D, E, F, and G) into four equal blocks. The number 176 represents the set of defining contrasts: A, ABCDEFG, and (BCDEFG), and 167 represents A, BCDEFG and (ABCDEFG). The "*" indicates that the associated numbers appeared before in the list.

A	B	C	D	E	F	G	
0	0	0	0	0	0	0	(I)
1	1	0	0	0	0	0*	ab
0	0	0	1	1	0	0*	de
1	1	0	1	1	0	0	abde
0	0	0	0	0	1	1*	fg
1	1	0	0	0	1	1	abfg
0	0	0	1	1	1	1	defg
1	1	0	1	1	1	1	abdefg
0	0	1	1	0	1	0*	cdf
1	1	1	1	0	1	0	abcdf
0	0	1	0	1	1	0	cef
1	1	1	0	1	1	0	abcef
0	0	1	1	0	0	1	cdg
1	1	1	1	0	0	1	abcdg
0	0	1	0	1	0	1	ceg
1	1	1	0	1	0	1	abceg
1	0	0	1	0	1	0*	adf
0	1	0	1	0	1	0	bdf
1	0	0	0	1	1	0	aef
0	1	0	0	1	1	0	bef
1	0	0	1	0	0	1	adg
0	1	0	1	0	0	1	bdg
1	0	0	0	1	0	1	aeg
0	1	0	0	1	0	1	beg
1	0	1	0	0	0	0	ac
0	1	1	0	0	0	0	bc
1	0	1	1	1	0	0	acde
0	1	1	1	1	0	0	bcde
1	0	1	0	0	1	1	acfg
0	1	1	0	0	1	1	bcfg
1	0	1	1	1	1	1	acdefg
0	1	1	1	1	1	1	bcdefg

TABLE E.5a Treatment combinations of the principal block for the 1/4-replicate of a 2^7 factorial design. The factors are A, B, C, D, E, F, and G and the defining contrasts are ABCDE, ABCFG and (DEFG). The treatment combinations are represented by the numbers 0 and 1 (mod 2) and also equivalently by the lower case letters. "1" represents the letter which exists in the treatment combinations and "0" otherwise. The above treatment combinations satisfy the following modulo equations (mod 2) for the principal block: $x_1+x_2+x_3+x_4+x_5 = 0$ and $x_1+x_2+x_3+x_6+x_7 = 0$

Block 1 (principal)	Block 2	Block 3	Block 4
I	F	D	A
AB	ABF	ABD	B
DE	DEF	E	ADE
ABDE	ABDEF	ABE	BDE
FG	G	DFG	AFG
ABFG	ABG	ABDFG	BFG
DEFG	DEG	EFG	ADFG
ABDEFG	ABDEG	ABEFG	BDEFG
CDF	CD	CF	ACDF
ABCDF	ABCD	ABCF	BCDF
CEF	CE	CDEF	ACEF
ABCEF	ABCE	ABCDEF	BCEF
CDG	CDFG	CG	ACDG
ABCDG	ABCDFG	ABCG	BCDG
CEG	CEFG	CDEG	ACEG
ABCEG	ABCEFG	ABCDEG	BCEG
ADF	AD	AF	DF
BDF	BD	BF	ABDF
AEF	AE	ADEF	EF
BEF	BE	BDEF	ABEF
ADG	ADFG	AG	DG
BDG	BDFG	BG	ABDG
AEG	AEFG	ADEG	EG
BEG	BEFG	BDEG	ABEG
AC	ACF	ACD	C
BC	BCF	BCD	ABC
ACDE	ACDEF	ACE	CDE
BCDE	BCDEF	BCE	ABCDE
ACFG	ACG	ACDFG	CFG
BCFG	BCG	BCDFG	ABCFG
ACDEFG	ACDEG	ACEFG	CDEFG
BCDEFG	BCDEG	BCEFG	ABCDEFG

TABLE E.5b The four blocks of effects for the $1/4 \times 2^7$ factorial design with factors A, B, C, D, E, F and G and defining contrasts ABCDE, ABCFG and (DEFG). Treatment combinations of blocks 2, 3 and 4 satisfy the three pairs of modulo equations:

$$x_1+x_2+x_3+x_4+x_5 = 0 \pmod 2$$
$$\text{and } x_1+x_2+x_3+x_6+x_7 = 1 \pmod 2,$$
$$x_1+x_2+x_3+x_4+x_5 = 1 \pmod 2$$
$$\text{and } x_1+x_2+x_3+x_6+x_7 = 0 \pmod 2, \text{ and}$$
$$x_1+x_2+x_3+x_4+x_5 = 1 \pmod 2$$
$$\text{and } x_1+x_2+x_3+x_6+x_7 = 1 \pmod 2 \text{ respectively.}$$

Effect		Aliases	
I	ABCDE	ABCFG	DEFG
A	BCDE	BCFG	ADEFG
B	ACDE	ACFG	BDEFG
C	ABDE	ABFG	CDEFG
D	ABCE	ABCDFG	EFG
E	ABCD	ABCEFG	DFG
F	ABCDEF	ABCG	DEG
G	ABCDEG	ABCF	DEF
AB	CDE	CFG	ABDEFG
AC	BDE	BFG	ACDEFG
AD	BCE	BCDEG	AEFG
AE	BCD	BCEFG	ADFG
AF	BCDEF	BCG	ADEG
AG	BCDEG	BCF	ADEF
BC	ADE	AFG	BCDEFG
BD	ACE	ACDFG	BEFG
BE	ACD	ACEFG	BDFG
BF	ACDEF	ACG	BDEG
BG	ACDEG	ACF	BDEF
CD	ABE	ABDFG	CEFG
CE	ABD	ABEFG	CDFG
CF	ABDEF	ABG	CDEG
CG	ABDEG	ABF	CDEF
DE	ABC	ABCDEFG	FG
DF	ABCEF	ABCDG	EG
DG	ABCEG	ABCDF	EF
ADF	BCEF	BCDG	AEG
ADG	BCEG	BCDF	AEF
BDF	ACEF	ACDG	BEG
BDG	ACEG	ACDF	BEF
CDE	ABEF	ABDG	CEG
CDG	ABEG	ABDF	CEF

TABLE E.6 Alias groups in the $1/4 \times 2^7$ factorial design with factors A, B, C, D, E, F and G and defining contrasts ABCDE, ABCFG and (DEFG). The aliases are obtained by multiplying (mod 2) each effect by the defining contrasts.

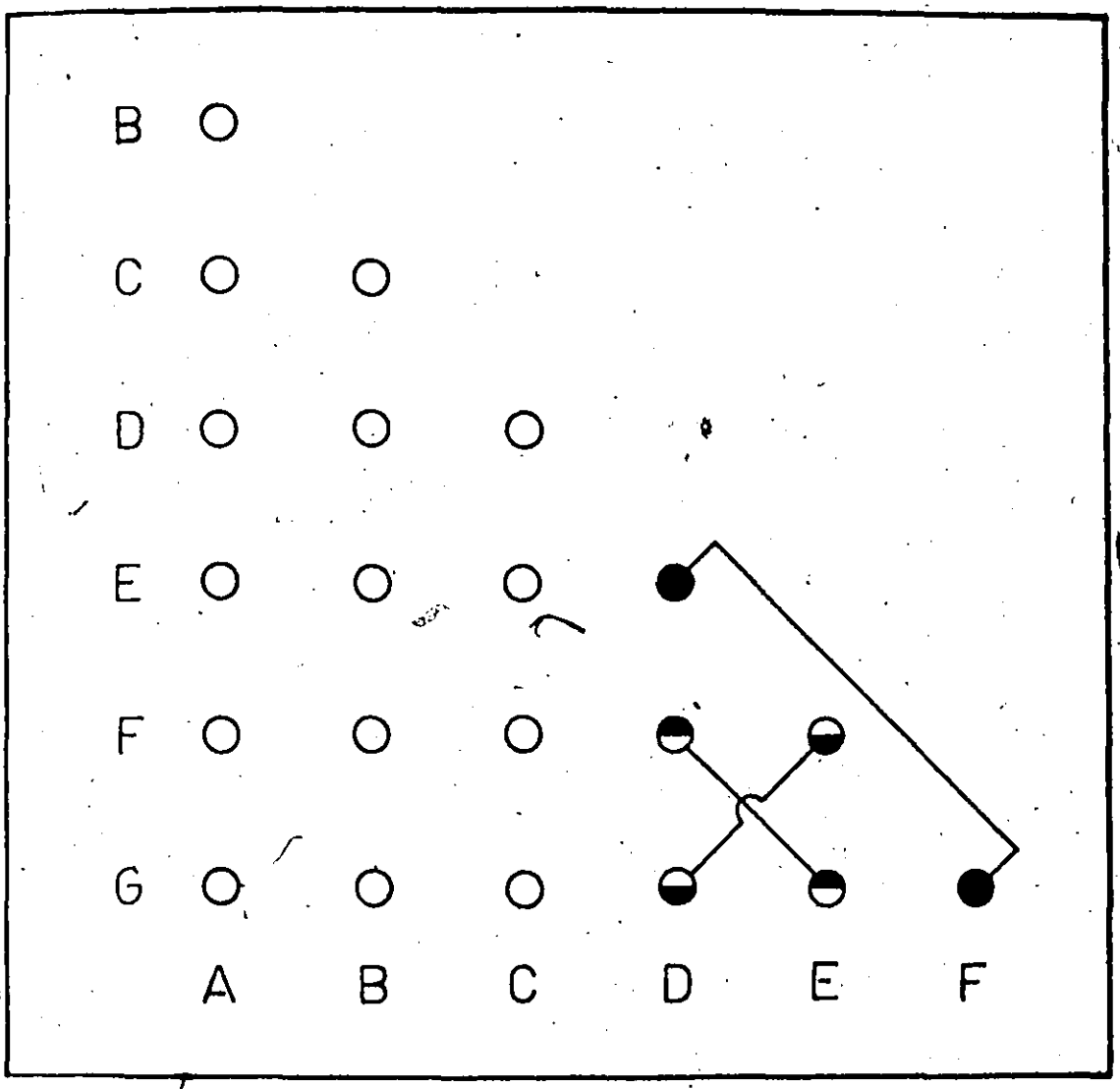

FIGURE E.1 Confounding pattern for the 2-factor interactions

1	ACDE	17	CDF
2	BCDE	18	ABCDF
3	ABDE	19	ADF
4	DE	20	BDF
5	AC	21	CEF
6	BC	22	ABCEF
7	I	23	AEF
8	AB	24	BEF
9	CDG	25	ACDEFG
10	ABCDG	26	BCDEFG
11	ADG	27	DEFG
12	BDG	28	ABDEFG
13	CEG	29	ACFG
14	ABCEG	30	BCFG
15	AEG	31	FG
16	BEG	32	ABFG

TABLE E.7 Order of performing the 32 experimental runs for the 1/4-replicate factorial design.

ANALYSIS OF VARIANCE TABLE(ANOV)

EFFECT	SUM OF SQUARE	DEG. OF FREEDOM	MEAN SUM OF SQUARE	MEAN SQUARE RATIO	
(A)B	100.543	1.0	100.543	9.804	**FL
(A)C	5.831	1.0	5.831	.569	
BC	2.838	1.0	2.838	.277	
(D)E	29.234	1.0	29.234	2.851	
(A)B(D)E	.051	1.0	.051	.005	
(A)C(D)E	2.393	1.0	2.393	.233	
BC(D)E	17.440	1.0	17.440	1.701	
(A)(D)E	3.696	1.0	3.696	.360	
B(D)E	28.876	1.0	28.876	2.816	
C(D)E	.013	1.0	.013	.001	
(A)BC(D)E	138.353	1.0	138.353	13.491	**(FS)x(WL)
(A)EF	83.728	1.0	83.728	8.164	**(WH)x(WL)
BEF	22.438	1.0			
CEF	2.523	1.0			
(A)BCEF	9.777	1.0			
(A)(D)G	1026.294	1.0	1026.294	100.072	***WL
B(D)G	198.025	1.0	198.025	19.309	***(WL)x(FL)
C(D)G	7.310	1.0	7.310	.713	
(A)BC(D)G	24.416	1.0	24.416	2.381	
(A)EG	12.560	1.0	12.560	1.225	
BEG	6.292	1.0			
CEG	1.043	1.0			
(A)BCEG	19.459	1.0			
FG	17.003	1.0	17.003	1.658	
(A)BFG	1.315	1.0	1.315	.128	
(A)CFG	2.741	1.0	2.741	.267	
BCFG	182.405	1.0	182.405	17.786	***FS
(D)EFG	1276.893	1.0	1276.893	124.508	***WH
(A)B(D)EFG	.656	1.0	.656	.064	
(A)C(D)EFG	3.200	1.0	3.200	.312	
BC(D)EFG	.890	1.0	.890	.087	

.... Cont'd p.170

RESIDUAL	61.533	6.0	10.256

CRITICAL VALUES:

F(1,6,0.90) = 3.78 F(1,6,0.95) = 5.99 F(1,6,0.999) = 13.75

TABLE E.8 Analysis of variance table

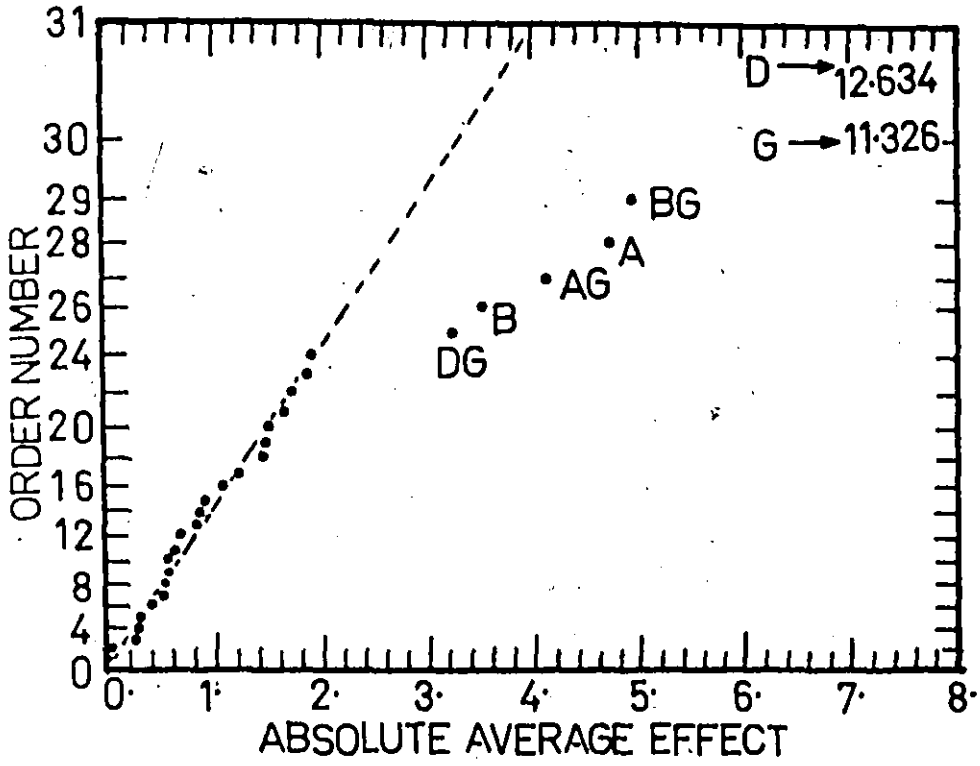

FIGURE E.2 Half-normal plot for the absolute average effects

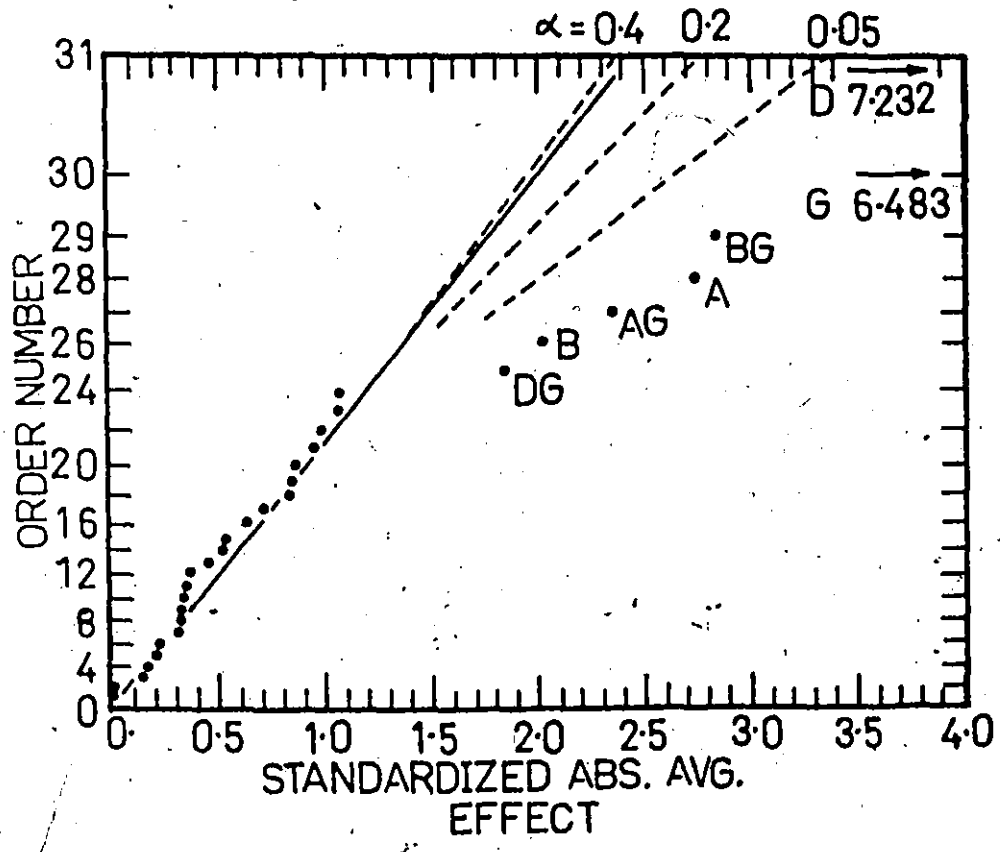

FIGURE E.3 Standardized half-normal plot for the absolute average effects

APPENDIX F

Half-normal Plot

The following discussion on half-normal plot is adapted from the work by Daniel (49) and also from the text by Johnson and Leone (48).

The results from a complete factorial (2^P) or a fractional factorial (2^{P-q}) experimental design can be studied using the analysis of variance (ANOVA) table. Sometimes there is a question as to which effects can reasonably be pooled together into the residual sum of squares, i.e. assumed to be zero. The half-normal plot proposed by Daniel (49) is helpful in solving this problem. The plotting can also be used to detect such defects as the existence of wild values in a set of observations (effects), the error variance being not the same for all observations, or the planned randomization being inadvertently modified (e.g. by plot splitting).

The half-normal plotting is based on the fact that the theoretical cumulative distribution of the absolute values of the average effects ($u' = |u|$, where u has a normal distribution) is a straight line through the origin on a half-normal probability paper. The slope of the straight line is determined by the population standard deviation.

In the half-normal plot, the average effects are arranged in the order of estimated absolute magnitude. The effects are then plotted on half-normal probability paper. The half-normal probability paper is obtained by modifying the vertical scale of the normal probability paper. The range of P less than 50% is deleted and the range of P greater than 50% is modified to

$$P' = 2P - 100$$

where P is the cumulative probability of the normal distribution and P' the cumulative

distribution used in the half-normal paper. Instead of a cumulative probability for the vertical scale, an ordered rank of i = 1, 2, 3, ..., n for the emperical data is used. A general conversion formula for the vertical scale is

$$P' = (i - 1/2)/n \qquad i = 1,2, \ldots n)$$

where n is the number of orthogonal contrasts and n+1 is then the number of observations (effects) in the experimental design. The abscissae are the absolute values of the average effects.

In a standardized half-normal plot, the average effects are standardized and significance limits can be placed on the chart. The standardization is performed by using u_α as an approximation to the standard deviation (σ). u_α is the absolute value of the rank order statistic from the n average effects that is nearest to (0.683n + 0.5). Values of u_α for different values of n are given below

			d		
n	τ	rank of u_α	α =0.05	0.20	0.40
15	2.09	11	0.94	0.26	-0.14
31	2.42	22	0.94	0.33	-0.05
63	2.69	44	0.66	0.23	-0.04
127	2.88	88	0.66	0.25	0.00

where n = number of orthogonal contrasts

τ = expected value of the ratio of the largest absolute value of the n observed values to the corresponding σ-estimator, u_α

α = frequency of false positives per experiment

d = deviations to right of centre line.

The "centre line" and "significance limits" for the standard plot are determined using the constants in the above table,

Centre line: Through points (0,0) and (τ , n)

Significance limit: Through points (τ + d, n) and (1, rank (u_α)).

APPENDIX G

Computer Program for Mass-Transfer Experiments

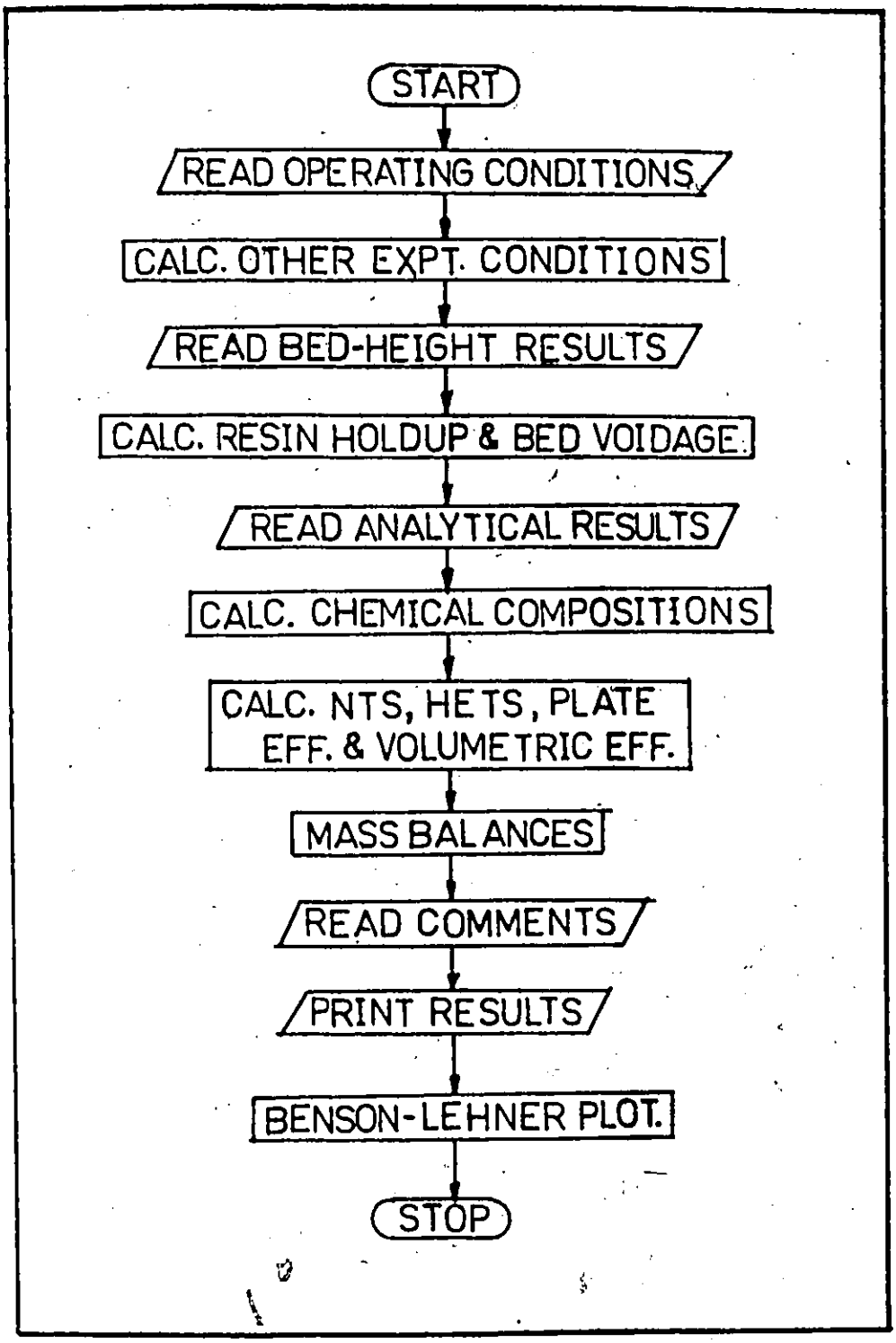

FIGURE C.1 Flow chart of the computer program for analysing the results of mass-transfer experiments

```
C COMPUTER PROGRAM TO CALCULATE THE NUMBER OF THEORETICAL STAGES
C (NTS), HEIGHT EQUIVALENT OF A THEORETICAL STAGE (HETS), AND PLATE
C AND VOLUMETRIC EFFICIENCIES OF A CONTINUOUS COUNTERCURRENT MULTI-
C STAGE IONEXCHANGE COLUMN WITH FLUID DIODE DOWNCOMER
C THE PROGRAM ALSO PLOTS THE EQUILIBRIUM DIAGRAM, OPERATING LINES ,
C AND THE THEORETICAL STAGES USING THE BENSON-LEHNER PLOTTING SYSTEM
C WRITTEN BY C.Y.F. LAW
C JULY, 1973

      DIMENSION X(20),Y(20),COM(80),FBED(12),SBED(12)
      DIMENSION RVI(4),RVF(4),TVI(4),TVF(4),CLMVI(4),CLMVF(4),PHI(4),
     1          PHF(4)
      DIMENSION RI(4),RF(4),CLI(4),CLF(4),HI(4),HF(4)
      DIMENSION XEQ(400),YEQ(400),XP(20),YP(20)
      REAL INTER,LABXTP,LABYTP,LABXBP,LABYBP

      WRITE TITLE
      WRITE(6,10)
   10 FORMAT( 1H1, * CONTINUOUS COUNTERCURRENT MULTISTAGE ION-EXCHANGE W
     1ITH* // * FLUID DIODE DOWNCOMER* /// * EXPERIMENTS WERE PERFORMED
     2WITH A COLUMN OF FOUR INCHES INSIDE* // * DIAMETER.  THE EXCHANGER
     3 HAS SIX STAGES SPACED 4.5 INCHES APART*        // * THE ION-EXCHAN
     4GE SYSTEM IS SODIUM ION-DOWEX-50WX8 RESIN-HYDROGEN ION*)
      COUNTER=1.0
   40 CONTINUE

C READ AND WRITE RUN NUMBER
      READ(5,20)RUN
   20 FORMAT(A10)
      IF(EOF(5))999,30
   30 CONTINUE
      IF(COUNTER.EQ.1.0)WRITE(6,40)RUN
   40 FORMAT(/// * RUN NUMBER  *, A10, /, 15H **************)
      IF(COUNTER.GT.1.0)WRITE(6,35)RUN
   35 FORMAT(1H1, * RUN NUMBER  *, A10, /, 17H  ****************)

C READ WEIR TYPE NUMBER
C TYPE=1.0 FOR STRAIGHT WEIR
C TYPE=2.0 FOR CYLINDRICAL WEIR
C TYPE=3.0 FOR CONICAL WEIR
      READ(5,80)TYPE
   80 FORMAT(F10.0)

C READ AND WRITE OPERATING PARAMETERS
C COLUMN DIMENSION IN INCHES, SODIUM CONCENTRATION IN MEQ/ML AND
C PARTICLE SIZE IN MESH NUMBERS
      READ(5,50)FL,FS,SIC,WL,WH,DC,DLD,DP
   50 FORMAT(7F10.0,A10)
      WRITE(6,60)FL,FS,SIC
   60 FORMAT(//, * OPERATING PARAMETERS* ///,
     15X, *LIQUID FLOW RATE(ML/SEC)=*, F7.3, //,
     25X, *SOLID FLOW RATE(ML/SEC)=*, F6.3, //,
     35X, *INITIAL SODIUM CONC.(MEQ/ML)=*, F6.3)
      IF(TYPE.EQ.1.0)WRITE(6,95)WL
   95 FORMAT( /, 5X, *STRAIGHT WEIR LENGTH(INCH)=*, F6.3)
      IF(TYPE.EQ.2.0)WRITE(6,105)WL
  105 FORMAT( /, 5X, *CYLINDRICAL WEIR DIAMETER(INCH)=*, F6.3)
      IF(TYPE.EQ.3.0)WRITE(6,205)WL
  205 FORMAT( /, 5X, *CONICAL WEIR DIAMETER(INCH)=*, F6.3)
```

```
      F(6,254)H,DC,DLD,DP
  FORMAT( /, 5X, *WEIR HEIGHT(INCH)=*, F6.3, //,
     *, *DOWNCOMER CLEARANCE(INCH)=*, F6.3, //,
     *, *DIODE LATERAL DISPLACEMENT(1/20 INCH)=*, F6.3, //,
     *, *RESIN PARTICLE SIZE(MESH)= *, A10)
C
C  CALCULATE AND WRITE OTHER OPERATING CONDITIONS
      ITE(6,2)
  FORMAT(///, 5X, *OTHER EXPERIMENTAL CONDITIONS*)
      =.0687*2.54
      =D/2.0
      IF(TYPE.GT.1.0)GO TO 215
      L=WL*2.54
      =SQRT(R**2.0-(WL/2.0)**2.0)
      IF(H.EQ.0.0)THETA=1.5708
      IF(H.GT.0.0)THETA=ATAN(WL/(2.0*H))
      ECTOR=(R**2.0)*THETA
      EGMENT=SECTOR-(WL*H/2.0)
C     AC IS THE CATCHING AREA OF WEIR
C     AD IS THE BOTTOM AREA OF WEIR
      AC=AD=SEGMENT
      GO TO 225
  CONTINUE
      IF(TYPE.GT.2.0)GO TO 285
      AC=AD=0.25*3.1416*(WL*2.54)**2.0
      GO TO 225
  CONTINUE
      AC=0.25*3.1416*(WL*2.54)**2.0
      AD=0.25*3.1416*(0.6875*2.54)**2.0
      CONTINUE
      AT=3.1416*(R**2.0)
      AF=AT-AD
      AR1=AF/AT
      AR2=AD/AT
      AR=AF/AC
      WRITE(6,100)AT,AF,AC,AR1,AR2,AR
  FORMAT(///, 5X, *CROSS-SECTIONAL AREA(SQ.CM.)=*, F7.3, //,
     *, *FLUIDIZATION AREA(SQ.CM.)=*, F7.3, //,
     *, *DOWNCOMER CATCHING AREA(SQ.CM.)=*, F7.3,//,
     *, *FRACTION OF FLUIDIZATION AREA=*, F6.3, //,
     *, *FRACTION OF DOWNCOMER AREA=*, F6.3, //,
     *, *FLUIDIZATION TO DOWNCOMER AREA RATIO=*, F6.3)
      =FL/AT
      =FL/AF
      WRITE(6,110)CSV,TSV
  FORMAT(///, 5X, *OVERALL COLUMN SUPERFICIAL VEL.(ML/SQ.CM-SEC)=*,
     *F6.3, //, 5X, *FLUIDIZATION SUPERFICIAL VEL(ML/SQ.CM-SEC)=*, F6.3)
      =(WH-DC)*2.54
      WRITE(6,130)DS
  FORMAT( //, 5X, *DOWNCOMER SEAL(CM)=*, F6.3)
C     BAFFLE SPACING IS PS IN INCHES
      =4.4531
      =(PS-DC)*2.54
      WRITE(6,120)TDL
  FORMAT(///, 5X, *TOTAL DIODE LENGTH(CM)=*, F6.3)

C     RESIN VOIDAGE AND WATER FLOW RATE IN RESIN FEED
```

```
      READ(5,270)VOID,WATER
  270 FORMAT(2F10.0)

C     READ AND WRITE EXPERIMENTAL RESULTS IN BED HEIGHT
C     AND HEIGHT INPUT DATA IN INCHES
      WRITE(6,135)
  135 FORMAT(///,' EXPERIMENTAL RESULTS')
      READ(5,145)(FBED(I),I=1,12)
      READ(5,145)(SBED(I),I=1,12)
  145 FORMAT(8F10.4)
      DO 155 I=1,12
      FBED(I)=FBED(I)*2.54
      SBED(I)=SBED(I)*2.54
  155 CONTINUE
      CALL STAT(FBED,12,FMEAN,FSTD)
      CALL STAT(SBED,12,SMEAN,SSTD)
C     THE VOLUME OCCUPIED BY THE DIODE IS ACCOUNTED FOR IN CALCULATING THE
C     BED VOLUMES
      DTHICK=0.8281*2.54
C     THE DIODE WIDTH WITH ZERO LATERAL DISPLACEMENT IS 1.2562 INCHES
      DWIDTH=(1.2562+0.05*DLD)*2.54
      DAREA=DTHICK*DWIDTH
      FDS=FMEAN+TDL-PS*2.54
      IF(FDS.LE.0.0)DELTAFV=0.0
      IF(FDS.GT.0.0)DELTAFV=FDS*DAREA
      SDS=SMEAN+TDL-PS*2.54
      IF(SDS.LE.0.0)DELTASV=0.0
      IF(SDS.GT.0.0)DELTASV=SDS*DAREA
      FBMV=FMEAN*AF-DELTAFV
      SBMV=SMEAN*AF-DELTASV
      FBMVOID=(FBMV-SBMV*(1.0-VOID))/FBMV
      WRITE(6,165)FMEAN,SMEAN,FSTD,SSTD,FBMV,SBMV
  165 FORMAT(/, 25X, *FLUIDIZED     SETTLED*, /, 28X, *BED*, 10X, *BED*,
     1 /, 5X, *MEAN HEIGHT(CM)*, F13.3, F13.3,
     2 /, 5X, *HEIGHT STD DVN*, F14.3, F13.3,
     3 /, 5X, *MEAN VOL(C.C.)*, F14.3, F13.3)
      WRITE(6,70)FBMVOID
   70 FORMAT(///, 5X, *MEAN FLUIDIZED BED VOIDAGE=*, F6.3)
      WH=FMEAN*2.54
      WRITE(6,175)WH
  175 FORMAT(/, 5X, *(NOTE9 WEIN HEIGHT(CM)=*, F6.3, *)* )

C     READ ANALYTICAL RESULTS, CALCULATE AND WRITE THE INITIAL AND FINAL
C     RESIN CAPICITIES, SODIUM CONCENTRATIONS AND HYDROGEN CONCENTRATIONS
C     AND NUMBER OF SETS OF SAMPLE DATA (MAXIMUM OF FOUR)
      READ(5,275)RN
  275 FORMAT(F10.0)
C     RN IS THE SODIUM HYDROXIDE TITRANT NORMALITY(=MEQ/ML)
      TVOL=0.1
C     WRITE HEADINGS
      WRITE(6,280)
  280 FORMAT(///,1X, *RESIN CAP.(MEQ/ML)*, 5X, *CHLORIDE(MEQ/ML)*, 5X,
     1 *HYDROGEN(MEQ/ML)*, //,10X, *INITIAL*, 4X, *FINAL*, 7X, *INITIAL*,
     2 7X, *FINAL*, 5X, *INITIAL*, 4X, *FINAL*, / )
C     BED VOLUME IN ML OF PACKED BED, TITRANT VOLUME IN ML, CHLORIDE
C     CONCENTRATION IN MV, AND HYDROGEN CONCENTRATION IN PH VALUE
```

```
      READ(5,45)(CLMVI(I),I=1,N)
      READ(5,45)(PHI(I),I=1,N)
      READ(5,45)(CLMVF(I),I=1,N)
      READ(5,45)(PHF(I),I=1,N)
      READ(5,45)(RVI(I),I=1,N)
      READ(5,45)(TVI(I),I=1,N)
      READ(5,45)(RVF(I),I=1,N)
      READ(5,45)(TVF(I),I=1,N)
   45 FORMAT(4F10.3)
      DO 33 I=1,N
      RI(I)=TNORM*TVI(I)/(RVI(I)*(1.0-VOID))
      RF(I)=TNORM*TVF(I)/(RVF(I)*(1.0-VOID))
      SLOPE=-0.018805
      INTER=-0.0954754
      YI=CLMVI(I)*SLOPE+INTER
      YF=CLMVF(I)*SLOPE+INTER
      IF(YI.LE.0.0)CLI(I)=1.0/10.0**(ABS(YI))
      IF(YI.GT.0.0)CLI(I)=10.0**YI
      IF(YF.LE.0.0)CLF(I)=1.0/10.0**(ABS(YF))
      IF(YF.GT.0.0)CLF(I)=10.0**YF
      HI(I)=1.0/(10.0**(PHI(I)))
      HF(I)=1.0/(10.0**(PHF(I)))
      WRITE(6,55)RI(I),RF(I),CLI(I),CLF(I),HI(I),HF(I)
   55 FORMAT(F15.3,F11.3,F13.4,F10.4,F10.3,F11.4)
   33 CONTINUE

C     CALL STAT TO CALCULATE MEANS AND STANDARD DEVIATIONS OF CONCENTRATION
C     DATA AND PRINT RESULTS
      CALL STAT(RI,N,RIMEAN,RISTD)
      CALL STAT(RF,N,RFMEAN,RFSTD)
      CALL STAT(CLI,N,CLIMEAN,CLISTD)
      CALL STAT(CLF,N,CLFMEAN,CLFSTD)
      CALL STAT(HI,N,HIMEAN,HISTD)
      CALL STAT(HF,N,HFMEAN,HFSTD)
      WRITE(6,65)RIMEAN,RFMEAN,CLIMEAN,CLFMEAN,HIMEAN,HFMEAN
   65 FORMAT( /, 5X, *MEAN*, F6.3,F11.3,F13.4,F10.4,F10.3,F11.4)
      WRITE(6,75)RISTD,RFSTD,CLISTD,CLFSTD,HISTD,HFSTD
   75 FORMAT( /, 3X, *STD DVN*, F5.3,F11.3,F13.4,F10.4,F10.3,F11.4)
      RIC=RIMEAN
      RFC=RFMEAN
      CLIC=CLIMEAN
      CLFC=CLFMEAN
      HIC=HIMEAN
      HFC=HFMEAN

C     WARNING STATEMENT WHEN THERE IS AN INSUFFICIENT WASH OF RESIN
C     AFTER REGENERATION
C     IS THE EXCHANGEABLE RESIN CAPACITY OBTAINED EXPERIMENTALLY
C     (=2.65)
      DELTA=EXRC-RIC
      IF(DELTA.GE.0.0)GO TO 115
      WRITE(6,125)EXRC
  125 FORMAT(//, 5X, *EXCHANGEABLE RESIN CAPACITY(MEQ/ML)=*, F6.3)
      WRITE(6,185)
  185 FORMAT(/, 5X, *NOTE9 INITIAL RESIN CAPACITY GREATER THAN EXCHANGEA
     1BLE RESIN CAPACITY*, //, 11X, *DUE TO INSUFFICIENT WASHING AFTER R
     2EGENERATION.  Y(IN)*, //, 11X, *SET EQUAL TO ZERO*)
```

```
   NTINUE

   LCULATE AND WRITE ION FLOWS RATIO AND SLOPE OF FLOW OPERATING LINE
   C=CLIC
   F=FS*RIC/(FL*SIC)
   ITE(6,140)RIF
   MAT(//, 5X, *RATIO OF HYDROGEN TO SODIUM ION FLOW=*, F6.3)
   S IS THE SLOPE OF THE FLOW OPERATING LINE
   =1.0/RIF
   ITE(6,25)FOLS
   MAT(/, 5X, *SLOPE OF FLOW OPERATING LINE(CC/RQ)=*, F6.3)

   LCULATE THE INITIAL AND FINAL ION FRACTIONS ON SODIUM BASIS
   XB IS THE ION FRACTION IN THE LIQUID PHASE
   YB IS THE ION FRACTION IN THE RESIN PHASE
   FC=SIC-FS*(RIC-RFC)/FL
   T=RFC/(SIC+HIC)
   B=SIC/(SIC+HIC)
   TA=DELTA/EXRC
   F(DELTA.LT.0.0)YT=0.0
   F(DELTA.GE.0.0)YB=(EXRC-RFC)/EXRC
   F(DELTA.LT.0.0)YB=(RIC-RFC)/EXRC

   ALCULATE AND WRITE THE SLOPE OF THE ANALYSIS OPERATING LINE
   AOLS IS THE SLOPE OF THE ANALYSIS OPERATING LINE
   OLS=(YB-YT)/(XB-XT)
   RITE(6,15)AOLS
   MAT(/, 5X, *SLOPE OF ANALYSIS OPERATING LINE((YB-YT)/(XB-XT))=*
  1, F6.3)

   LCULATE THE NUMBER OF THEORETICAL STAGES
   C IS THE INITIAL SODIUM CONCENTRATION IN NORMAL(=MEQ/ML)
   =(-ALOG10(SIC)+17.75)/12.5
   =
   (1)=YB
   15  I=1,20
   (I)=Y(I)/(EK-(EK-1.0)*Y(I))
   F(X(I)-XT)160,160,170
   (I+1)=YB-(XB-X(I))*AOLS
   =J+1
   NTINUE
   F(J)180,180,190
   J=J+ (XT-X(I-1))/(X(I)-X(I-1))
    TO 195
   =(XT-XB)/(X(I)-XB)
   NTINUE

   LCULATE HETS, AND PLATE AND VOLUMETRIC EFFICIENCIES
   S*2.54
   =6.0
   =(PS*PN)/RNTS
   =RNTS*100.0/PN
   =3600.0*(FL+FS)/(HETS*AT)
   TE(6,200)
   AT(//, 5X, *X IS THE SODIUM ION FRACTION IN LIQUID PHASE*, //,
  , *Y IS THE SODIUM ION FRACTION IN RESIN PHASE*)
   TE(6,210)XB,XT,YT,YB,RNTS,HETS,PEFF,VEFF.
```

```
    FORMAT( /, 5X, *X(IN)=*, F6.3, 10X, *X(OUT)=*, F6.3, //
   1, *Y(IN)=*, F6.3, 10X, *Y(OUT)=*, F6.3, //,
   2, *NTS=*, F6.3, 11X, *HETS(CM)=*, F7.3, //,
   3, *PLATE EFFICIENCY(PERCENT)=*, F7.3, //,
   4, *VOLUME EFFICIENCY(1/HR)=*, F7.3)

    CHECK MASS BALANCE FOR CHLORIDE AND HYDROGEN IONS
    CHLORIDE BALANCE
    CLIN=CLIC*FL
    CLOUT=CLFC*(FL+WATER)
    DELTACL=CLIN-CLOUT
    ERRORCL=(ABS(DELTACL)/CLIN)*100.0
    HYDROGEN BALANCE
    HIN=RIC*FS+HIC*FL
    HOUT=RFC*FS+HFC*(FL+WATER)
    DELTAH=HIN-HOUT
    ERRORH=(ABS(DELTAH)/HIN)*100.0
    WRITE(6,220)CLIN,HIN,CLOUT,HOUT,DELTACL,DELTAH,ERRORCL,ERRORH
220 FORMAT(///, *IONIC MASS BALANCES*, //, 25X, *CHLORIDE*, 5X,
   1*HYDROGEN*, //, 5X, *ION IN(MEQ/SEC)*, F11.3, F13.3, //, 5X,
   2*ION OUT(MEQ/SEC)*, F10.3, F13.3, //, 5X, *IN-OUT(MEQ/SEC)*,
   3F11.3, F13.3, //, 5X, *ABS(IN-OUT)/ION IN*, F8.3, F13.3, /,
   4 4X, *(PERCENT)*)

    READ AND WRITE COMMENTS
    EIGHT CARDS ARE REQUIRED.  THE FIRST 50 COLUMNS OF EACH CARD ARE USED
    READ(5,230)(COM(I),I=1,40)
230 FORMAT(5A10)
    WRITE(6,240)
240 FORMAT(///, * COMMENTS*)
    WRITE(6,250)(COM(I),I=1,10)
250 FORMAT(//, 5X, *FLUIDIZATION9  *, 5A10, /, 20X, 5A10)
    IF(COM(6).NE.1CH          )WRITE(6,235)
235 FORMAT(*                  *)
    WRITE(6,255)(COM(I),I=11,20)
255 FORMAT(5X, *RESIN FLOW9  *, 5A10, /, 18X, 5A10)
    IF(COM(16).NE.1OH           )WRITE(6,235)
    WRITE(6,245)(COM(I),I=21,30)
245 FORMAT(5X, *OVERALL OPERATION9  *, 5A10, /, 25X, 5A10)
    IF(COM(26).NE.1OH           )WRITE(6,235)
    WRITE(6,265)(COM(I),I=31,40)
265 FORMAT(5X, *OPERATION TIME9  *, 5A10, /, 22X, 5A10)

    THE FOLLOWING SECTION PLOTS THE EQUILIBRIUM DIAGRAM, OPERATING LINES,
    AND THE THEORETICAL STAGES

    IF(COUNTER.GT.1.0)GO TO 400
    DEFINE PLOTTER UNIT AS CENTIMETER
    CALL PLOT(0.0,0.0,-20)

    DEFINE PLOTTER ORIGIN
    CALL PLOT(5.0,2.0,-3)

    PLOT NAME AND DATE
    CALL DATE(THEDATE)
    CALL LETTER(9,0.6,90.0,1.0,3.0,9HC.Y.F.LAW )
    CALL LETTER(10,0.6,90.0,2.1,3.0,THEDATE)
```

```
      DEFINE NEW PLOTTER ORIGIN
      CALL PLOT(5.0,0.0,-3)
      GO TO 510
  410 CONTINUE
      CALL PLOT(21.5,0.0,-3)
      CONTINUE

C     DEFINE PLOTTING SCALE FACTOR AND BOUNDARIES FOR X AND Y
      XSCALE=1.0/15.0
      YSCALE=1.0/15.0
      V=-3.5*XSCALE
      W=-1.0*YSCALE
      XMIN=-3.5*XSCALE
      XMAX=18.0*XSCALE
      YMIN=-1.0*YSCALE
      YMAX=18.0*YSCALE
      CALL PLTIN(XSCALE,YSCALE,V,W,XMIN,XMAX,YMIN,YMAX)

C     MARK CORNERS OF EACH PLOT
      IF(COUNTER.GT.1.0)GO TO 410
      CALL PLOT(1.0,0.0,3)
      CALL PLOT(0.0,0.0,2)
      CALL PLOT(0.0,2.0,2)
      CALL PLOT(0.0,26.0,3)
      CALL PLOT(0.0,27.5,2)
      CALL PLOT(1.0,27.5,2)
      GO TO 510
  410 CONTINUE
      CALL PLOT(1.0,0.0,2)
      CALL PLOT(0.0,27.5,3)
      CALL PLOT(1.0,27.5,2)
      CONTINUE
      CALL PLOT(21.5,27.5,3)
      CALL PLOT(21.5,27.5,2)
      CALL PLOT(21.5,26.0,2)
      CALL PLOT(21.5,2.0,3)
      CALL PLOT(21.5,0.0,2)
      CALL PLOT(20.5,0.0,2)

C     PLOT RUN NUMBER
      CALL LETTER(3,0.5,0.0,3.5,25.5,3HRUN)
      CALL LETTER(4,0.5,0.0,5.5,25.5,RUN)

C     PLOT FRAME OF THE EQUILIBRIUM DIAGRAM
      CALL PLOT(3.5,25.0,3)
      CALL PLOT(18.5,25.0,2)
      CALL PLOT(18.5,10.0,2)
      CALL PLOT(3.5,10.0,2)
      CALL PLOT(3.5,25.0,2)
      DO 420 I=1,9
      C=I
      YY=25.0-1.5*C
      CALL PLOT(3.5,YY,3)
      XX=3.7
      IF(I.EQ.5)XX=3.9
      CALL PLOT(XX,YY,2)
```

```
      CONTINUE
      DO 440 I=1,9
      CI=I
      XX=3.5+1.5*CI
      CALL PLOT(XX,10.0,3)
      YY=10.2
      IF(I.EQ.5)YY=10.4
      CALL PLOT(XX,YY,2)
      CONTINUE
      DO 440 I=1,9
      CI=I
      YY=10.0+1.5*CI
      CALL PLOT(18.5,YY,3)
      XX=18.3
      IF(I.EQ.5)XX=18.1
      CALL PLOT(XX,YY,2)
      CONTINUE
      DO 450 I=1,9
      CI=I
      XX=18.5-1.5*CI
      CALL PLOT(XX,25.0,3)
      YY=24.8
      IF(I.EQ.5)YY=24.6
      CALL PLOT(XX,YY,2)
      CONTINUE

C     GENERATE POINTS FOR THE EQUILIBRIUM CURVE
      XEQ(1)=0.0
      DO 520 I=1,301
      YEQ(I)=EK*XEQ(I)/(1.0+(EK-1.0)*XEQ(I))
      XEQ(I+1)=XEQ(I)+1.0/300.0
      CONTINUE

C     PLOT EQUILIBRIUM CURVE
      CALL PLTMPL(XEQ,YEQ,301)

C     PLOT ANALYSIS OPERATING LINE
      CALL UNITTO(XB,YB,XBP,YBP)
      CALL UNITTO(XT,YT,XTP,YTP)
      CALL GRAF(XBP,YBP,0.4,3HCIR)
      CALL PLOT(XBP,YBP,3)
      CALL PLOT(XTP,YTP,2)
      CALL GRAF(XTP,YTP,0.4,3HCIR)

C     PLOT FLOW OPERATING LINE
      FOLS=XB-YB/FOLS
      FXT=0.0
      CALL UNITTO(FXT,FYT,FXTP,FYTP)
      IF(ABS(FXTP-XTP).LT.0.1)GO TO 460
      CALL DASH(FXTP,FYTP,XBP,YBP,3)
      CONTINUE

C     PLOT OUT THE THEORETICAL STAGES
      CALL PLOT(XBP,YBP,3)
      NSTEP=J+1
      DO 470 I=1,NSTEP
      CALL UNITTO(X(I),Y(I),XP(I),YP(I))
```

```
      CONTINUE
      DO 490 I=1,NSTEP
      CALL PLOT(XP(I),YP(I),2)
      IF(XP(I).LT.XT)GO TO 490
      CALL PLOT(XP(I),YP(I+1),2)
  490 CONTINUE
      CONTINUE
      CALL PLOT(XP(I),FYTP,2)

C     LABEL EQUILIBRIUM DIAGRAM
      CALL LETTER(13,0.5,90.0,3.0,14.0,13HY RESIN PHASE)
      CALL MATH(3.15,14.6,0.8,90.0,6HLPAREN)
      CALL MATH(3.15,20.1,0.8,90.0,6HRPAREN)
      CALL LETTER(11,0.5,0.0,8.0,9.0,11HX LIQ PHASE)
      CALL MATH(8.6,9.85,0.8,0.0,6HLPAREN)
      CALL MATH(13.1,8.85,0.8,0.0,6HRPAREN)
      LABXTP=XTP+0.3
      LABYTP=9.6
      CALL LETTER(5,0.3,0.0,LABXTP,LABYTP,5HXT,YT)
      LABXBP=XBP+0.1
      LABYBP=YBP-0.6
      CALL LETTER(5,0.3,0.0,LABXBP,LABYBP,5HXB,YB)
      CALL LETTER(3,0.3,0.0,18.1,9.6,3H1.0)
      CALL LETTER(3,0.3,0.0,2.6,9.6,3H0.0)
      CALL LETTER(3,0.3,0.0,2.6,24.8,3H1.0)

C     WRITE INITIAL SODIUM ION CONCENTRATION OF EXPERIMENTAL RUN
      CALL LETTER(1,0.5,0.0,4.5,23.5,1HC)
      CALL LETTER(1,0.3,0.0,5.0,23.5,1H0)
      CALL MATH(5.3,23.50,0.5,0.0,5HEQUAL)
      CALL NUMBER(5.9,23.5,0.5,0.0,SIC,6H(F5.4))

C     WRITE RESULTS OF EXPERIMENTAL RUN
      CALL LETTER(29,0.5,0.0,3.0,7.5,29HION FRACTIONS ON SODIUM BASIS)
      CALL LETTER(2,0.5,0.0,3.0,6.5,2HXB)
      CALL MATH(4.0,6.5,0.5,0.0,5HEQUAL)
      CALL NUMBER(4.5,6.5,0.5,0.0,XB,6H(F5.3))
      CALL LETTER(2,0.5,0.0,9.5,6.5,2HYB)
      CALL MATH(10.5,6.5,0.5,0.0,5HEQUAL)
      CALL NUMBER(11.0,6.5,0.5,0.0,YB,6H(F5.3))
      CALL LETTER(2,0.5,0.0,3.0,5.5,2HXT)
      CALL MATH(4.0,5.5,0.5,0.0,5HEQUAL)
      CALL NUMBER(4.5,5.5,0.5,0.0,XT,6H(F5.3))
      CALL LETTER(2,0.5,0.0,9.5,5.5,2HYT)
      CALL MATH(10.5,5.5,0.5,0.0,5HEQUAL)
      CALL NUMBER(11.0,5.5,0.5,0.0,YT,6H(F5.3))
      CALL LETTER(3,0.5,0.0,3.0,4.5,3HNTS)
      CALL MATH(4.5,4.5,0.5,0.0,5HEQUAL)
      CALL NUMBER(5.0,4.5,0.5,0.0,RNTS,6H(F5.3))
      CALL LETTER(9,0.5,0.0,9.5,4.5,9HPLATE EFF)
      CALL MATH(14.0,4.5,0.5,0.0,5HEQUAL)
      CALL NUMBER(14.5,4.5,0.5,0.0,PEFF,6H(F6.3))
      CALL LETTER(22,0.5,0.0,3.0,3.5,22HANALYSIS OF LINE SLOPE)
      CALL MATH(14.0,3.5,0.5,0.0,5HEQUAL)
      CALL NUMBER(14.5,3.5,0.5,0.0,AOLS,6H(F5.3))
      CALL LETTER(18,0.5,0.0,3.0,2.5,18HFLOW OF LINE SLOPE)
      CALL MATH(12.0,2.5,0.5,0.0,5HEQUAL)
```

```
      CALL NUMBER(12.5,2.5,0.5,0.0,FOLS,6H(F5.3))
      COUNTER=COUNTER+1.0
      GO TO 260
      CONTINUE

C     PRINT THE NUMBER OF EXPERIMENTAL RUNS PROCESSED BY THE PROGRAM
      WRITE(6,290)COUNTER-1.0
290   FORMAT(1H1, ' NUMBER OF EXPERIMENTAL RUNS=', F6.1)
      CALL PLOT(30.0,0.0,-3)
      CALL PLOT(0.0,0.0,999)
      STOP

C
      SUBROUTINE NUMBER(X,Y,HEIGHT,ANGLE,ANUM,FMT)
C     SUBROUTINE TO ENCODE NUMBERS
C
      ENCODE(10,FMT,BCD)ANUM
      CALL SYMBOL(X,Y,HEIGHT,BCD,ANGLE,10)
      RETURN
C
      SUBROUTINE STAT(X,N,XMEAN,XSTD)
C     SUBROUTINE TO CALCULATE THE MEAN AND STANDARD DEVIATION OF X
C
      DIMENSION X(4)
C
      SSQ=0.0
      XSUM=0.0
      DO 10 I=1,N
      SSQ=SSQ+X(I)*X(I)
      XSUM=XSUM+X(I)
10    CONTINUE
      XMEAN=XSUM/FLOAT(N)
      XSTD=SQRT((SSQ-XMEAN*XMEAN*FLOAT(N))/FLOAT(N-1))
      RETURN
```

CD TOT 0549

SAMPLE COMPUTER OUTPUT

CONTINUOUS COUNTERCURRENT MULTISTAGE ION-EXCHANGE WITH
FLUID BEDS DOWNCOMER

EXPERIMENTS WERE PERFORMED WITH A COLUMN OF FOUR INCHES INSIDE
DIAMETER. THE EXCHANGER HAS SIX STAGES SPACED 4.5 INCHES APART
THE ION-EXCHANGE SYSTEM IS SODIUM ION-DOWEX-50WX8 RESIN-HYDROGEN ION

RUN NUMBER 74
****

OPERATING PARAMETERS

LIQUID FLOW RATE(ML/SEC)= 40.300
SOLID FLOW RATE(ML/SEC)= 1.600
INITIAL SODIUM CONC.(MEQ/ML)= .100
STRAIGHT WEIR LENGTH(INCH)= 3.781
WEIR HEIGHT(INCH)= 2.000
DOWNCOMER CLEARANCE(INCH)= 1.047
BEDS LATERAL DISPLACEMENT(1/20 INCH)= 2.000
RESIN PARTICLE SIZE(MESH)= -30+35

OTHER EXPERIMENTAL CONDITIONS

CROSS-SECTIONAL AREA(SQ.CM.)= 79.810
FLUIDIZATION AREA(SQ.CM.)= 55.097
DOWNCOMER CATCHING AREA(SQ.CM.)= 24.713
FRACTION OF FLUIDIZATION AREA= .690
FRACTION OF DOWNCOMER AREA= .310
FLUIDIZATION TO DOWNCOMER AREA RATIO= 2.229

OVERALL COLUMN SUPERFICIAL VEL.(ML/SQ.CM-SEC)= .501
FLUIDIZATION SUPERFICIAL VEL(ML/SQ.CM-SEC)= .726

DOWNCOMER SEAL(CM)= 2.421

TOTAL DIODE LENGTH(CM)= 8.651

EXPERIMENTAL RESULTS

	FLUIDIZED BED	SETTLED BED
MEAN HEIGHT(CM)	5.583	2.910
HEIGHT STD DVN	.532	.429
MEAN VOL(C.C.)	286.407	158.534

MEAN FLUIDIZED BED VOIDAGE= .631

(NOTE: WEIR HEIGHT(CM)= 5.080)

RESIN CAP.(MEQ/ML)		CHLORIDE(MEQ/ML)		HYDROGEN(MEQ/ML)	
INITIAL	FINAL	INITIAL	FINAL	INITIAL	FINAL
2.648	.687	.1317	.1199	.000	.0693
2.649	.687	.1317	.1194	.000	.0695
2.635	.689	.1022	.1189	.000	.0697
2.659	.687	.1022	.1184	.000	.0698
MEAN 2.648	.688	.1320	.1192	.000	.0696
STD DVN .010	.001	.0003	.0007	.000	.0002

RATIO OF HYDROGEN TO SODIUM ION FLOW= 1.039

SLOPE OF FLOW OPERATING LINE(LC/RQ)= .963

SLOPE OF ANALYSIS OPERATING LINE((YB-YT)/(XB-XT))= .962

X IS THE SODIUM ION FRACTION IN LIQUID PHASE

Y IS THE SODIUM ION FRACTION IN RESIN PHASE

X(IN)= 1.000 X(OUT)= .231

Y(IN)= .001 Y(OUT)= .741

NTU= 2.329 HETS(CM)= 29.143

PLATE EFFICIENCY(PERCENT)= 38.812

VOLUME EFFICIENCY(1/HR)= 64.399

ION MASS BALANCES.

	CHLORIDE	HYDROGEN

ION IN(MEQ/SEC)	4.079	4.236
ION OUT(MEQ/SEC)	4.967	4.000
IN-OUT(MEQ/SEC)	-.888	.236
ABS(IN-OUT)/ION IN (PERCENT)	21.778	5.568

COMMENTS

FLUIDIZATION: COMPLETE AND QUITE SMOOTH

RESIN FLOW: CONTINUOUS BUT FLOW RATE HAS SLIGHT PERIODIC VARIATION

OVERALL OPERATION: GOOD-EXCELLENT

OPERATION TIME: 24 MIN.

RUN 74

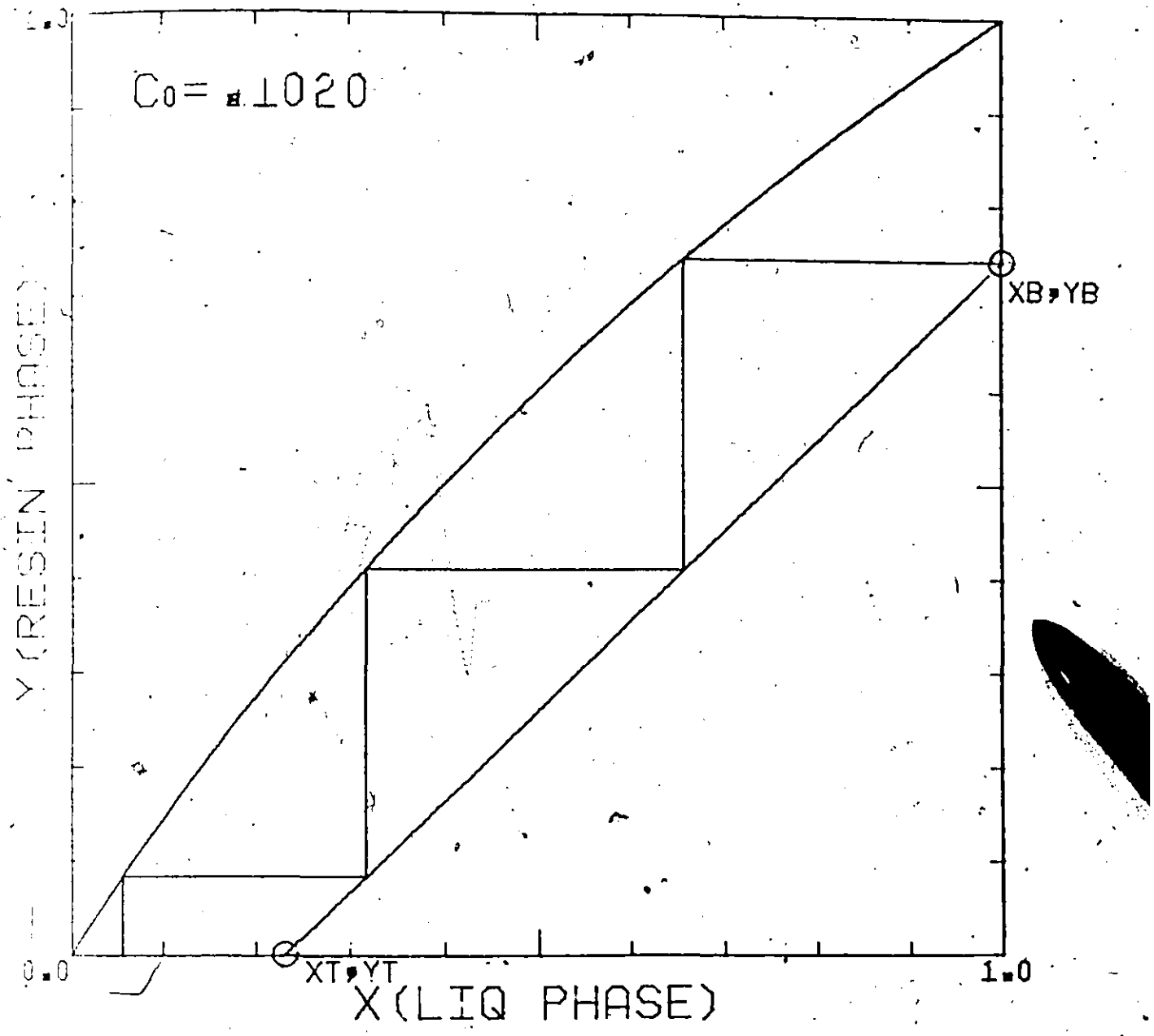

ION FRACTIONS ON SODIUM BASIS

XB=1.000 YB= .741

XT= .231 YT= .001

NTS=2.329 PLATE EFF=38.812

ANALYSIS OP LINE SLOPE= .962

FLOW OP LINE SLOPE= .963

APPENDIX H

Computer Program for Fractional Factorial Experimental Design

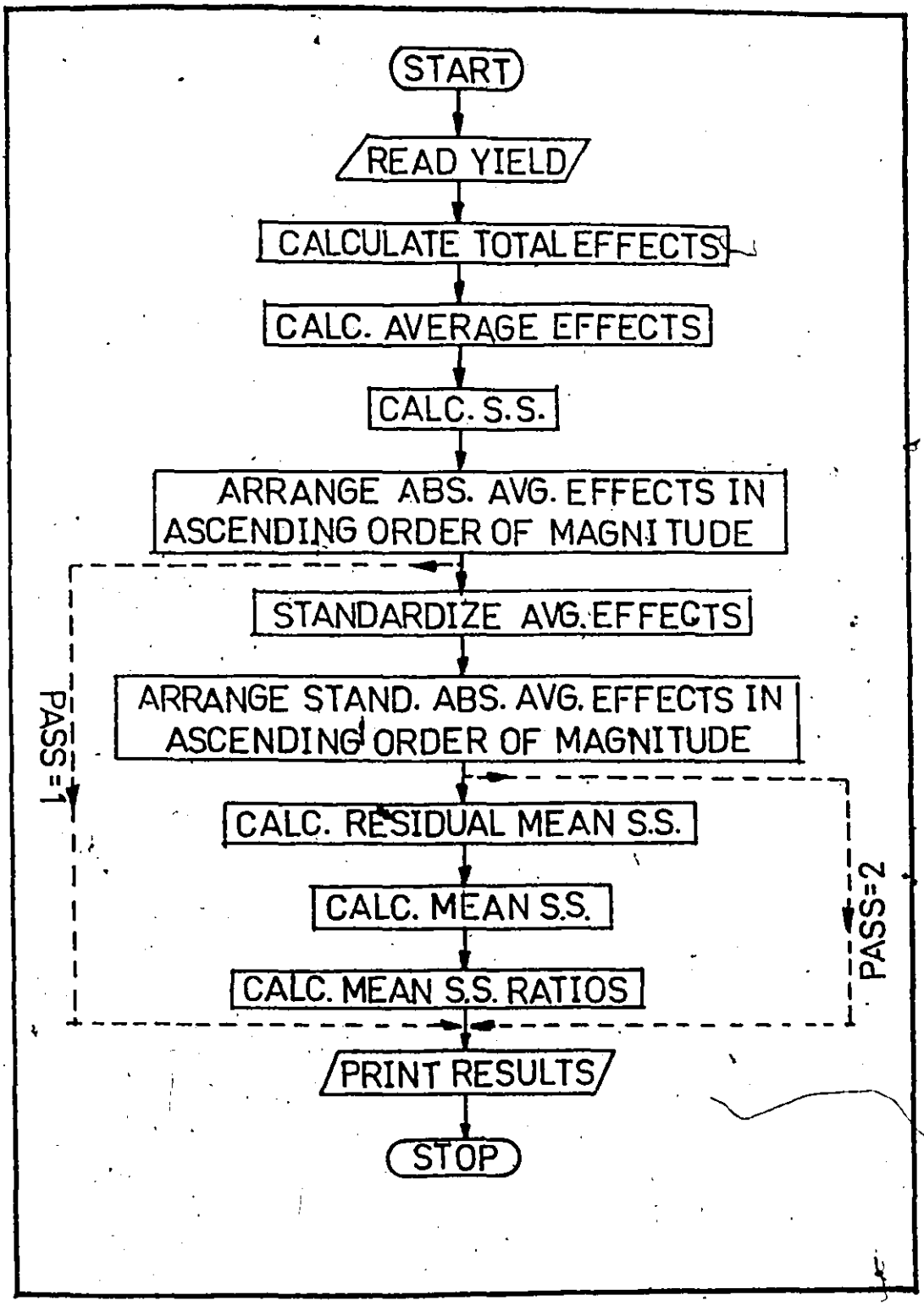

FIGURE H.1 Flow chart of the computer program for analysing the results of factorial experimental design

```
C  GENERAL PROGRAM FOR ANALYSING FRACTIONAL FACTORIAL EXPERIMENTAL
C  DESIGN TO ANY NUMBER OF FACTORS AND PERFORMING THE ANALYSIS OF
C  VARIANCE(ANOV)
C  THE PROGRAM IS DIVIDED INTO THREE FUNCTIONAL PARTS.  THE PASS NUMBER
C  IN THE DATA DECK CONTROL THE SECTION OF THE PROGRAM TO BE USED.
C  THE FOLLOWING RESULTS ARE OBTAINED FROM THE PASS NUMBERS WHEN
C  PROPER DATA IS PROVIDED IN THE DATA DECK,
C  PASS=1.   YATES ANALYSIS AND
C            AVERAGE EFFECTS LISTED IN ASCENDING ORDER
C  PASS=2.   YATES ANALYSIS,
C            AVERAGE EFFECTS AND
C            STANDARDIZED EFFECTS LISTED IN ASCENDING ORDER
C  PASS=3    YATES ANALYSIS,
C            AVERAGE EFFECTS AND
C            STANDARDIZED EFFECTS LISTED IN ASCENDING ORDER, AND
C            THE ANALYSIS OF VARIANCE TABLE
C  WRITTEN BY C.Y.F. LAW
C  SEPTEMBER, 1973

      DIMENSION CODE(100),YIELD(100),SYIELD(100),EFFECT(100),
     1          AVGEFF(100),SS(100),SCODE(100),SEFF(100)
      DIMENSION FACTOR(160),COM(8)
      DIMENSION POSI(50),NPOSI(50),MSS(100),MSSR(100),DF(100)
      DIMENSION CVALUE(3)
      INTEGER A,B,C
      REAL MSS, MSSR

C     READ THE PASS NUMBER
      READ(5,240)PASS
  240 FORMAT(F10.0)

C     SECTION FOR THE ANALYSIS BY YATES TECHNIQUE

C     READ NUMBER OF FACTORS IN FACTORIAL DESIGN
    1 CONTINUE
      READ(5,10)RK
   10 FORMAT(F10.0)
      IF(EOF(5))999,100
  100 CONTINUE
      PRINT(RK+0.01)

C     READ THE FRACTION OF THE FRACTIONAL FACTORIAL DESIGN (EXPRESSED
C     AS 2**(-M)), I.E. READ M
      READ(5,10)RM
      PRINT(RM+0.01)

C     READ THE FACTORS IN THE FACTORIAL DESIGN (ONE FACTOR IN ONE CARD)
C
      READ(5,140)(FACTOR(I),I=1,C)
  140 FORMAT(8A10)

C     READ THE TYPE OF YIELD IN THE DESIGN
      READ(5,200)(COM(I),I=1,8)
  200 FORMAT(8A10)

C     FIND THE SIZE OF THE FRACTIONAL FACTORIAL DESIGN
      RN=(2.0**RK)/(2.0**RM)
      PRINT(RN+0.01)
```

```
[illegible] TREATMENT COMBINATION AND TOTAL YIELD
  [illegible], I=1,N
[illegible](5,*) NCOMB(I),YIELD(I)
 [illegible]T(A1,F10.0)
  TINUE

[illegible] TOTAL YIELD DATA
  [illegible] I=1,N
[illegible](I)=YIELD(I)
  TINUE

CALCULATE TOTAL EFFECTS
[illegible]=4
[illegible]=1
DO 60 J=1,A
DO 70 I=1,B,2
EFFECT(1+I/2)=YIELD(I+1)+YIELD(I)
EFFECT(1+N/2+I/2)=YIELD(I+1)-YIELD(I)
CONTINUE
IF(J.EQ.A)GO TO 80
DO 90 L=1,N
YIELD(L)=EFFECT(L)
CONTINUE
CONTINUE
CONTINUE

CALCULATE AVERAGE EFFECTS
DIV1=2.0**(RK-RM-1.0)
DO 100 I=1,N
AVEFF(I)=EFFECT(I)/DIV1
CONTINUE

CALCULATE SUMS OF SQUARES
DIV2=2.0**(RK-RM)
DO 110 I=1,N
SS(I)=(ABS(EFFECT(I)))**2.0/DIV2
CONTINUE

WRITE TITLE
WRITE(6,20)
20 FORMAT(1H1, * YATES TECHNIQUE FOR THE ANALYSIS OF FRACTIONAL FACTO
 [illegible]AL*, //, * EXPERIMENTAL DESIGN*)
  FRACT=1.0/(2.0**RM)
  WRITE(6,120)K,FRACT
120 FORMAT(//, * NUMBER OF FACTORS IN DESIGN= *, I2,
  , * FRACTION OF FACTORIAL DESIGN=*, F5.3)
  WRITE(6,230)
230 FORMAT(//, * FACTORS9*)
  WRITE(6,130)(FACTOR(I),I=1,C)
130 FORMAT(/, 5X, 8A10)
  WRITE(6,210)(COM(I),I=1,8)
210 FORMAT(//, * YIELD9 *, //, 5X, 8A10)

  WRITE RESULTS
  WRITE(6,150)
150 FORMAT(//, 4X, *TREATMENT*, 5X, *YIELD*, 6X, *TOTAL*, 6X,
 [illegible]ERAGE*, 5X, *SUM OF*, /, 3X, *COMBINATION*, 15X, *EFFECT*, 5X,
```

```
      *EFFECT*, 6X, *SQUARE*)
        WRITE(6,220)CODE(1),SYIELD(1),EFFECT(1)
  220   FORMAT(/, 3X, A10,F10.3,F12.3)
        DO 240 I=2,N
        WRITE(6,170)CODE(I),SYIELD(I),EFFECT(I),AVGEFF(I),SS(I)
  170   FORMAT(/, 3X, A10,F10.3,F12.3,F11.3,F12.3)
  240   CONTINUE

C     CALCULATE THE ABSOLUTE VALUES OF THE AVERAGE EFFECTS AND STORE CODES
        DO 7  I=2,N
        AVGEFF(I)=ABS(AVGEFF(I))
        SCODE(I)=CODE(I)
    7   CONTINUE

C     ARRANGE THE ABSOLUTE AVERAGE EFFECTS IN ASCENDING ORDER
        M1=N-1
        DO 540 I=2,M1
        M2=I+1
        DO 560 J=M2,N
        IF(AVGEFF(I).LE.AVGEFF(J))GO TO 560
        STORE1=SCODE(I)
        STORE2=AVGEFF(I)
        SCODE(I)=SCODE(J)
        AVGEFF(I)=AVGEFF(J)
        SCODE(J)=STORE1
        AVGEFF(J)=STORE2
  560   CONTINUE
  540   CONTINUE
        IF(PASS.GT.1.0)GO TO 660

C     PRINT THE ABSOLUTE AVERAGE EFFECTS IN ASCENDING ORDER
        WRITE(6,620)
  620   FORMAT(////, * AVERAGE EFFECTS IN ASCENDING ORDER FOR HALF NORMAL
     *T*,///, 3X, *ORDER*, 5X, *EFFECT*, 6X, *AVERAGE EFFECT*, /,
     *  *(ABSOLUTE)*)
        DO 640 I=2,N
        WRITE(6,640)I-1,SCODE(I),AVGEFF(I)
  640   FORMAT(/, I6,5X,A10,F14.3)
        CONTINUE
        GO TO 300

  660   CONTINUE
C     READ THE ORDER OF THE EFFECT WHICH IS USED FOR STANDARDIZATION
        READ(5,650)RNUM
  650   FORMAT(F10.0)
        NUM=INT(RNUM+0.01)+1

C     CALCULATE THE ABSOLUTE STANDARDIZED EFFECTS
        DO 680 I=2,N
        SS(I)=AVGEFF(I)/AVGEFF(NUM)
  680   CONTINUE
C     PRINT THE AVERAGE EFFECTS AND THE STANDARDIZED EFFECTS IN ASCENDING
C     ORDER
        WRITE(6,550)
  550   FORMAT(////,* AVERAGE EFFECTS AND STANDARDIZED EFFECTS ARE ARRANGE
     *D*, //, * ASCENDING ORDER FOR HALF NORMAL AND STANDARDIZED HALF
     *NORMAL*, //, * PLOTS RESPECTIVELY*)
```

```
      WRITE(6,580)
  580 FORMAT(//, 3X, *ORDER*, 5X, *EFFECT*, 7X, *ABSOLUTE*, 7X, *ABSOLUT
     *E*, /, 26X, *AVG EFF*, 8X, *STD AVG*)
      DO 590 I=2,N
      WRITE(6,590)I-1,SCODE(I),AVGEFF(I),SEFF(I)
  590 FORMAT(/, I6,5X,A10,F11.3,F15.3)
      CONTINUE

      IF(ISS.EQ.2.)GO TO 300

C     SECTION FOR THE ANALYSIS OF VARIANCE

C     READ THE NUMBER OF EFFECTS POOLED TOGETHER AS THE RESIDUAL VARIANCE
      READ(5,310)RNN
  310 FORMAT(F10.0)
      NN=INT(RNN+0.01)

C     READ THE POSITIONS OF THOSE EFFECTS
      READ(5,320)(POSI(I),I=1,NN)
  320 FORMAT(8F10.0)
      DO 430 I=1,NN
      NPOSI(I)=INT(POSI(I)+0.01)
  430 CONTINUE

C     READ CRTICAL VALUES IN THE ORDER OF 0.90, 0.95 AND 0.99 LEVEL OF
C     CONFIDENCE
      READ(5,470)(CVALUE(I),I=1,3)
  470 FORMAT(3F10.0)

C     CALCULATE THE RESIDUAL MEAN SUM OF SQUARES
      SUM=0.0
      DO 330 I=1,NN
      KK=NPOSI(I)
      SUM=SUM+SS(KK)
  330 CONTINUE
      MSS(N+1)=SUM/RNN
      DF(N+1)=RNN

C     CALCULATE THE MEAN SUM OF SQUARES
      DO 340 I=1,N
      MSS(I)=SS(I)
      DF(I)=1.0
  340 CONTINUE

C     CALCULATE THE MEAN SUM OF SQUARES RATIO
      DO 350 I=1,N
      FR(I)=SS(I)/MSS(N+1)
  350 CONTINUE

C     PRINT RESULTS

      WRITE(6,460)
  460 FORMAT(////, * ANALYSIS OF VARIANCE TABLE(ANOV)*)
      WRITE(6,420)
  420 FORMAT(//, 5X, *EFFECT*, 7X, *SUM OF*, 4X, *DEG. OF*, 4X,
     *  MEAN SUM*, 4X, *MEAN SQUARE*, /, 18X, *SQUARE*,
     *  *REEDOM*, 4X, *OF SQUARE*, 6X, *RATIO*)
```

```
      I=2,N
      J=1,NN
     .EQ.NPOS1(J))GO TO 380
     CONTINUE
     MSSR(I).LT.CVALUE(1))GO TO 510
     MSSR(I).GE.CVALUE(1).AND.MSSR(I).LT.CVALUE(2))WRITE(6,480)
     (I),SS(I),DF(I),MSS(I),MSSR(I)
     MAT(/, 3X, A10,F11.3,F9.1,F14.3,F14.3, 2H *)
     MSSR(I).GE.CVALUE(2).AND.MSSR(I).LT.CVALUE(3))WRITE(6,490)
     (I),SS(I),DF(I),MSS(I),MSSR(I)
     AT(/, 3X, A10,F11.3,F9.1,F14.3,F14.3, 3H **)
     MSSR(I).GE.CVALUE(3))WRITE(6,500)CODE(I),SS(I),DF(I),MSS(I),
     R(I)
     ORMAT(/, 3X, A10,F11.3,F9.1,F14.3,F14.3, 4H ***)
     TO 520
     CONTINUE
     WRITE(6,390)CODE(I),SS(I),DF(I),MSS(I),MSSR(I)
     ORMAT(/, 3X, A10,F11.3,F9.1,F14.3,F14.3)
     CONTINUE
     TO 360
     CONTINUE
     WRITE(6,400)CODE(I),SS(I),DF(I)
     ORMAT(/, 3X, A10,F11.3,F9.1)
     CONTINUE
     WRITE(6,410)SUM,DF(N+1),MSS(N+1)
     ORMAT(/, 3X, *RESIDUAL*, F13.3,F9.1,F14.3)
     WRITE(6,440)NN,CVALUE(1),NN,CVALUE(2),NN,CVALUE(3)
     ORMAT(//,* CRITICAL VALUES*, //, 3X, *F(1,*, I1, *,0.90)=*, F5.2
     ,3X,*F(1,*, I1, *,0.95)=*, F5.2, 3X, *F(1,*, I1, *,0.99)=*, F5.2)
     CONTINUE
     TO 180
```

CD TOT 0263

SAMPLE COMPUTER OUTPUT

YATES TECHNIQUE FOR THE ANALYSIS OF FRACTIONAL FACTORIAL EXPERIMENTAL DESIGN

NUMBER OF FACTORS IN DESIGN= 7

FRACTION OF FACTORIAL DESIGN= .250

FACTORS:

A=RESIN FLOW RATE
B=LIQUID FLOW RATE
C=RESIN PARTICLE SIZE
D=WEIR HEIGHT
E=DIODE LATERAL DISPLACEMENT
F=DOWNCOMER CLEARANCE
G=WEIR LENGTH

YIELD:

PLATE EFFICIENCY

TREATMENT COMBINATION	YIELD	TOTAL EFFECT	AVERAGE EFFECT	SUM OF SQUARE
I	26.340	727.575		
(A)	18.952	-56.722	-3.545	100.543
(B)	17.488	-13.660	-.854	5.831
(C)	21.136	9.530	.596	2.838
(D)	39.335	-30.586	-1.912	29.234
(E)	29.408	-1.272	-.080	.051
(AB)	27.912	8.750	.547	2.393
(AC)	38.078	23.624	1.477	17.440
(BC)	29.758	10.875	.680	3.696
(ABC)	50.314	30.398	1.900	28.876
(D)	41.550	-.635	-.040	.013
(AD)	34.329	-66.539	-4.159	138.353
(BD)	16.623	-51.762	-3.235	83.728

[illegible]EF	23.708	-26.795	-1.675	22.438
[illegible]EF	22.473	8.986	.562	2.523
[illegible]CEF	17.004	17.688	1.106	9.777
(A)[illegible]EG	29.353	-181.222	-11.326	1026.294
B(D)G	13.894	-79.604	-4.975	198.025
C(D)G	27.840	15.294	.956	7.310
(A)BC(D)G	18.878	27.952	1.747	24.416
(A)EG	16.586	20.048	1.253	12.560
BEG	8.563	14.190	.887	6.292
CEG	16.101	-5.775	-.361	1.043
(A)BCEG	8.486	-24.954	-1.560	19.459
EG	17.290	-23.325	-1.458	17.003
(A)BEG	9.242	-6.488	-.405	1.315
(A)CEG	13.784	-9.366	-.585	2.741
BCEG	8.942	76.400	4.775	182.405
(D)EFG	26.587	202.140	12.634	1276.893
(A)B(D)EFG	14.665	4.582	.286	.656
(A)C(D)EFG	23.129	10.120	.632	3.200
BC(D)EFG	19.837	5.338	.334	.890

AVERAGE EFFECTS AND STANDARDIZED EFFECTS ARE ARRANGED IN ASCENDING ORDER FOR HALF NORMAL AND STANDARDIZED HALF NORMAL PLOTS RESPECTIVELY

ORDER	EFFECT	ABSOLUTE AVG EFF	ABSOLUTE STD AVG
1	C(D)E	.040	.023
2	(A)B(D)E	.080	.046
3	(A)B(D)EFG	.286	.164
4	BC(D)EFG	.334	.191
5	CEG	.361	.207

6	(A)BFG	.405	.232
7	(A)C(D)E	.547	.313
8	CEF	.562	.321
9	(A)CFG	.585	.335
10	BC	.596	.341
11	(A)C(D)EFG	.632	.362
12	(A)(D)F	.680	.389
13	(A)C	.854	.489
14	BEG	.887	.508
15	C(D)G	.956	.547
16	(A)BCEF	1.106	.633
17	(A)EG	1.253	.717
18	FG	1.458	.835
19	BC(D)E	1.477	.845
20	(A)BCEG	1.560	.893
21	BEF	1.675	.959
22	(A)BC(D)G	1.747	1.000
23	B(D)F	1.900	1.088
24	(D)E	1.912	1.094
25	(A)EF	3.235	1.852
26	(A)F	3.545	2.029
27	(A)BC(D)F	4.159	2.380
28	BCFG	4.775	2.733
29	B(D)G	4.975	2.848
30	(A)(D)G	11.326	6.483
31	(D)FFG	12.634	7.232

ANALYSIS OF VARIANCE TABLE(ANOV)

EFFECT	SUM OF SQUARE	DEG. OF FREEDOM	MEAN SUM OF SQUARE	MEAN SQUARE RATIO

(A)B	100.543	1.0	100.543	9.804 **
(A)C	5.831	1.0	5.831	.569
BC	2.838	1.0	2.838	.277
(A)F	29.234	1.0	29.234	2.851
(A)B(D)E	.051	1.0	.051	.005
(A)C(D)E	2.393	1.0	2.393	.233
BC(D)E	17.440	1.0	17.440	1.701
(A)(D)F	3.696	1.0	3.696	.360
B(D)F	28.876	1.0	28.876	2.816
C(D)F	.013	1.0	.013	.001
(A)BC(D)F	138.353	1.0	138.353	13.491 **
(A)EF	83.728	1.0	83.728	8.164 **
BEF	22.438	1.0		
CEF	2.523	1.0		
(A)BCEF	9.777	1.0		
(A)(D)G	1026.294	1.0	1026.294	100.072 ***
B(D)G	198.025	1.0	198.025	19.309 ***
C(D)G	7.310	1.0	7.310	.713
(A)BC(D)G	24.416	1.0	24.416	2.381
(A)FG	12.560	1.0	12.560	1.225
BFG	6.292	1.0		
CFG	1.043	1.0		
(A)BCFG	19.459	1.0		
EG	17.003	1.0	17.003	1.658
(A)BEG	1.315	1.0	1.315	.128
(A)CEG	2.741	1.0	2.741	.267
BCEG	182.405	1.0	182.405	17.786 ***
(D)FG	1276.893	1.0	1276.893	124.508 ***
(A)B(D)EFG	.656	1.0	.656	.064
(A)C(D)EFG	3.200	1.0	3.200	.312
BC(D)EFG	.890	1.0	.890	.087

(A)B	100.543	1.0	100.543	9.804 **
(A)C	5.831	1.0	5.831	.569
BC	2.838	1.0	2.838	.277
(D)E	29.234	1.0	29.234	2.851
(A)B(D)E	.051	1.0	.051	.005
(A)C(D)E	2.393	1.0	2.393	.233
BC(D)E	17.440	1.0	17.440	1.701
(A)(D)E	3.696	1.0	3.696	.360
B(D)E	28.876	1.0	28.876	2.816
C(D)E	.013	1.0	.013	.001
(A)BC(D)E	138.353	1.0	138.353	13.491 **
(A)EF	83.728	1.0	83.728	8.164 **
BEF	22.438	1.0		
CEF	2.523	1.0		
(A)BCEF	9.777	1.0		
(A)(D)G	1026.294	1.0	1026.294	100.072 ***
B(D)G	198.025	1.0	198.025	19.309 ***
C(D)G	7.310	1.0	7.310	.713
(A)BC(D)G	24.416	1.0	24.416	2.381
(D)FG	12.560	1.0	12.560	1.225
BFG	6.292	1.0		
CFG	1.043	1.0		
(A)BCFG	19.459	1.0		
EFG	17.003	1.0	17.003	1.658
(A)BFG	1.315	1.0	1.315	.128
(A)CFG	2.741	1.0	2.741	.267
BCFG	182.405	1.0	182.405	17.786 ***
(D)EFG	1276.893	1.0	1276.893	124.508 ***
(A)B(D)EFG	.656	1.0	.656	.064
(A)C(D)EFG	3.200	1.0	3.200	.312
BC(D)EFG	.890	1.0	.890	.087

RESIDUAL 61.533 6.0 10.256

CRITICAL VALUES:

F(1,6,0.90)= 3.79 F(1,6,0.95)= 5.99 F(1,6,0.99)=13.75